AUTHOR: SHEHU, H.

TITLE: Innovative hydrocarbons recovery and utilization technology using reactor-separation membranes for off-gases emission during crude oil shuttle tanker transportation and natural gas processing.

YEAR: 2018

This work was submitted to- and approved by Robert Gordon University in partial fulfilment of the following degree:
Doctor of Philosophy, School of Engineering

Innovative Hydrocarbons Recovery and Utilization Technology Using Reactor-Separation Membranes for Off-gases emission during Crude Oil Shuttle Tanker Transportation and Natural Gas Processing

HABIBA SHEHU

A thesis submitted in partial fulfilment
of the requirements of the
Robert Gordon University
for the degree of Doctor of Philosophy

This research programme was carried out in collaboration with the Center for Process Integration and Membrane Technology

May, 2018

Abstract

The increase in greenhouse gas (GHG) concentrations in the atmosphere, as well as the high rate of depletion of hydrocarbon-based resources have become a global concern. A major source of emissions of hydrocarbon vapours occur during loading and offloading operations in crude oil shuttle tanker transportation. The emitted gases have a typical composition of 60 % N_2, 10 % CO_2, 5% O_2, 5 % C_3H_8, 10% CH_4, 5% C_2H_6 and 5 % higher hydrocarbons. As a result, various methods aimed to add value to GHG to produce valuable fuels and chemical feedstock are being developed. This work incorporates the use of silica, polyurethane/zeolite and y-type zeolite membrane on an alumina support to selectively permeate methane and carbon dioxide from inert gases and higher hydrocarbons. The recovered gas is upgraded by dry reforming reactions employing rhodium/alumina membrane incorporated into a shell and tube reactor. Mixed gas permeation tests have been carried out with the permeate and feed gases sent to the online gas chromatograph (GC) equipped with a mass spectrometry (MS) detector and an automated 6-port gas sampling valve with a 30 mm HP- Plot Q column. The question is what mesoporous membrane can be highly selective for the separation of methane and carbon dioxide from inert gases and higher hydrocarbons, and what is the effect of temperature and feed gas pressure on the conversion of separated gases? Characterisation of the modified membranes was carried out using nitrogen physisorption measurements and showed the hysteresis isotherms corresponding to type IV and V, which is indicative of a mesoporous membrane. The surface area and the pore size were determined using the Barrett, Joyner, Halenda (BJH) desorption method, which showed the silica membrane had a larger surface area (10.69 $m^2\ g^{-1}$) compared to zeolite (0.11 $m^2\ g^{-1}$) and polyurethane/zeolite membrane (0.31 $m^2\ g^{-1}$). Fourier Transform Infrared spectroscopy, Scanning Electron Microscope and Energy Dispersive X-ray Analysis confirmed the asymmetric deposition of silica, polyurethane, rhodium and zeolite crystals in the matrix of the alumina support. Single gas permeation tests showed that the synthesised y-type zeolite membrane at 293 K had a CH_4/C_3H_8 selectivity of 3.11, which is higher than the theoretical value of 1.65. The permeating CH_4 and C_3H_8 flux at 373 K and a pressure of 1 x 10^5 Pa was 0.31 and 0.11 mol $s^{-1}\ m^{-2}$ respectively proving that zeolite has molecular sieving mechanism for separation of methane and propane. The silica membrane exhibited higher effectiveness for

Abstract

the separation of CO_2 than the other membranes. For methane dry reforming using a supported rhodium membrane, an increase of the reaction temperature from 973 K to 1173 K showed an increase in conversion rate of CO_2 and CH_4 from less than 20% to over 90% while increasing the gas hourly space velocity (GHSV) did not have a noticeable effect. The study revealed the high potential of the zeolite and rhodium membrane for gas separation and dry reforming reactions concept in creating value-added carbon-based products from CO_2 and CH_4.

Dedication

This thesis is dedicated to my soul mate, the person who touched my hands and I could reach the stars, my husband Colonel Mohammed Bako Shehu and my father that started me in the right path late Malam Sanusi Karaye Madakin Galadiman Karaye.

Declaration

I hereby declare that no portion of the work in this thesis has been submitted in support for an application for another degree or qualification of this or other university or other institute of learning. I confirm that the material presented in this report is my own work. Where this is not the case, the source of material has been duly acknowledged.

Acknowledgement

The success and final outcome of this project required a lot of guidance and assistance from many people and I am extremely privileged to have got this all along to the completion of my project. All that I have done is only due to the supervision and assistance that I received and I would not forget to thank them.

I owe my deep gratitude and respect to my surpervisor Professor Edward Gobina, for providing me with the opportunity to undertake my research work at the Center for Process Intergration and Membrane Technology, Robert Gordon University and giving me the opportunity to be part of a group that was more like family and provided all the support and guidance which made me complete the project duly. I am extremely thankful to him for providing such support and guidance, although he has a busy schedule I can count on his support even on weekends.

My thanks goes to our health and safety personel Alan Mclean for making sure I know all the hazards of working in a laboratory, our technical staff David Howie, David Smith, Mark and Martin, who took keen interest in my work, helped build my experimental rig and even give up their lunch break to offer assistance. To my colleagues, Abubabakar Alkali, Nasir Kajama, Ngozi Nwogu, Edidiong Okon and Ifeyinwa Orakwe, thank you for all the assistance and the shoulder to lean on.

I would not forget to mention Mr Iain Tough of the School of Pharmacy and Life Sciences RGU for the tireless lessons on the use of the Scanning Electron Microscope and the Xray Diffraction.

I am thankful and fortunate enough to get constant encouragement, support, guidance and help of babysitting from my sister Karima Bakare, my mother Habiba Sanusi, my nephews Adamu and Sanusi Jagafa for braving the Aberdeen cold and being with me. My sisters Fatima and Maryam Sanusi, my brothers Ado and Ibrahim Sanusi, thank you for being supportive.

I will not forget to mention my source of joy my children whom at the start of my PhD used to say mum drop your yabtop (laptop) and carry us to the end of my PhD now as matured lovely kids, Usman, Hadiza, Nurain and Zahra Shehu, I love you guys, you are my inspiration.

Habiba Shehu

Table of Contents

Table of Figures

Table of Tables

Acronyms

BET	Brunauer, Emmett and Teller
BJH	Barrett-Joyner-Halenda
CETS	Chemical energy transmission systems
CMR	Catalytic Membrane Reactor
COSHH	Control of substances hazardous to health regulations
CPOX	catalytic partial oxidation
DRM	Dry reforming methane
EDAX	Energy Dispersive X-Ray analyser
EPA	Environmental Protection Agency
FPSO	Floating Production Storage and Offloading units
FSO	Floating Storage Offloading units
FTIR	Fourier Transform Infrared spectrometer
FTS	Fischer-Tropsch synthesis
GC-MS	Gas chromatography coupled mass spectrometry
GHG	Greenhouse gases
GTL	Gas to liquid
GWP	Global Warming Potential
HC	Hydrocarbons
INDC	Intended Nationally Determined Contributions
ICOM	International Conference on Membranes and Membrane Process
IG	Inert Gas
IMO	International Maritime Organization
LHHW	Langmuir-Hinshelwood-Hougen-Watson
MARPOL	Marine Pollution
MMMs	Mixed matrix membranes
MS	Maxwell-Stefan
NMP	*N*-methylpyrrolidone
NMVOC	Non- Methane Volatile Organic Compounds

PBR	Packed bed reactor
PMA	Poly(methacrylic acid)
POX	Partial oxidation
PSF	Polysulfone
PU	Polyurethane
SEM	Scanning Electron Microscope
SLPM	Standard litre per minute
SMR	Steam methane reforming
TEOS	Tetraethoxysilane
TOC	Total Organic Compounds
UNFCCC	United Nations Framework Convention on Climate Change
VECS	Vapour Emission Control System
VOC	Volatile Organic Compounds
WGS	Water gas shift

Symbols

P	permeance	mol m^{-2} s^{-1} Pa^{-1}
A	membrane surface area	m^2
Δp	pressure difference	Pa
$\alpha_{i,j}$	ideal gas selectivity	-
D	diffusivity coefficient	m^2s^{-1}
S	solubility coefficient	mol m^3 Pa
SF	separation factor	-
X	concentration (permeate)	%
Y	concentration (feed)	%
Q	molar gas flow	mol s^{-1}
r_p	pore radius	m
R	molar gas constant	J Kg^{-1} mol^{-1}
M	molar mass	g mol^{-1}

T	temperature	K
K	Knudsen number	
λ	mean free path	m
J	gas flux	mol m^{-2} s^{-1}
$\bar{P}$	mean pressure across a membrane	Pa
A	constant representing Knudsen flow	
B	constant representing viscous flow	

Scientific Achievement

Memberships

- European Membrane Society (EMS) 01/2015 – date
- International Association of Engineers (IAENG) 03/2015 – date
- Association for Women in Science (AWIS) 08/2017 - date

Invited World Conferences

1. An Initial Study on the Use of Membranes for Hydrocarbons Recovery from Shuttle Tankers during Crude Oil Transportation at the 3rd International Conference on Challenges in Environmental Science and Computer Engineering, London, United Kingdom 21st to 22nd June 2014.
2. Characterization of composite mesoporous membranes using nitrogen isothermal measurements at the 18th International Conference on Composite structures, Lisbon Portugal, 15th to 18th June 2015.
3. The Use of Nano-composite Ceramic Membranes for Gas Separations at the World Congress on Engineering 2015; July 1st to 3rd, 2015, London, UK.
4. Study of the selectivity of methane over carbon dioxide and inert gases using composite inorganic membranes at the 3rd International conference on Mechanical and Aerospace Engineering 5th to 7th October 2015, San Francisco, USA.
5. Recovery of VOC from Onshore and Offshore Shuttle Tankers using Structured Membranes at the World Congress on Engineering, 21st to 23rd October 2015, San Francisco, USA
6. Novel Zeolite-Polyurethane Membrane for Environmental Applications at the Nanotech France 2016 International Conference and Exhibition 1st to 3rd June 2016, Paris, France.
7. Separation of C_3H_8 and CO_2 from CH_4 in polyurethane/y-type zeolite mixed matrix membrane at the International Conference on Nanotechnology and Nanomaterials in Energy (ICNNE 2016) 2nd to 4th June 2016, Paris, France.
8. A Fickian Model for Gas Transport through a Zeolite Membrane at the World Congress on Engineering and Computer Science 2016, 19th to 21st October 2016, San Francisco, USA. **(Award: Best Student Paper).**
9. Experimental study of CO_2 conversion from flue gas using catalytic rhodium membrane at the 13th International Conference on Catalysis in Membrane Reactors July 10th to 13th, 2017, Houston, Texas, USA.
10. Innovative Hydrocarbons Recovery and Utilization Technology Using Reactor-Separation Membranes for Off-gases emission at the Global Conference on Catalysis and Reaction Engineering. October 19-21, 2017 at Hampton Inn Tropicana and Event Centre, Las Vegas, Nevada, USA **Oral Presentation**

Poster Presentations

1. Innovative Hydrocarbons Recovery Technology using Separation Membranes for Crude Oil Shuttle Tanker transportation and Natural Gas Processing. Conference on "Emerging and Hybrid Membrane Technologies" organized by institution of chemical engineers (IChemE) advancing chemical engineering worldwide, 10 June 2016, Swansea University, UK.
2. Experimental study of CO_2 conversion from flue gas using catalytic rhodium membrane at the 13th International Conference on Catalysis in Membrane Reactors July 10th to 13th, 2017, Houston, Texas, USA.
3. Characterization of Y-Type zeolite membrane for natural gas processing at the 13th International Conference on Catalysis in Membrane Reactors July 10th to 13th, 2017, Houston, Texas, USA.
4. Effect of Polyurethane on Hydrocarbons separation using an Inorganic Membrane at the International Conference on Catalysis and Chemical Engineering 22nd to 24th February 2017 Baltimore, USA.

Journal Publication

1. Shehu H, Kajama M, Gobina E. Effect of Temperature on Gas Separations Using Porous Alumina Membranes. International Journal of Modern Sciences and Engineering Technology (IJMSET). 2014; 1(5):22-30

2. Habiba Shehu, Edidiong Okon, Mohammed Kajama, Ngozi Nwogu, Ify Orakwe and Edward Gobina. An Initial Study of The Selectivity of Methane Over Carbon Dioxide and Inert Gases Using a Y- Type Zeolite Membrane. International Journal of Current Research, Vol. 7, Issue, 04, pp.14986-14990, 2015. http://www.journalcra.com.

3. Habiba Shehu, Edidiong Okon, Mohammed Nasir Kajama, Edward Gobina. Characterization of Y-Type Zeolite Membrane using the Fickian Approach for VOC Recovery from Shuttle Tankers. American International Journal of Research in Science, Technology, Engineering & Mathematics, Vol. 1(11), pp. 19-22' 2015.

4. H. Shehu, E. Okon, E. Gobina. A Fickian Model for Gas Transport through a Zeolite Membrane. Proceedings of the World Congress on Engineering and Computer Science 2016 Vol II WCECS 2016, October 19-21, 2016, San Francisco, USA. http://www.iaeng.org/publication/WCECS2016/

5. Habiba Shehu, Edidiong Okon, Ifeyinwa Orakwe and Edward Gobina. Study of the Selectivity of Methane over Carbon Dioxide Using Composite Inorganic Membranes for Natural Gas Processing. http://dx.doi.org/10.4172/2090-4568.1000150

6. H. Shehu, E. Okon, E. Gobina, "Separation of Methane from Shuttle Tanker Vents Gases by Adsorption on a Polyurethane/Zeolite Membrane", Key Engineering Materials, Vol. 733, pp. 42-46, 2017. 10.4028/www.scientific.net/KEM.733.42

7. Kajama MN, **Shehu H,** Okon E, Orakwe I, Gobina E. VOC oxidation in excess of oxygen using flow-through catalytic membrane reactor. *International Journal of Hydrogen Energy.* 2016; 41(37):16529-16534.

8. Okon E, **Shehu H**, Gobina E. Evaluation of the performance of α-alumina nano-porous ceramic composite membrane for esterification applications in petroleum refinery. *Catalysis Today.* 2017.

9. H. Shehu, E. Okon, E. Gobina, Novel Zeolite-polyurethane membrane for environmental applications and gas separation, Mat´eriaux & Techniques. EDP Sciences, 2017 DOI: 10.1051/mattech/2017031 www.mattech-journal.org. Accepted manuscript still in press

Book Chapters

1. Habiba S, Ajayi A, Edidiong O and Gobina E. Recovery of VOC from Offshore and Onshore Shuttle Tankers Using Structured Y-Type Zeolite Membranes. Recovery of VOC from Offshore and Onshore Shuttle Tankers Using Structured Y-Type Zeolite Membranes. *The World Congress on Engineering and Computer Science*: Springer; 2015. p. 541-553.

2. Habiba S, Edidiong O, Gobina E. Novel Composite Inorganic Ceramic Membranes for Gas Separations and Environmental Applications. Transactions on Engineering Technologies.: Springer; 2016. p. 59-72.

3. Shehu H, Okon E and Gobina E. A Fickian Model for the Recovery of Methane from Carbon dioxide, Propane, and Inert gases in Natural Gas Purification Process. *Iaeng Transactions On Engineering Sciences: Special Issue For The International Association Of Engineers Conferences 2016*: World Scientific; 2017. p. 175.

4. H. Shehu, E. Okon, E. Gobina. Separation of Methane from Shuttle Tanker Vents Gases by Adsorption on a Polyurethane/Zeolite Membrane. Key Engineering Materials, Vol. 733, pp. 42-46, 2017. 10.4028/www.scientific.net/KEM.733.42

1 Introduction

This chapter introduces the motivation of the research and the benefits for the recovery and utilisation of two major greenhouse gases, carbon dioxide and methane. Various sources of emission of these gases, as well as separation and catalytic conversion methods are discussed. In addition, the use of membrane technology for gas separation and catalytic action will be introduced. The gas transport mechanism and catalytic properties of the membranes with comparison to the current state-of-the art technology used in industry is examined. Applications of the separation products (i.e. methane and carbon dioxide) and conversion products (i.e. carbon monoxide and hydrogen) are explored.

1.1 Motivation

In the past century, human activities have caused the release of large quantities of carbon dioxide and other greenhouse gases (GHG) into the atmosphere. The greenhouse effect is caused by GHGs that behave like a layer around the Earth, confining the energy in the atmosphere there by resulting in an increase in the Earth's temperature. This is a natural process and it is vital for life on earth. However, the build-up of GHGs can alter the Earth's climate, resulting in harmful effects to human health and to the ecosystem. The GHG that are purported to cause the greenhouse effect include methane (CH_4), carbon dioxide (CO_2), oxides of nitrogen (N_2O), and fluorinated gases (F-gases). Figure 1(a) presents the distribution of GHG globally, it shows that CO_2 and CH_4 are the most abundant gases as they are the major pollutants from industrial processes. Thus, they are the major GHGs responsible for contributing most to the greenhouse effect or global warming. GHG emissions are significantly connected to the world increasing population, which has also necessitated an increase in energy demand. This is evidenced by the fact that CH_4 and CO_2 emissions are mostly released from oil and gas extraction activities, agriculture and combustions of fossil fuel. Globally, advanced countries are pushing for the enforcement of the reduction of greenhouse gas emissions. Hence, various countries presented their plans to lower GHG emissions or Intended Nationally Determined Contributions (INDCs) at the 21st Conference of Parties in Paris (also known as COP21), under the United

Nations Framework Convention on Climate Change (UNFCC) as a plan to reducing GHG emissions, and all nations that are signatory to the UNFCC were asked to publish at the 2015 United Nations Climate Change conference held in Paris, France in December 2015. Various methods were proposed by the COP21 participants, namely; making specific policy actions, reductions from everyday sources and reducing the intensity, thus these goals are not easily quantifiable (1).

The call for 100% renewable energy future is gaining a tremendous amount of support, although due to the various sectors involved in environmental GHG emissions (figure 1b) and the different countries with different policies involved, it looks like a difficult achievement. However, the concept is clear and simple but due to global complexity, achievable goals in one country may not necessarily be feasible in another, thus making its implementation futile. The 2015 Paris agreement signalled by various countries in undertaking to hold the world average temperature increase below 2 °C, or a preferred value of 1.5 °C, will need the removal of carbon-based energy. Finding solutions for some sectors is easier than for others due to the financial, environmental and social implications (1).

The Europe 2020 Strategy adopted on June 2010 gave the present direction for the European Union for economic renewal with a goal to subsequently lower GHG emissions by 30% before 2020 (2). The global warming potential (GWP) of methane is higher than that of CO_2 with a factor of about twenty-one, hence it is regarded as a GHG. Moreover, gases like butane, ethane, propane, hexane and pentane combine with oxides of nitrogen to form ground-level ozone that can be harmful to the vegetation, animals and people as well. Carbon dioxide is an important source of carbon for fuels and chemical feedstock.

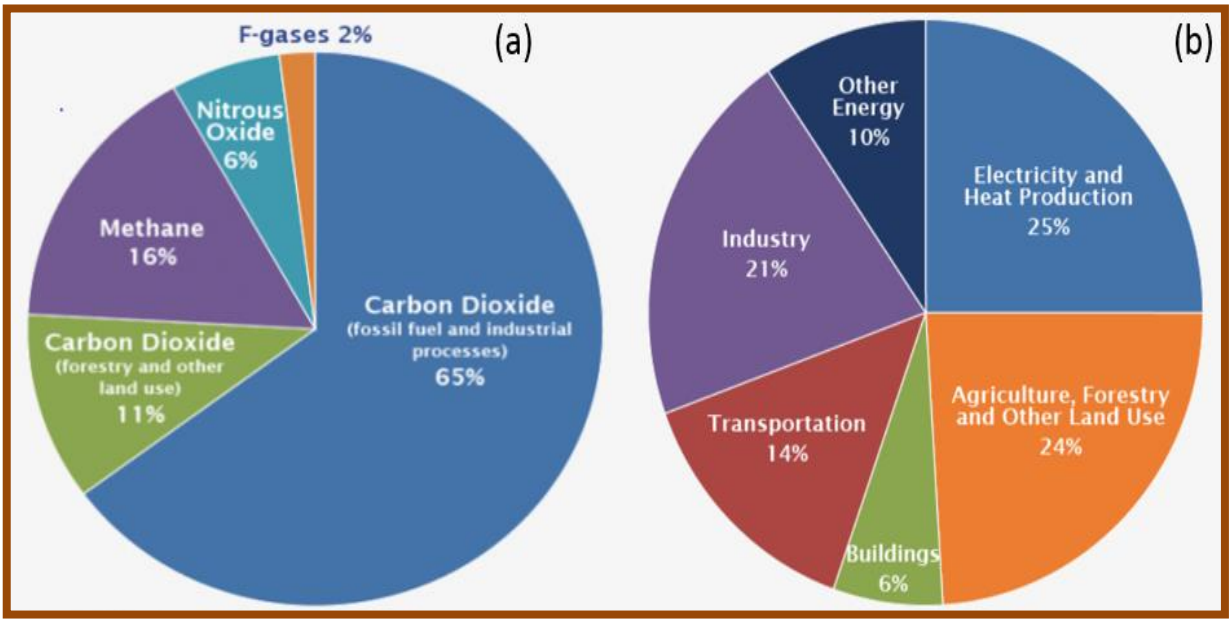

Figure 1-1: Global greenhouse gas emissions by (a) gas and (b) economic sector. Adapted from www.epa.gov.

In recent years, industrial routes for one-step conversion of methane to fuels and chemicals have been and are still limited. The most technologically advanced routes involve high temperature indirect conversion of methane (methane steam reforming (SMR)) to fuels and chemicals. A good number of hydrocarbon resources in the world consist mainly of methane with a significant amount not being fully utilised. With the scale of oil, gas and petrochemical industries today, the use of catalytic membrane reactors to produce fuels from methane and carbon dioxide, rather than from crude oil, will significantly impact the whole hydrocarbon chain value and produce a much cleaner society.

Figure 1-1(b) shows the global emissions of GHG by economic sector. This shows that electricity and heat production generate the highest percentage of GHG emissions. The transport, storage and production of crude oil are among the major pathways for the emissions of volatile organic compounds (VOCs) in the environment (3). However, VOC emissions happens during filling and discharging of crude oil from floating production storage and offloading units (FPSOs and FSOs) (4). When filling the units, lower hydrocarbons vaporise and occupy the space between the roof of the tank and the crude oil. There has been recent development in the use of membrane technology for environmental applications due to their low energy consumption and small footprint. Poly dimethyl siloxane (PDMS) is a type

of polymeric membrane that is commonly used as selective permeation layer. It can be easily fabricated and thus is readily available for its use on large scales. The use of dimensionless solubility parameters showed that PDMS has good selectivities towards a wide variety of VOCs (e.g., hydrocarbons). However, these polymeric membranes can have a problem of being easily fouled due to harsh operating conditions. Inorganic membranes can be competitive with processes like distillation, adsorption, extraction and crystallisation (5). Catalytic membrane reactors also offer potential for improved conversion rates at reduced operating temperature due to process intensification (5). In this work the separation of CH_4 from inert gases and propane (C_3H_8) has been studied using silica, y-type zeolite and polyurethane polymer/zeolite on an alumina membrane. The separated gases were used as constituents in a simulated methane reforming process designed using a rhodium membrane for flue gas reforming of methane to form carbon monoxide and hydrogen, as described in equation [1].

$$CH_4 + CO_2 \rightleftharpoons 2H_2 + 2CO \; [\Delta\hat{H}_{rection}\,(298\,K) = 247.3\,KJ\,mol^{-1}] \qquad \textit{Equation 1}$$

This reaction is important for the reduction of emissions and syngas production. High yield of carbon monoxide and hydrogen can represent the starting point for methanol synthesis (6–8), for Fischer-Tropsch reactions (9, 10) and subsequently to produce ammonia. The use of the membrane reactor for this reaction can be competitive when compared to the conventional method that involves the application of packed bed reactors that do not incorporate a membrane. Moreover, the catalytic membrane reactor will also have an improved yield and reduce capital cost due to process intensification.

1.2 Background

Volatile organic compounds (VOCs) vapourises easily to the atmosphere due to their high vapour pressure. Light hydrocarbons like methane, ethane and propane are considered as VOCs (3). As stated previously, methane has a global warming potential (GWP) 21 times greater than CO_2. Table 1.1 shows the GWP for methane, carbon dioxide and several hydrocarbon gases, butane has a slightly higher GWP than propane this is due to the 100-year GWP calculation, butane stays longer than propane in the atmosphere. Figure 1-1(a) shows the percentage of the GHGs emitted.

Table 1.1: Global warming potentials for several VOC components. Adapted from reference 11.

Components	*GWP*
Methane	21
Ethane	5.5
Propane	3.3
Butane	4
Carbon dioxide	1

Worldwide emissions of GHG can be presented according to the economic activities that lead to their production, as indicated in Figure 1-1(b) (12). These include,

- Electricity and heat production: This sector accounts for the highest percentage of GHG emissions at 25% (in 2010), as reported by the United States Environmental Protection Agency (EPA). Hence, the burning of fossil fuels (*i.e.* coal, natural gas and oil) for electricity and heat generation are the main activities that contribute to the global increase of GHG.
- Industry: GHG emissions from industry primarily involve onsite burning of fossil fuels for energy. This area incorporates emissions from mineral transformation processes which are not as a result of energy consumption, chemical, metallurgical and emissions from activities of waste management. This sector accounts for 21% of GHG (Figure 1-1(b)).
- Agriculture, forestry and other land uses: GHG emissions from this sector originate primarily from deforestation, cattles and planting of trees. This value does not include carbon dioxide removed from the atmosphere by dead organic matter, carbon sequestering in biomass and soils, which reduces about 20% of emissions from this sector.
- Transportation: GHG emissions from transportation includes the use of fossil fuels that are burned for rail, road, water and air transportation. Petroleum-based fuels account for about 96% of global transportation energy, this is mainly from diesel and gasoline.
- Buildings: This area accounts for the smallest GHG emissions (6%) and the

emissions mainly arise from onsite energy generation and burning fuels for heat in buildings or cooking in homes.

- Other Energy: Other sources of GHG emissions come from the Energy sector which are not directly associated with electricity or heat production. For example, oil and gas extraction, refining, processing, and transportation.

The work carried out in this research considers the economic sector of GHG emissions namely, transportation and storage of crude oil as well as natural gas processes. A technology to separate the major GHGs methane and carbon dioxide and further utilise them in valuable feed stock has been explored. The retentate could also constitute a valuable stream for further utilisation. This is outside the scope of this thesis.

1.3 Transportation- Shuttle Tankers for Crude Oil Transportation

VOC emissions to the atmosphere, from shuttle tankers has not been globally quantified and evaluated methodically. Obviously, emissions represent a financial deficit worldwide. Moreover, dangerous environmental ramifications due to emission of distinctive lower hydrocarbons are not fully understood, however, could be more significant than the financial deficit. It has been ascertained that several VOC compounds represent greenhouse gases. Moreover, these gases can combine with NOx to form ozone in the presence of sunlight. Furthermore, H_2S which is a strong poison can be found in the oil vapour.

The International Maritime Organisation (IMO) adopted a goal of thirty percent reduction in the discharge of non-methane volatile organic compounds (NMVOCs) at the end of 1999, as the Directive on Integrated Pollution Prevention and Control (IPPC) (96/61/EC) entered into force in 1999 (4). It aims to prevent or minimise pollution to air, water or land from various industrial sources throughout the European Union. The Commission has been undertaking a review of the IPPC Directive and related legislation on industrial emissions and on the 21st December 2007 adopted a proposal for a Directive on industrial emissions. The proposal recasts seven existing Directives relating to industrial emissions into a single legislative instrument (4).

In marine pollution (MARPOL) Annex VI of 1997 it is stated that each nation has the right to determine what they need for lowering NMVOC emission in their docks and regional waters. Various nations have adopted a national goal of thirty percent reduction in NMVOC emission. For example, in Norway, nearly 50% of their overall Norwegian NMVOC discharge arises from asea oil transportation that includes crude oil loading operations in the North Sea. Reduction of emissions in this area could be accomplished in an economical manner. Hence, clearly it is vital to control emissions from shuttle tankers. A huge amount of VOC emission is as a result of floating production, storage, and offloading units (FPSOs and FSOs). However, there are some measures that are put in place to regulate these emissions (4). However, the major challenge in the recovery of volatile organic compounds from shuttle tankers, FPSOs and FSOs is that the hydrocarbons that have evaporated are mixed in large volume of inert nitrogen gas as the cargo tanks are being loaded, the gas mixture is displaced by the inflow of oil. There have been previous studies on the feasibility of a number of concepts, based on the application of measures to depress the evaporation at the outset, combined with conventional processes for recovery of oil vapour. Hence, the concepts consist of particular combinations of measures that are separately known but which so far have not been evaluated or come into practical use. Simulation programs have been used extensively in the evaluation of these concepts. The philosophy is that the equipment for recovery of VOCs can be made simpler and cheaper than solutions for recovery that have been employed to date.

The challenge is to find a solution that is economic and yet does not sacrifice to the emission reduction potential. Gas return from cargo tanks to oil terminals is practiced using absorption where the gas return system is made in accordance to the MARPOL requirements for the Vapour Emission Control System (VECS). In this technology, VOC emissions from cargo tanks are collected by a manifold system, passed through a de-mister and condensed. Once condensed, the heavier non-methane elements are passed into an absorption column where they are absorbed into a stream of crude and returned to the cargo tank. The lighter compounds – ethane, methane and inert gases are not condensable and are vented. Thus, the use of membrane for the recovery of these vented gases will offer a chance to utilize the lighter gases as well (4). Figure 1-2 presents a diagram for proposed hydrocarbon recovery and utilisation from a shuttle tank vent using membrane technology.

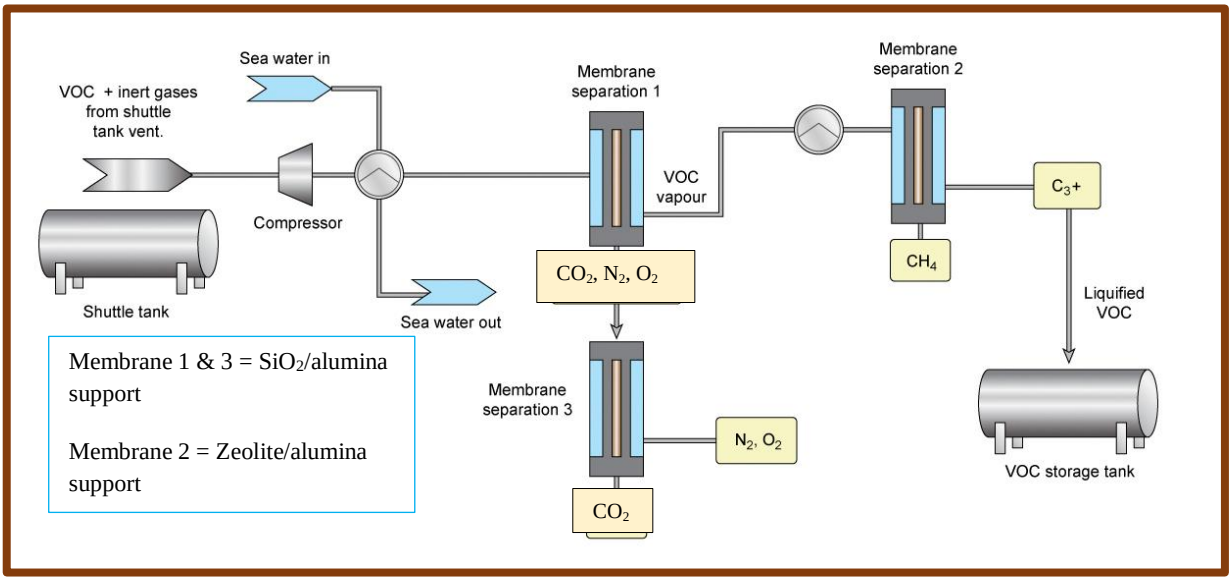

Figure 1-2: Process of hydrocarbon recovery using membrane technology.

Different countries in the world have regulations in place that tightly regulate these emissions. The ambient air quality standard as suggested EPA should have no more than a concentration of hydrocarbon content of 1.6 x 10^{-4} kg m^{-3} (0.24 ppm) (13). There is a standard concentration of thirty-five gram of total organic compounds (TOC) per cubic meter of gasoline loaded that was set in Europe (13). In 1999, the EU adopted the Gothenburg Protocol to abate acidification, eutrophication and ground level ozone. Moreover, it set emission levels for sulfur, nitrous oxide, VOCs and ammonia. It is expected that European VOC emission will be down by 40% as compared to 1990 when the protocol is fully implemented (14). In various nations, the regulation of VOC and NMVOC discharge are not regulated. As such, they result in acute pollution of the environment and financial deficit. Due to the high flammability of VOCs, their emissions can present a safety hazard during loading and unloading operations. Different steps have been taken to lower the number of VOCs emitted from operations at oil terminals.

1.4 Volatile Organic Compounds (VOCs) from Shuttle Tankers

VOCs are a large group of organic compounds that evaporate easily into the atmosphere. VOCs include lower hydrocarbons, like CH_4, C_2H_6, C_3H_8 and C_4H_{10} (15).

The main component of VOCs is CH_4, and it has a GWP of 21, while CO_2 has GWP of one. Therefore, the effect of one unit of methane discharged into the

atmosphere is equal to the effect of twenty-one units of carbon dioxide. C_3H_8 and C_4H_{10} are also known as NMVOC can chemically react with oxides of nitrogen to form harmful ground level ozone (16).

Figure 1-3 shows a schematic diagram of emissions from a shuttle tanker during crude oil loading. The storage, production and transportation of crude oil and gasoline lead to VOC emissions. From these operations, two main processes have been identified as the main sources of emissions. These are from storage tanks and from transport of crude oil during loading and offloading operations (15). As indicated in Figure 1-3, vent stream is considered as a major source of emissions from shuttle tankers.

Several measures have been put in place for the control of VOCs emitted from shuttle tankers. However, the main problem in the recovery of VOCs from tankers is that the evaporated hydrocarbons are diluted in vast amounts of inert gases when the gas mixture is displaced by the inflow of oil during loading of the cargo tanks (17).

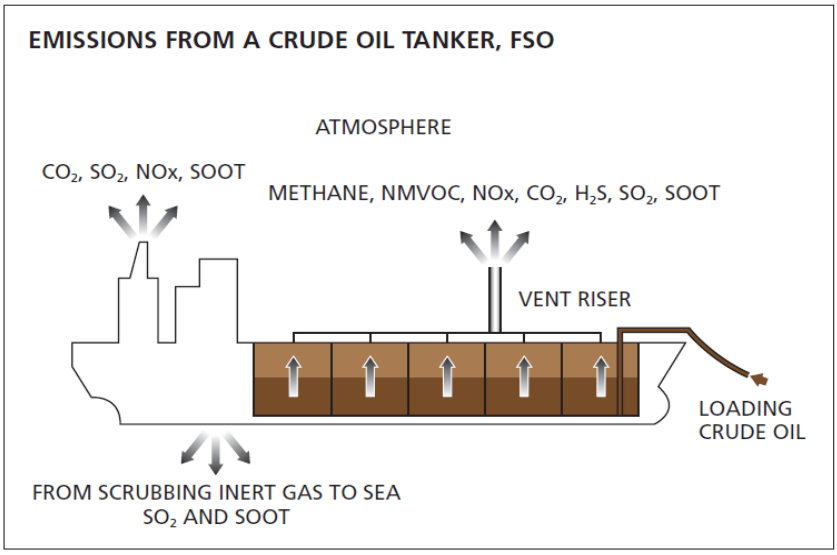

Figure 1-3: Schematic diagram of the emissions from a shuttle tanker (adapted from harmworthy)

1.5 Major Causes of VOC Emission from Shuttle Tankers

Several factors affect the emission of VOCs from FPSOs, FSOs and crude oil

transportation tankers. These factors are outlined as follows:

1.5.1 *Inert Gas (IG)*

In the process of off-loading crude oil at terminals, shuttle tanks are initially loaded with a layer of inert gases having a standard composition of 4% oxygen, 84% nitrogen and 12% carbon dioxide. These levels are used to keep the O_2 concentration low so as to lower the risk of an explosion. The equilibrium mechanism is altered by the inert gas, which prompts the emissions of hydrocarbon vapours from the crude oil and is dependent on the oil vapour pressure. Hence, the shuttle tank will have a layer of gases comprising of a mixture of inert gases and about twenty five percent hydrocarbon gases which will be emitted during the next loading operation (18).

1.5.2 *Light end Hydrocarbons*

The concentration and composition of light end hydrocarbons affect the rate at which they are emitted. A high concentration leads to an increased vaporisation rate and hence more hydrocarbons are emitted to the tank's atmosphere (18). Crude oil that exhibit high concentrations of methane and ethane tend to have hydrocarbon vapour lighter than IG and the two phases rapidly mix due to convection. This results in a more uniform IG/hydrocarbon composition in the tank. As such, vaporisation of the hydrocarbon gas from the loaded crude will occur. This will be displaced at the start of the loading operation (18).

1.5.3 *Loading Time*

The emission of hydrocarbon gases from a cargo tank is a non-equilibrium process. Therefore, emission increases with increased loading time. The longer the loading operation, the higher the percentage of hydrocarbon gases that is emitted. Figure 1-4 shows the increase in % hydrocarbon gases emitted from crude oil obtained from two different fields over time.

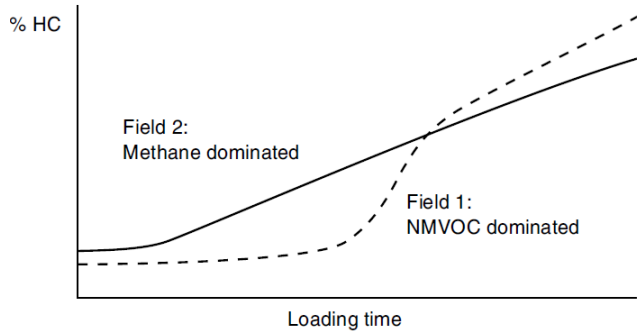

Figure 1-4: Hydrocarbon gas emission during loading operation adapted from (18).

1.5.4 *Effects of Weather*

Movements due to weather tend to increase circulation in the cargo tank between the crude oil and the atmosphere. This leads to greater mixing of hydrocarbon vapours and IG, which in turn increases the hydrocarbon vaporisation rate. This is more prevalent when the shuttle is short loaded, and the rolls or pitch could cause more splashing (18).

1.6 Methods for the Reduction of VOCs Emitted from Crude Oil Tankers

Procedures have been put in place, dating as far back as 1984, for the reduction of VOCs emitted during loading and unloading operations. Several different VOC emission reduction processes from shuttle tankers include adsorption, cryogenic condensation, sequential transfer and membrane separation (3).

1.6.1 *Condensation Process*

The use of condensation is commonly applied in the industrial separation of gases. This is based on the respective saturation temperatures of the gases. However, in some cases the components of the gas mixture contain non-condensing species like air and nitrogen (19). Hydrocarbon gases condense more easily than inert gases when the feed gases from cargo tanks are compressed and cooled. In this process inert gases and methane are generally not condensed but are vented into the atmosphere. Moreover, the condensed gases generally consist of propane and butane. These are usually collected in a pressurised deck storage tank (18). A

study investigating compression-assisted condensation has proved that these systems are effective, however, they operate at high cost (11). In addition, this process allows for the emission of methane. However, reduction of VOC emissions to permitted levels cannot be achieved by condensation alone, and a significant amount of nitrogen for safety reasons (to inert the condensable flammable gases) is required for this process (20).

1.6.2 *Adsorption*

Several adsorption techniques have been used to reduce VOC emissions from shuttle tanks during loading and unloading operations. These include,

- Adsorption using activated carbon (18-20).
- The use of Y-type zeolites for adsorption of VOCs. Zeolites have a crystalline structure and fixed pores. Hence, they adsorb selectively and act as a molecular sieve (21).

Adsorbers have been used to control the emission of VOC. The control of VOC emissions typically reduces the concentrations from between 400 and 2,000 parts per million (ppm) to under 50 ppm. Adsorption technology can now extend the range of VOC concentration from 20 ppm to one-fourth of the Lower Explosive Limit (19, 20). At the lower end of this range, such small concentrations may be difficult or uneconomical to control by another technology or even by all adsorbents. Incinerators, membrane separators, and condensers may be economically feasible when used in place of adsorbers at the upper end of the range. This is because when using membrane technology, the recovered VOC can be easily utilised without the need for further processing.

1.6.3 *Membrane Technology*

The permeability of gases through a membrane is distinctive. As such, membrane technology can be used for the separation of hydrocarbons from inert gases, and different hydrocarbon gases emitted can also be separated (18).

Several different types of membranes have been investigated for the separation of VOCs from inert gases. Several polymeric membranes have been characterised and their permeation properties for vapour recovery and the separation of propylene and toluene (22-25). An important feature in the preparation of polymer

membranes for gas separation is the process of spinning them into hollow fibre membranes. Moreover, the large surface area of the membrane means they are suitable for large-scale industrial applications (26). A major drawback is that polymeric membranes cannot withstand high temperatures and harsh chemical conditions. In petrochemical plants, natural gas treatment plants and refineries, feed gas streams of heavy hydrocarbons can lead to problems as polymer membranes can become swollen or plasticised (27).

1.6.4 *Sequential Transfer*

In this system, additional pipelines are installed on the shuttle tank and used during loading and unloading. The shuttle tank is divided into sections and the loading and discharging is performed sequentially. The gas out-flow from the first loaded section is piped to the bottom of the next section to be loaded. This process is repeated sequentially for the remaining sections. A cargo tank is connected into a VOC plant and the IG content emitted is considerably lower in this system, which improves the operating conditions in the recovery plant (18). The emission of VOC will be reduced when using this method but will not be completely eliminated. The problem with this method is that there is no recovery of the emitted VOC.

1.7 Energy Sector – Natural Gas

The energy supply sector is the largest contributor to GHG emissions. In 2010, for example approximately 35% of total anthropogenic GHG emissions were attributed to this sector. Notwithstanding, the growth in annual GHG emissions from the global energy supply sector accelerated from 1.7% per year (1990 – 2000) to 3.1% (2000 – 2010). Fast economic growth is always associated with a higher demand for power, heat, and transport services.

Natural gas is primarily used as a fuel source and raw material in manufacturing. It is also used domestically in furnaces, water heaters and cooking stoves. Industrially it is used as fuel in brick, cement, ceramic tile kilns and as a source of sulfur and carbon black as well as a raw material in petrochemical manufacturing to produce hydrogen, ethylene, methanol and ammonia. The produced ammonia can be used for fertilisers or as a secondary feedstock for other chemicals like nitric acid and urea (28).

Natural gas composition varies extensively from one gas field to another. A field might have approximately 95% methane, with small quantities of other hydrocarbons, nitrogen, carbon dioxide, hydrogen sulfide and water vapour. Whereas another field may contain 10% of lower hydrocarbons like propane, butane or ethane as well as a high carbon dioxide content (29).

Table 1.2: General composition of wet and dry natural gas (adapted from reference 28).

Constituents	Composition (vol %)	
	Wet	Dry
Methane	84.6	96.0
Ethane	3-8	
Propane	5.3	0.60
n-butane	1.4	0.12
Pentane	≤ 1	
Carbon dioxide	≤ 5	
Helium	≤ 0.5	
Nitrogen	≤ 10	
Water	trace	

Table 1.2 lists some of the components that may be present in wet and dry natural gas. Oxygen is the only constituent that is not naturally occurring and is present in natural gas because of leaking pipes and is responsible for a significant amount of corrosion in the gas processing system (30). Natural gas is considered 'dry' when it is almost pure methane, having had most of the heavier constituents removed. It is considered wet when the heavier hydrocarbons are present.

The separation of natural gas components is vitally important from an economic point of view. Particularly as the hydrocarbons present in the mixture have more value when they are recovered as natural gas liquids (NGLs). This is because NGLs are used in the petrochemical industries as feedstock. Moreover, reducing the concentration of higher hydrocarbons and water in natural gas is important for preventing the formation of hydrocarbon liquids and hydrates in the pipeline. Furthermore, gases such as CO_2, N_2, and He need to be removed as they reduce the heating value of the gas. Although there is variation in composition from one source to another, the major component of natural gas is methane but, it could also contain other hydrocarbons, and unwanted impurities. Hence, all natural gas

must undergo some form of treatment, with about 20% requiring extensive treatment before being transported via pipelines. This step is essential in view of the regulations that closely monitor the composition of natural gas that is transported to the pipelines. Membrane technology can be used to upgrade raw natural gas to pipeline quality by removing water and higher hydrocarbons. These unwanted constituents can lower the dew point of natural gas from 293 to 303 K. At present, membrane technologies only constitute about 5% of the market for processing natural gas in the United States. This percentage is expected to rise as suitable membranes to lower the hydrocarbon dew points and have better carbon dioxide selectivity are developed (31, 32). High pressures in the range of 3,000 to 10,500 kPa are usually required for the transportation of natural gas to a gas processing plant and for removal of impurities using a membrane. To minimise the recompression cost, the membrane must remove impurities from the gas entering the permeate stream. Although several types of membranes can be used to achieve these separations, the challenge lies in developing a membrane with high methane separation efficiency.

1.7.1 *Natural Gas Sources*

Natural gas produced from geological formations have different types of compositions that can be broadly categorised into four distinct groups:

- Non-associated gas, which is produced from geological formations, does not contain a high proportion of higher hydrocarbons with higher boiling points. This gas is directly controllable by the producer. It flows up the well with its own energy through wellhead control valves and along the flow line to a treatment plant. Treatment requires that the temperature of the gas is reduced to a point dependent on the pressure of the pipeline. This is done so that all the liquid present at the pipeline temperature and pressure condenses and gets removed (28).
- Associated gas is formed during crude oil production. Crude oil cannot be formed without some associated gases, which emanate from the solution at reduced pressure. Properly designed crude oil well completions and good reservoir management are used to minimise the amount of associated gas produced. This is done to maintain maximum energy in the reservoir and improve crude oil recovery (28).

- Coal bed methane is the generic name given to methane that is produced or released when the water pressure within buried coal is reduced by pumping from the vertical or horizontal surface of the wells. It is mainly formed during the coalification process, whereby organic matter is slowly transformed into coal as the temperature and pressure of the organic matter rises over time. During this process; a range of chemical reactions take place that give rise to substantial amounts of produced gas. The gas then escapes in to the underlying rock and a large amount is retained within the forming coal seams. However, the formed methane is distinctly trapped, while conventional natural gas reservoirs are adsorbed on the coal grain surfaces and held in place by the reservoir water pressure (28). This type of natural gas requires little treatment, as it is primarily methane gas mixed with water but not mixed with heavier hydrocarbons .
- Biogas typically refers to methane produced by the breakdown of organic matter such as agricultural waste, manure, municipal waste, plant material, sewage, green waste or food waste in the absence of oxygen.

1.7.2 *Chemical and Physical Properties of Natural Gas*

Natural gas is colourless, odourless, tasteless, and lighter than air (Table 1.3). Following appropriate treatment for acid gas reduction, odourisation, and hydrocarbon and moisture dew point adjustment, natural gas is sold within prescribed limits of pressure, calorific value, and possibly Wobbe index (often referred to as the Wobbe number). The Wobbe index (calorific value divided by specific gravity) gives a measure of the heat input to an appliance through a given aperture, at a given gas pressure. Using the Wobbe index as a vertical coordinate and the flame speed factor as the horizontal coordinate, a combustion diagram can be constructed for an appliance, or a whole range of appliances, with the aid of appropriate test gases. Such a diagram would indicate areas within which variations in the Wobbe index and flame speed factor of gases may occur for a given range of appliances without resulting in incomplete combustion, flame lift, or the lighting back of pre-aerated flames. This method of prediction of combustion characteristics is not sufficiently accurate to eliminate entirely the need for practical testing of new gases.

Table 1.3: Properties of natural gas (adapted from reference 28).

Properties	Values
Relative molecular mass g/mol	17-20
Hydrogen content, mol %	Trace–0.1
Oxygen content, mol %	Trace–0.1
Hydrocarbon/carbon atomic ratio	3.0-4.0
Relative density, 15 °C	0.72-0.81
Methane concentration, mol %	93.9
Ethane concentration, mol %	4.2
Propane concentration, mol %	0.1-1.5
Iso- Butane concentration, mol %	0.01–0.3
Normal- Butane concentration, mol %	0.01–0.3
Nitrogen concentration, mol %	1.0
Carbon dioxide concentration, mol %	0.05 – 1.0
Sulphur concentration (including H_2S), mgm^{-3}	≤ 50
Specific CO_2 formation, g/MJ	38-50
Boiling point °C	-162

1.7.3 *Natural Gas Treatment*

1.7.3.1 Dehydration of Natural Gas

For the elimination of water vapour from natural gas, the current technology used is glycol absorption (33). Water is an easily condensable compound, thus there are many membranes with high water permeability as well as high water/methane selectivity. The use of glycol absorption is quite prominent, and it has a low

operational cost and little fouling problems. Even though this process is widely accepted in industry, it has some challenges. The operational problems include contamination of the glycol solution, decomposition of the glycol, foaming that leads to carry-over of the glycol solution and low temperature operations leading to increased glycol viscosity. The use of membrane technology may be an alternative to the conventional glycol dehydration process as it does not use any solvent and has no moving parts. To be competitive the rate of loss of methane with the permeate water must be reduced (34).

1.7.4 *Removal of Trace Components*

1.7.4.1 Nitrogen

The specification of inert gases in the natural gas pipelines is less than 4%. Gas reserves that contain higher content are of low quality, although gas containing about 10% inert gases can be blended with low nitrogen content gas to achieve pipeline quality gas (34). The economic importance of the content of nitrogen in natural gas is high. In the United States, the value of shut-in gas containing 10 – 15% nitrogen is about $30 billion (35), consequently numerous processes have been evaluated for the removal of nitrogen. The current technology used on the large-scale is cryogenic plants. Cryogenic removal of nitrogen is a complex and expensive process. Gas containing 8 to 12 % N_2 can be compressed and passed through a silica/alumina membrane. The permeate will be expected to contain less than 6 % N_2 which can be sent to the pipelines. The N_2 rich residue gas can be collected for further use. This will offer an easy, low cost installation system. Moreover, a membrane unit requires low maintenance and being modular can easily be moved from one location to another. The challenge is to develop membranes with high methane/nitrogen separation efficiency (34).

1.7.4.2 Helium

Helium is a valuable product from natural gas processing. Unlike other trace components, a high concentration of helium is desirable as that is one of the major commercial sources of helium (36). Recovery of helium from a natural gas stream can be carried out using a cryogenic process, pressure swing adsorption, membranes or non-cryogenic adsorption. Membranes can offer a simpler unit for helium separation as most membranes have a high permeability for helium with a

high selectivity against methane and other natural gas constituents, hence the use of a membrane unit will be competitive for helium removal.

1.7.4.3 Oxygen

Oxygen is the only natural gas constituent that is not naturally occurring but originates from leaking valves and piping systems that operate at atmospheric pressures. The presence of oxygen in the gas processing system is responsible for significant amounts of corrosion (36). Oxygen can be removed using non-regenerative scavengers if it is present at low concentrations. At higher concentrations, it can be removed from the gas via a catalytic reaction to produce water. The water is then eliminated in the dehydration process (36).

1.7.5 *Carbon Dioxide Removal*

A typical plant for the removal of carbon dioxide from natural gas uses absorption technology. This consists of two towers. The first tower contains the feed gas, at high pressure, and an absorbent liquid that flow counter current to the feed gas. Absorbent liquid that contains absorbed carbon dioxide and heavy hydrocarbons is removed from the bottom of the tower (32). Membrane technology is competitive against absorption for the removal of carbon dioxide from natural gas (37), as the high-pressure absorber tower is an expensive, large thick walled heavy vessel. Moreover, the mass of the components absorbed is relative to the size of the tower. In addition, the absorbance units are difficult to maintain, and corrosion is a significant problem (32). Membrane technology could offer a more competitive choice for the removal of carbon dioxide from natural gas. However, the challenge is to synthesise a membrane that has a CO_2/CH_4 selectivity of 20 or greater (37).

1.8 Membrane Technology

Membranes can be defined as selective barriers between two components through which differential transport can occur (38). They can separate one or more gases from a feed mixture and can generate a specific gas rich permeate. Gas separation membranes are used for numerous applications. Table 1.4 shows the various applications of gas separation membranes.

Table 1.4: Applications of gas separation membranes (38).

Common gas separation	Applications
O_2/N_2	Oxygen enrichment and inert gas generation
H_2/Hydrocarbons	Refinery hydrogen recovery
H_2/N_2	Ammonia purge gas
H_2/CO	Syngas ratio adjustment
CO_2/Hydrocarbons	Acid gas treatment and landfill gas upgrading
H_2S/Hydrocarbons	Sour gas treatment
H_2O/Hydrocarbons	Dehydration of hydrocarbons
He/Hydrocarbons	Helium separation
He/N_2	Helium recovery
Hydrocarbons/Air	Pollution control and recovery of hydrocarbons
H_2O/Air	Air humidification

Membranes used for gas separations can be generally classified into organic polymeric membranes and inorganic membranes. The organic polymeric membranes that are used for gas separations are hollow, asymmetric and nonporous. They have large surface areas making them suitable for large-scale industrial applications (26). However, they have poor heat and chemical resistance. Alternatively, inorganic membranes can withstand high temperatures and harsh chemical conditions. The major drawback for inorganic membranes is their high cost, brittleness, low membrane area and low permeability in the case of highly selective dense membranes (27). Inorganic membranes based on alumina, zeolites, carbon and silica have been used for the capture of CO_2 at

elevated temperatures (39). For the separation of hydrocarbons, zeolite membranes have been shown to exhibit interesting separation characteristics. However, their separation efficiency is dependent on the operating conditions including temperature, gas composition and total pressure (40). A membrane's performance is determined by its permeability – the flux of a specific gas through the membrane – and its selectivity – the preference of the membrane to allow one gas to permeate and not another (41-43). An important aspect in the use of catalytic membrane reactor (CMR) technology includes the membrane architecture, membrane reaction design and the reactor sealing (44).

1.8.1 *Membranes for Natural Gas Applications*

The use of membranes for natural gas separation has been limited to carbon dioxide removal (28). Current membranes used for natural gas separation applications are produced as hollow fibres, flat sheets or spiral-wound modules. Hollow-fibre modules allow large areas of membrane to be packaged into compact membrane modules. This has proved advantageous in the choice of membranes for the removal of oxygen from air to leave a nitrogen rich retentate, which was an early large-scale membrane gas separation process. Nitrogen production from air uses relatively low permeability membrane materials to process clean air at low pressures, generally < 1000 kPa . Essentially all membrane nitrogen-from-air separation systems use hollow-fibre modules (32).

In contrast, as indicated earlier, natural gas streams contain multiple components, some of which are water, carbon dioxide, higher hydrocarbons and aromatic compounds. Some of these compounds can degrade and plasticise the membrane. Natural gas streams may also contain entrained oil mist, fine particles, and hydrocarbon vapours that can easily collect on the surface membrane, resulting in fouling of the membrane. In addition, the gas is typically treated at relatively high pressures of 3000-6000 kPa. Under these conditions, the high permeances of flat sheet membranes formed as spiral-wound modules can compensate for their higher cost as compared to hollow-fibre modules. At present several companies produce both types of membrane modules and no clear winner has emerged.

One trend that has emerged in commercial gas separation membranes is a move

to composite membranes. Base anisotropic membranes are used as a highly porous support to provide the mechanical strength required, and a thin layer of permselective material that has a thickness of about 0.2-1.0 *μm* is deposited on the support to perform gas separation functions. Hollow-fibre membranes and flat sheet membranes can be made in this composite membrane form. Composite inorganic membranes offer key advantages over polymeric membrane as they provide more mechanical strength and are relatively resistant to fouling due to their high resistance to chemical degradation. In addition, the layer that performs the separation can be synthesised from the same or different material used for the support. This makes the number of materials that can be used to make the membrane almost limitless. However, the downside of this membrane is that separation properties are often compromised in order to make membranes with sufficient mechanical strength. The addition of a polymeric layer to make a mixed matrix membrane has shown promise in tackling the problem of mechanical strength and separation efficiencies. Composite membranes consist of a microporous support layer coated with one or more thin layers. Moreover, each can be optimised separately as the separation and the mechanical support function are disconnected.

1.8.2 *Membrane Transport Mechanism*

In order to understand the fundamentals of membrane gas separation, a brief introduction to some laws and processes commonly employed is required.

1.8.2.1 Graham's law (Thomas Graham in 1848)

Graham's law which is also refered to as Knudsen diffusion states that the rate of diffusion of a gas is inversely proportional to the square root of its molecular weight. This can be written as,

$$\frac{Rate_a}{Rate_b} = ({}^{M_b}/_{M_a})^{1/2} \qquad \textit{Equation 2}$$

where $Rate_a$ is the rate of diffusion of the first gas (volume or number of moles per unit time), $Rate_b$ is the rate of diffusion for the second gas, and M_a and M_b are the molar masses of gases a and b in g mol^{-1}.

1.8.2.2 Fick's first law:

Fick's first law depicts the flux to the concentration of the specie under the assumption that the flow is at steady state. It postulates that the flux goes from regions of high concentration to regions of low concentration. The law fundamentally describes diffusion of species and was enunciated by Adolph E. Fick in 1855, who noted a similarity between diffusion of solutes and Fourier's law describing the flow of heat in solids. Fick's law was theoretically deduced in 1860 by James C. Maxwell from the kinetic theory of gases.

The separation of gases in membranes is possible due to the difference in the movement of the different species through the membrane. For membranes having large pore sizes of 0.1 to 10 μm, the gases permeate via convective flow and there is no separation of the gases observed. For mesoporous membranes, separation is based on the collision amongst the molecule and hence molecular diffusion is dominant and the mean free path (which is the average distance travelled by a gas molecule between collisions with another gas molecule) of the gas molecules is greater than the pore size. The diffusion here is governed by Knudsen mechanism and it follows from the kinetic theory of gases that the rate of transport of any gas is inversely proportional to the square root of its molecular weight, which coincides with Graham's law of diffusion (45). However, for a microporous membrane with pore size less than 2 nm, separation of gases is based mostly on molecular sieving. The transport mechanism in these type of membranes is often rather complex and involves diffusion that occurs when the permeating species exhibit a strong affinity for the membrane surface, thus adsorbing on the walls of the pores (45).

The permeation of gases through a membrane is dependent on both the diffusion and the concentration gradient of the species along the membrane. The selective transport of a gas molecule through a membrane is often associated with the pressure, temperature and concentration gradient. The permeability and selectivity are some of the parameters that are used to determine the performance of a membrane. The permeance, P (mol m^{-2} s^{-1} Pa^{-1}), represents the proportionality coefficient with a flux at steady state for a gas passing through a membrane and is defined by equation 3:

$$P = \frac{Q}{A.\Delta p} \qquad \textit{Equation 3}$$

Where Q is the gas molar gas flow through the membrane (mol s^{-1}), A is the membrane surface area (m) and Δp is the pressure difference across the membrane (Pa). The permeance is a measure of the quantity of a component that permeates through the membrane (46).

The ideal gas selectivity $\alpha_{i,j}$, is the ratio of the permeability coefficients of two different gases as they permeate independently through the membrane is given by equation 4:

$$\alpha_{ij} = \frac{P_i}{P_j} \qquad \textit{Equation 4}$$

Where P_i and P_j are the permeance of the single gases through the membrane respectively. The selectivity is the measure of the ability of a membrane to separate two gases and is used to determine the purity of the permeate gas, as well as determine the quantity of product that is lost. The permeability coefficient is related to the diffusivity coefficient, D (m^2s^{-1}), and the solubility coefficient, S (mol m^3 Pa), for a component, i, (45) and is given by:

$$P_i = D_i.S_i \qquad \textit{Equation 5}$$

Combining equation 4 and 5, the selectivity of a membrane can be expressed as:

$$\alpha_{ij} = \frac{D_i}{D_j}\frac{S_i}{S_j} \qquad \textit{Equation 6}$$

For a binary mixture of gases with components i and j, the separation factor SF is given by:

$$SF_{ij} = \frac{(Y_i/Y_j)}{(X_i/X_j)} \qquad \textit{Equation 7}$$

Where Y and X are the percentage concentrations in the permeate and feed end of the membrane respectively. During experiments, the concentration of the gases (X_i and X_j) are fixed while at the permeate side Y_i and Y_j are determined using gas chromatography (GC) in this work.

1.8.2.3 Knudsen diffusion

Knudsen diffusion arises from differences in the molecular weights of components to be separated. This proceeds at a speed that is inversely proportional to the square root of the molecular weight of the component. Separation by Knudsen diffusion requires that the pore diameter of the membrane to be smaller than the

mean free path of the components. Generally, diffusion of gases through porous membranes is dependent on the type of collisions that occur. At low concentrations, where there is predominantly molecule-pore wall collisions then the flow is Knudsen flow. Knudsen flow can be achieved with membranes whose pore size is greater than 4 nm. However, for it to dominate the pore size should be less than 50 nm (30). In addition, the separation factor for a mixture of binary gases can be estimated from the square root of the ratio of the molecular weights of the gases. This is because gas permeation by Knudsen diffusion varies inversely with the square root of the molecular weights of the gases. Hence an ideal Knudsen separation for a mixture of binary gases is equal to the inverse of the square root of their molecular mass ratio (47). The transportation equation for Knudsen and viscous flow is given by equation 8:

$$J = A\bar{P} + B \qquad \textit{Equation 8}$$

Where $\bar{P}$ is the average pressure across a porous membrane, and A and B are constants relative to the membrane structure, molecular weight and size. According to equation 8, A is the constant representing Knudsen flow while B is the constant representing viscous flow.

Moreover, the pore radius (r_p) of the membrane can be determined using the formula (48):

$$r_p = \frac{16.A.\mu}{3.B}\sqrt{\frac{8RT}{\pi M}} \qquad \textit{Equation 9}$$

Where R is the molar gas constant (J Kg^{-1} mol^{-1}), T is the temperature (K) and M is the molar mass of the gas (g mol^{-1}).

The Knudsen number *K* is given by:

$$K = \frac{2r_p}{\lambda} \qquad \textit{Equation 10}$$

Where r_p is the pore radius (m) and λ is the mean free path (m) of the molecules. This determines the flow regime of the membrane and when the diameter of the pores is lower than the mean free path of the molecules then Knudsen flow is dominant (48).

For cylindrical membranes, the gas flow in membranes governed by Knudsen flow is given by equation 11 (49):

$$J = \frac{4r_p\varepsilon}{3}.\sqrt{\left(\frac{2RT}{\pi M}\right)}.\frac{p_o - p_l}{lRT}. \qquad \textit{Equation 11}$$

Where ε is the porosity of the membrane, M is the molecular weight of the gas, J is the flux, r_p is the pore radius, l is the pore length, p_o and p_l are the absolute pressures of the gas species at the beginning of the pore and at length l.

The above equations are for single gas permeation. In the case of gas mixtures, other factors must be taken into consideration when determining the separation of the gases. The gases in the mixture will have different molecular masses as well as move at different speeds. For separation by Knudsen diffusion for a binary mixture of gases having molecular masses M_1 and M_2, the ratio of their flux J_1 and J_2 is given by (50):

$$\frac{J_1}{J_2} = \sqrt{\frac{M_1}{M_2}} \qquad \textit{Equation 12}$$

To predict the selectivity of a gas over another gas in the case of binary mixtures of gases, the Knudsen selectivity (α_k) is calculated as:

$$\alpha_k = \frac{1}{\sqrt{\frac{M_1}{M_2}}} \qquad \textit{Equation 13}$$

For membrane separations, this indicates a limitation of the Knudsen flow mechanism (50). For the separations of CO_2 and H_2, the ratio of the square root of the molecular weight of CO_2 over that of H_2 is 4.69, which means that in practice separation must take place in multiple stages (50). For the separation of CO_2 from natural gas the ratios of the square root of the molecular weight of CO_2 over that of CH_4 is 1.66. Therefore, it is very difficult to achieve economic separation of CO_2 from methane using Knudsen separation alone.

1.8.2.4 Poiseuille flow

This is also known as viscous flow. At high concentrations, where collisions are predominantly molecule–molecule then viscous flow dominates. Thus, when the pore radius r_p is greater than the mean free path λ, the mechanism governing the transport of gases across a membrane is Poiseuille flow and the rate of a gas transport through the membrane is given by the Hagen-Poiseuille equation:

$$J = \frac{{r_p}^2\varepsilon}{8\,\eta} * \frac{[p_o - p_l][p_o + p_l]}{lRT} \qquad \textit{Equation 14}$$

Where r_p is the pore radius of the membrane, ε is the membrane porosity, p_o is the

gas inlet pressure, p_l is the permeate gas pressure, R is the molar gas constant, l is the effective length of the membrane, η is the gas viscosity and T is the temperature. The assumption made by Hagen-Poiseuille is that the pores of the membranes are cylindrical. This is not normally the case and is a limiting factor of this equation (51).

1.8.2.5 Slip flow

When the pore radius and the mean free path are approximately equal, slip flow occurs. Slip flow is in the intermediate range between Knudsen and Poiseuille flow (50). The flow rate is given by the equation:

$$J = \frac{r_p}{M\bar{v}l}\frac{(p_o - p_l)}{2} \qquad \textit{Equation 15}$$

Where $\bar{v}$ is the mean velocity of the gas.

1.8.2.6 Molecular sieving

The molecular sieving effect in gas separations occurs when the pores of a membrane decrease to the 5 to 10 $\times$ 10^{-10} m range. If the gases to be separated have different kinetic diameters then the smaller molecules will permeate through the membrane while the larger molecules will be retained. Very high separation can be achieved using this effect (47). The kinetic diameter of a gas is defined as the intermolecular distance of closest approach for two molecules colliding with zero initial kinetic energy. This is dependent on the molecular shape, size and dipole-dipole interactions (52). Table 1.5 lists the kinetic diameters and molecular weights of several molecules found in natural gas or shuttle tanker exhaust off-gases.

Research in the production of membranes exhibiting these properties has accelerated. Zeolites and ceramic membranes can be modified to achieve these properties. None of the membranes that have exhibited these properties are known to be commercially available. However, there have been reports indicating the separation of gases that differ in size by just 0.1$\times$ 10^{-10} m (30).

Table 1.5*: Kinetic diameter and molecular mass of various molecules found in off-gases (52).*

Gas	Kinetic Diameter ($\times\ 10^{-10}\ m$)	Molecular weight ($g\ mol^{-1}$)
CO_2	3.30	44.01
CH_4	3.80	16.04
N_2	3.64	28.01
CO	3.76	28.01
Ar	3.40	39.95
O_2	3.46	32.00
SO_2	3.60	64.07
NO_2	3.30	46.01
He	2.60	4.00
H_2	2.89	2.02

1.8.2.7 Surface diffusion

Surface diffusion and adsorption is a further mechanism that governs the permeation of gases through membranes that have small pore sizes. When the pore diameter of a membrane is in the range of 50 to 100 Å then adsorption on the walls of the membrane is observed depending on the nature of the gas and the support. It is often noted that the amount of gas that is adsorbed on the membrane pore walls is greater than the amount of gas that is not adsorbed. The adsorbed gas molecules then move by surface diffusion through the membrane with the flow rate obeying Fick's law (30). The contribution to permeation by surface diffusion j_s is given by:

$$j_s = -D_s \frac{dc_s}{r_p} \qquad \textit{Equation 16}$$

Where dc_s is the diffusion rate of the component, D_s is a surface diffusion coefficient and r_p is the pore size.

1.8.2.8 Capillary condensation

Capillary condensation occurs when a porous membrane is in contact with a vapour and the saturation vapour pressure in the pores is different from the saturation vapour pressure of the components (53). In addition, capillary condensation can occur with increasing gas pressures at temperatures below the critical temperature

(54). Therefore, condensed gas molecules are transported across the membrane pores. Capillary condensation pressure in a cylindrical pore is given by the kelvin equation (54):

$$\frac{RT}{V_m} ln \frac{p_t}{p_o} = -2 \frac{\alpha cos\phi}{r} \qquad \textit{Equation 17}$$

Where p_o is the saturated vapour pressure, α is the interfacial tension, r is the pore radius of the capillary membrane, V_m is the liquid molar volume and ϕ is the contact angle of the molecule and the membrane. For a capillary modified with a condensate, the effective capillary pressure (p_ε) can be given as:

$$p_\varepsilon = -2\alpha(r - t_o)^2 \, cos \frac{\phi}{r^2} \qquad \textit{Equation 18}$$

Where t_o is the thickness of the condensate. Using Darcy's law (that describes the flow of liquid through a porous media) and combing equations 17 and 18, the gas flux, J_c, of a capillary can be written as (55):

$$J_c = \frac{\varphi RT}{\mu V_m L} [\frac{(r-t_1)^2}{r^2} ln \frac{p_1}{p_0} - \frac{(r-t_2)^2}{r^2} ln \frac{p_2}{p_0}] \qquad \textit{Equation 19}$$

Where φ is a constant related to the structure of the membrane pores and μ is the gas viscosity. For transport measurements, the molecular fluxes of the gases need to be determined from the uneven concentration profile, which can be used to determine the diffusion coefficient (54).

1.8.3 *Membrane Architecture in Chemical Reactions*

Architecture is vital in determining the performance of a membrane. The architecture can be studied from:

i. A symmetrical angle that is self-supported (symmetrical) or supported (asymmetrical) membranes.
ii. A configurational angle that is planar or tubular membranes.

The tubular membrane design exhibits several advantages over the planar design, including a higher surface area/volume ratio. Consequently, it is more widely used by researchers (56-61). Yin *et al.* (62) previously prepared a three-layered, asymmetric tubular membrane comprising of a porous cathode layer, a dense composite membrane layer and a porous composite anode layer that also acts as a catalyst. The cathode layer had a thickness of about 10 μm and the catalytic

anode layer where the partial oxidation of methane occurred serves as the support for the reactor. While the authors reported almost 100 % CH_4 conversion with high selectivity for CO and H_2, the oxygen permeation flux of the YSZ-Ag composite membrane was shown to be limited.

For successful preparation of a supported inorganic membrane, three key issues need addressing (56):

i. The thermal and chemical performance of the membrane layer and the support should match.
ii. There should be proper interfacial bonding of the membrane layer and the support
iii. The layer should be defect free.

1.8.4 *Membrane Function*

The basic function of a membrane in a membrane reactor can be divided into the several categories, which are discussed in this section.

1.8.4.1 Preferential Removal of a Specie

For a separation membrane, the preferential removal of one species over another is made possible by differences in the rate of movement (flux) of the individual species through the membrane. In this research, the permeate end was maintained at atmospheric pressure throughout the gas permeation process and the flux of the gas was then calculated using equation 20:

$$J = \frac{Q}{A} \qquad \textit{Equation 20}$$

Where J is the flux in mol s^{-1} m^{-2}, Q is the molar flowrate in mol s^{-1} and A is the effective membrane area in m^2.

The selectivity of the membrane for gas A over B ($\alpha_{A/B}$), which provides a measure of the ability of the membrane to preferentially permeate specie A compared to B has been calculated from pure gas permeation tests as given by equation 21:

$$\alpha_{\frac{A}{B}} = \frac{J_A}{J_B} \qquad \textit{Equation 21}$$

Where J_A and J_B are the flux of gases A and B respectively measured at STP.

The incorporation of a catalyst in the membrane reactor can result in the preferential removal of one species by shifting the equilibrium of the chemical

reaction. This generally leads to higher conversion via selective permeation of one of the reaction products. The general reaction for preferential removal of one species is shown in Figure 1-5.

A and B are reactants, while C and D are the products. The removal of product C through the membrane produces an equilibrium shift effect towards more production of C. Balachandran *et al.* (70) and Evdou *et al.* (71) have previously reported hydrogen production reactions where membrane was used to selectively remove the product hydrogen and hence, resulting in an increased product yield.

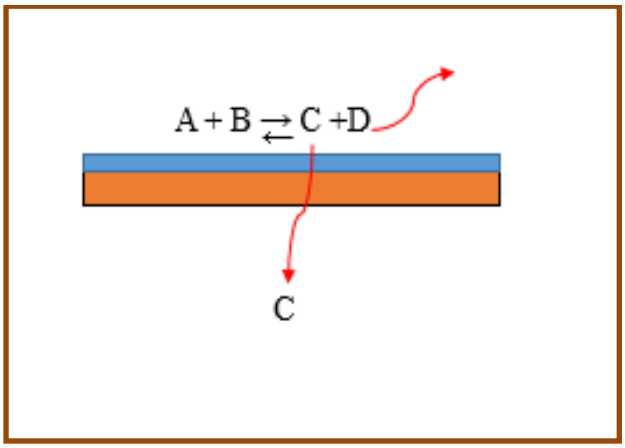

Figure 1-5: Preferential removal of a species in a membrane.

1.8.4.2 Distribution of Reactant

The membrane can also be configured to serve as a distributor for one of the reactants (72). A general reaction path is shown in Figure 1-6. Y and X are the reactants, Z is the desired product and T, U, V and X are fed into the feed end of the membrane. X is distributed to react with Y at the permeate. This type of membrane can be suitable for consecutive and parallel reactions like partial oxidation (73, 74), oxidative coupling (75, 76) and oxidative dehydrogenation of hydrocarbons (75, 77, 78).

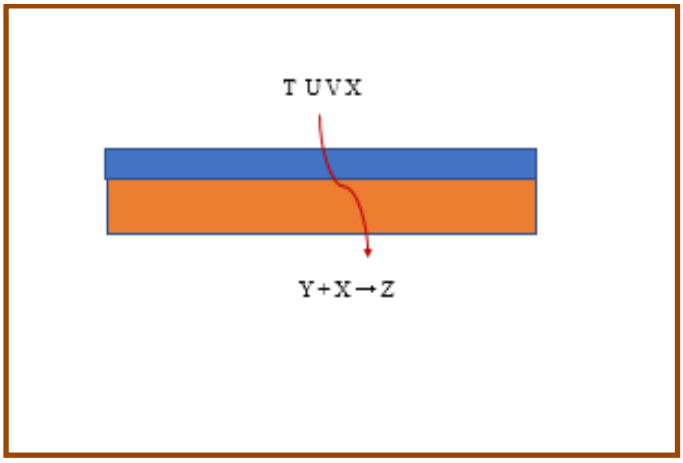

Figure 1-6: Distribution of reactants with a membrane

1.8.4.3 Coupling of Multiple Reactions

An interesting concept regarding the membrane reactor is that it can couple the above functions on both sides of the membrane.

1.9 Advantages of Membrane Process

There are several advantages of using membranes for industrial processes. In 2002, an *ad hoc* committee at the International Conference on Membranes and Membrane Processes (ICOM 2002) prepared a report on membrane technology perspectives and needs. The following advantages of membrane processes were listed.

1. It does not involve any phase changes or chemical additives.
2. It is simple in concept and easy to operate.
3. Scale up is relatively easy.
5. Greater efficiency for raw material use and potential for recycling of by-products.
6. The size of equipment used for operation is decreased and it is possible to intensify processes.

In addition, a further advantage for membrane devices for industrial processes is that they usually operate under continuous steady-state conditions. Baldus and

Tillmman (79) have stated that the simple rules for gas separation by membranes is said to be favourable under the following conditions,

1. When moderate purity recovery is sufficient.
2. When the components to be separated are in a considerable amount.
3. When the feed gas is available at the necessary pressure, or when the residue stream is needed at high pressure.
4. When the feed gas contains no substances harmful to the membrane.
5. When a membrane with sufficient selectivity is available.

The choice of membrane material for gas separation applications is based on specific physical and chemical properties. Therefore, a material should be tailored in an advanced way to separate gas mixtures. Membrane material should be robust, *i.e.* it should be long lasting and should be stable towards gas separation processes. The properties of a gas separation membrane depend on the following factors.

1. Permeability of the membrane, which is measured in terms of separation factors.
2. Membrane structure and thickness.
3. Membrane configuration.
4. Module and system design.

However, there are several practical problems or weaknesses with membranes. Membrane performance generally decreases with time. This decrease can be caused by concentration polarisation and fouling. Concentration polarisation occurs when there is limited permeation of certain species. The concentration of these species builds up over time on the membrane surface thereby, reducing transport across the membrane. The magnitude of this effect depends on the type of species used and the flow setup. However, concentration polarisation is not a very severe problem for gas separation membranes, compared to fouling. Fouling of the membrane occurs when the adsorbed species are on the membrane surface as well as inside the pores and thus limit or block the permeation of the gas species. Notable fouling species of gas separation membranes are sulphur-containing

compounds such as H_2S and SO_2. To reduce or eliminate the effects of fouling, membranes can be cleaned using heating, and purging with non-adsorbing gases. Small particles can best be removed from the feed flow using a filter. Membrane deterioration may also be caused by compaction, *i.e.* a reduction in pore size due to pressurisation. This phenomenon occurs with polymeric membranes and is usually irreversible. Most often the pore size does not return to its original value when the pressure is decreased.

Other practical considerations can come into play when making choices to obtain optimal membrane system design. One of these is the effect of the thermal stresses on structural integrity. If temperature variation occurs, several parts of the system may experience different degrees of expansion. If there is no room to accommodate these differences in expansion, the system can be seriously damaged. In addition, a pressure drop over a membrane unit is directly proportional to the module length. It would be advantageous to apply shorter modules to reduce the pressure drop. However, shorter modules require more seals. An additional issue to consider is the ease by which the unit can start up and shut down. A system design needs to accommodate these effects before it can be used for gas separation and a scale up module can be considered.

1.10 Off-gas Utilisation by CH_4 Reforming Reaction with CO_2

The most important GHG that arises from anthropogenic activities is CO_2. Its emissions have increased significantly in recent years. In order to minimise its impact on the environment, its capture and utilisation remain one of the most important processes in gas and petrochemical industries. Being able to store CO_2 can help to reduce the overall amount emitted to the atmosphere. However, long term storage could be hazardous due to potential risks. Therefore, the application of CO_2 as a raw material for various processes such as in the reforming of methane to generate products that can be used as feed stock in the chemical industry is a highly desirable process. Reforming reactions with CO_2 on a large scale to generate syngas can be used for several applications (Figure 1-7).

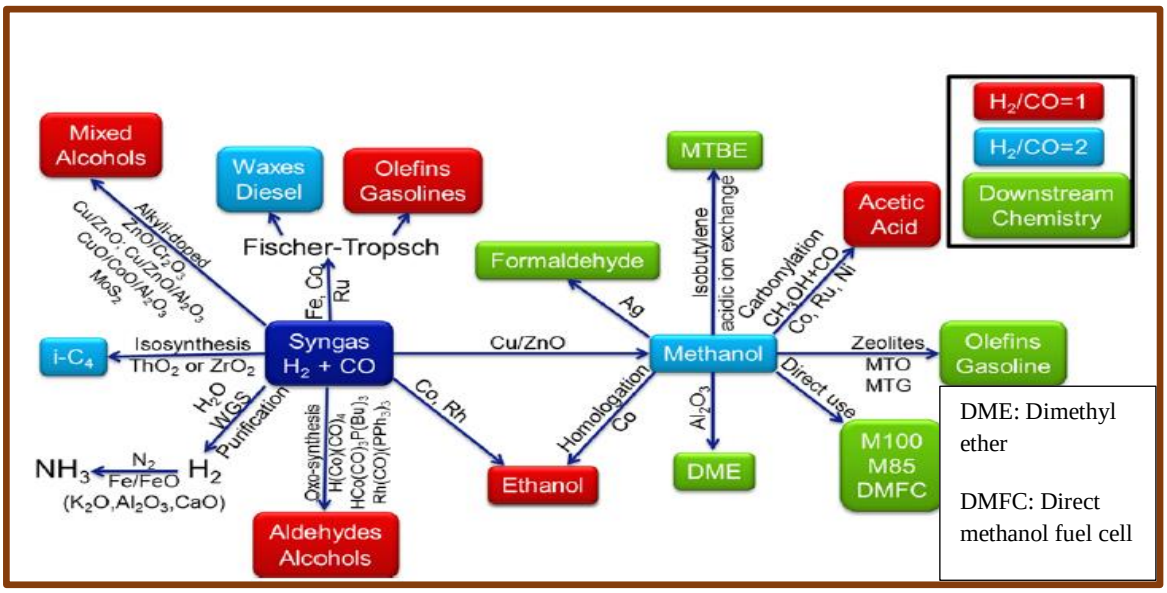

Figure 1-7: Use of syngas in the chemical industry (80).

Several studies have been carried out to investigate the reforming of methane with CO_2 at low pressures ($1 - 7 \times 10^5 Pa$) (81-85). However, there is a drawback due to upstream and downstream operations that affect the ratio of H_2/CO produced. This is an important aspect of syngas production, as its use for certain processes is more efficient when conducted with low H_2/CO ratios. Commercial methane reforming processes are conducted at high temperatures (773 – 1223 K) to enhance conversion rates (85) with either noble (86, 87) or transition metals as catalyst (88, 89). Noble metals are generally more expensive and have increased resistance to coking in comparison to transition metals. In a previous work, nickel was used as a substitute for the noble metals, but it is prone to coking as carbon can dissolve in the Ni layer (90). There are various reforming processes for the production of syngas from of CH_4. These include steam reforming, partial oxidation and dry reforming.

1.10.1 *Steam Reforming*

Steam methane reforming (SMR) is the reaction whereby methane and steam react in a reformer at temperatures ranging from 1073 – 1173 K and a pressure of $\approx 3 \times 10^6 Pa$ in the presence of a metal-based catalyst to produce syngas (91). Syngas then reacts further to produce more hydrogen and carbon dioxide via the water gas shift (WGS) reaction.

$$CH_4 + H_2O \rightleftharpoons CO + 3H_2 [\Delta H_{reaction}(298) = 206.1\ KJ\ mol^{-1}] \quad \textit{Equation 22}$$

$$CO + H_2O \rightleftharpoons CO_2 + H_2 [\Delta H_{reaction}(298) = -412\ KJ\ mol^{-1}] \quad \textit{Equation 23}$$

This process is widely applied for the production of syngas from natural gas and represents 50 % of the global processes of conversion of natural gas and hydrogen production. This percentage in the United States can reach up to 90 %. SMR is an endothermic process, which requires high temperatures and is thus very expensive (92).

1.10.2 *Partial Oxidation (POX) and Catalytic Partial Oxidation (CPOX)*

This reaction occurs when a sub-stoichiometric fuel-air mixture is partially combusted at a high temperature (93), producing hydrogen rich gas. POX could be more economic than steam or dry reforming because it is an exothermic reaction, requiring less thermal energy. However, it is an expensive process, as it requires the flow of pure oxygen. This poses a hazard as both reactants (CH_4 and O_2) are highly flammable and could result in an explosion if not handled carefully (94).

$$CH_4 + 1/2\ O_2 \rightleftharpoons CO + 2H_2\ [\Delta H_{reaction}(298) = -36\ KJ\ mol^{-1}] \quad \textit{Equation 24}$$

In the CPOX reaction, methane is converted with oxygen or air over a noble or transition metal catalyst to syngas, this can only be effectively carried out if the sulfur content of the fuel is below 50 ppm

1.10.3 *Dry Reforming*

CO_2 is available in large quantities from fossil-fuelled power plants and a number of other chemical and metallurgical processes and it can be used in place of steam for the reforming of methane. This not only offers a cheaper alternative to reforming reactions, but it also reduces the GHG effect of CO_2 in the environment. This is a promising technology to produce syngas. Dry reforming is slightly more endothermic than steam reforming, however, it is favoured at low pressure (95). The main disadvantage of dry reforming of methane is the significant deposition of carbon on the catalyst, which lowers the efficiency of the catalyst. The challenging aspect of the industrial application of this process is the development of an active catalyst material with a very low coke formation rate either on the catalyst or in the cold zones of the reactor. Moreover, carbon formation can be

controlled by using a catalyst support that favours the dissociation reaction of CO_2 into CO and O. These gases are responsible for cleaning the surface of the metal preventing coke formation (94).

1.10.3.1 Catalyst Development for Methane Dry Reforming

Heterogeneous catalysts used for methane dry reforming are solid state metals, this differs from the gaseous state of the reactants. Heterogeneous catalysts increase the rate of reforming reactions without being used up in the reaction. However, they are subject to changing properties as a result of deactivation mechanisms. The design of these catalysts starts with the ideal mixture of active metal and support, which are designed in relation to the reforming conditions. This involves several preparation methods to control the chemical reactions and the crystallographic structures of the active metal and support. Moreover, promoters are added as non-active additives. These are used to improve the metallic dispersion over the support, minimising carbon deposition and active metal sintering. The basis for selecting an efficient heterogeneous catalyst includes selectivity, activity, stability, morphology, ease of regeneration, low toxicity, economical cost, and mechanical and thermal properties of the catalyst (96-98). These criteria can be achieved and are characterised by:

1. The amount of the active metal, chemical promoters, selective blocking additives, and the selected support (99).
2. Ensuring the active metal particles are on a scale of 1-10 nm on a support surface that is between 20-50 nm, and porous support body having a macroscopic scale of 1-2 mm (98).
3. Achieving large surface area, proper mesoporous volume as well as increased active metal distribution (98).

1.10.3.2 Active Metal Species for Methane Dry Reforming

There is increased interest from both academia and industry towards the methane dry reforming process in order to produce syngas of low H_2/CO ratios for use as raw material for gas to liquid technologies (100). Applied active metal catalysts usually belong to Group eight of the periodic table and they can be classed into two groups: transition metals and noble metals. Most catalysts today are nickel based because of its good activity and economical cost (100). Catalyst deactivation

mechanisms have promoted research on the combination of other metals such as cobalt or noble metals to produce alloys of enhanced properties. The noble metals, Rh, Ru, Ir, Pt and Pd show good catalytic performance and exhibit low sensitivity to deposition of carbon. On the other hand, their low availability and expensive market value limits their use as a single metal catalyst in large-scale industrial processes.

1.10.3.3 Ni Based Catalyst

Nickel is catalytically active for the dry reforming reaction. Moreover, it is a readily available and economical metal. However, it experiences excess carbon deposition on its surface and this results in its deactivation (101-103). Deposited carbon on the catalyst surface originates from methane decomposition. This is explained in further detail in equations 53 - 56 with dependence on the thermodynamic variables and active metal species (104). Researchers are now focusing on improving Ni based catalysts with the addition of promoters (105-111). Moreover, using different types of supports has also shown that deposition of coke can be reduced depending on the nature of the support (112-117). Noble metals have shown that they are less sensitive to carbon depositions (112, 118-121), however, one major advantage of nickel is its low cost and high availability.

1.10.3.4 Noble Metal Based Catalysts

Noble metals have been shown to be good for the prevention of catalyst deactivation due to their highly selective and stable reactivity, increased resistance in high temperature applications and their significant reduction in reaction energy (122). However, they are very costly, making their applications in industrial scale applications challenging. This has motivated researchers to examine their implementation as low percentage second metals in bimetallic catalysts based on Ni or Co. Thermodynamic analysis reveals that methane dry reforming reactions require reaction temperatures in the region of 1173 K to obtain high syngas yields. Nickel is the preferred catalyst metal for methane dry reforming reactions as per the literature (117, 123-126). However, an encased metal rhodium catalyst has been used in these works to eliminate coke deposition and reactor fouling. In this research, the use of low catalyst loading to achieve optimum conversion has been carried out to make up for the high cost of the catalyst. Noble metal characteristics that provide the best functionality in reforming processes include (127, 128):

- The capability to be dispersed into nanoscale particles is better than most other transition metals, enabling easy adsorption of H_2/O_2.
- The electrons presented in the filled d-subshell can promote the dissociative adsorption of H_2/O_2.
- There is ease of noble bimetallic catalyst preparation via the impregnation method.

1.10.3.5 Ruthenium and Rhodium

To ascertain the noble metal effectiveness, catalytic activity and stability of rhodium (Rh), ruthenium (Ru), palladium (Pd), iridium (Ir) and platinum (Pt) metals have been studied and compared with a non-noble metal. Ru and Rh reveal the best resistance toward catalyst deactivation by carbon deposition amongst other noble metals (129, 130). The activities of noble metals have been compared systematically in terms of conversion rates, product yield and susceptibility to coking. However, an analysis of results obtained by several researchers are contradictory when comparing the relative catalytic activity of these metals (131). Similar to abundant earth metals, it has been shown that noble metals have varrying catalytic actions which is dependent on the type of support. This arises from reactions that occur chemically between the metal and support. Modifications to the catalytic actions of the metals have been explained in terms of how sensitive the reaction is and the changes that occur in the reaction mechanism, due to the nature of the support in the activation of either CH_4 or CO_2 (132). Considering that the support participates in the activation it is anticipated that the noble metal-support interface plays a significant role in DRM reactions. It has been shown that the activity and selectivity of Ru catalysts is highly dependent on the oxidation state of the metal, which can change according to the reaction conditions and the support (133). Moreover, it has been shown that the support can have a significant influence on the type of carbonaceous species formed during reaction. The stability and durability of Rh active sites have been shown to be affected by catalyst supports in different reaction mechanisms (134). On a SiO_2 support, which is considered to be the most inert (134), the entire reforming process occurs on the Rh phase and leads to rapid ageing of the catalyst. The rapid ageing is thought to be related to the large residence time of surface carbon intermediates which favours polymerisation and graphitisation. Less inert supports like Al_2O_3 act as a collector of CH_x species, which reduces the residence time of carbon species on

the Rh phase and therefore leads to more stable catalysts. In this research Al_2O_3 has been chosen as the support.

1.10.3.6 Comparison of Rhodium and Ruthenium with Other Active Metals

There are a number of research work that analysed the catalytic action of noble metals with the aim to ascertain the metal that has excellent catalytic actions and also exhibit good hinderance to carbon deposition. Hou *et al.* (135) compared the reactivity and stability of rhodium (5 wt%), ruthenium (5 wt%) and nickel (10 wt%) as supported metals. The noble metals exhibited high resistance coking, however, they showed lesser catalytic action than nickel. Thus, it can be seen that the activity dependency of the nobel metal on different supports and the thermodynamic conditions are still not fully confirmed (136-138). Hou *et al.* (135) studied the effect of various noble metals supported on alumina and came to the conclusion, in agreement with Matsui (139), that noble metal (5 wt%) supported catalysts lead to high coke resistance and stability in the order of Rh >Ru >Ir >Pd >Pt. The following performance criteria have been identified in order to develop ideal catalysts:

- No coke formation
- High sulfur tolerance
- Ultra-rapid reaction rate
- High-temperature resistance
- Low temperature start-up, in a very short time
- Non-toxic
- Low production cost

1.11 Research Aim

The aim of this research is to develop and experimentally test membrane concepts for the separation of CH_4 from inert gases and higher hydrocarbons. The application of a catalytic membrane to utilise the separated gases (CH_4 and CO_2) as a feed-stock for the methane dry reforming reaction is tested experimentally.

Catalytic membrane reactor design development was also identified as an important aspect. This is a constant feature discussed in this research.

1.12 Thesis Outline

Chapter 1 introduces the motivation of the research and the various sources of VOC emissions. Gas separation and catalytic conversion methods are discussed. The gas transport mechanism of the relevant membranes are discussed.

Chapter 2 investigates the design of a silica membrane and determines gas separation through the silica layer at various temperatures. Parameters are evaluated by determining the flow mechanism that governs the transport of gases through the membrane layer.

Chapter 3 presents the design and gas transport properties of a y-type zeolite membrane on an alumina support at various temperatures. This is achieved by carrying out gas permeation studies and data evaluation.

Chapter 4 presents ways to increase the performance of the membrane studied in chapter 3. This was carried out by incorporating a polyurethane polymer to the y-type zeolite membrane. The objective is achieved through evaluation of gas transport properties of the mixed matrix layer.

Chapter 5 determines the conversion rate of the separated gases (CH_4 and CO_2) using a rhodium impregnated catalyst on an alumina support. This is achieved by investigating various reaction parameters, including feed flowrate and reaction temperature.

Chapter 6 presents the overall discussion and the major findings.

Chapter 7 gives the conclusion and recommendation for further work.

1.13 Overview of Safety Procedures

1.13.1 *Ethical Issues*

Robert Gordon University's research governance policy has been strictly adhered to throughout this research work. This ensures that the research is carried out with the highest ethical standards and the codes of practice. The Research Degrees

Registration (RDR) has been executed together with the Research Ethics Students and Supervisors Appraisal (RESSA). The following are the measures were put in place to ensure that the research is conducted with highest ethical standards

1. To protect the researcher: The University has measures in place to protect the researcher both legally and morally. A Research Governance Policy is helpful in clarifying responsibilities, accountabilities and obligations.

2. To improve the quality of the research: A Research Governance Policy is in place to help promote efficient practices and to help maintain high ethical standards.

3. To protect the position of those affected by the research: The University's Research Ethical Policy requires researchers to consider the impact of the research.

4. To protect the rights of fellow researchers: There is need for mutual respect between researchers and to duly acknowledge the input of every individual researcher as well as put into account the confidentiality of results obtained with commercial sensitivity.

The following ethical conducts were strictly adhered to by the researcher throughout the project work:

- Maintained high quality research
- Displayed responsibility towards other researchers
- Displayed and maintained competence in the research work
- Risks to the researcher and other laboratory users was minimised.

1.13.2 *Health and Safety*

Robert Gordon University's health and safety policy was strictly followed during this research work. Risk assessment of all chemicals used in this work was carried out by the researcher and any hazards are identified and the control measures put in place to reduce any risk. The policy includes:

- Guidance on working and disposal of dangerous and hazardous substances (COSHH) assessment.

- Lone working and out of hours access policy is in place to ensure persons and researchers are not exposed to unacceptable levels of risks.
- Manual handling of equipment was avoided to minimise risk of injury.
- The work place was always kept clean and dry to minimise slips and trips.
- Personal protection gear was always worn in the laboratory.
- The researcher worked in a responsible and safe manner.

2 Design and Evaluation of Gas Transport Through a Silica Membrane

This chapter presents a detailed description of the design, fabrication and characterisation of a silica membrane coated on an alumina support. The evaluation of gas transport mechanism and effectiveness of the membrane was carried out by single gas permeation tests. Characterisation was carried out by Scanning Electron Microscope (SEM), Fourier Transform Infrared spectrometry (FTIR) and liquid nitrogen adsorption/desorption measurements. The quality of the membrane is important for application to gas separation and this membrane is known to withstand harsh operating conditions and have a high carbon dioxide permeation flux. It was chosen for analysis because of the above factors. Moreover, it is economic to synthesise as silicon elastomer is readily available.

2.1 Introduction

The ability of a microporous flat sheet membrane that was dipped into a silica sol for a few seconds and having a pore diameter of less than 2 nm to allow the passage of one molecule over another through its pores has been previously studied (140). State-of-the-art silica membranes usually consists of a thin silica layer on a mesoporous γ-alumina support with pore size ranging from 2 to 50 nm. Microporous silica (SiO_2) membranes are prominent representatives of inorganic membranes. The first successful silica membranes for gas permeation and separation that were effective and had high gas flux were synthesised in 1989 via the sol-gel method (141). SiO_2 sols were first prepared by acid catalysed hydrolysis of tetraethoxysilane (TEOS) in alcoholic solution. The acid catalyst reduces hydrolysis but enhances polycondensation rates during the sol preparation process. This results in the polymeric sol containing silica particles of uneven shape and structure. The tubular porous support was then dipped into the SiO_2 gel solution for a few hours followed by drying and calcination at 673 K. This process was repeated several times to increase the thickness of the membrane layer. In sol-gel method synthesised silica membranes, the process parameters strongly affect the flux and selectivity of the resulting membrane and must be controlled

(142, 143). A major problem of microporous silica membranes is that they don't have good hydrothermal stability particularly in humid atmospheres resulting in the loss of permeability (144). This is due to the closure of membrane pore channels by densification.

$$\equiv Si - OH + \equiv Si - OH \Rightarrow \equiv Si - O - Si \qquad \textit{Equation 25}$$

Several methods can potentially be used to improve the stability of sol-gel derived silica membranes. One particular method is to dope a small amount of inorganic oxides, such as TiO_2, ZrO_2, Fe_2O_3, Al_2O_3 and NiO. In this work the sol-derived silica has been deposited on a composite support consisting of TiO_2, ZrO_2 and Al_2O_3, to avoid instability at high operating temperatures of up to 673 K. An approach for the synthesis of silica membranes is to make the silica membrane hydrophobic by replacing the $-OH$ group on the pore surface with $-CH_3$ groups. This is done by using a hydrophobic methyl template covalently bonded to silica in the sol-gel process (145).

Hove, Nijmeijer and Winnubst (146) previously reported dosing a silica precursor with zirconia to synthesise a silica membrane with a Si/Zr ratio of 10:1. The resulting membrane revealed an increase in H_2 selectivity over CO_2, N_2 and CH_4, however, a decrease in permeance of He and H_2 was found when compared to the silica membrane. Yoshioka *et al.* (147) prepared a sol-derived microporous silica membrane which showed high performance CO_2 permeance and selectivity over N_2. Boffa *et al.* (148) synthesised a microporous niobia-silica membrane where the separation is based on a combination of molecular sieving and variations in molecule wall interactions between gas molecules. The resulting membrane had a Si/Nb ratio of 3:1 and revealed an increase in CH_4 selectivity over CO_2 from 3.3 to 7.0 at 353 K.

2.2 Materials and Experimental method

2.2.1 *Materials*

The materials, chemicals and gases used for this experimental work include,

1. Silicone elastomer SYLGARD 184 supplied by Dow Corning, UK.
2. Deionised Water by Purelab Flex, Elga.
3. Isopentane (2-methyl butane) supplied by Fisher Scientific, UK.
4. SYLGARD 184 silicon elastomer curring agent supplied by Dow Corning, UK.
5. Gases (oxygen, propane, methane, nitrogen, helium, and carbon dioxide) 99 % purity supplied by BOC, UK.

2.2.2 *Instrumentation and Equipment*

The instruments and equipment used for this experimental work together with the respective manufacturer include,

1. Magnetic Stirrer by Fisher Scientific
2. Automated gas sorption analyser by Quantachrome instruments
3. Beakers by Fisher Scientific
4. Weighing Balance by Sartorius
5. Electric water bath by Clifton
6. pH meter by Checker
7. Electric oven by Carbolite
8. Graphite seals by Gee graphite (Figure 8a)
9. Scanning Electron Microscope by Oxford Instruments
10. Energy Dispersive X-ray Detector by Zeiss Instruments
11. 15 nm pore size α-alumina support which consists of 77% alumina and 23% TiO_2 and has a permeable length of 348 mm and an internal and external diameter of 7 and 10 mm respectively, supplied by Ceramiques Techniques

et Industrielles (CTI), France.

12. Thermocouple by RS
13. Rotatory dryer Weir 413D
14. Power Regulator by Barnstead Electro thermal
15. Thermometer by Digitron
16. Hand tools (spanners and screw drivers)
17. Pressure gauge by omega
18. Flow meter by Roxspur
19. Nicolet i S 10 FT-IR spectrometer by Thermo Scientific, UK.

2.2.3 *Methods*

The silica membrane was prepared using the dip-coating method (Figure 2-1). The support was initially weighed using a weighing balance and then dipped in a solution comprising of silicone elastomer, curing agent and isopentane with a volumetric ratio of 10:1:100. The volume of each substance used is provided in Table 2.1. Silicone elastomer has been used because of its high tensile strength and good adhesion, in comparison to a silicon dioxide solution. The solution was homogenised using a magnetic stirrer for 2 h before the support was dipped for 1 h and kept in a central vertical position to ensure an even coating of the silica across the surface of the support. Both ends of the support were sealed to ensure only the outer surface was coated with the silicone elastomer. The solution was stirred constantly using a magnetic stirrer to stop it from coagulating. The membrane was then carefully withdrawn from the solution and air dried for 30 min using the WEIR 413D motor powered rotary dryer as shown in Figure 2-2.

Table 2.1: Composition of the modification solution for silica membrane.

Substance	Amount (ml)
Silicon elastomer curing agent	5
Isopentane	500
Silicone elastomer	50

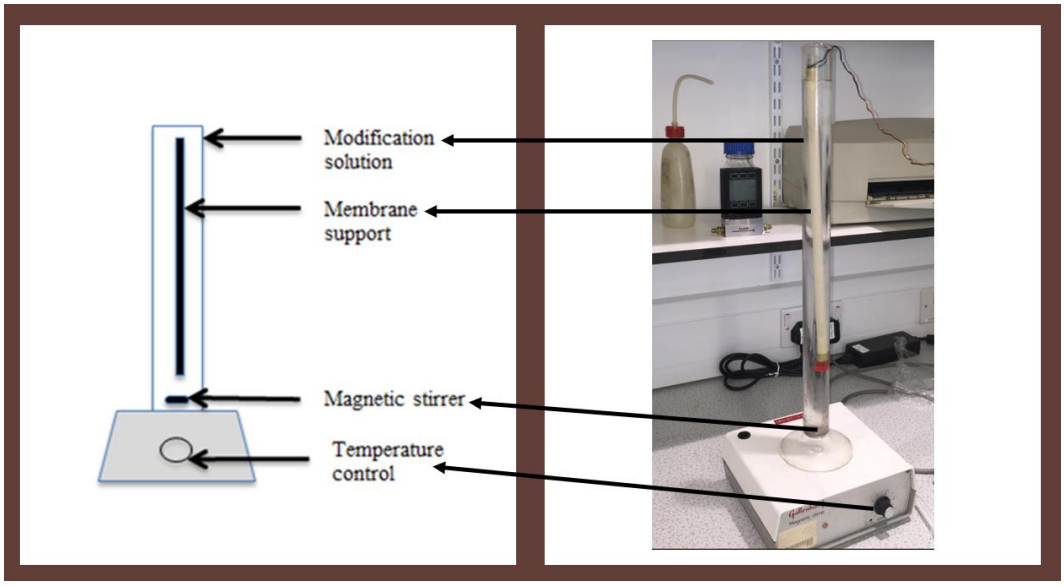

Figure 2-1: Dip-coating method for silica membrane preparation

The air dried composite membrane was thermally treated at 873 K for 10 h at a temperature gradient increase of 2 ^{o}C per min in an oven (Carbolite). This was done to ensure better adhesion of the silica layer to the alumina support. The weight of the membrane was then taken after calcination. This was used to determine the thickness of the membrane. Prior to gas permeation test, the resulting membrane was fitted into the stainless steel membrane reactor and sealed at both ends using graphite seals (Gee graphite). The graphite seals were securely fitted to ensure that there were no leaks. The membrane was pressurised to 2 × 10^{6} Pa at 293 K with an inert gas and tested for leaks. Gas permeation

measurements were carried out at a temperature range of 293 to 333 K and with a transmembrane pressure drop of 0.1 to 1 × 10^6 Pa. The feed gas flow was controlled using a valve and the permeating gas flow rate was determined using a digital gas flow meter at atmospheric pressure. The retentate gas outlet was connected to the fume cupboard to discard any gas that did not permeate through the membrane.

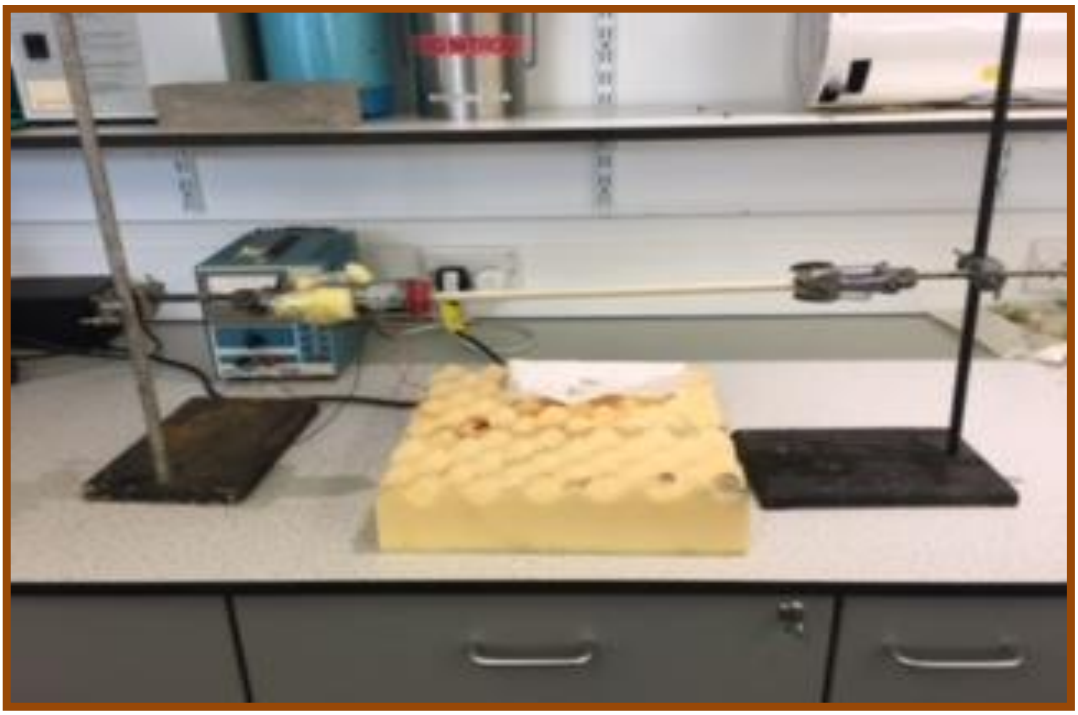

Figure 2-2: Motor powered rotatory dryer

2.2.4 *Silica Membrane Characterization*

The functional groups in the synthesised silica membrane have been investigated using an Attenuated total reflection (ATR) Nicolet i S 10 FT-IR spectrometer in the range 400-4000 cm^{-1}. A Zeiss model Evo LS10 Scanning Electron Microscope (SEM) with an Oxford Instruments INCA System Energy Dispersive X-Ray analyser (EDAX) was used to determine the morphology and elemental composition of the prepared membrane. Nitrogen physisorption measurements (Figure 2-3) have been carried out using a Quantachrome autosorb® gas analyser to determine the pore size and surface area.

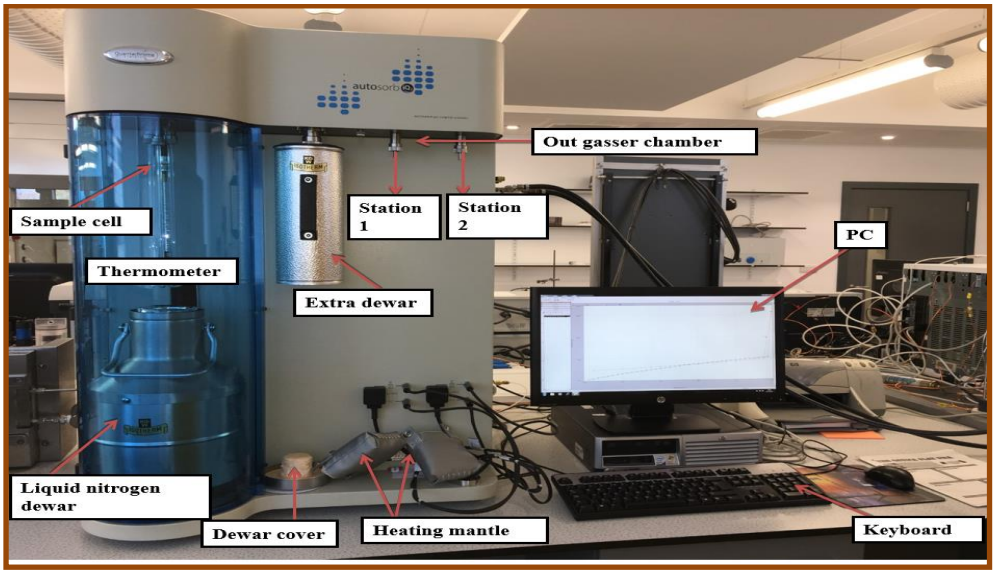

Figure 2-3: Quantachrome autosorb® gas analyser.

2.2.4.1 FTIR Analysis

Fourier Transform Infrared spectrometry has been used to determine the infrared spectra of compounds and can be used to determine the different bonds present in a compound to gain information about the functional groups present in a substance. The recognition of one or two important absorbance, and the identification of the functional group with which they associate are necessary to identify a compound. This can be achieved with the aid of correlation tables, which show typical absorbance frequencies in the form of bands for functional groups. Light moves through space with a velocity *v*, which is equal to 3.0 x 10^8 m s^{-1} and the frequency *f*, at which the peaks pass a point is given by equation 26.

$$f = \frac{v}{\lambda} = \frac{3.0\times10^8}{\lambda}\ hertz\ (Hz) \qquad \textit{Equation 26}$$

The energy *E*, of light is related to a frequency by Plank's constant *h*, which has the value 6.23 X 10^{-24} J s.

$$E = h\ f \qquad \textit{Equation 27}$$

In the context of infrared, it is normal to measure the wavelength in wavenumbers. This is merely the inverse of wavelength and has the unit cm^{-1}. The most useful infrared region lies between 4000 – 670 cm^{-1}.

2.2.4.2 Scanning Electron Microscope (SEM) and Enery Dispersive Xray (EDAX) Analysis

In SEM a variety of signals that give information about the morphology, size, shape, crystalline structure and thickness of materials that make up the membranes are generated by a focused beam of high-energy electrons. A 2-dimensional image that displays spatial variation in the properties of the sample is generated (151). Electron-sample interactions produce accelerated electrons, which dissipate forming a variety of signals. Secondary electrons, photons, diffracted electrons, visible light and heat are some of the signals produced. SEM images are the major constituent of secondary electrons and they are instrumental in revealing the morphology of samples. The basic components of an SEM include a display unit (pc), signal detectors, electron source, sample stage and electron lenses. The sample preparation includes preparing a stub where the sample to be examined was placed. A suspension of silver from Agar Scientific was added to the stub. The sample was then placed on the stub and allowed to dry for 24 h prior to obtain SEM images. Operating parameters for both the SEM and EDAX is provided in Table 2.2.

Table 2.2: SEM and EDAX operating parameters

Parameters	SEM	EDAX
Working distance (mm)	8.5	8.5
Gun beam (pA)	1	10
Magnification (x)	any	200

2.2.4.3 **Nitrogen *Physisorption Measurements***

One of the most important techniques for the characterisation of nano-sized porous materials in regards to the surface area, pore volume and pore size distribution is the physical adsorption of gas on the material's surface. Several types of physisorption isotherms (Figure 2-4) are observed for different materials. Type I isotherms are governed by adsorption in a microporous sample (pore size less than 2 nm), type II is regarded as a non-porous or macroporous samples (pore size greater than 50 nm), type III are also non-porous or microporous but with weak adsorbent-adsorbate interaction. Type IV are also typical mesoporous adsorbent with initial monolayer-multilayer coverage on external and mesoporic surfaces.

This is followed by capillary condensation in the mesopores with different types of hysteresis. An example is presented for water adsorption on activated carbon (152). The specific surface area of a given material can be determined if the number of molecules in a monolayer of the adsorbate and the space occupied by one molecule are known. Several mathematical models have been developed to assess the monolayer capacity of a given adsorbent. The BET model developed by Brunauer, Emmett and Teller is most often used. It is based on a simplified model of monolayer-multilayer adsorption that represents an extension of the Langmuir model. It is used as a universal method for the determination of specific surface areas of samples (153). The BET surface area can be expressed as in equation 28:

$$\frac{p}{n_{ads}(p_o - p)} = \frac{1}{cn_m} + \frac{(c-1)}{cn_m} \times \frac{p}{p_o} \qquad \textit{Equation 28}$$

Where p and p_o are the equilibrium and saturation pressures of the adsorptive species at the adsorption temperature, n_{ads} is the amount of gas adsorbed by unit mass of the adsorbent, c is the empirical constant related to the heat of adsorption and indicates the magnitude of adsorbent-adsorbate interaction energy and n_m is the monolayer capacity (153).

The BET equation requires a linear relationship between $p/n_{ads}(p_o - p)$ and p/p_o as shown in the BET plot in Figure 2-5. Linearity is usually observed only if the relative pressure (p/p_o) value is between 0.05 and 0.3. At higher p/p_o values, capillary condensation occurs, and the BET equation is no longer valid.

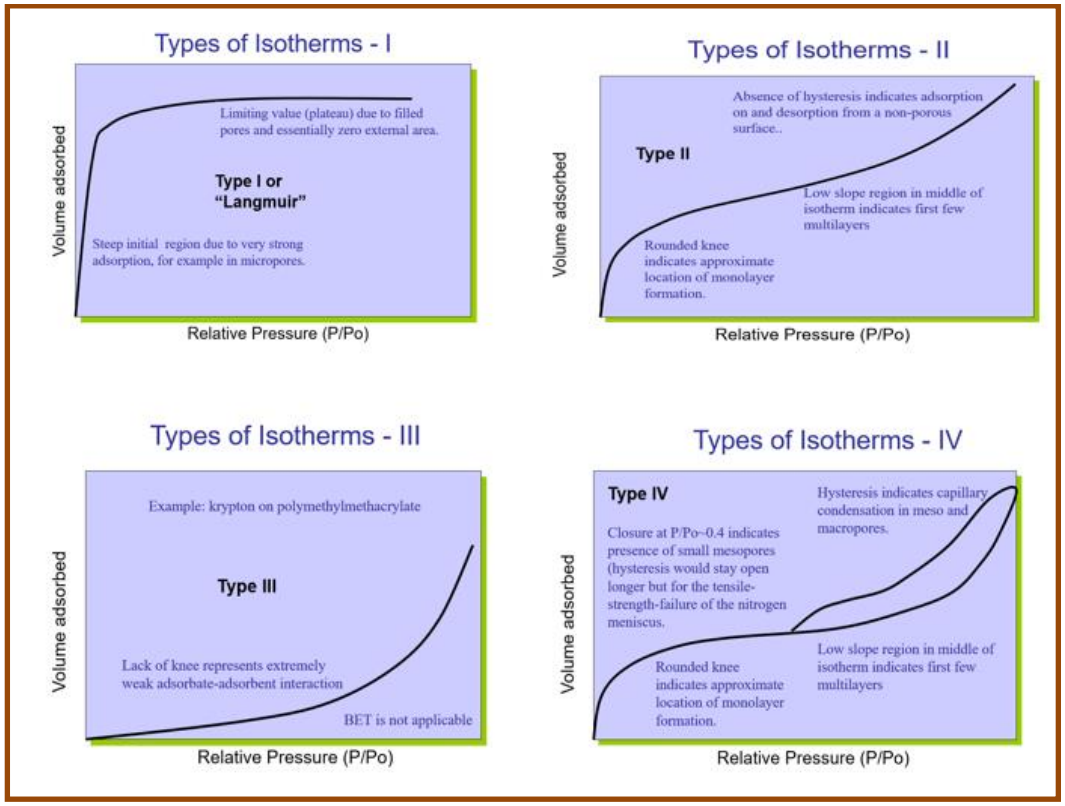

Figure 2-4: Types of Physisorption Isotherms (adapted from Quantachrome Instruments).

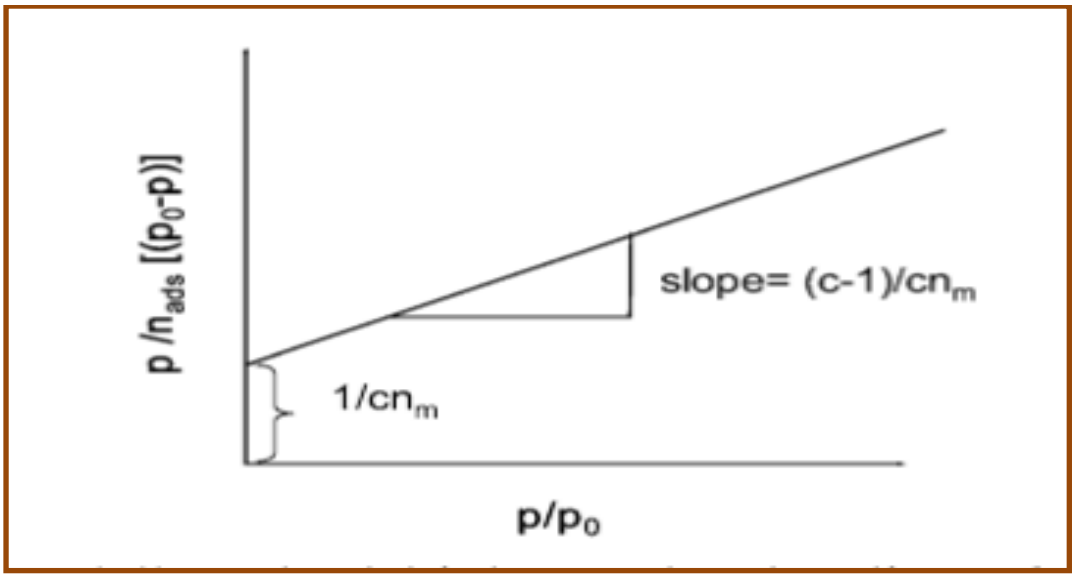

Figure 2-5: BET plot and relation between c and n_m to slope and intercept of y-axis (153).

The specific surface area of the silica membrane has been determined from the adsorption of nitrogen on the external and internal surface of the membranes at

77.35 K using a Quanta chrome adsorption gas analyser. The operating conditions of the instrument are provided in Table 2.3.

The adsorption behaviour of mesoporous materials is determined by the adsorbent-adsorbate interactions. A Barrett-Joyner-Halenda (BJH) graph can be used to indicate the adsorption and desorption branches, which are used to determine the pore sizes of the membrane. Hence, the Kelvin equation, which is based on the existence of cylindrical pores in the membrane, has been used for the evaluation of the pore size distribution of the samples. The Kelvin equation is given as:

$$r_p = r_k + t \qquad \textit{Equation 29}$$

Where r_p is the pore radius of the membrane layer, r_k is the Kelvin radius and t is the thickness of the membrane layer.

Table 2.3**:** Optimum operating conditions of the Quantachrome Gas Analyser

Parameter	Value
Area (A^2 mol^{-1})	16.2
Non-Ideality (1/mm Hg)	6.58 x 10^{-5}
Sample cell type (mm)	12
Analysis time (mins)	237
Mol weight (g mol^{-1})	28.0134
Ambient temperature (K)	300
Bath temperature (K)	77

2.2.5 *Gas Permeation Test*

To evaluate the performance of the fabricated membrane, a reactor fitted with digital pressure gauges and Cole-Palmer digital flow meter has been used to determine the movement of the gases through the membrane. Gas permeation tests have been carried out with single-component gases, namely, carbon dioxide,

oxygen, methane, nitrogen and propane all at 99.5% purity as supplied by BOC, United Kingdom. A schematic diagram of the gas transport system is shown in Figure 2-6. The gas permeation experiment was performed by pressurising one side of the membrane with the gas while keeping the other end at atmospheric membrane shell pressure. The permeate end of the reactor was connected to flow meter to measure the flow of the permeated gas (L/min). The flow rate was converted to molar flow rate (mol/s) and normalised by dividing with the active membrane area to determine the flux of the gases through the membrane. Transmembrane pressure was controlled by a pressure controller and the flow of the gases through the membrane was measured with a digital flow meter.

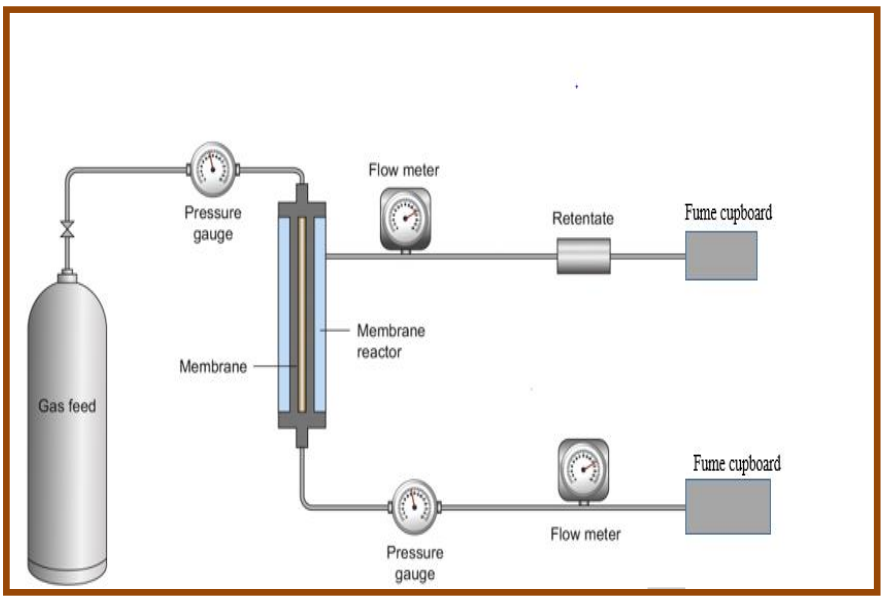

Figure 2-6: Gas permeation setup.

2.3 Results and Discussion

2.3.1 *FTIR Analysis*

The FTIR spectrum of the alumina support is presented in Figure 2-7. Three bands have been identified on the spectrum. The band at 2335 cm^{-1} indicates the presence of C−H functional groups, while the bands at 2167.34 and 1977.73 cm^{-1} reveal the presence of C=O functional groups.

The FTIR spectrum of the silica membrane is presented in Figure 2-8. This reveal adsorption bands arising from asymmetric (1088.10 cm^{-1}) and symmetric (below

1000 cm^{-1}) Si–O vibrations. The adsorption bands between 1000.89 cm^{-1} and 1257.44 cm^{-1} can be described as the superimposition of several signals from SiO_2 peaks, Si–OH bonding and peaks due to residual organic groups (154). Water shows an intense characteristic absorption band at the region of 3000 cm^{-1}. This can be assigned to O–H stretching in H-bonded water.

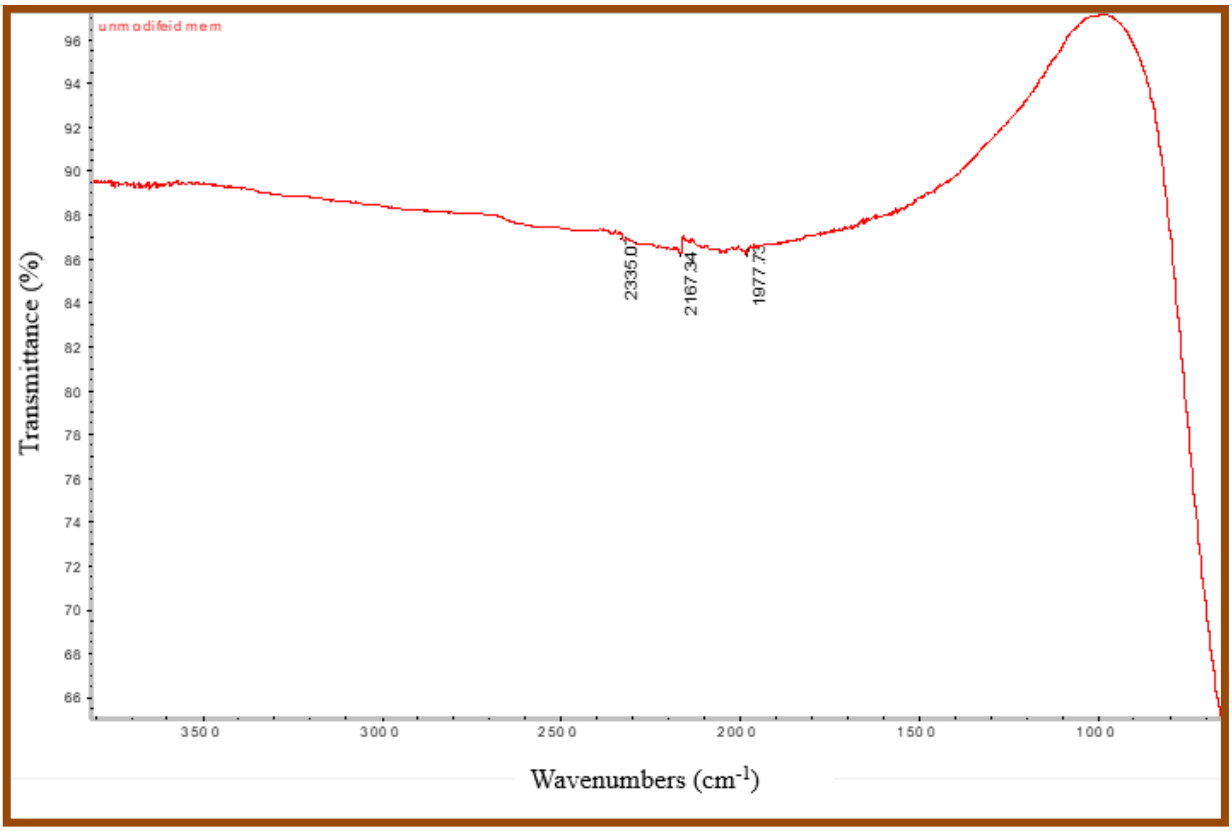

Figure 2-7: FTIR spectra of the alumina support.

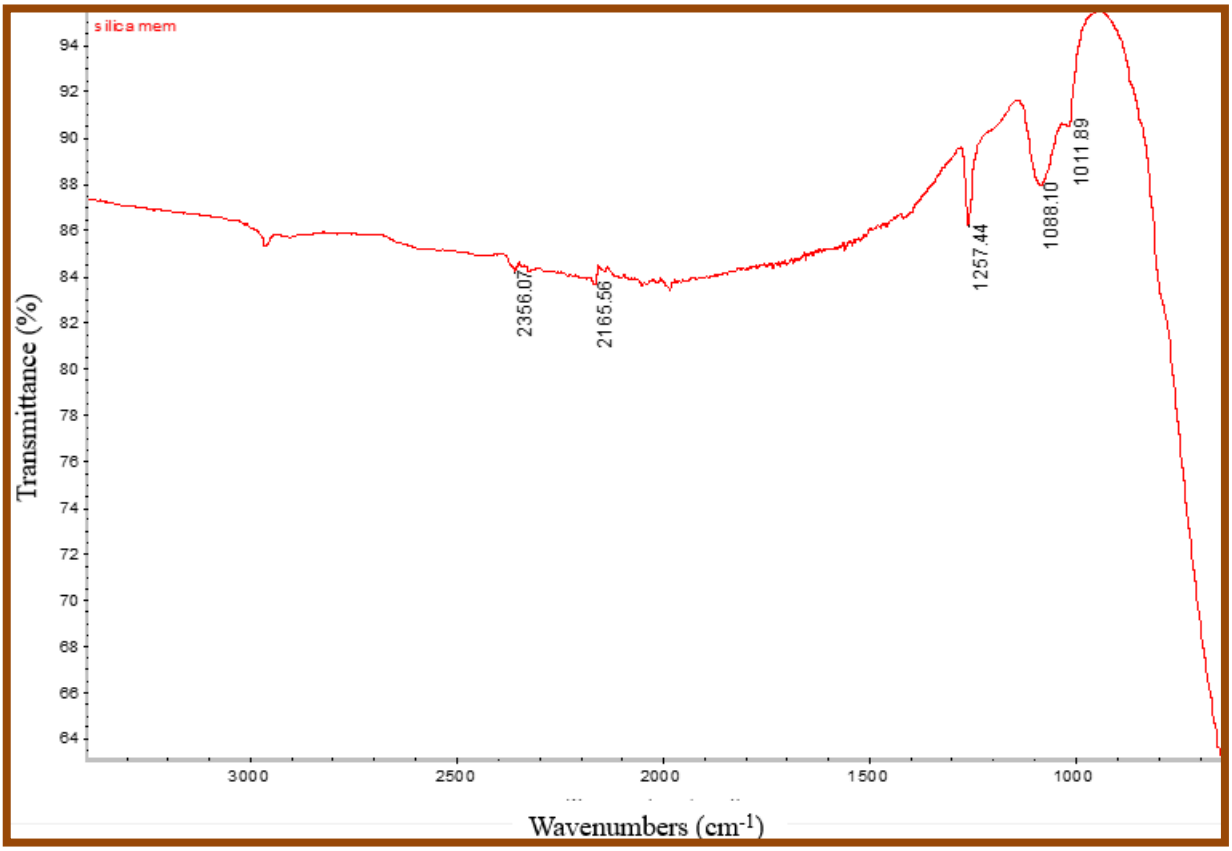

Figure 2-8: FTIR spectra of the silica membrane.

2.3.2 *SEM and EDAX*

SEM images revealing the surface morphology of the alumina support and the silica membrane are presented in Figures 2-9 (a) and (b). The samples have been examined at magnifications of 2.00 KX with a scale of 10 μm. The smooth clear surface of the alumina support can be observed (Figure 2-9a). Moreover, the silica particles with uneven pores distributed can be observed (Figure 2-9b), upon modification with silica sol.

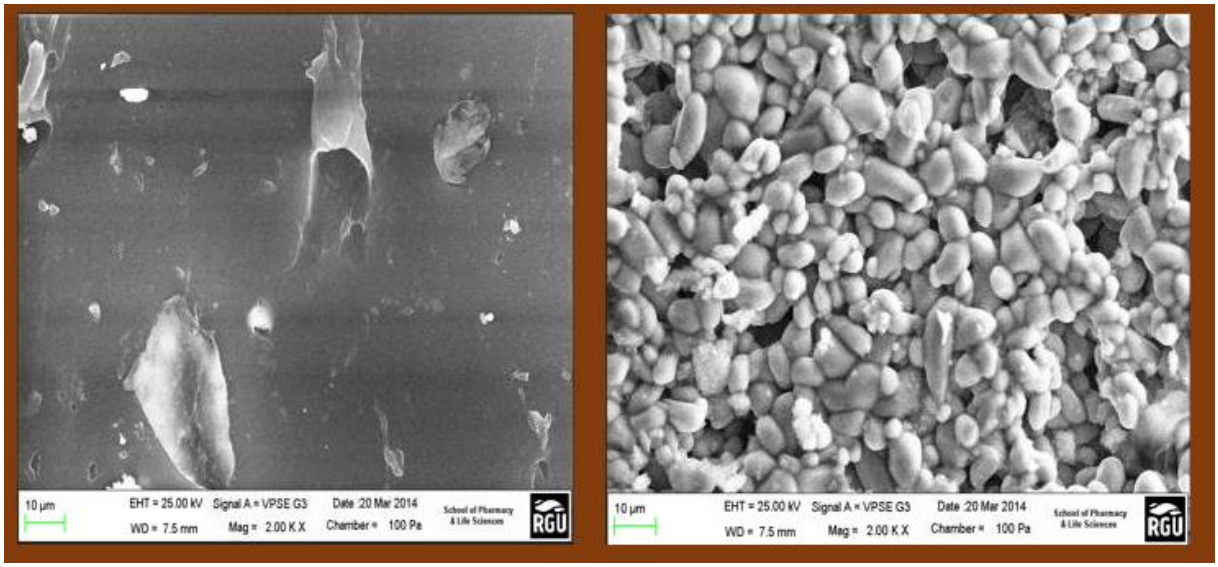

(a) **(b)**

*Figure 2-9**:** SEM images of the outer surface of (a) silica membrane and (b) alumina support*

The elemental compositions of the alumina support and silica membrane have been determined using Energy Dispersive X-|ray Analysis (EDAX) and are presented in Figures 2-10 and 2-11 respectively. The elemental composition of the membrane is given in Table 2.4.

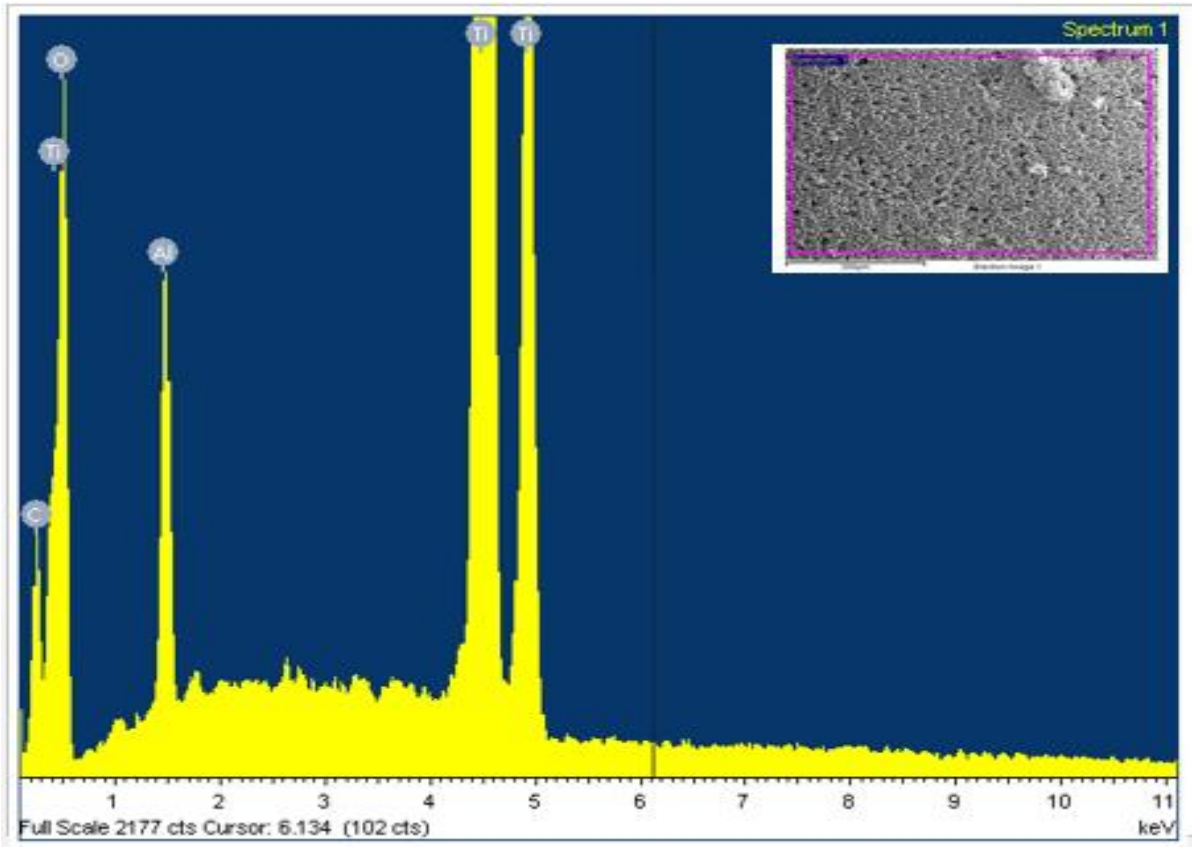

Figure 2-10: EDAX spectrum of the alumina support.

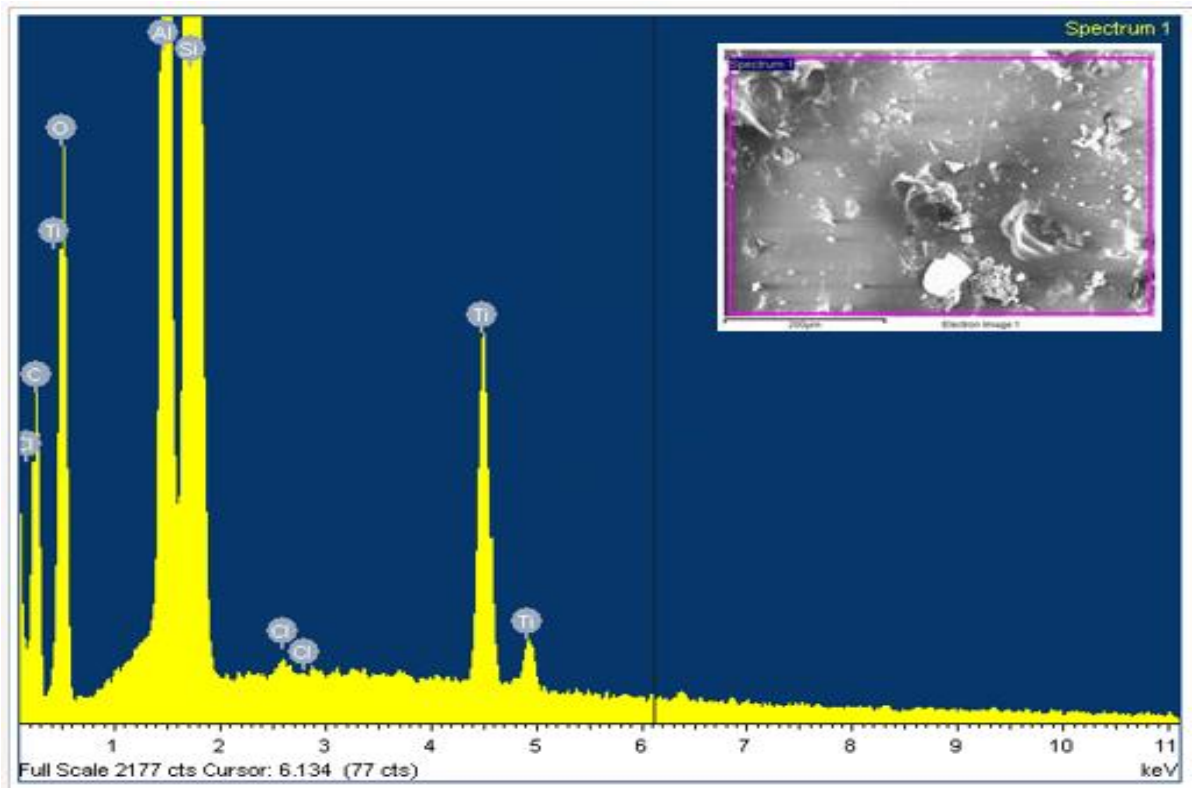

Figure 2-11: EDAX of the silica modified membrane.

Table 2.4: Elemental composition of the alumina support and silica membrane

Element	Alumina support weight (%)	Silica membrane weight (%)
C	6.92	31.97
O	40.45	26.74
Al	2.17	5.81
Ti	50.46	3.20
Si	-	32.21
Cl	-	0.08

2.3.3 *Nitrogen Physisorption Measurements*

The hysteresis isotherms of the silica membrane shown in Figure 2-12 correspond to type IV. This indicates that the membrane is mesoporous and can undergo capillary condensation during hysteresis.

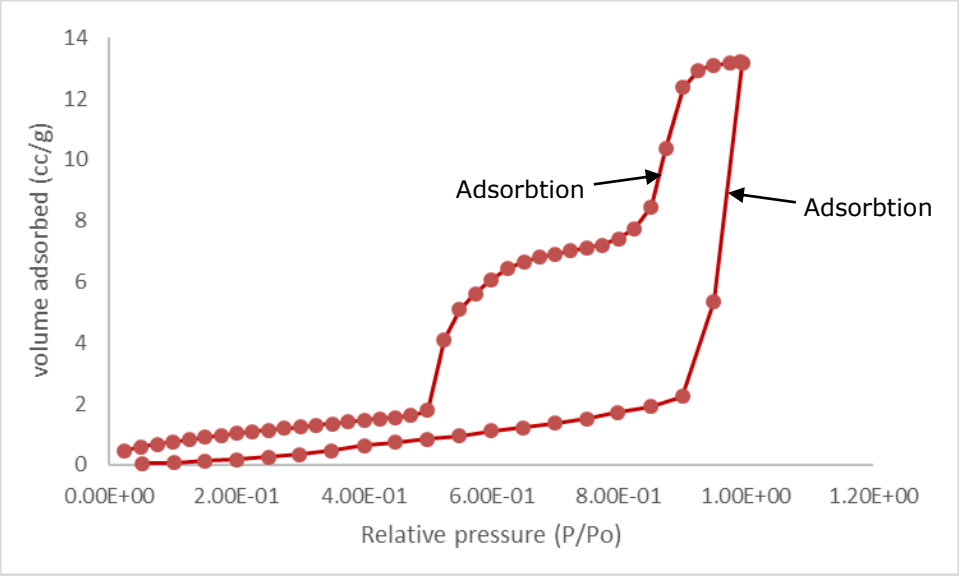

Figure 2-12: N_2 adsorption/desorption isotherm of silica membrane.

The pore size distribution of the membrane is presented in Figure 2-13. This has

been used to determine the pore size of the membrane using the BJH method (Equation 34). Table 2.5 provides a summary of the desorption process and calculated parameters for the membrane and support. Although the mean pore size of the support is actually 15 nm, nitrogen adsorption did not show this. This could be because N_2 adsorption/desorption is more suited for determination of nanopores. Mecury porosimetry can be used for the determination of actual pore sizes in the 15 nm range.

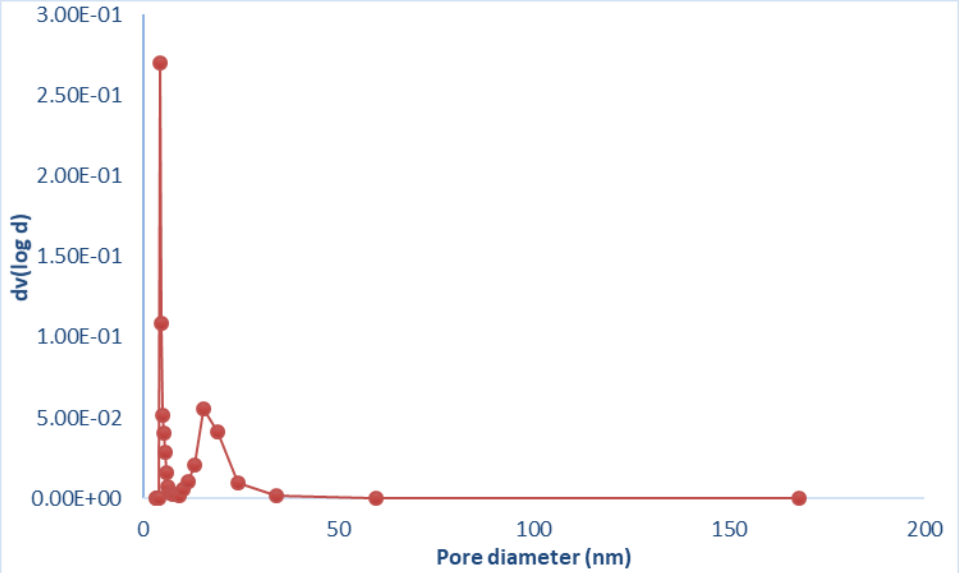

Figure 2-13: Pore-size distribution of silica membrane measured by N_2 adsorption/desorption.

Table 2.5: N_2 adsorption/desorption summary of the alumina support and silica membrane.

	AlO_2 support	Silica membrane
Surface Area (m^2g^{-1})	1.33	15.894
Pore Volume (cc/g)	0.001	0.027
Pore Diameter (nm)	3.135	4.183

2.3.4 *Gas Permeation*

2.3.4.1 Effect of Mean Pressure on Gas Permeation

The plot of permeance against mean feed pressure is presented in Figure 2-14 for the silica membrane. The mean pressure ($\bar{P}$) was determined by equation 30.

$$\bar{P} = \frac{p_1 + p_2}{2} \qquad \textit{Equation 30}$$

Where p_1 is the inlet gas pressure (Pa) and p_2 is the permeate gas pressure that is assumed to be atmospheric pressure.

The permeance was observed to decrease with an increase in feed pressure. CO_2 was found to have the lowest permeance, but the highest molecular weight. He has the lowest molecular weight, but highest permeance. Therefore, an inverse relationship between molecular weight and permeance has been found. This follows the flow mechanism of Knudsen flow (48). At pressures higher than 0.1 bar, the plots indicate a flow that is consistent with Knudsen flow for a membrane that is free from defects. The order of molecular weights is CO_2 > Ar > N_2 > He. Nitrogen and argon exhibit close permeances, however their molecular weights are not so close. This could imply that a different flow mechanism was responsible for the transport of these gases across the membrane.

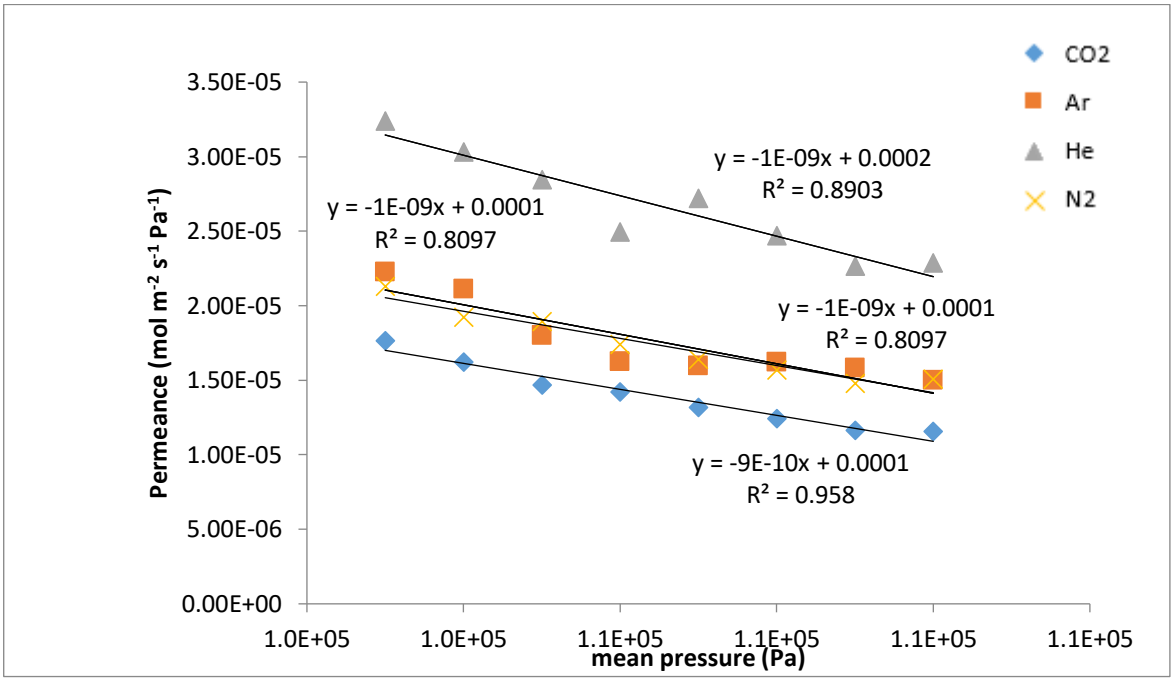

Figure 2-14: Effect of mean pressure on gas permeance through the alumina support at 293 K

Recal equation 8:

$$J = A\bar{P} + B$$

The slope (A) of the graph shown in Figure 2-14 is the Knudsen contribution, while the intercept (B) is the contribution due to Poiseulle flow. Equation 9 has been used to calculate the pore radius. The values for A and B were obtained from the graph plotted in Figure 2-14 using linear regression. In this work the value of B is very low as the membrane does not exhibit Poiseulle flow. The pore radii and the mean free paths of the molecules have been calculated and are presented in Table 2.6.

Table 2.6: Calculated pore radius of the membrane and mean free path of the gases

Gas	r_p ($\times 10^{-9}$m)	Λ ($\times 10^{-3}$m)
Ar	0.037	1.48
He	0.312	6.24
N_2	0.044	2.93
CO_2	0.029	1.99

The theoretical pore radius of the membrane is meant to be the same despite the gas used to determine it. However, the values in Table 2.6, clearly show that the pore radius values are different for the different gases used. This is because depending on their kinetic diameter, gases see a different pore size as they negociate their way through a membrane pore. The calculated pore radius was found to be much lower than the mean free path which implies that the dominant flow of the gases is Knudsen flow.

The Knudsen selectivity has been calculated using the ratios of the square roots of the gas molecular weights using equation 4 (47). The pure gas selectivity obtained experimentally was determined by calculating the ratios of the permeance of the gases at different pressures. The selectivity of CO_2 with respect to other gases at room temperature has been determined across a range of pressures. Figure 2-15 shows both the permselectivities and the Knudsen selectivities. Calculated Knudsen selectivity values for the gases are tabulated in Table 2.7.

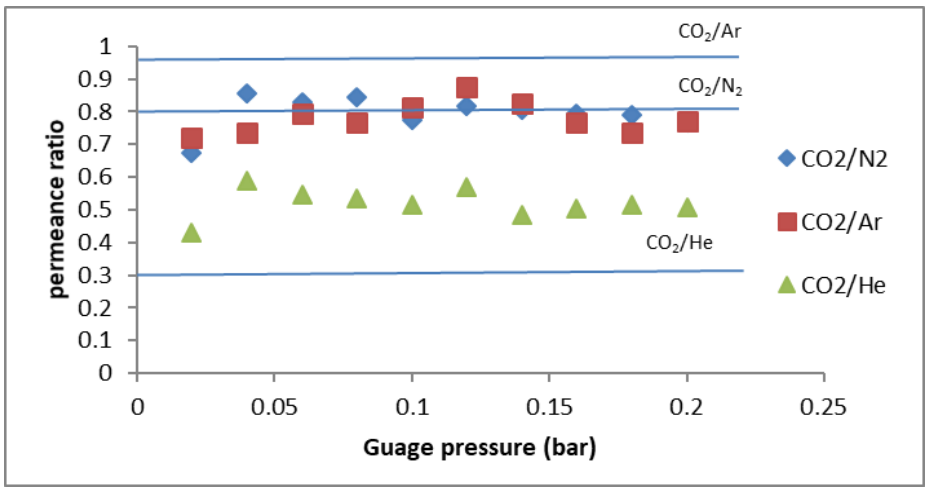

Figure 2-15: Knudsen selectivity of CO_2 at 293 K.

Table 2.7: Knudsen selectivity calculated using the molecular weights of the gases.

Gases	Knudsen selectivity
CO_2/N_2	0.799
CO_2/Ar	0.952
CO_2/He	0.302

The pure gas selectivity for CO_2/Ar (indicated by the blue line) was found to be higher than the theoretical values at all the pressures. This indicates that in order for CO_2 to be recovered from Ar, the membrane has to be modified. Moreover, factors including the temperature and pore size of the membrane could be reduced to further enhance the Knudsen selectivity. Alternatively, zeolite membranes use the molecular sieving separation mechanism and could be effective as a gas separation membrane for the off gases (155). However, another flow mechanism could be employed for the separation of these gases.

For CO_2/He, the pure gas selectivity was found to be higher than the theoretical value. This indicates that the recovery of CO_2 from helium is possible. The pure gas selectivity of CO_2/N_2 was found to vary with changes in pressure. Pure gas permselectivity was found to approach Knudsen selectivity value at pressures between 2000 to 8000 Pa, and at room temperature. This indicates that under these conditions CO_2 can be selectively recovered from nitrogen. The membrane permeance was calculated using equation 3. A permeance in the range of 10^{-6} mol m^{-2} Pa^{-1} for CO_2, Ar, N_2 and He at 294 K was determined. This value is equivalent to similar membranes reported in the literature (156).

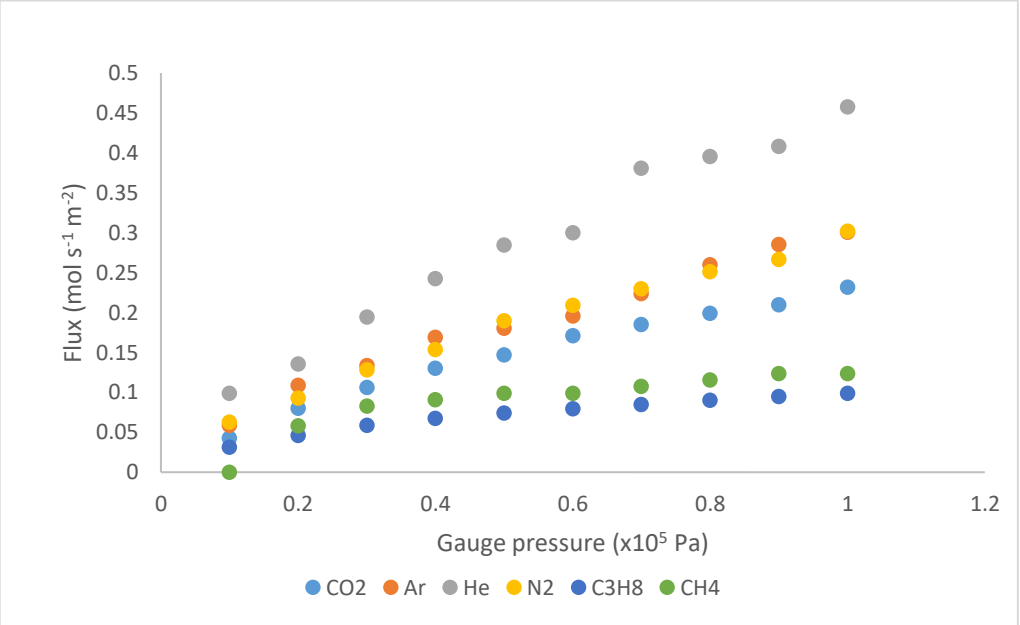

Figure 2-16: Molar flux of single gases through silica membrane at 293 K

The molar flux of all the gases increases with increase in pressure as can be seen in Figure 2-16. CH_4 has the least flux through the silica membrane. The order of molar flux of the single gases through the membrane with increase in pressure drop is He > Ar > N_2 > CO_2 > CH_4 > C_3H_8. The order of gas molecular weight starting from the lightest is He > CH_4 > N_2 > Ar > CO_2 > C_3H_8. This does not agree with Graham's law of diffusion and does not follow Knudsen flow mechanism.

Table 2.8 shows the ability of the membrane to selectively separate gas mixtures based on their single gas permeances while the Knudsen selectivities are given in parentheses. The highest separation factor for the separation of methane from the inert gases is achieved at 293 K. The selectivity of methane towards propane, CO_2 and inert gases can be improved by using a membrane that uses a different flow mechanism compared to the silica membrane. Increasing the temperature did not increase the selectivity of the silica membrane.

Table 2.8: Maximum selectivity of methane through a silica membrane at 293 K, 303 K and 333 K

Temp (K)	CH_4/CO_2 **(1.65)**	CH_4/N_2 **(1.32)**	CH_4/He **(0.50)**	CH_4/C_3H_8 **(1.65)**	CH_4/Ar **(1.58)**
293	1.4	1.4	1.1	1.1	1.1
303	1.3	0.8	0.6	-	0.8
333	1.2	0.9	0.6	-	0.8

2.3.4.2 Effect of Gas Kinetic Diameter on Gas Permeation

A plot of gas permeance at 293 K *vs.* the kinetic diameter of the gas molecules is shown in Figure 2-17. This plot was generated to further investigate the flow mechanism of the membrane. Moreover, it was used to investigate whether or not the mechanism could be molecular sieving, whereby smaller molecules permeate and larger molecules are retained (47). In Figure 2-17, it can be seen that the permeance of the gases through the membrane does not follow the order of kinetic diameter, this could be due to the transport mechanism exhibited by the silica membrane. Propane has the largest kinetic diameter (0.43 nm) and is expected to have the lowest permeance. Whereas, helium has the smallest kinetic diameter (0.265 nm) is expected to have the highest permeance (157).

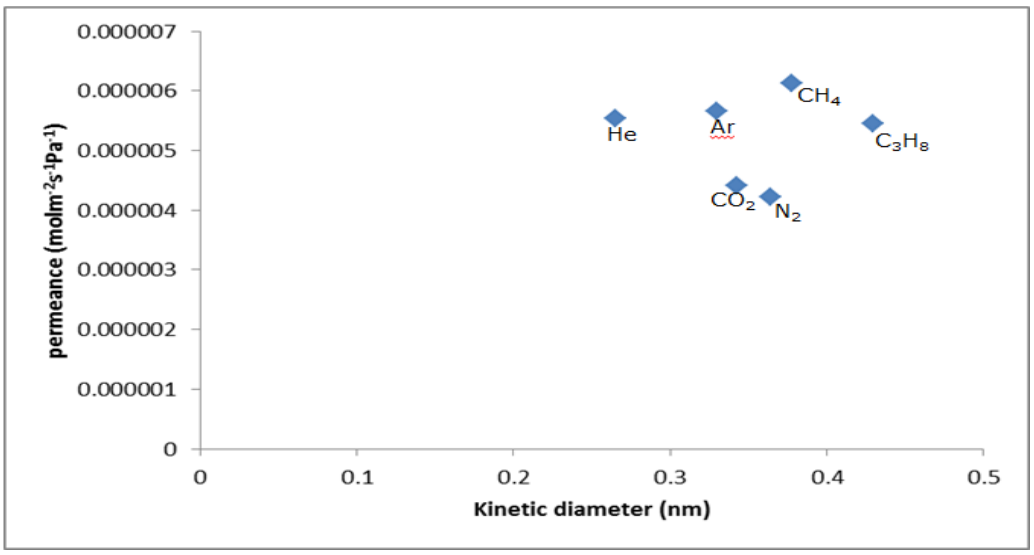

Figure 2-17: Effect of kinetic diameter on gas permeance at 293 K and 10^4 Pa.

Asymmetric membranes were obtained by dip-coating the alumina/titania support

in the prepared silica sol gel solution. Single gas permeation measurements determined the efficiency of the membrane by calculating the selectivities of the gases in relation to methane. The selectivity of methane towards other components such as propane, CO_2 and inert gases can be improved by using a membrane that uses a different flow mechanism compared to the silica membrane. Hence, the alumina support was modified with y-type zeolite to achieve this higher selectivity.

3 Design and Evaluation of Gas Transport Through a Zeolite Membrane on an Alumina Support

This chapter details the synthesis and applications of zeolite membranes (gas separation and zeolite-membrane reactors). Gas separation is still not carried out at industrial level for zeolite membranes. Related areas, such as the possibility of incorporating a zeolite membrane in a reactor for possible catalytic action of the zeolite particles and scale-up issues are also discussed. The basic concept of mass transport through the zeolite layer has been presented. Zeolites can enhance the selectivity of methane in relation to CO_2, C_3H_8 and inert gases more effectively than silica membrane and this is discussed in more detail.

3.1 Introduction

Zeolites are natural or synthetic compounds that are composed of hydrated alumina-silica structures of alkaline and alkaline-earth metals. They have attracted increased interest because of their similar pore size on the molecular scale, which enables the separation of liquid and gaseous mixtures in a continuous way (158). Zeolites have good chemical and thermal stability. As such, they can be used for high temperature processes and for processes that employ organic solvents. In addition, zeolite materials exhibit intrinsic catalytic property, which promotes the use of zeolite membranes as catalytic membrane reactors (CMRs).

In the previous two decades, enormous progress has been made on zeolite membrane synthesis. However, only 20 out of approximately 170 zeolite structures are used for the preparation of a membrane (159). The high cost and poor reproducibility of the synthesis hinders the application of the zeolite membranes on a large industrial scale (160, 161). Zeolite frameworks are made of silicon oxides and aluminium oxides. Moreover, the silicon and aluminium atom centres have a tetrahedral shape, which are linked to each other by bridging oxygen atoms. The strong acidity and uniformity of the micropores (less than 2 nm in diameter), together with a unique crystal structure ensures that zeolites have a high selectivity for separation based on the shape or chemical configuration of molecules in different chemical reactions. For example, alkylation,

aromatisation, cracking, pyrolysis, and hydrodesulfurisation.

In comparison to natural zeolites, synthetic zeolites (*i.e.* X, Y and A) are often more applicable in membrane technology due to their uniform particle size and high purity. In addition, they can be designed to separate hydrocarbons. van Bekkum *et al.* (162) have previously prepared an MFI-type (Mordenite Framework Inverted) zeolite membrane on a porous stainless-steel disk. These exhibited a high permselectivity for *n*-butane (*n*-C_4H_{10}) over *i*-butane (*i*-C_4H_{10}) at room temperature. Jia *et al.* (163) reported on a zeolite membrane that showed a *n*-C_4H_{10}/*i*-C_4H_{10} selectivity of approximately 50 at 20 °C. However, the authors reported no data at elevated temperatures. Yan *et al.* (164) previously prepared an MF (Mordenite Framework) membrane on an alumina porous disk. The authors reported a *n*-C_4H_{10}/*i*-C_4H_{10} permselectivity of 6.2 at 108 °C and 9.4 at 185 °C. Vroon *et al.* (165) reported the formation of an MFI-type membrane on an alumina support. This was shown to exhibit a *n*-C_4H_{10}/*i*-C_4H_{10} permselectivity of 90 at 25 °C and 11 at 200 °C. Thus, reproducibility in the membrane formation process is one of the vital factors for the application of zeolite membranes.

In addition, the effect of the supporting substrate on permeation properties of zeolite membranes is critical. Yan *et al.* (164) reported that the membrane morphology changed for the same porous substrate, under different synthetic conditions. Kusakabe *et al.* (155) produced an MFI-type zeolite membrane on the exterior surfaces of a porous alumina support tube using a hydrothermal reaction. The authors found no direct relationship between film morphology and permselectivity. The authors also synthesised a Y-type zeolite membrane on a porous α-alumina support tube and carried out single gas permeation test on CO_2, N_2, CH_4, C_2H_6 and SF_6. The authors found that the selectivity of CO_2/CH_4 through the membrane was higher at permeation temperatures that are lower, and tends to decrease with increases in temperature

3.2 Synthesis of Zeolite Membrane

Zeolite membranes are normally synthesised on porous alumina supports or stainless steel, because a self-standing zeolite layer is very fragile. The commonly employed procedures used for zeolite membrane synthesis include:

(a) vapour-phase transport

(b) direct *in situ* crystallisation

(c) secondary growth

The structured pores of zeolites, and the ability of zeolites to withstand high temperatures and pressures have made them a unique material for designing membranes. Significant high-profile research is currently being undertaken to develop the synthesis of zeolite membranes. Several of the developed methods for the synthesis of zeolite membranes are reviewed in this section.

3.2.1 *Polymeric- Zeolite filled membranes*

This method involves embedding zeolite crystals in to a polymer matrix (166). The space between the zeolite crystals is sealed with a gas-tight polymeric structure. A major concern with this preparation method has been pore sizes that are different across the matrix and poor thermal stability. The embedded method of zeolite preparation is shown in Figure 3-1.

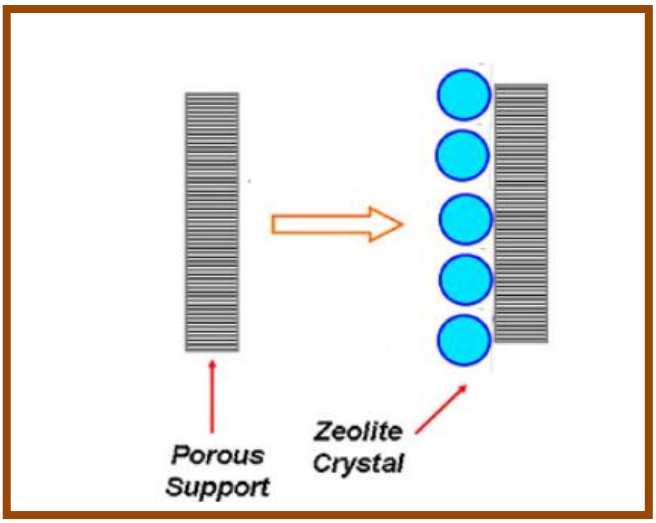

Figure 3-1: Embedded method of Zeolite Preparation adapted from reference 167.

3.2.2 *Zeolite films that are Free-Standing*

For molecular sieving applications, this method of preparation is most commonly

employed. Teflon and cellulose supports are used as temporary supports for the synthesis (166). This preparation method has been discontinued because of the fragility of the self-supported membrane.

3.2.3 *Supported Zeolite Membrane*

This is the most commonly synthesised zeolite membrane. An *in-situ* hydrothermal synthesis process is used in the preparation. This method is direct and can produce good membranes. In this process a thin layer of zeolite is crystallised on the pores of the porous support. Various forms of porous inorganic materials can be used as supports. These include titania, alumina, dense glass, carbon and stainless steel. Crystal growth on the support involves the pre-treatment of the support, preparation of zeolite crystals and the seeding of the crystals . Seeding can be achieved by employing several methods including, rub-coating, dip-coating, vacuum seeding, spin coating and filtration seeding (167). A schematic of the secondary growth method for zeolite membrane preparation is shown in Figure 3-2.

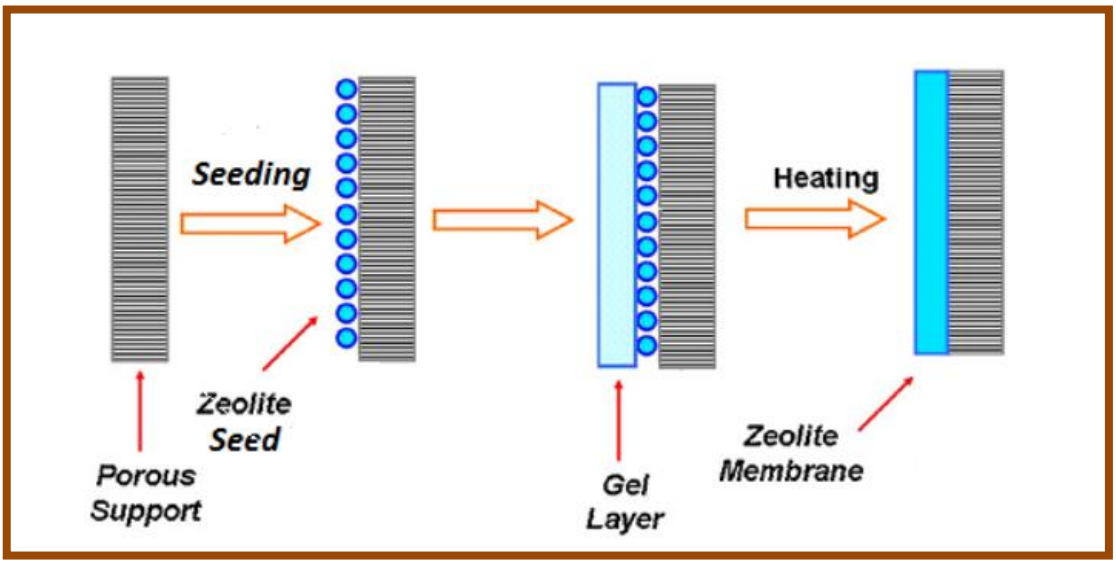

Figure 3-2: Secondary growth method of zeolite preparation adapted from reference 167.

3.3 Zeolite Membrane Characterisation

The morphology of zeolite membranes can be determined using several

techniques. In this work, the thickness and morphology of the zeolite membrane have been determined using SEM. The outer surface and cross-sectional view shows the thickness of the zeolite layer on the support and a top view shows the size and shape of the crystals. EDAX has been used to determine the Si/Al ratio as well as the elemental compositions of zeolite membranes.

Fluorescence confocal optical microscopy is a good instrument for the non-destructive analysis of zeolite membranes. The defects of the membrane and the grain boundary network of the zeolite can be observed along the thickness of the membranes and defects may be clearly visualised (168). N_2 physisorption experiments are typically used to determine the pore volume and porosity of the zeolite powders and membranes. However, this method is difficult to use for supported zeolite membranes, because the supports generally do not fit inside the sample tubes within commercial equipment.

Therefore, in this work, a witness sample of the supported zeolite was used for all characterisation measurements. This is shown in Figure 3-3, alongside a mortar and pestle that was used to further grind the samples. An alternative method for the determination of porosity in thin films is the porosimetry, which allows analysis of the contribution of micropores and defects to the overall flux through the membrane (169).

Figure 3-3: Picture of (a) witness sample for characterisation and (b) mortar and pestle for grinding the sample.

3.4 Zeolite Membrane Reactors

Zeolite membrane reactor concept has been developed for equilibrium-limited reactions, products removal and increased reactant conversion rates. They have been used for the in-situ removal of hydrogen in dehydrogenation reactions. Zeolite membranes having an MFI structure have been used for the conversion of alkanes to olefins. Also, isobutane dehydrogenation has been studied in a membrane reactor combining a platinum/zeolite catalyst and a supported MFI membrane with a tubular configuration (170). The results provide proof that isobutene yield was found to be about four times greater than the values observed when using a normal reactor. Another study of the dehydrogenation of isobutane revealed that the H_2/iso-butane mixture separation factor was close to one at a temperature of about 23 °C and increased to seventy at 500 °C (171). These results can be related to the fact that, at reduced temperature, permeation is controlled by adsorption and the permeate is enriched in i-butane. Diffusion becomes the dominant mechanism when the temperature is increased, this is because the i-butene is adsorbed less. Furthermore, for the various conditions that were considered experimentally, the membrane reactor showed increased isobutane conversion with respect to the conversion obtained using a normal reactor (Figure 3-4).

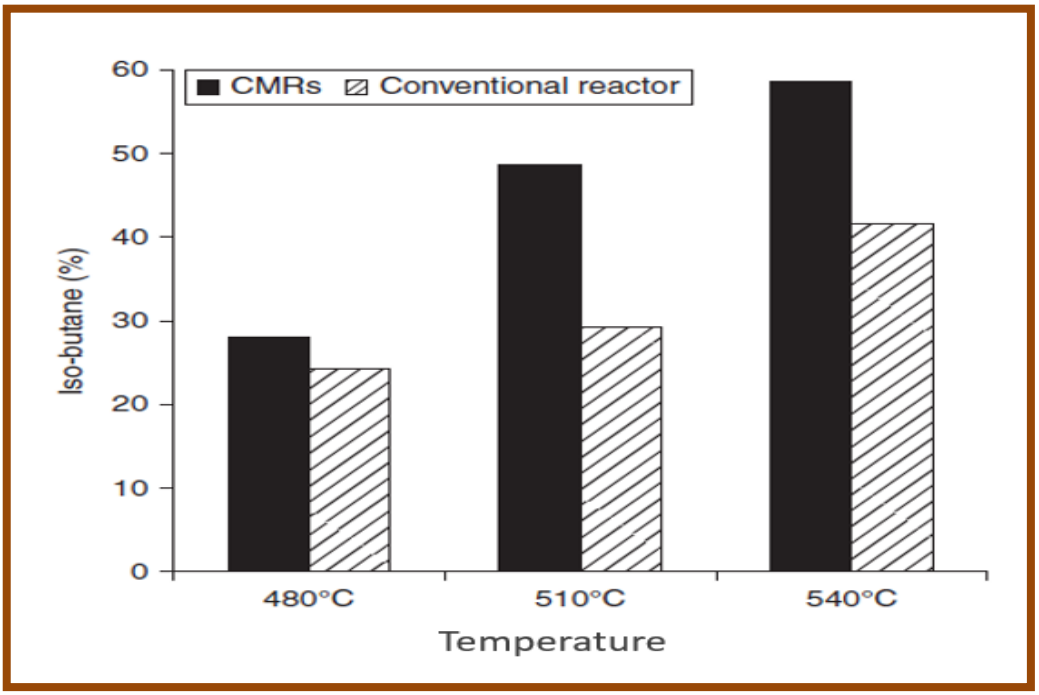

Figure 3-4: Iso-butane conversion to iso-butene with and without H_2 removal. Weight-hourly-space-velocity (WHSV)=0.5 h^{-1}. Adapted from reference 171.

Qi et al. (172) prepared MFI zeolite membranes that contain partial modification of the zeolite channels and are able to obtain a high selectivity and permeance during hydrogen separation following a water gas shift reaction at an elevated temperature. Gu *et al.* (173) have previously modified a zeolite membrane by *in-situ* catalytic cracking of methyl diethoxysilane. The synthesised zeolite membrane showed a H_2/CO_2 permselectivity of 68.3 with a hydrogen permeance of 2.94 × 10^{-7} mol m^{-2} s^{-1} Pa^{-1}. The membrane also presented a high stability in the temperature range 400–550°C. Moreover, the membrane reactor achieved a carbon monoxide conversion of 81.7 % at 550°C. This is higher than that obtained using a PBR.

Fischer–Tropsch synthesis (FTS) allows for the synthesis of liquid hydrocarbons from various feedstocks, including coal and natural gas. The removal of water from this synthetic process is important for the following reasons:

- To increase reactor productivity.
- To reduce deactivation of the catalysts.
- To increase the conversion of CO_2 to long-chain hydrocarbons by shifting the equilibrium of the water gas shift reaction (174).

Different hydrophilic zeolite membranes have been used for the selective removal of water from mixtures of H_2 and CO. For example, ZSM-5 and mordenite membranes have been used for the water removal under normal FTS conditions (175). Mordenite membranes have exhibited increased H_2O fluxes and high permselectivities. An A-type (NaA) zeolite membrane was used to study the permeation of single components of H_2O vapour, CO, H_2, CH_4 and their binary mixtures (176). The permeance of water vapour in the binary mixture is almost close to the value found in the single gases. However, the permeance of each gas component went down with increasing water content. The results obtained can be used to explain how the adsorbed water molecules in the membrane blocks the other gas molecules. On raising the temperature, the amount of water adsorbed in the membrane goes slightly lower and the selectivity for water in the binary mixture reduces.

Zeolite membranes act also as distributors to regulate the number of reactants

added to a catalyst and thus limits side reactions. The use of membrane reactors is also highly relevant for carrying out oxidative dehydrogenation of alkanes to control the oxygen feed, in order to limit total combustion that is highly exothermic (177). Zeolite membranes have also been found to be active for the partial oxidation of propane at 550 °C. Another possible application of these membranes is to use them as an active contactor, which is catalytically active but not necessarily permselective (178). Bernado et al. (179) showed how a catalytic zeolite membrane, with catalytically active particles dispersed in to a thin zeolite layer ensures ultimate contact between reactants and the active site of the catalyst. This reduces by-pass problems that occur in PBR and reduces the pressure drop. The same authors have also studied carbon monoxide selective oxidation (Selox) from hydrogen-rich gas streams using catalytic zeolite membranes.

3.5 Mass Transfer Through a Zeolite Membrane

The process of mass transport through a zeolite layer arises via the five steps listed below (180-181):

1. Adsorption of the substance on the outer surface of the membrane.
2. Mass transport from the outer surface into the zeolite pore.
3. Diffusion of intra-crystalline zeolite.
4. Mass transport out of the zeolite pores to the external surface.
5. Desorption from the outer surface to the bulk.

Adsorption and desorption of species from the outer surface of a zeolite layer depends on the permeation conditions (*i.e.* temperature and pressure), type of crystalline material and the nature of the chemical species. Steps 2, 3 and 4 are usually activated processes (182).

Intra-crystalline permeation through a zeolite membrane can be described using several approaches (183). The Fickian approach considers the concentration gradient as the driving force in a zeolite membrane. Alternatively, the gradient of the thermodynamic potential is the driving force in the Maxwell-Stefan (MS)

approach. The MS approach allows for the approximation of the flux through the membrane for multicomponent gas mixtures by using information about single gas permeations (45). The Fickian approach can be applied for permeation of single gas components through a zeolite membrane at a wide range of temperatures. Moreover, it can be assumed that the total flux N is the combination of the surface flux N_s, which takes place at low to medium temperatures, and the activated gaseous flux N_g, which is prevalent at high temperatures (180, 181, 184). This is given by equation 31:

$$N = N_s + N_g \qquad \textit{Equation 31}$$

Fick's diffusivity D_s is given by equation 32:

$$D_s = D_o \Gamma \qquad \textit{Equation 32}$$

Where D_o is the intrinsic or corrected diffusivity and Γ is the thermodynamic correction factor, which is expressed as:

$$\Gamma = \frac{dlnp_i}{dlnc_i} \qquad \textit{Equation 33}$$

Where P_i and c_i are the pressure and concentration of component i.

The transport diffusivity is dependent on the temperature. This is more apparent at higher temperature. The assumption of an Arrhenius type dependence on temperature can be assumed (45), giving:

$$D_o = \frac{D_g}{RT}\left(\frac{dp}{dz}\right) \qquad \textit{Equation 34}$$

The dependence on temperature will be affected by the adsorption of the component on the zeolite as well as the operating conditions. Moreover, the adsorption phenomena can be negligible at elevated temperatures. Under these conditions molecules can be considered to be in a quasi-gaseous state in the zeolite framework. This is referred to as activated Knudsen diffusion or gas translational diffusion. When this occurs, the flux is expressed as:

$$N_g = -\frac{D_g dp}{RTdz} \qquad \textit{Equation 35}$$

Where dp/dz is the pressure gradient and also the permeance driving force. The diffusion coefficient that is dependent on the gas molecular velocity is given by:

$$D_g = d_p u_m e^{-E_e/RT} \qquad \textit{Equation 36}$$

Where d_p is the pore diameter and u_m is the average velocity.

For ideal gases, kinetic theory can be used to calculate the molecular velocity given by equation 37:

$$u_m = \sqrt{\frac{8RT}{\pi M}} \qquad \textit{Equation 37}$$

From the equations above, it is clear that gas transport through a zeolite membrane is dependent on the adsorptive interaction between the permeating gas molecule and the zeolite. Moreover, the permeating flux is meant to increase with an increase in temperature. This is true for a defect free zeolite membrane. However, Knudsen and viscous flow can contribute to the overall flux and will strongly influence the expected temperature dependence when defects are present (45).

The ramification of predicting the mass transport and separation through synthesised zeolite membranes, where defects of inter-crystalline nature also need to be considered, is evident even though a simple approach has been used. High-selectivity separations can be achieved by using nearly perfect zeolite membranes. In addition to high permselectivity, zeolite membranes should exhibit a high permeation flux in order to be suitable for industrial scale applications. This can be achieved with minimal membrane thickness. Regrettably, decreasing the membrane thickness results in negative effect of inter-crystalline defects on permselectivity and this can be limiting. The thickness of a zeolite layer is dependent on the synthesis routes, conditions and on the number of depositions. For example, White et al. (185) obtained a ZSM-5 membrane by direct *in-situ* crystallisation with a two-step deposition and showed a thickness between 30–40 μm. At laboratory level, zeolite membranes with a thickness of a few microns can be obtained with sufficient quality. Currently there are ongoing investigations to find a way to avoid, reduce or eliminate the presence of inter-crystalline defects, which, aside from poor synthesis reproducibility, are the main obstacle to the widespread industrial application of zeolite membrane. Moreover, if mixtures of gas and vapour having high molecular masses, or liquid mixtures of two species with different volatility and surface tension, are considered, the separation factors and permeation fluxes can be very interesting. However, these separations cannot be extrapolated from the permeances of the pure gases.

3.6 Materials and method

3.6.1 *Materials*

The chemicals, materials and gases used for the experimental work carried out in this chapter are listed as follows:

1. 0.1M sodium hydroxide (NaOH) supplied by Sigma-Aldrich, UK.
2. Aluminium oxide (Al_2O_3) supplied by Sigma-Aldrich, UK.
3. Deionised Water by Purelab Flex, Elga.
4. Gases (Oxygen, Propane, Methane, Nitrogen, Helium, and Carbon dioxide) supplied by BOC, UK.
5. Silicon dioxide (SiO_2) supplied by Sigma-Aldrich, UK.
6. Y-type Zeolite powder supplied by Sigma-Aldrich, UK

3.6.2 *Instrumentation and Equipment*

The instruments and equipment used for the experimental work carried out in this chapter, alongside the respective manufacturers are listed as follows:

1. 15 nm pore size α-alumina support which consists of 77% alumina and 23% TiO_2 and has a permeable length of 348 mm and an internal and external diameter of 7 and 10 mm respectively, supplied by Ceramiques Techniques et Industrielles (CTI), France.
2. Automated gas sorption analyser by Quantachrome instruments
3. Beakers by Fisher Scientific
4. Electric oven by Carbolite
5. Electric water bath by Clifton
6. Energy Dispersive X-ray Detector by Zeiss Instruments
7. Flow meter by Roxspur
8. Hand tools (spanners and screw drivers)
9. Magnetic Stirrer by Fisher Scientific
10. PH meter by Checker
11. Power Regulator by Barnstead Electro thermal
12. Pressure gauge by omega
13. Scanning Electron Microscope by Oxford Instruments

14. Thermocouple by RS
15. Thermometer by Digitron
16. Vernier calliper by Mitutoyo Diamond
17. Weighing Balance by Sartorius
18. Weir 413D

3.6.3 *Zeolite Synthesis*

A y-type zeolite membrane was synthesised by mixing NaOH, Al_2O_3, SiO_2 and deionised H_2O with a molar ratio of $1SiO_2$:$10Al_2O_3$:14NaOH:$798H_2O$. The NaOH and Al_2O_3 were first dissolved in H_2O. This was followed by the addition of SiO_2 and the mixture was agitated with a magnetic stirrer for 24 h at 293.15 K. 2 g of NaX powder was then added. The γ-alumina support, which consists of 77% alumina and 23% TiO_2 and has a permeable length of 348 mm and an internal and external diameter of 7 and 10 mm respectively was subsequently dipped in the resulting sol and kept under magnetic agitation at 343.15 K for 20 h making sure that it was kept central to the measuring cylinder and also vertical. This allowed the solvent to evaporate and resulted in the deposition of y-type zeolite crystals on the support matrix. The resulting membrane was then washed with deionised H_2O until the pH of the wash water was neutral. The membrane was then air dried for 2 h, using a motor powered rotatory drier at room temperature. It was then subjected to thermally treatment at 338.15 K in an oven for 20 h. The α-alumina support was weighed before and after zeolite deposition to determine the amount of zeolite loaded on the support. A schematic of the crystallisation process is shown in Figure 3-5. Moreover, in Figure 3-6 laboratory photos showing the zeolite synthesis process are presented.

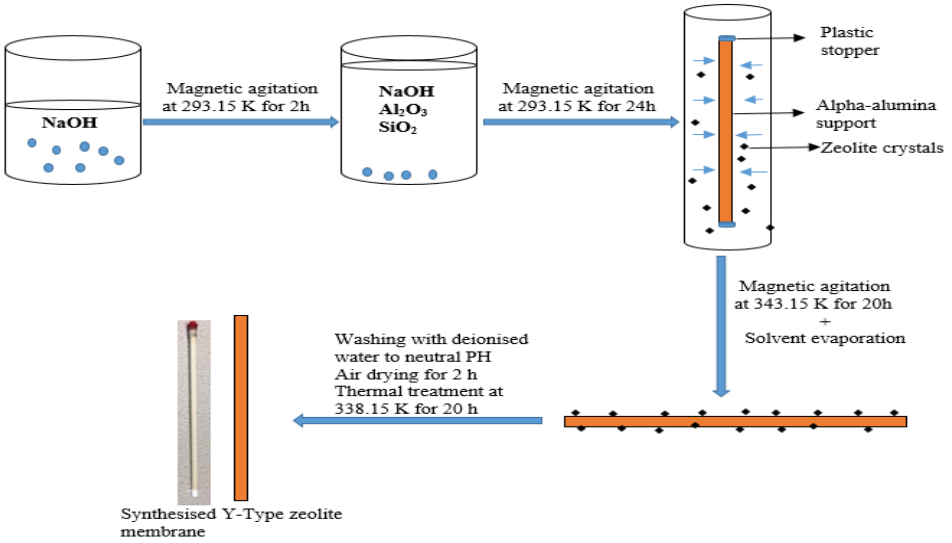

Figure 3-5: Schematic of the solid-state crystallisation route for y-type zeolite synthesis.

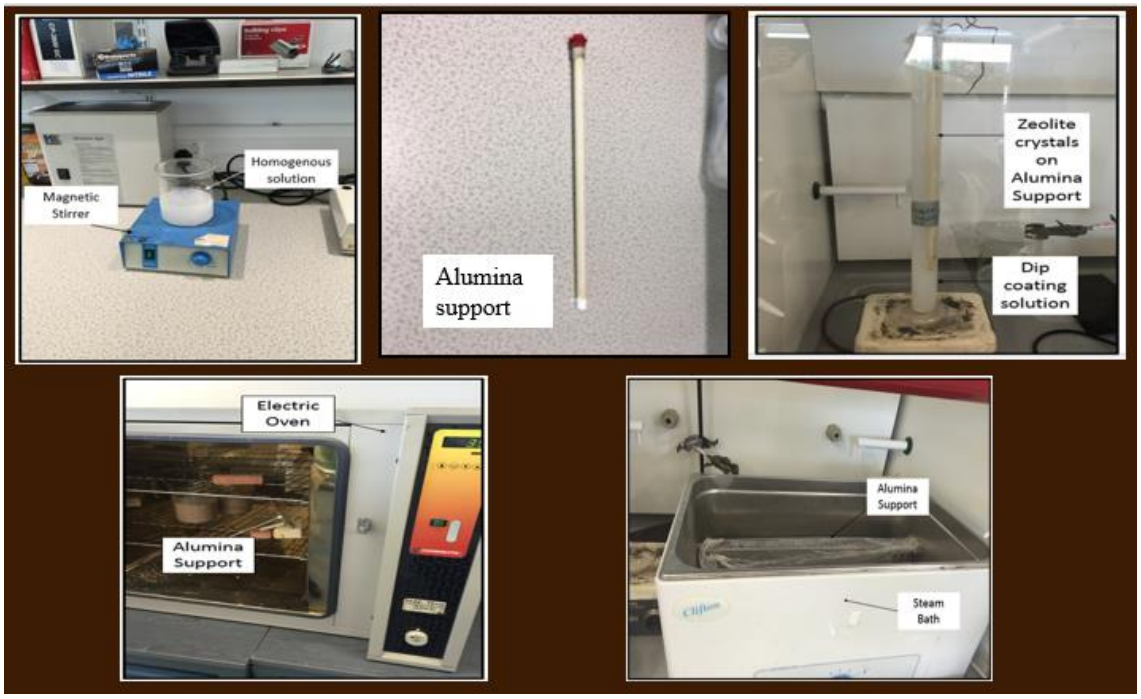

Figure 3-6: Pictures of the zeolite synthesis process.

3.6.4 *Zeolite Membrane Characterisation*

3.6.4.1 SEM and EDAX analysis

SEM and EDAX analyses were carried out using a Zeiss Evo LS10 S with an Oxford Instruments INCA System Energy Dispersive X-Ray analyser. Samples were

prepared by dusting the zeolite powder onto the adhesive side of the sample stub. A silver suspension was added to the prepared sample stub and dried for 24 h. All samples were subsequently sputter coated with a thin gold film to reduce charging effects. The SEM and EDAX images were obtained at a working distance of 8.5 mm.

3.6.4.2 Nitrogen Physisorption Analysis

Nitrogen adsorption/desorption isotherms (BET) were obtained at 77 K on a Quantachrome analyser. Since zeolites are highly porous, have high surface areas and are natural sorbents, they contain a large amount of water and contaminants that are adsorbed from the environment. Therefore, they are degassed at 573.15 K for up to 3 h. The pore size distribution was determined using the Barrett-Joyner-Halenda (BJH) method.

3.6.4.3 FTIR Analysis

Functional groups in the synthesised zeolite membrane were investigated using an ATR Nicolet i S 10 FT-IR spectrometer, in the range 400-4000 cm^{-1}.

3.6.4.4 Gas Permeation Test

The synthesised y-type zeolite membrane was housed inside a stainless-steel reactor and the retentate valves were kept closed. A schematic of the setup used to measure gas permeation is presented in Figure 3-7. This consists of a feed gas delivery system and a pressure gauge, which monitors the pressure in the reactor. Throttling the feed gas via a valve is used to control the flow. Gas permeations have been carried out at various temperatures up to 573.15 K. A digital flow meter was connected downstream of the permeate exit to the membrane reactor and was placed after a pressure gauge in order to measure the flow rate of the gas at standard litre per minute (SLMP).

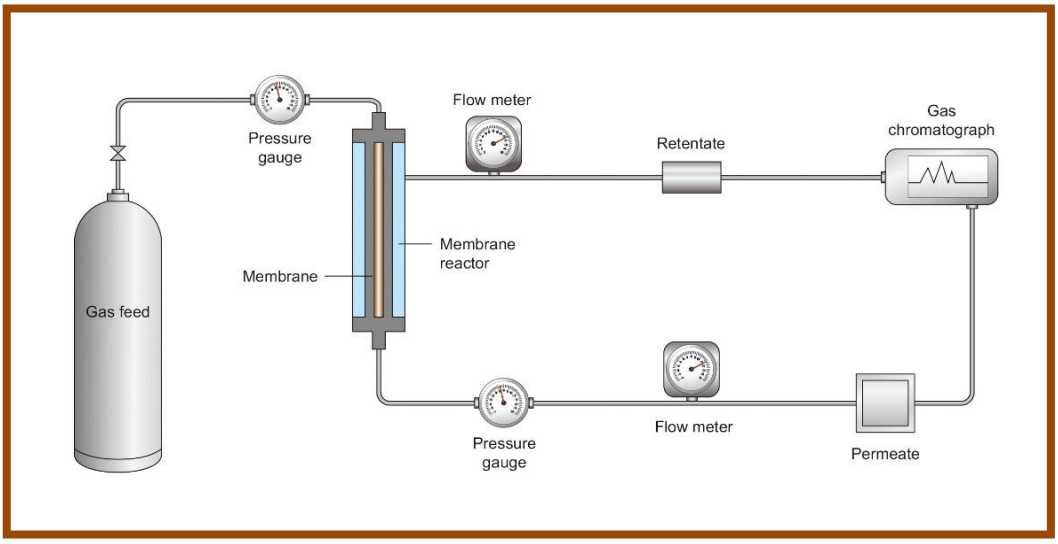

Figure 3-7: Schematic diagram of the gas permeation setup.

3.7 Results and Discussion

3.7.1 *SEM and EDAX Observation of Solid-State Crystallisation Deposition on the Alumina Support*

SEM and EDAX have been carried out for different synthesis conditions to reveal the solid-state crystallisation of the zeolite on the support. Zeolite nanoparticles have been found to have an average size of 0.18 to 3.72 nm (Figures 3-8a and b). Figure 3-8c shows the SEM of a fresh support. Following crystallising in a mixture of sodium, aluminium and silicone oxides for 24 h the membrane revealed zeolite nanoparticles embedded in the matrix of the support (Figure 3-8d). These nanoparticles began aggregating in several locations that had unclear boundaries. Moreover, the nanoparticles have a spherical shape and a uniform particle size. The high magnification SEM image (Figure 3-8b) revealed that the particles could be mesoporous. This has been attributed to the assembly of many nanoparticles of 0.35 to 0.37 nm.

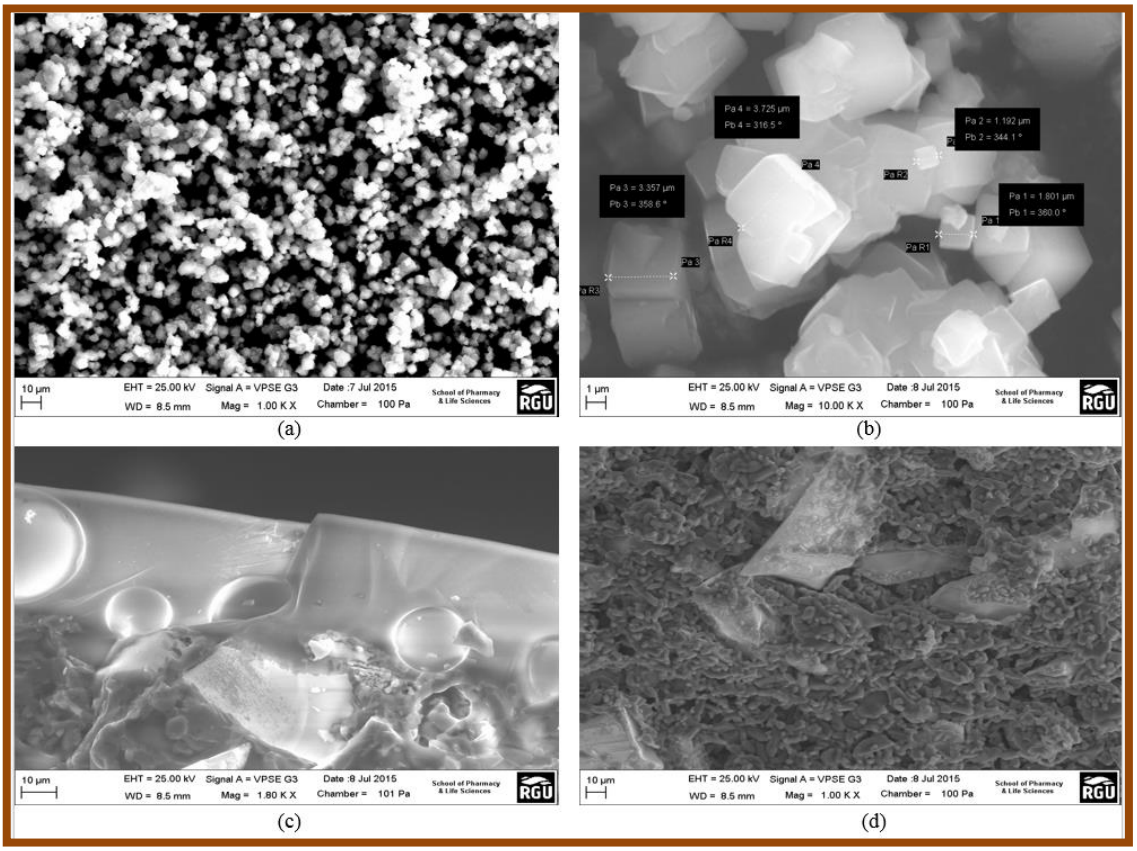

Figure 3-8: SEM of the zeolite particle samples at (a) before deposition (b) higher magnification before deposition (c) 24 h crystallisation (d) alumina support.

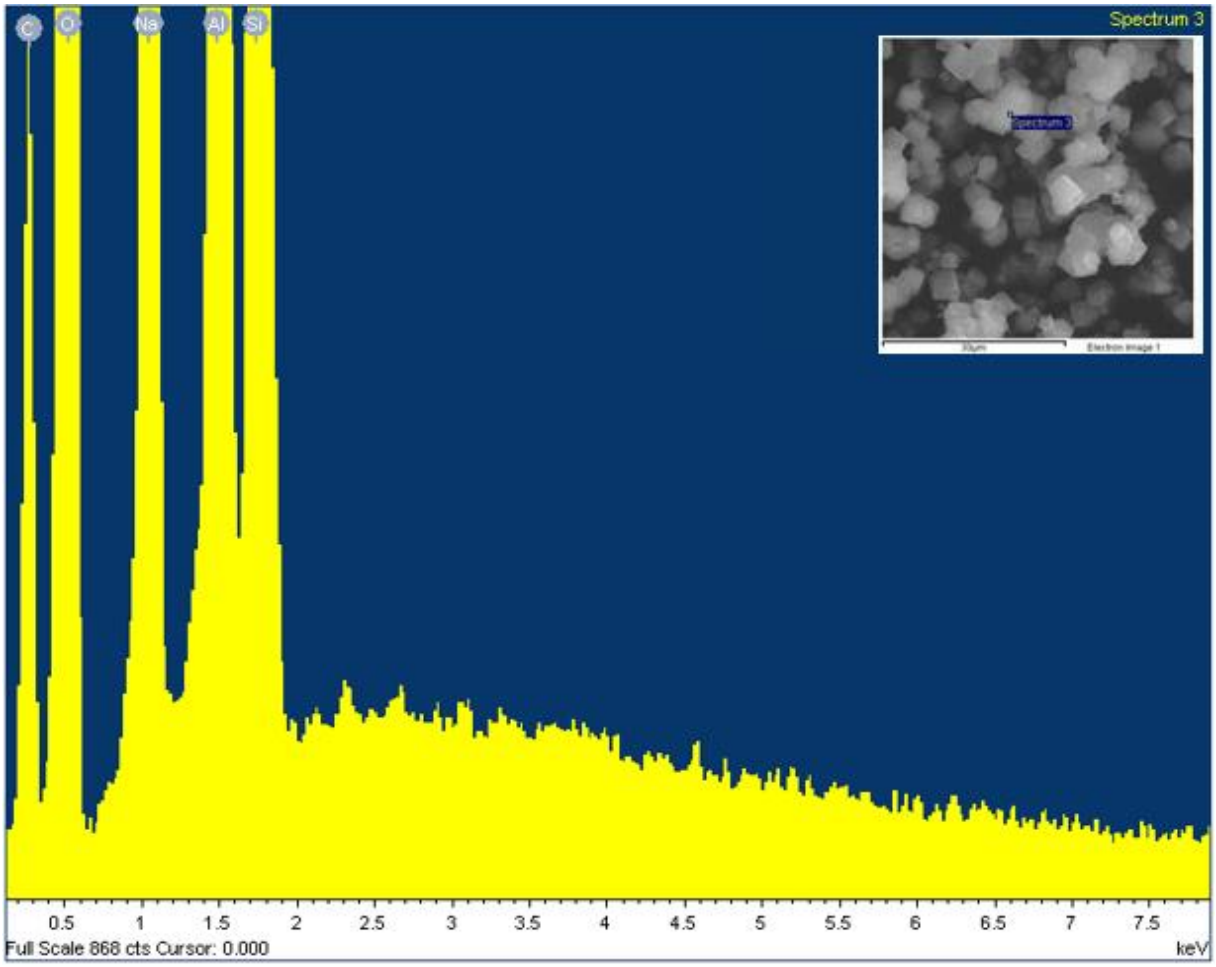

Figure 3-9: EDAX spectrum of zeolite powder before deposition on alumina support.

Figure 3-9 shows an EDAX spectrum for zeolite powder. The EDAX spectrum provides details about the elemental composition of the sample. The results confirm the molecular formula of zeolite to be TO_4, where T is either silicon or/and aluminium. Therefore, the elemental composition indicates that the zeolite powder is made up of tetrahedral units of AlO_4 and SiO_4. The percentage weights of O, Al and Si are 138.04, 34.27 and 37.05 respectively. The percentage weight of Oxygen present is approximately four times that of aluminium and silicon.

In addition, an elemental composition analysis of the y-type zeolite membrane has been determined using EDAX. This is presented in Figure 3-10 and 3-11. The associated data is provided in Table 3.1.

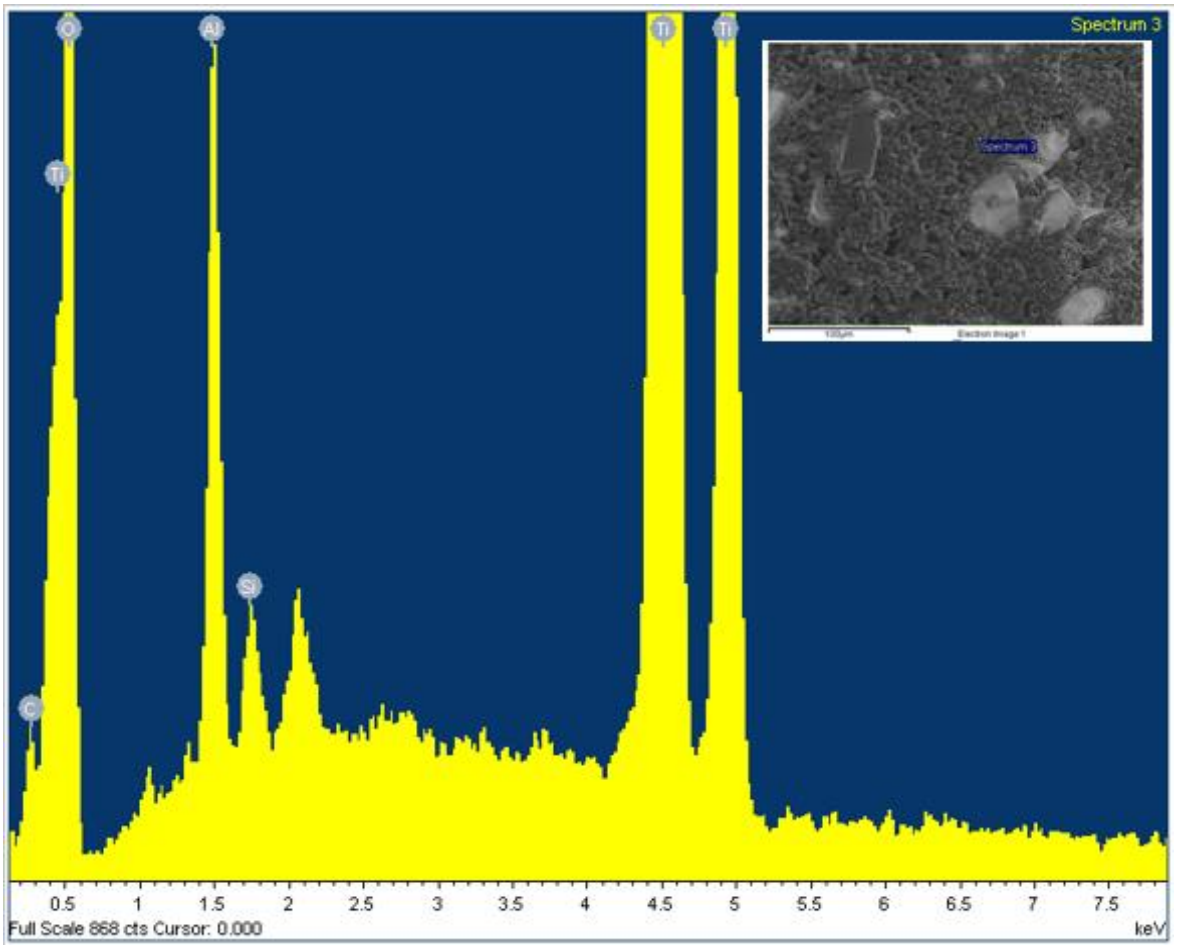

Figure 3-10: EDAX spectrum of y-type zeolite membrane 24 h after deposition.

Table 3.1: Elemental composition of the zeolite powder and the synthesised y-type zeolite membrane.

Element	Zeolite powder weight (%)	Synthesised y-type zeolite membrane weight (%)
C	53.72	3.82
Al	34.27	3.11
O	138.04	53.19
Si	37.05	0.50
Ti	-	60.63
Na	30.46	-

3.7.2 *Nitrogen Physisorption Measurements*

Nitrogen adsorption isotherms of the membrane are shown in Figure 3-11. A summary of the adsorption/desorption data is provided Table 3.2. The pore diameters have been calculated using the Barret-Joyner-Halenda (BJH) model. The BET surface areas for the support and zeolite membranes were found to be 10.69 and 0.106 m^2/g. Zeolites are believed to have large surface areas, however, the synthetic Y-type zeolite has a lower surface area than the support.

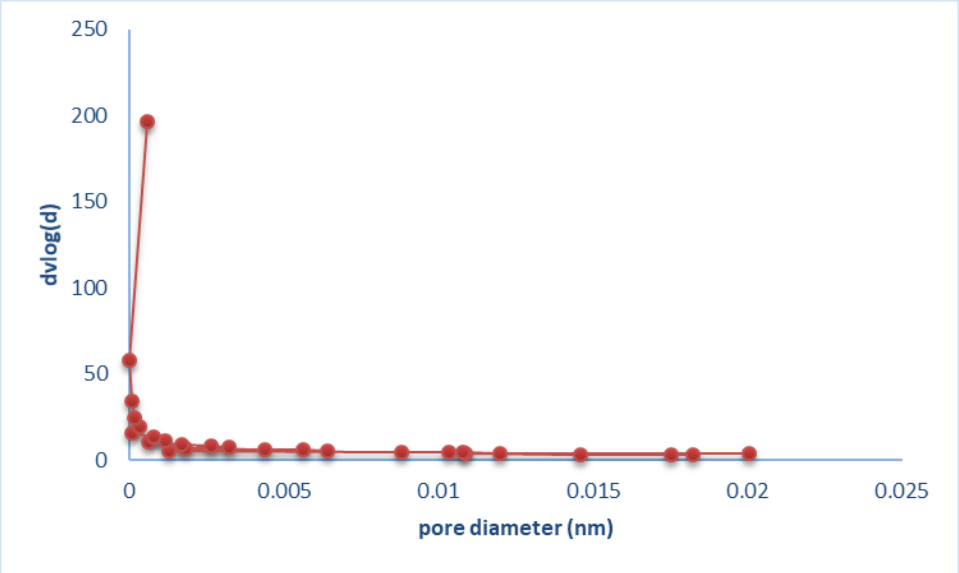

Figure 3-11: Pore-size distribution of zeolite membrane measured by N_2 adsorption/desorption

Table 3.2: BET surface area, average pore diameter and pore volume of the membrane

Membrane	BET surface area (m2/g)	Pore diameter (nm)	Pore volume (cm^3/g)
y-type zeolite membrane	0.106	3.139	0.025

3.7.3 *Gas Permeation*

3.7.3.1 Effects of Temperature on Single Gas Permeation

The single gas permeances for CO_2, N_2, O_2, CH_4 and C_3H_8 have been determined using the gas permeation setup shown in Figure 3-12. The permeate stream has been measured at standard temperature and pressure. The flux of the permeate gas has been measured using a volumetric digital flow meter (L min^{-1}). Gas phase conditions have been employed exclusively in the feed and the permeate sides. Subsequently, single gases were fed into the membrane reactor at a gauge pressure range of 10 to 100 kPa and at temperatures of 293, 373, 473 and 573 K. Data indicating the change in the flux of the gases through the zeolite membrane, as a function of temperature, are presented in Figures 3-13 and 3-14. The flux is shown to be different for each gas. On increasing the temperature from 273 K to 373 K, propane showed an increase of 146 % in its flux, whereas there was only a 17% increase for methane. The extent of the effect of temperature is determined by the adsorption of the component on the zeolite. As observed from Figure 3-13, zeolite has a higher affinity towards methane compared to propane. Moreover, the influence of adsorption is greater than that of temperature. At elevated temperatures, it is likely that adsorption is negligible and the molecules exist in a quasi-gaseous state in the zeolite framework. Diffusion in this state is referred to as activated Knudsen diffusion or gas translational diffusion.

Selectivity is a measure of the ability of a membrane to separate two gases. It is used to determine the purity of the permeate gas and to determine the quantity of product lost. Figure 3-14 shows that C_3H_8/CH_4 selectivity increases from 0.3 at 293 K to 0.9 at 373 K. The higher temperature favours the separation of CH_4 over C_3H_8. However, changes in temperature did not show much significant difference in the separation factors for the CO_2/CH_4 and N_2/CH_4. Moreover, for O_2/CH_4, separation is found to be more favourable at lower temperature (293 K).

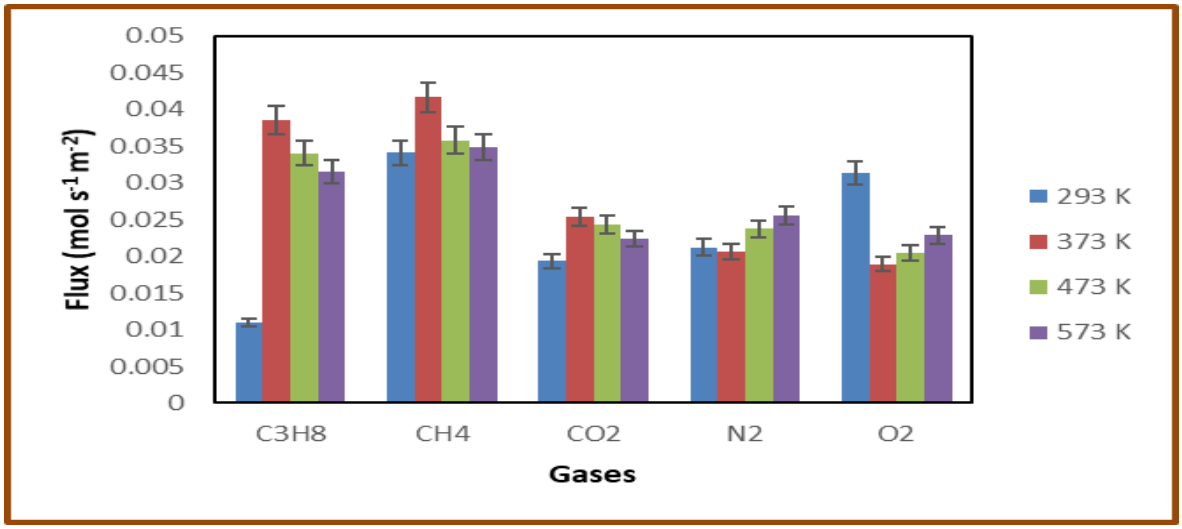

Figure 3-12: Flux of gases with increase in temperature at 1×10^4 *Pa (error bars represent standard deviation at n = 5).*

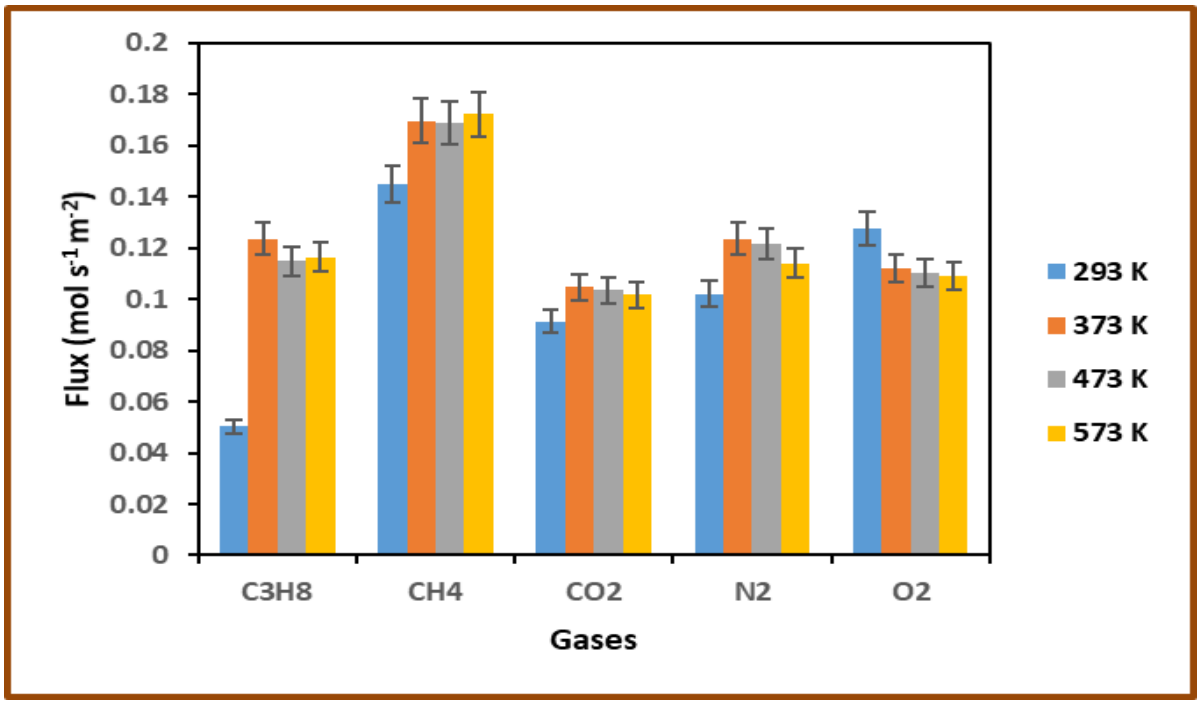

Figure 3-13: Flux of gases with increase in temperature at $1\,x\,10^5$ *Pa (error bars represent standard deviation at n = 5).*

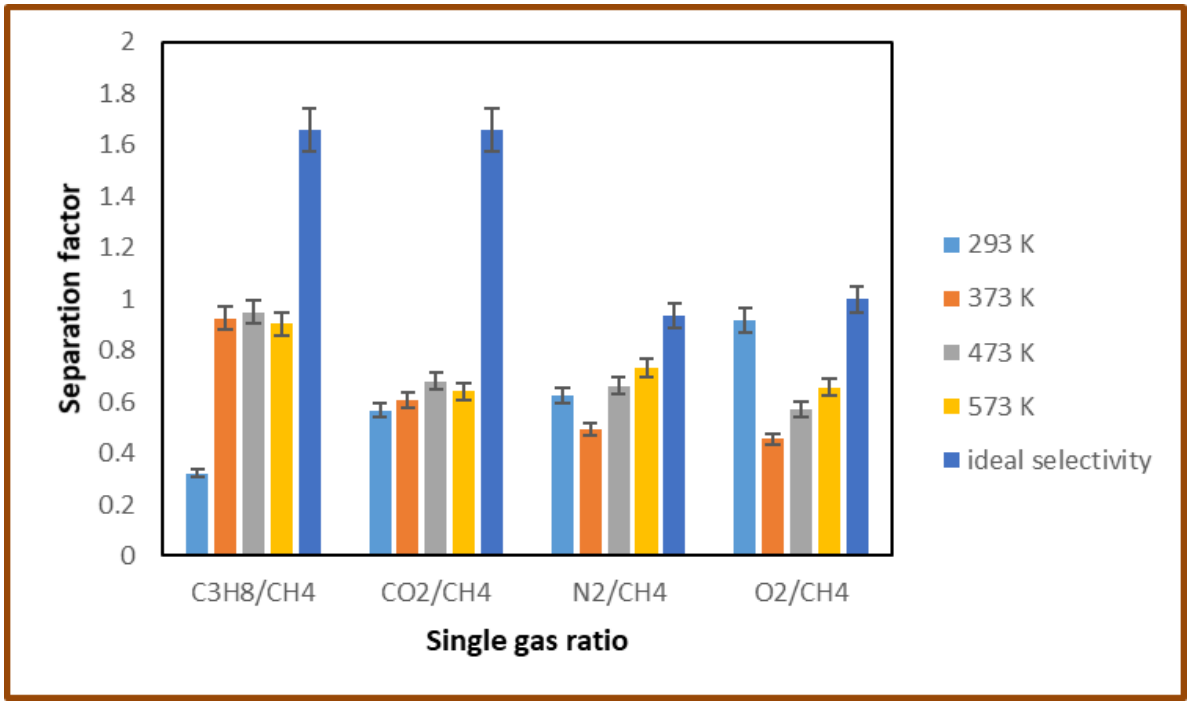

Figure 3-14: Separation factor of gases with increasing temperature (error bars represent standard deviation at n = 5).

The gas flux J through membrane can be written as an Arrhenius dependency equation:

$$J_o = J_\infty exp^{-\Delta E/RT} \qquad \textit{Equation 38}$$

Equation 38 can then be re-written as:

$$lnJ_o = lnJ_\infty - \frac{\Delta E}{RT} \qquad \textit{Equation 39}$$

Where J_o is the flux (mols^{-1}m^{-2}), J_∞ is the Arrhenius-type pre-exponential constant (m^{2}s^{-1}), T is the temperature (K), R is the molar gas constant (8.3144621 Jmol^{-1}K^{-1}), and ΔE is expressed as the activation energy of surface diffusion or heat of adsorption.

Equation 39 is a straight-line equation of the form:

$$y = c - mx \qquad \textit{Equation 40}$$

Therefore, a plot of lnJ_o against $\frac{1}{T}$ can be used to determine the activation energy ΔE. Moreover, a positive slope indicates the heat of adsorption and a negative slope indicates the activation energy of surface diffusion.

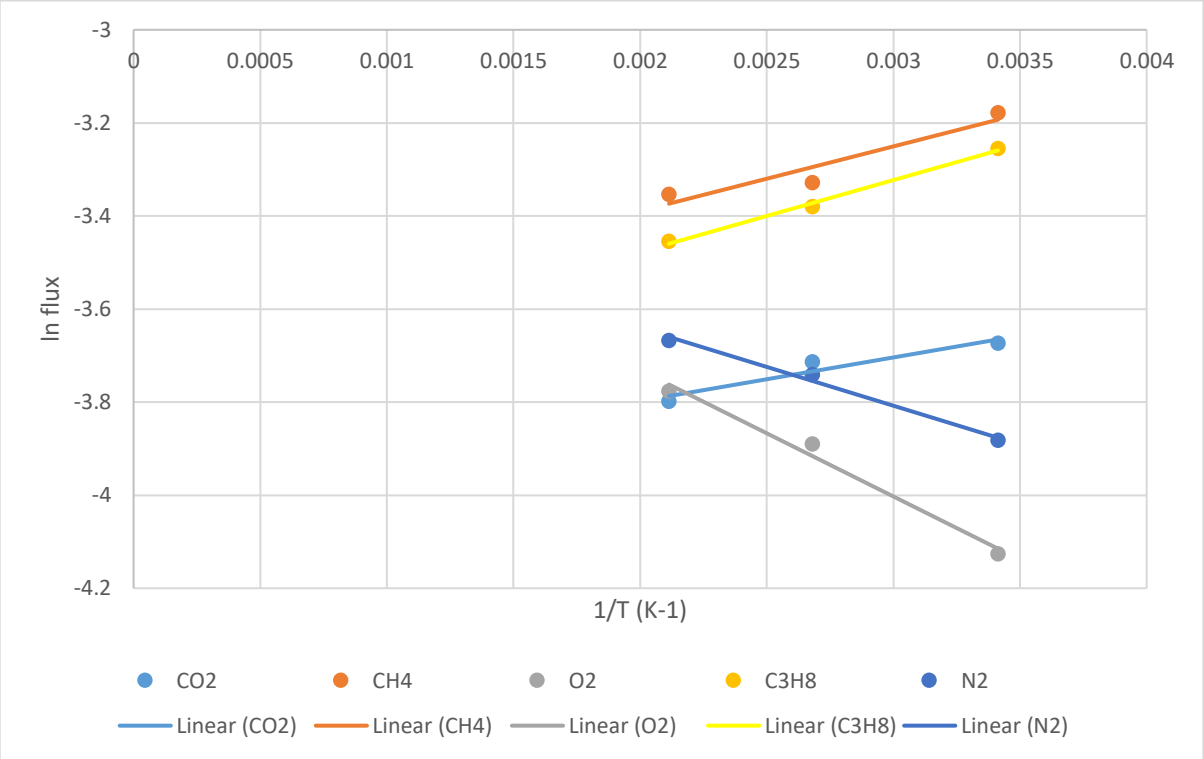

Figure 3-15: Effect of temperature on single gas flux through a zeolite membrane

The fluxes for CO_2, CH_4, O_2, C_3H_8 and N_2 have been determined at 372 K, 473 K and 573 K. Plots of the flux vs. 1/T for each gas are presented in Figures 3-15. These plots have been used to determine the activation energies or heat of adsorption of the gases using equation 39. A summary of the results is presented in Table 3.3.

Table 3.3: Activation energies calculated from flux and temperature dependence

Gas	Activation energy or heat of adsorption ($Jmol^{-1}$)
Carbon dioxide	134.449
Methane	226.7104
Oxygen	-425.592
Propane	239.1156
Nitrogen	-260.742

The activation energy of a gas provides a numerical indicator of the level of resistance offered by the membrane to gas transport. Therefore, the negative value for both oxygen and nitrogen indicates a lower resistance for these gases to pass through the zeolite and support layer. Moreover, the result indicates that

carbon dioxide, methane and propane adsorb on the surface of the zeolite layer. These results coincide with the expected transport mechanism for gases through a zeolite layer.

3.7.3.2 Mixed Gas Permeation using a Gas Chromatogragh Mass Spectrometer (GCMS)

The selectivity of mixed gases (50/50) of CH_4/CO_2, CH_4/N_2 and CH_4/C_3H_8 was determined by the measure of the concentration of feed and permeate gases through the GCMS using equation 7. Details of the GCMS column, carrier gas and operating conditions are given in section 5.6.7. The values calculated for the different binary gas pairs are listed in Table 3.4.

Table 3.4: selectivity of methane through a zeolite membrane at 293 K

	CH_4/CO_2 (1.65)	CH_4/N_2 (1.32)	CH_4/C_3H_8 (1.65)
293 K (mixed gases)	1.3	1.8	2.5
293 K (single gases)	1.1	1.6	3.1

3.7.3.3 Transport Mechanism Determination Using Gas Permeation

It has been previously postulated that the linear proportionality of single gas permeance to the inverse of the square root of the molecular weight of the gases indicates that the mode of transport through the membrane is Knudsen diffusion (158). Figure 3-16 plots the relation between the molar gas flux and the inverse of the square root of the gas molecular weight at 10 kPa guage pressure and 293 K. Based on this plot it can be deduced that the gas molar flux is dependent on the molecular weight as previously reported.

The order of molecular weight is $CH_4 > O_2 > N_2 > CO_2 > C_3H_8$. However, the R^2 value of 0.807 suggests there is a deviation from Knudsen flow mechanism. CO_2

and C_3H_8 have a similar molecular weight of 44.01 g/mol but the molar flux of CO_2 is greater than that of C_3H_8, this could be explained by molecular sieving flow mechanism, as the kinetic diameter of CO_2 (0.38 nm) is lower than that of C_3H_8 (0.43 nm). Figure 3-17 shows the relation between the molar flux and the kinetic diameter of the gases at $1\,x\,10^4$ Pa and 293 K. For gases to flow via a molecular sieving mechanism, the smaller molecules must move with a higher molar flux than the larger molecules. There was a deviation to this mechanism, as the order of kinetic diameter is O_2 > N_2 > CH_4 > CO_2 > C_3H_8. Moreover, CO_2 and C_3H_8 are observed to permeate through the membrane layer based on their size as C_3H_8 has higher size as compared to CO_2.

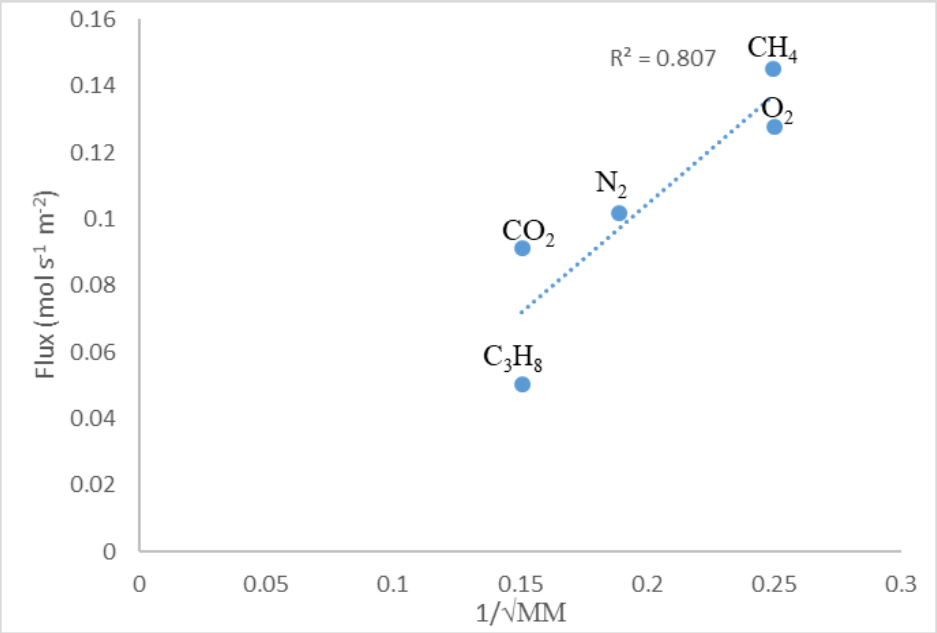

Figure 3-16: Gas molar flux against the inverse square root of molecular weight.

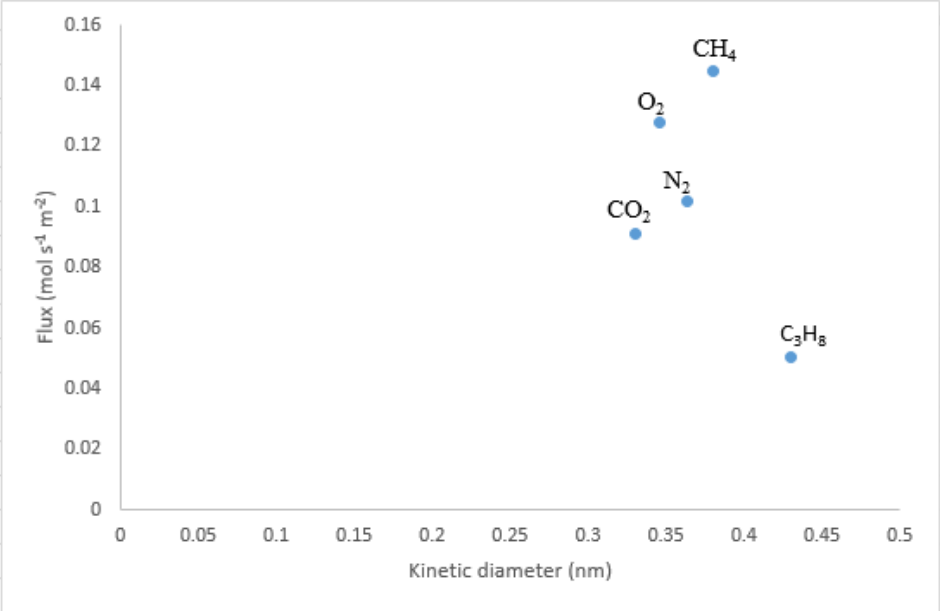

Figure 3-17: Gas molar flux against kinetic diameter of gases.

3.8 Conclusions

An evaluation of the performance of y-type zeolite/γ-alumina membrane for natural gas processing has been carried out for separation ability. The transport of gases through the membrane has been shown to be governed by Knudsen diffusion. However, CO_2 and C_3H_8 have been shown to exhibit a molecular sieving mechanism. N_2 adsorption/desorption showed that at a lower surface area of 0.106 m^2/g, the membrane is more effective at the separation of methane compared to the support. The SEM images revealed asymmetric structure deposition of the zeolite layer. Further investigation using a mixed matrix polyurethane/zeolite membrane for improved membrane performance in the separation of methane from the heavier components of natural gas mixtures, CO_2 and inert gases was carried out.

4 Design and Evaluation of Gas Transport Through a Polyurethane/Zeolite Membrane on an Alumina Support

This chapter looks at the preparation of the nanocomposite polyurethane/zeolite membrane and its gas separation applicability. The use of a polyurethane/zeolite membrane is an approach to improve the module design of gas separation of zeolite membranes. Mixed matrix membranes (MMMs) have lately appeared as hopeful alternatives for gas separation. High permeability and selectivity to CH_4 and CO_2, with good mechanical strength and thermal stability as well as increased separation efficiency is expected of this membrane.

4.1 Introduction

Polyurethane (PU) is a polymer composed of a chain of organic units joined together by urethane links. Whilst most PUs are thermosetting polymers that do not melt when heated, thermoplastic PUs are also available. The properties of PU are greatly influenced by the type of incorporated chemical functionality, *i.e.* isocyanates and polyols.

Materials with high permeance and separation factor for methane and carbon dioxide are required for off-gas separation membrane design. MMMs have recently appeared as promising materials for gas separation, they are based on the addition of small organic molecules or mineral particles such as carbon molecular sieves or zeolites into the matrix of a polymer. Zeolites have an intrinsic ability to absorb molecules and have been considered as ideal materials for gas separation and purification. MMMs are anticipated to have improved gas separation properties due to the combination of the separation properties of both polymers and fillers (186-188).

Tantekin-Ersolmaz et al. (189) have studied the effect of zeolite loading on the separation of *n*-pentane from *i*-pentane. The researchers selected polydimethylsiloxane as the polymer phase and HZSM-5, NaZSM-5, 4A, and 5A as zeolite fillers. Moreover, the results indicated no enhancement on *n*-pentane/i-

pentane ideal selectivity in comparison with pure polymer. An alternative study investigated the gas separation properties of PU membrane by incorporation of TiO_2 nanoparticles, which revealed a decrease in gas permeability together with an increase in gas selectivity (190).

Kim *et al.* (191) investigated the gas permeability of polysulfone with incorporated mesoporous MCM-41 nanoparticles. The authors showed that permeability increased significantly. Moreover, constant ideal gas selectivity was maintained in comparison to the pure polysulfone. Additionally, the surface of mesoporous silica was modified with hydrophobic trimethylsilyl groups. This lead to a significant enhancement of CO_2/CH_4 selectivity through MMMs (191). The morphology and performance of polyethersulfone/polyimide blend membranes for gas separation have also been studied (191). The thickness of the dense layer was found to increase with higher polymer concentrations or lower solvent to nonsolvent ratio, a longer solvent evaporation period prior to quenching in coagulant. This has led to the formation of a membrane, which exhibits high selectivity and low permeability.

An MMM containing polysulfone and nano-ZnO particles has been made from a mixture of solution dispersion blending and phase-inversion (192). Several changes in membrane morphology, surface roughness, and hydrophilicity were observed with the addition of nano-ZnO particles. The resulting membrane was hydrophilic and had a dense surface. This produced a high water flux and an effective permeability barrier. Furthermore, the membrane had the sponge-like structure with uniform and well-interconnecting pores (192).

Li *et al.* (193) investigated the effect of membrane preparation method, zeolite loading, and pore size of zeolite on the gas separation performance of polyethersulfone–zeolite MMMs. The results showed a decrease in permeability with increasing zeolite content. The authors concluded that this phenomenon can be attributed to two hypotheses. The first is that polymer chain rigidification near the zeolite. The second is partial pore blockage of zeolites by the polymer chains. In addition, their results satisfied the molecular sieving mechanism.

Sadeghi et al. (194, 195) have studied gas transport properties of polyimide/polysulfone in the presence of ZSM-5 zeolite. The results of this research revealed a decrease in permeability with an increase in the polyimide concentration

at constant zeolite loading. Moreover, gas separation properties of polyether-based PU–silica nanocomposite membranes have been studied by the same group. Afarani et al. (188) investigated the effect of silica particles on the gas permeation properties of polycaprolactone-based PU membranes. Their results revealed a reduction in permeability of all gases studied coupled with an enhancement in the selectivity of the gases by silica nanoparticles through nanocomposite membranes (188).

In their study, Mohaghehian et al. (196) focused on improving the performance of polymeric membranes via several methods (196). The authors concluded that the addition of silica nanoparticles to the polymer matrix improved the separation performance of CO_2/CH_4 and CO_2/N_2 gases. Furthermore, Bai *et al.* (197) have investigated a nanocrystalline cellulose/ polysulfone composite membrane. This was primed, and the composite membranes were coagulated in different coagulation baths and at different concentrations. The results revealed that the connection of nanocrystalline/polysulfone composite membrane pores are superior to that of pure polysulfone membrane macrovoids. Moreover, short finger-like pores were created with the addition of methanol, ethanol, or isopropanol into the coagulation bath.

Rajesh and Murthy (198) have reported the synthesis and characterisation of an asymmetric ultrafiltration membrane made from polysulfone. The authors used 2,2-methylene-bis (6-tert-butyl-4- ethylphenol) (MBEP) as an additive. The addition of MBEP lead to a membrane with higher thermal stability. The presence of the additive was also shown to affect the surface roughness, membrane morphology, and mechanical strength. Furthermore, the presence of MBEP had a significant effect on the polysulfone– membrane performance. More recently, Tirouni et al. (199) studied the effect of the zeolite particles on the separation of hydrocarbons from methane through PU membranes and it was found that zeolite particles enhance the separation of hydrocarbons from methane through PU membranes.

The main purpose of the research carried out in this chapter is to improve the gas separation properties of PU membranes by incorporating zeolite particles. Moreover, to identify the effect of zeolite pore size on gas separation properties, of PU membranes. The support used is a 15 nm pore size α-alumina support which

consists of 77% alumina and 23% TiO_2 and has a permeable length of 348 mm and an internal and external diameter of 7 and 10 mm. Upon modification, the pore size is expected to decrease. The membrane pore size together with the mean free path of gas molecules are some of the factors that determine the flow mechanism and separation of gas components through a membrane. The choice of membrane material is dependent on the particular application of the membrane. The aim of the work presented in this chapter is to evaluate the performance and effects of zeolite and the polymer mixture on the separation of hydrocarbon gases. This is the first systematic study on hydrocarbon vapour permeance and selectivity properties of a PU/zeolite alumina-based membrane.

4.2 Mixed Matrix Membrane Preparation

Polymer/inorganic membranes can be classified according to their structure (a) polymer/inorganic phases connected by covalent bonds and (b) polymer/inorganic phases connected by van der Waals forces or hydrogen bonds (201). The large difference in properties between the polymer and inorganic materials and strong aggregation of the nanofillers means that polymer–inorganic nanocomposite membranes cannot be prepared using common methods, such as melt blending and roller mixing. The preparation technologies most employed for the fabrication of nanocomposite membranes can be divided into the following three types; namely solution blending, in-situ polymerisation and sol-gel (202).

4.2.1 *Solution Blending*

Solution blending is an easy way of fabricating a polymer/inorganic nanocomposite membrane. The polymer is first dissolved in a solvent to form a solution. Then inorganic nanoparticles are added to the solution and dispersed by stirring. The nanocomposite membrane is cast by removing the solvent. Genne *et al.* (203) previously prepared polysulfone (PSF)/ZrO_2 nanocomposite membranes using 18 wt.% PSF solution in *N*-methylpyrrolidone (NMP). Moreover, various amounts of ZrO_2 nanoparticles were added. The membrane permeability was found to increase as the ZrO_2 weight fraction was increased. In addition, War *et al.* (204) reported the fabrication of cellulose/Al_2O_3 nanocomposite membranes using solution blending. The solution blending method is easy to operate, suitable for all kinds of inorganic materials and the concentrations of the polymer and inorganic

components are easy to control (205). However, a disadvantage of this method is that the inorganic materials are liable to aggregate in the membrane (206).

4.2.2 *In Situ Polymerisation*

In the in-situ polymerisation method, nanoparticles are first mixed with organic monomers and then the monomers are polymerised. There are often several functional groups such as hydroxyls and carboxyls on the surface of the inorganic particles. These can generate initiating cations or anions under high-energy radiation, in plasmas or other circumstances that may initiate the polymerisation of the monomers on the surface. For example, nanocomposite membranes of poly(methacrylic acid) (PMA)/TiO_2 have been synthesised from TiO_2 nano-powder/methacrylic acid dispersions under microwave radiation (207). In the in-situ polymerisation method, inorganic nanoparticles with functional groups can be connected by polymer chains via covalent bonds. However, it is challenging to avoid aggregation of inorganic nanoparticles in the formed membranes.

4.2.3 *Sol-Gel Method*

The sol–gel method is the most widely used preparation technology for nanocomposite membranes. In this method organic monomers, oligomers or polymers, and inorganic nanoparticle precursors are mixed together in solution. The inorganic precursors then hydrolyse and condense into well-dispersed nanoparticles in the polymer matrix. The advantage of this method is that the reaction conditions are moderate – usually room temperature and ambient pressure, and the concentrations of organic and inorganic components are easy to control in the solution. In addition, the organic and inorganic components are dispersed at the molecular or nano level in the membranes. Therefore, the membranes are homogeneous.

4.3 Materials and Methods

4.3.1 *Materials*

The method of Tirouni *et al.* (199) has been adapted and modified for the membrane preparation. The porous ceramic support used in this work (inner diameter 7 mm, outer diameter 10 mm, length 366 mm and a pore size of 15 nm) consisted of a α-alumina support, which was supplied by CTI, France. All chemicals used have been purchased from Sigma-Aldrich, U.K. These include analytical grade SiO_2, Al_2O_3, NaOH, zeolite crystal, poly(tetramethylene glycol) (MW 2000 g/mol), butanediol (MW 90.12 $gmol^{-1}$), hexamethylene diisocyanate, dimethyl formamide and N, N-dimethylacetamide.

4.3.2 *Polymer Synthesis*

The molar ratio of polyol and hexamethyl diisocyanate used was 1:3 as per Tirouni *et al.* (199). The solution was kept at 30 – 40 °C for 2 h under a N_2 atmosphere to obtain macro-diisocyanate. A chain extender, butanediol, was added and the mixture was kept at 20 °C. The molar ratio of the components in the synthesised polymer was 1:3:2.

4.3.3 *Membrane Preparation*

The PU/zeolite membrane has been prepared by dissolving 1 g of zeolite powder in 2.4 mL of dimethyl formamide (10 wt%). This was stirred for 15 min at 20 °C. The resulting solution was then added to the prepared polymer solution. The volumetric ratio of the resulting polymer/zeolite solution was 1:129. The alumina support was then immersed in a zeolite/polymer solution using the dip-coating method. Subsequently, it was left in the solution for 17 h at 60 °C. It was then retrieved and air-dried for 30 min. Finally, it was oven dried for 2 h at 65 °C.

4.4 Results and Discussion

4.4.1 *Characterisation*

4.4.1.1 SEM and EDAX Analysis

The SEM micrograph (Figure 4-1) reveals that polyurethane has been embedded in the pores of the zeolite. This confirms deposition of polyurethane and zeolite on the support. From the micrographs, it can be observed that both the PU and zeolite are bonded on the surface of the alumina support.

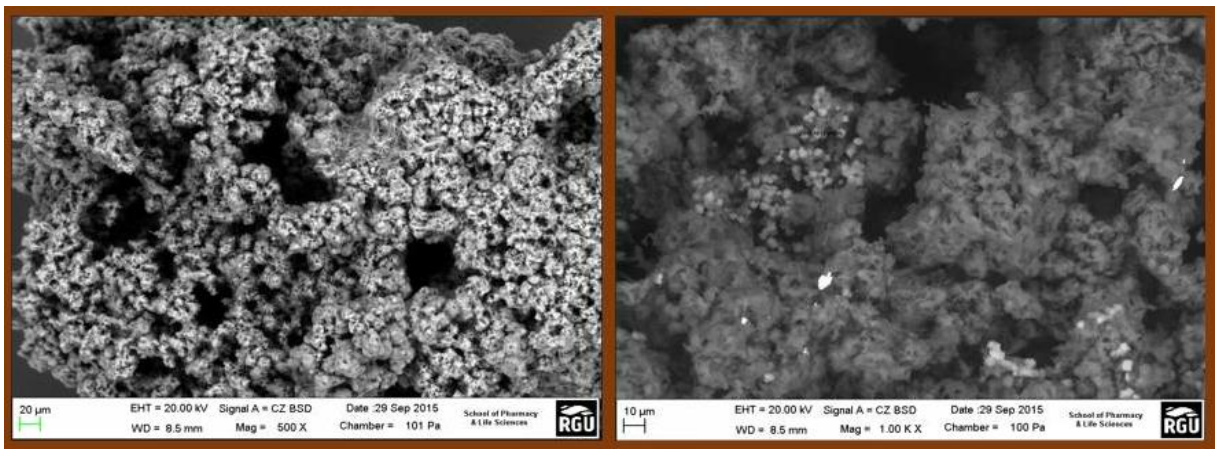

Figure 4-1: SEM micrographs of the polyurethane/zeolite membrane

4.4.1.2 N_2 Desorption/Adsorption Measurements

The pore size of the PU/zeolite membrane has been determined using the BJH method (Figure 4-2). Table 4.1 summarises key data for the PU/zeolite membrane. The pore size is 3.32 nm is close to that of the zeolite membrane, while the surface area is 0.309 m^2/g larger. The increase in the surface area may arise due to the polymer filling the zeolitic pores and this difference should be reflected in the flow and separation of gases through these materials

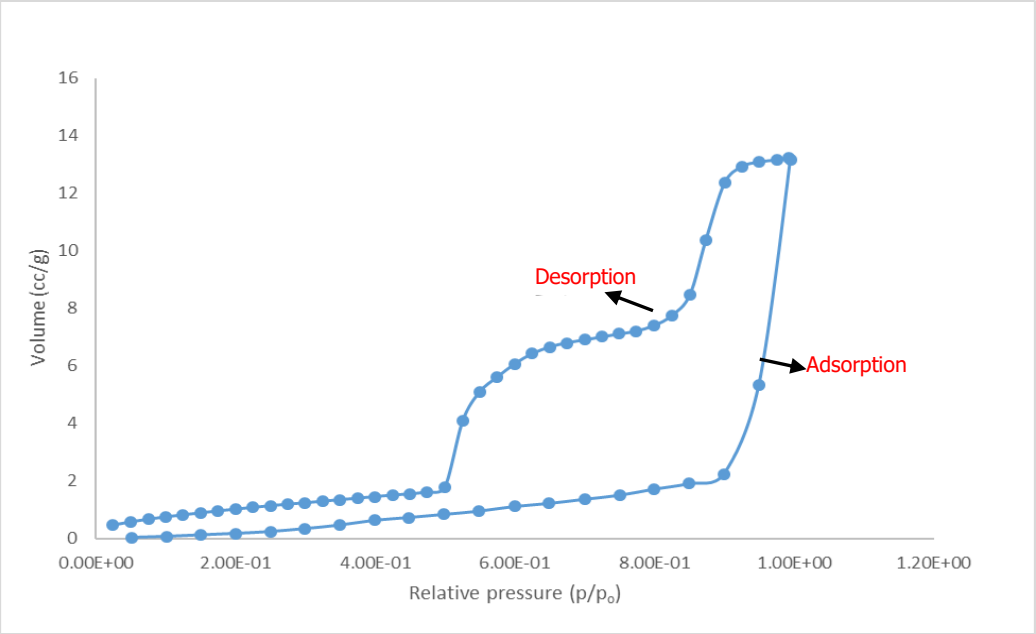

Figure 4-2: Physisorption isotherm for polyurethane/zeolite membrane.

Table 4.1: Pore size and surface area of polyurethane/zeolite membrane.

Parameter	Polyurethane/zeolite membrane
Pore size (x10^{-9} m)	3.32
Specific surface area (m^2/g)	0.31

4.4.1.3 FTIR Analysis

Structural characteristics of the PU/zeolite membrane were determined using FTIR analysis (Figure 4-3). An asymmetric Si-O-Si vibration peak is observed at 1072.2 cm^{-1}. Absorption peaks for the urethane carbonyl group have been found in the region of 1615.65 cm^{-1}. This signal was absent in the zeolite membrane, indicating the presence of the polymer mixture in the zeolite matrix.

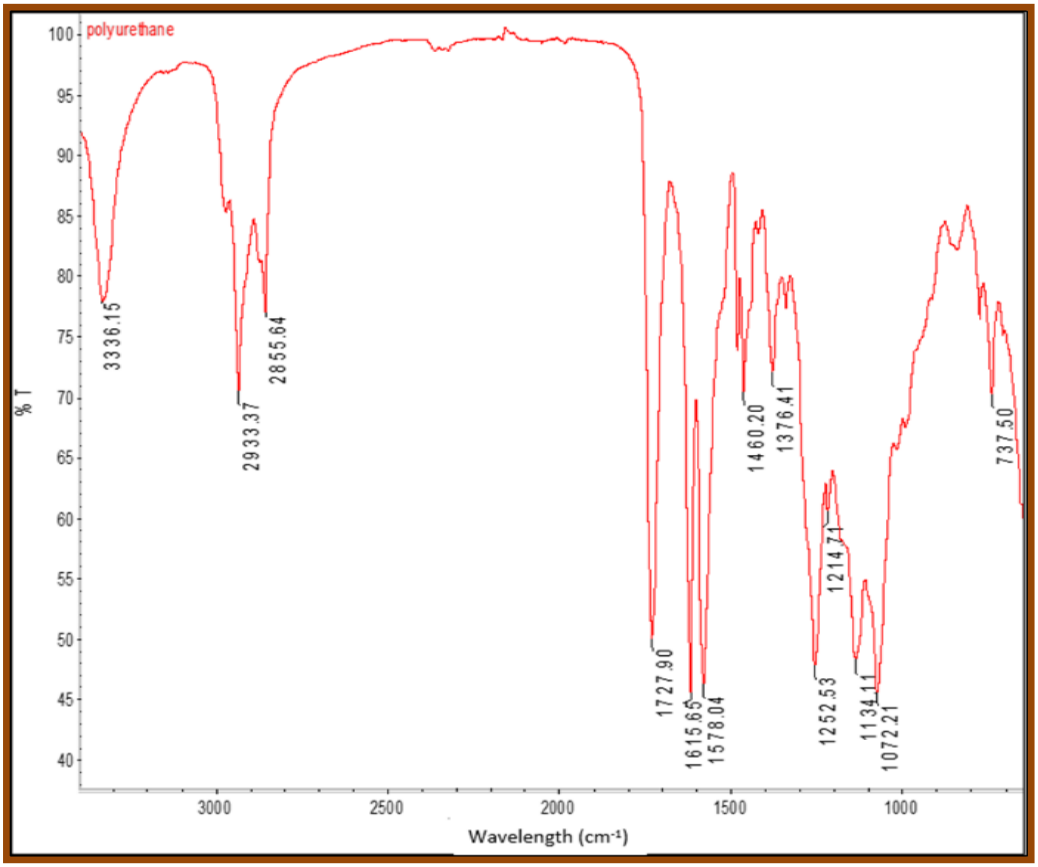

Figure 4-3: FTIR functional groups of the polyurethane/zeolite membrane.

4.5 Gas Transport Through a Polyurethane/Zeolite Membrane

Gases are transported through both polymeric and inorganic phases. Moreover, the zeolite particles can act as molecular sieves within the polymer matrix. The flux and selectivity of the gases through the membrane are expected to increase as the performance of the membrane is increased. The fundamentals of transport through the polymeric layer involve sorption, diffusion and permeation. The driving force for this process is the concentration difference between the two phases, the feed side and the permeate side, which are separated by the membrane. The transport process tries to equalise the concentration difference or the chemical potential between the feed and the permeate side of the membrane. This process is described by Fick's law of diffusion which states that the flux *J* in the direction of flow is proportional to the concentration gradient *(dc/dx)*. This relation is applicable when diffusion is in steady state, *i.e.* the concentrations of the species do not vary with time. Alternatively, Fick's second law describes the unsteady state. This is described by the rate of change of the concentration gradient (d_c/d_t)

at a plane within the membrane and is given by the equation below (200).

$$\frac{d_c}{d_t} = D\left(\frac{d_c^2}{d_x^2}\right) \qquad \textit{Equation 41}$$

Where D is the diffusivity coefficient.

Figure 4-4 reveals that the molar fluxes of the single gases increase with an increase in gauge pressure. Methane is seen to exhibit a higher flux than C_3H_8 and CO_2 at a pressure drop of 1.0 x10^5 Pa. The contribution of viscous flux to the overall mass transfer at higher pressures for the zeolite membrane may have caused this.

The molar fluxes for C_3H_8 and CO_2 are close. This indicates that the PU/zeolite membrane will not be suitable for their separation. A plot of separation factors vs. pressure is shown in Figure 4-5. This graph indicates that the separation factor for CH_4/CO_2 is higher at lower pressure. Moreover, the separation factor for CH_4/C_3H_8 is lower at lower pressures, but subsequently increases as the pressure increases.

PU and zeolite have been successfully embedded on the surface of an alumina support. The molar fluxes for C_3H_8 and CO_2 indicate that this membrane will not be suitable for their separation. This could be because of their identical molar mass (44.1 g mol^{-1}) as the transport mechanism exhibited by these gases through the membrane was based on their molar mass rather than their respective kinetic diameters (0.38 and 0.43 nm).

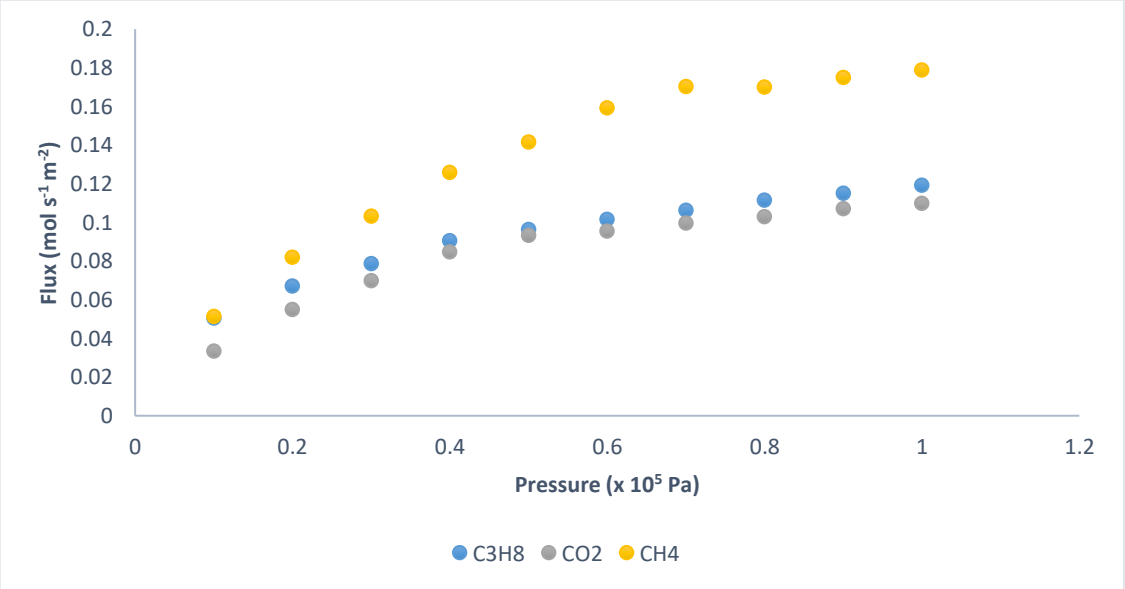

Figure 4-4: Flux of C_3H_8, CO_2 and CH_4 through the polyurethane/zeolite membrane.

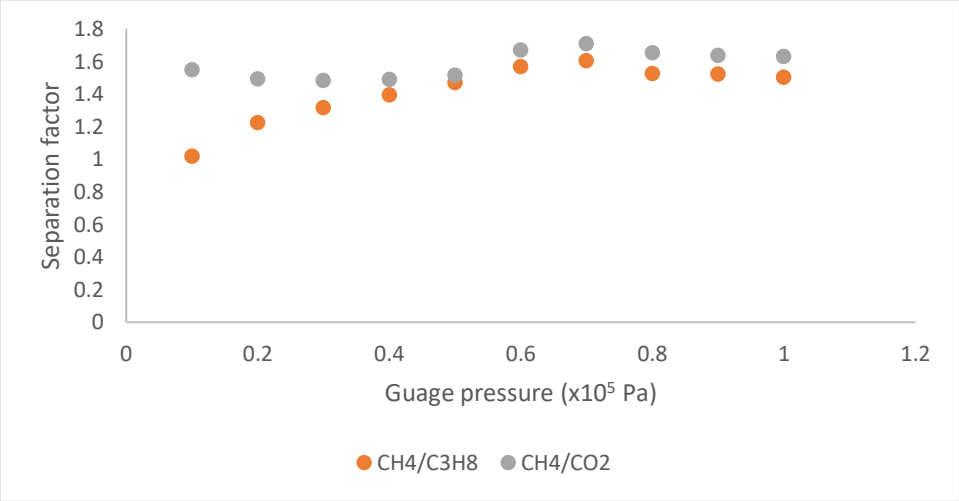

Figure 4-5: Separation factor of CH_4 against C_3H_8 and CO_2.

Methane has been shown to have a higher molar flow rate of 0.179 mol s^{-1} m^{-2} (molar mass 16.04 g mol^{-1}, kinetic diameter 0.37 nm) compared to CO_2 (0.109 mol s^{-1} m^{-2}) at 1 x 10^5 Pa. The addition of PU to the zeolitic pore did not reveal a significant difference in the flux of the gases. This is despite the reduction in the membrane pore size. The results obtained in this chapter were compared with the results from chapter 2 and 3 to determine the best membrane for scale up. The proposed membrane for the utilization of the recovered VOC through methane dry reforming using carbon dioxide is discussed in chapter 5.

5 Design and Evaluation of VOC Utilisation with a Rhodium Membrane impregnated on the Alumina Support

In this chapter a catalyst has been incorporated to utilise greenhouse gases CO_2 and CH_4 that have been separated from off-gases, to form value-added products using methane dry reforming reaction with carbon dioxide. The principle is to have an advanced catalytic membrane reactor that can perform high CH_4 and CO_2 conversions in one unit. The products expected from this reaction are H_2 and CO, which form the base for the production of ammonia, methanol, and long-chain hydrocarbons via Fischer-Tropsch synthesis. The catalyst employed was the noble metal rhodium that was loaded on a gamma-alumina membrane support with a loading percent of 0.52 %. The effect of temperature, molar gas flow rate through the membrane reactor and the stability of the membrane when exposed to impurities like nitrous oxide has been studied. Temperature has been found to have more effect on the reaction rate than the molar flow rate of the gases.

5.1 Introduction

The methane dry reforming reaction is highly endothermic and is catalysed by transition metals supported on various oxides and the mechanism has been previously studied (208-210). The rate-limiting step of the process has been shown to be the C-H bond activation of methane, which occurs on the transition metal (208). For the C-O bond in CO_2, the acidity or basicity of the oxide determines where the activation occurs. For a neutral support, activation occurs on the metal (210). A further challenge with dry reforming of methane is the deactivation of the catalyst due to carbon poisoning. It has been suggested that the deactivation of the metal catalyst is more pronounced in the case when metals are supported on neutral supports, as both the C-H bond activation in methane and C-O bond activation in CO_2 are thought to occur on the metal surface.

The use of basic supports like CeO_2 and La_2O_3 has been shown to minimise carbon formation by facilitating dissociation of CO_2. This occurs via low-energy barriers through the formation of oxy-carbonates that provide surface oxygen atoms, which

facilitates the removal of surface carbon atoms formed during C-H bond activation in methane (127, 210). An additional approach to suppress carbon formation is to synthesise very small metal particles that are well dispersed on the support. A minimum metal particle size is required for the formation of extended carbon structures. Therefore, synthesising very small, well-dispersed metal particles destabilises the formation of extended carbon structures and enhances the interaction between the support and the metal, increasing the probability of O atoms, formed from CO_2 dissociation on the support, to oxidise C atoms on the metal which have been formed from methane dissociation (209). While there have been many attempts to minimise carbon formation through the routes discussed above, industrial implementation of the process remains a significant challenge.

Rhodium catalyst have been deposited on an alumina porous tubular support using rhodium (III) chloride precursor and incorporated into a shell and tube membrane reactor to measure conversion yield of CH_4 and CO_2. The main assumption in this work is that the reaction of feed gases produces a mixture consisting of CO, O_2, H_2, H_2O and solid carbon (C). The effect of temperature and feed flow rate was studied to determine the yield of syngas produced. Results showed that temperature has a greater effect on the conversion rate than the feed gas flowrate.

5.2 Dry Reforming Technology

The development of a stable CH_4 dry reforming technology is important from an environmental and economical point of view. Aside from GHG utilisation, the reaction is a more favourable route for the production of syngas with low H_2:CO ratios which has been shown to be well suited for use in gas-to-liquid production. Syngas is normally produced by methane steam reforming or partial oxidation of methane. This results in high H_2:CO ratios. However, synthesis required for methanol and long-chain liquid hydrocarbons via the Fischer-Tropsch process needs a low H_2:CO ratio as the starting feedstock. Consequently, methane dry reforming reaction is a more desired route to generate low H_2:CO syngas ratios. In addition, the reaction is highly endothermic which makes it suitable to store abundant thermal solar or nuclear energy as chemical energy in chemical energy transmission systems (CETS) (211). Under the CETS scheme, thermal energy from fossil fuel, solar or nuclear sources is used to achieve equilibrium of a reversible

endothermic reforming reaction. The products can be stored or can be used as feedstock for various processes. However, when energy is required the reverse exothermic reaction can be driven to equilibrium hence, producing heat. The exothermic reaction products can then be recycled back to the original reactor to be reformed through the use of the thermal energy source. This process, when conducted with methane steam reforming reaction is known as the Eva-Adam process (211). However, dry reforming is more endothermic, and will be more favourable to CETS. The major disadvantage of the dry reforming reaction is the thermodynamic tendency for the formation of coke during the reaction process, which leads to the deactivation of the catalyst. In this study, a stability test with the Rh/g-AlO_3 catalytic membrane reactor has addressed the problem of coke formation due to continual removal of product and water from the reaction stream.

Rh catalysts on various supports have been investigated for use in CH_4 dissociation, CO_2 dissociation, and the dry reforming reaction (129). The dissociation of CH_4 on Rh was observed at 423 K, producing H_2 and small amounts of C_2H_6. The intermediate species is CH_3, which can rapidly decompose to form surface carbon and hydrogen atoms. For the decomposition of CH_4, Al_2O_3 was shown to be the best support for Rh, followed by TiO_2, MgO, and SiO_2. The same study showed that CO_2 dissociation was promoted by the addition of CH_4 and the H_2 formed from CH_4 decomposition promotes CO_2 dissociation. Erdohelyi *et al.* (129) suggested that adsorbed O, which is formed from the CO_2 decomposition facilitates CH_4 dissociation. This contradicts the findings of Rostrup-Nielsen, which showed that oxygen atoms only affected CH_4 chemisorption and activation by restricting the number of available sites on Ni catalysts and also showed that the rate of carbon aging from reactive carbidic carbon to amorphous carbon to graphite increases with increasing temperature. However, no deactivation of the Rh catalysts was found in the dry reforming studies they concluded. This indicates that the formed surface carbon reacted before stable amorphous or graphitic carbon was formed. Furthermore, the ratio of H_2:CO was found to be greater than one, indicating the occurrence of secondary processes.

5.3 Thermodynamics of Methane Dry Reforming Process

Several side reactions are known to occur simultaneously with the dry reforming

reaction. These may lead to coke formation or change the amount of species being produced. A possible side reaction is the reverse of the water-gas-shift (WGS). The water-gas-shift reaction is given in equation 42:

$$CO + H_2O \rightleftharpoons CO_2 + H_2 \qquad \textit{Equation 42}$$

Other side reactions that can occur and result in coke formation are shown below:

$$2CO \rightleftharpoons C + CO_2 \qquad \textit{Equation 43}$$

$$CO + H_2 \rightleftharpoons C + H_2O \qquad \textit{Equation 44}$$

$$CH_4 \rightleftharpoons C + 2H_2 \qquad \textit{Equation 45}$$

Equation 43 shows CO disproportionation, while equation 44 indicates CO reduction and equation 45 shows the decomposition of CH_4. To understand the conditions at which these reactions to occur, the Gibbs free energy has been determined. Taking the change in Gibbs energy $\Delta G < 0$ to predict thermodynamic favourability for the forward reaction to occur, the dry reforming reaction has been determined to not be favoured below 650 °C. Moreover, the WGS reaction is favoured up to 825 °C. Above this temperature the reverse reaction is favourable. However, because of the low magnitude of ΔG for the WGS, the presence of either product or reactant species could shift the reaction in either direction. CO disproportionation and CO reduction reactions have been determined to be favoured at temperatures up to 700 °C and 675 °C respectively. Moreover, CH_4 decomposition becomes favourable at temperatures above 550 °C. In the temperature range of 550 to 675 °C, deposition of carbon is favoured by disproportionation of CO, decomposition reactions of CH_4 and CO reduction. In this region, severe coking is expected.

Fischer and Tropsch conducted the first comprehensive dry reforming experiments in 1928 (212). They studied the reaction over iron, cobalt, nickel, copper, molybdenum and tungsten catalyst supported on clay, silica and $MgCO_3$ or and $MgCO_3/Al_2O_3$ mixes. Compositions of the gases produced were determined by thermodynamic calculations and Ni and Co were found to be the preferred catalysts with activity increasing with loading of Al_2O_3. Moreover, Bodrov *et al.* (213), found that the kinetics for dry reforming over a Ni film matched the kinetic model that Fischer and Tropsch had constructed from a study of steam reforming (213).

Recently, Wei and Iglesia (214) conducted studies of CO_2 and H_2O reforming of

methane over Rh/Al_2O_3 and Rh/ZrO_2 catalyst and measured the forward rates and activation energies for CO_2 and H_2O methane reforming. The forward CH_4 reaction rates were found to be affected by CH_4 pressures but were unaffected by the concentration of the reactants or products at 600 °C. The forward rates were calculated using equation 46 by correcting measured net rates for approach to equilibrium ŋ:

$$ŋ = \frac{[P_{CO}]^2 \left[P_{H_2}\right]^2}{[P_{CH_4}][P_{CO_2}]} \times \frac{1}{K_{eq}} \qquad \textit{Equation 46}$$

Where K_{eq} is the equilibrium constant at a given temperature and P is the prevalent partial pressures of each species. The forward rate, r_f, was given in terms of the net rate r_n, shown in equation 52.

$$r_f = \frac{r_n}{1-ŋ} \qquad \textit{Equation 47}$$

The authors also found out that the concentration of reactants influenced net rates. However, the effects disappeared when the thermodynamic reactions were considered, and the experimental net rates were converted to the forward reaction rates. The forward CO_2 rates increase linearly with increases in CH_4 partial pressures, but were found to be independent of CO_2 pressures.

5.4 Reaction Mechanism for Methane Dry Reforming Process

The reaction mechanism for the dry methane reforming reaction depends on the type of catalyst used, and the nature of the support. However, most mechanisms that have been proposed are based on the Langmuir-Hinshelwood-Hougen-Watson (LHHW) kinetic models, where one reaction is assumed to be slow and is rate determining, while the others are at thermodynamic equilibrium (215). The main steps involved in dry reforming of methane are methane and carbon dioxide dissociation, followed by adsorption of intermediates on the catalyst active sites which leads to the formation of the products CO, H_2 and H_2O. These are eventually desorbed.

5.4.1 *Methane Activation*

The adsorption and activation of methane is the most significant step kinetically in dry methane reforming reaction. CH_4 dissociates directly on the active metal site

(216) forming carbon, CH_x radicals and hydrogen atoms (217-219), as shown in equations 53-56.

$$CH_{4(g)} \rightleftharpoons CH_3 + H \qquad \textit{Equation 48}$$

$$CH_3 \rightleftharpoons CH_2 + H \qquad \textit{Equation 49}$$

$$CH_2 \rightleftharpoons CH + H \qquad \textit{Equation 50}$$

$$CH \rightleftharpoons C + H \qquad \textit{Equation 51}$$

While the activation of methane is generally postulated to occur on the metal sites, Zhang *et al.* (220) have found that when Ni was supported on an acidic support (Al_2O_3), as compared to the basic support like La_2O_3, the conversion of CH_4 is higher. This is due to the acid sites of the alumina support that promotes the breaking of methane to carbon species. However, a drop in activity due to the higher amount of carbon deposition on the alumina support has been reported. Moreover, Nielsen and Hansen (209) reported that there is the possibility of formation of three types of carbon species during the reforming process. These include,

- Encapsulating amorphous carbon formed via polymerisation at temperatures below 773 K.
- Pyrolytic carbon nanotubes formed from methane cracking at temperatures greater than 873 K.
- Whisker-type carbon (formation temperature above 723 K).

The reaction temperature has been found to determine the type of carbon that is formed. As the reactions in this work have been carried out at temperatures above 873 K, the formation of carbon on the membrane was expected.

Wei and Iglesia (221) have used isotopic and kinetic investigations to examine the reaction mechanism over Ni/MgO catalyst. The authors observed similar first-order rate constant and turnover rate for decomposition of methane. They concluded that methane dissociation is a relevant step kinetically for the dry methane reforming reaction and that the behaviour of Ni catalyst is similar to that of supported noble metal catalysts (*i.e.* Rh, Ru, Ir and Pt). Ferreira-Aparicio *et al.* (222), suggested that the formation of methoxo (CH_xO) species is aided by the availability of surface oxygen species from hydroxyls that is from the acidic supports. The FTIR spectroscopy analysis of methane adsorption on alumina was

observed by Li *et al.* (223), it showed the presence of two hydroxyl signals at 3750 cm^{-1} and 3665 cm^{-1}, which shifted to 3707 cm^{-1} and 3640 cm^{-1} with the adsorption of methane. These results predict the occurrence of weak interaction of surface hydroxyls with methane, a phenomenon also observed with iridium catalysts during decomposition of methane (224).

5.4.2 *Carbon Dioxide Activation*

CO_2 dissociation depends on the type of the catalyst support. An acidic or inert support (*e.g* SiO_2) causes CO_2 chemisorption and dissociation to occur on the surface of a transition metal and is dominated by electron transfer, which requires the formation of an anionic CO_2^- precursor (133) as depicted in equations 52 and 53.

$$CO_{2(g)} \rightleftharpoons CO_{2(a)} \qquad \textit{Equation 52}$$

$$CO_{2(a)} \rightleftharpoons CO_{(a)} + O_{(a)} \qquad \textit{Equation 53}$$

The adsorbed O atoms, from the CO_2 dissociation, then react with either the methyl radicals or adsorbed H atoms as shown in equations 54 – 58.

$$CH_{x(a)} + O_{(a)} \rightarrow CO_{(a)} + xH_{(a)} \qquad \textit{Equation 54}$$

$$H_{(a)} + O_{(a)} \rightleftharpoons OH_{(a)} \qquad \textit{Equation 55}$$

$$H_{(a)} + OH_{(a)} \rightleftharpoons H_2O_{(a)} \qquad \textit{Equation 56}$$

$$2H_{(a)} \rightarrow H_{2(g)} \qquad \textit{Equation 57}$$

$$CO_{(a)} \rightarrow CO_{(g)} \qquad \textit{Equation 58}$$

There is a limit to CO adsorption because of the availability of the active metal site. This leads to large accumulation of carbon deposits, that can gradually lead to catalyst deactivation. In the presence of a basic support like La_2O_3, CO_2 can easily be activated on these sites, forming an oxycarbonate.

5.5 Membrane Reaction Design

In this research, supported tubular membranes consisting of a γ-alumina support with thin silica, zeolite, polyurethane/zeolite and rhodium layer as porous supports have been used and are shown in Figure 5-1. The material used determines the function of the membrane.

Figure 5-1: pictures of (a) zeolite/γ-alumina membrane, (b) un-activated Rh/ γ-alumina membrane, (c) SiO_2/ γ-alumina membrane and (d) activated Rh/ γ-alumina membrane

The membranes in a membrane reactor can be designed to carry out the following functions:

The membranes used in this research have been housed in stainless-steel tubing (Figure 5-2), which have the following dimensions:

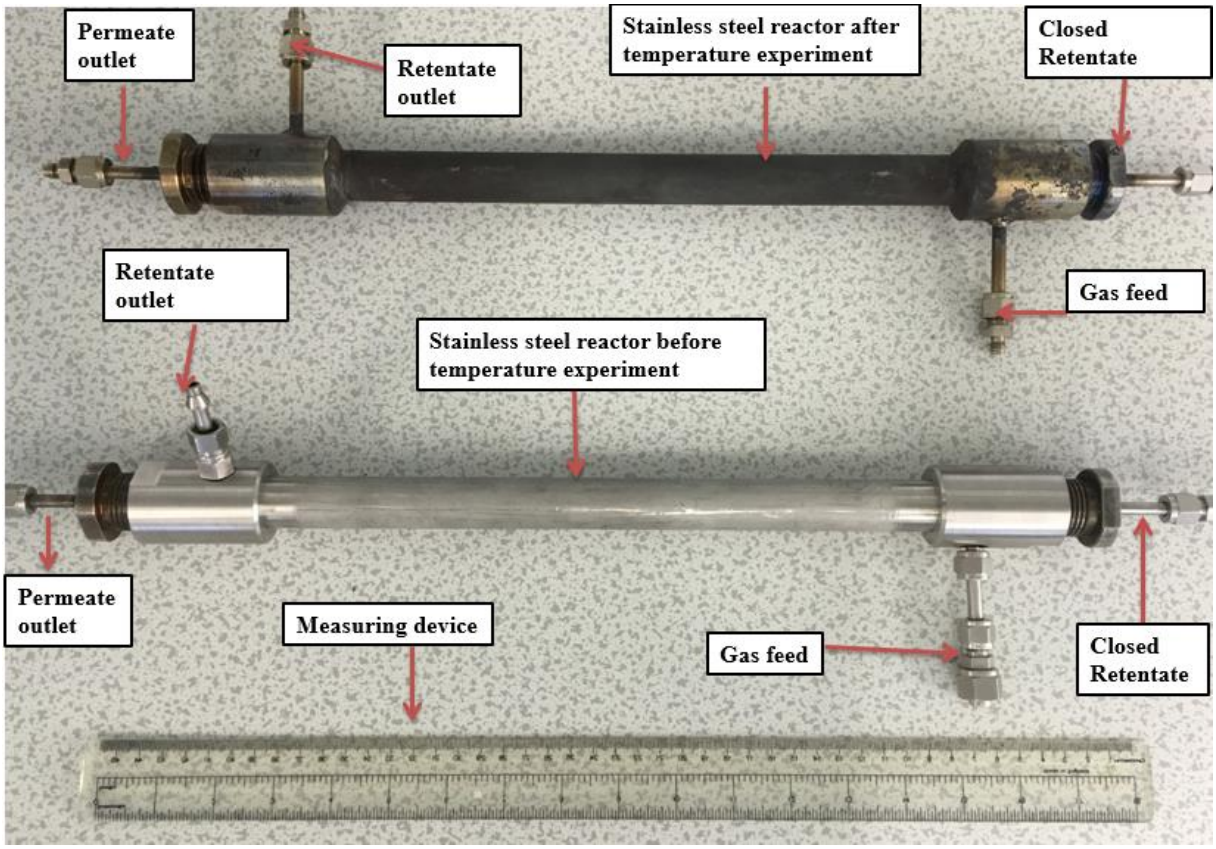

Figure 5-2: Membrane reactor before and after reaction at elevated temperature.

Length of reactor = 395 mm

Outer diameter = 36 mm

Inner diameter = 28 mm

Thickness = 5 mm

The design was adapted from the patent by Edward Gobina (63). It was designed in four sections; the gas feed, the reaction chamber, permeate and retentate sides. For operations at elevated temperatures, a heating system consisting of a heating jacket, heating mantel, thermo-couples and a thermometer were added to the setup.

5.5.1 *Membrane Reactor Sealing*

In order to develop a ceramic membrane reactor for large-scale applications, the reactor must be properly sealed. Sealing problems remain a significant technical challenge that must be addressed. There is a major problem with the development of high performance and effective sealants. Moreover, there are only a few studies

that have focused on this subject (64-68). For a membrane reactor sealant to be effective, it must be able to withstand high temperatures and pressures. In addition, it must be stable over operating times, withstand both oxidising and reducing conditions and be generally unreactive as there will be various components that will come in contact with the sealant. Most existing studies refer to the development of sealants for Solid Oxide Fuel Cell applications. The same trend is observed for sealing the membrane reactor (44). Sealants that are currently used for ceramic membrane reactors are either metal-based materials or glass-based composite oxides. Glass-based sealants are a promising sealing material for CMR because of their ability to seal both ceramics and metallic components. However, poor bond strength and changes in the physical properties due to chemical interaction with the membrane material leads to leakage with long-term use. Metal-based sealants offer long term-advantages due to their strength. However, high temperature oxidation and thermal expansion are a major challenge. In this research, a graphite seal (Figure 5-3) has been used to tackle problems encountered with seals. Moreover, graphite can withstand high temperatures with an estimated sublimation (1.01×10^5 Pa) and boiling point at 4000 and 4560 K respectively (69).

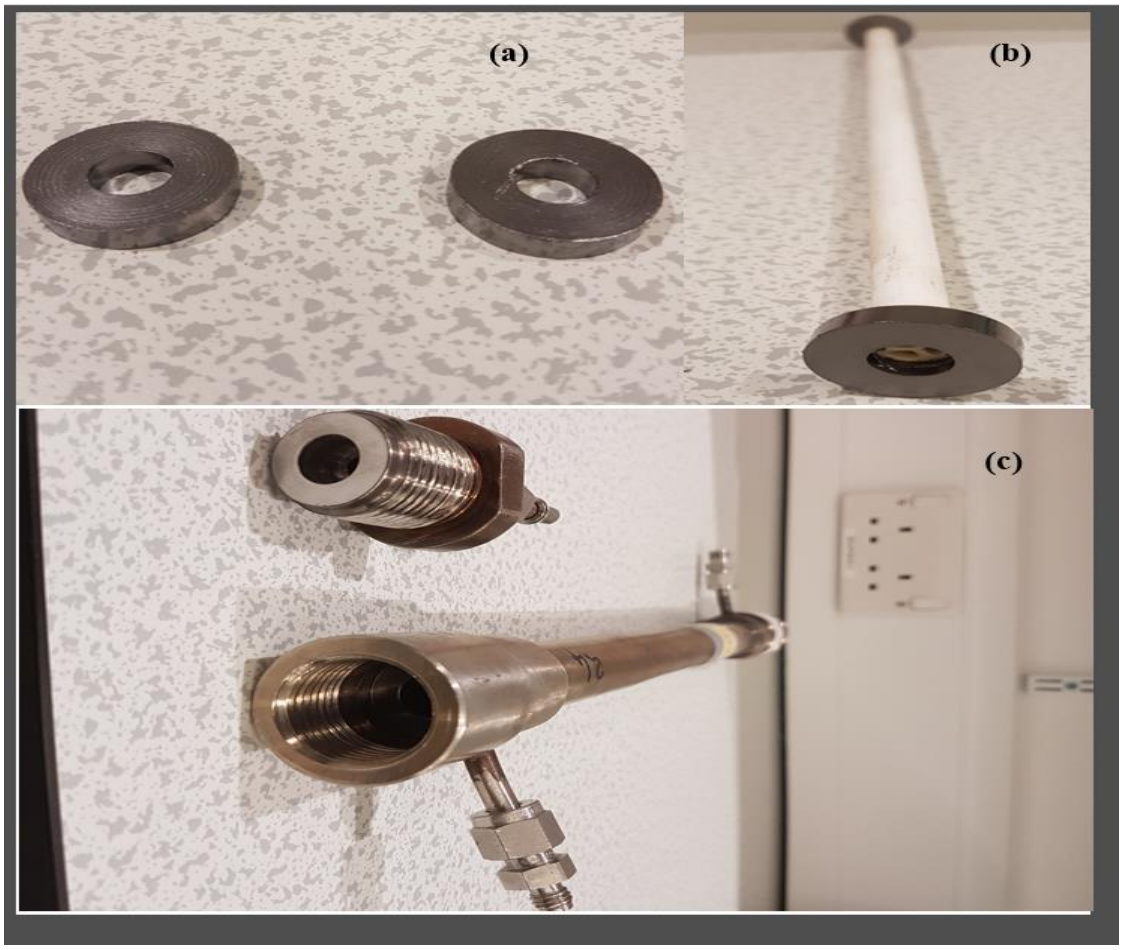

Figure 5-3: Pictorial presentation of (a) Graphite seals (b) membrane with the seal fitted at both ends (c) Membrane reactor tube and shell casing.

Graphite rings used in this research have the following dimensions:

Inner diameter = 10 mm

Outer diameter = 24 mm

Thickness = 7 mm

5.6 Reactor Design and Specifications

5.6.1 *Reactor*

A photograph of the membrane reactor, enclosed in the heating jacket and with heating jacket loosened to reveal reactors is presented in Figure 5-4. The reactor consists of a high temperature stainless steel tubular membrane holder with zonal heating and a power controller to control the temperature of the membrane. The

membrane itself is centralised inside a stainless-steel tube. The stainless-steel tube (thickness of 0.3 cm) forms the main body of the reactor. The two ends of the reactor are fitted with screw caps, which create a seal via compression of moulded graphite seal rings. The rings also help to centralise the membranes in the reactor. Three Ni-Cr thermocouples (Cole – Palmer, London, UK) have been inserted in the top, middle and bottom of the furnace through 0.32 cm bored-through fittings. The three thermocouples are in direct contact with the reactor shell. The furnace used in the reactor setup is custom designed and consists of four split zones (Horst, Frankfort, Germany). The first zone serves to preheat the incoming feed gases. The second and third zones serve to maintain the isothermal conditions for the membrane, and the fourth zone maintains the reactor temperature to avoid any condensation inside the reactor. The four heating zones of the heating unit are digitally controlled using separate two-point temperature controllers (Horst R2400, Frankfort, Germany) with LCD displays. The particular temperature in each of the four zones are adjustable. By maintaining the four temperatures in each zone the entire membrane reactor is operated at a desired reaction temperature.

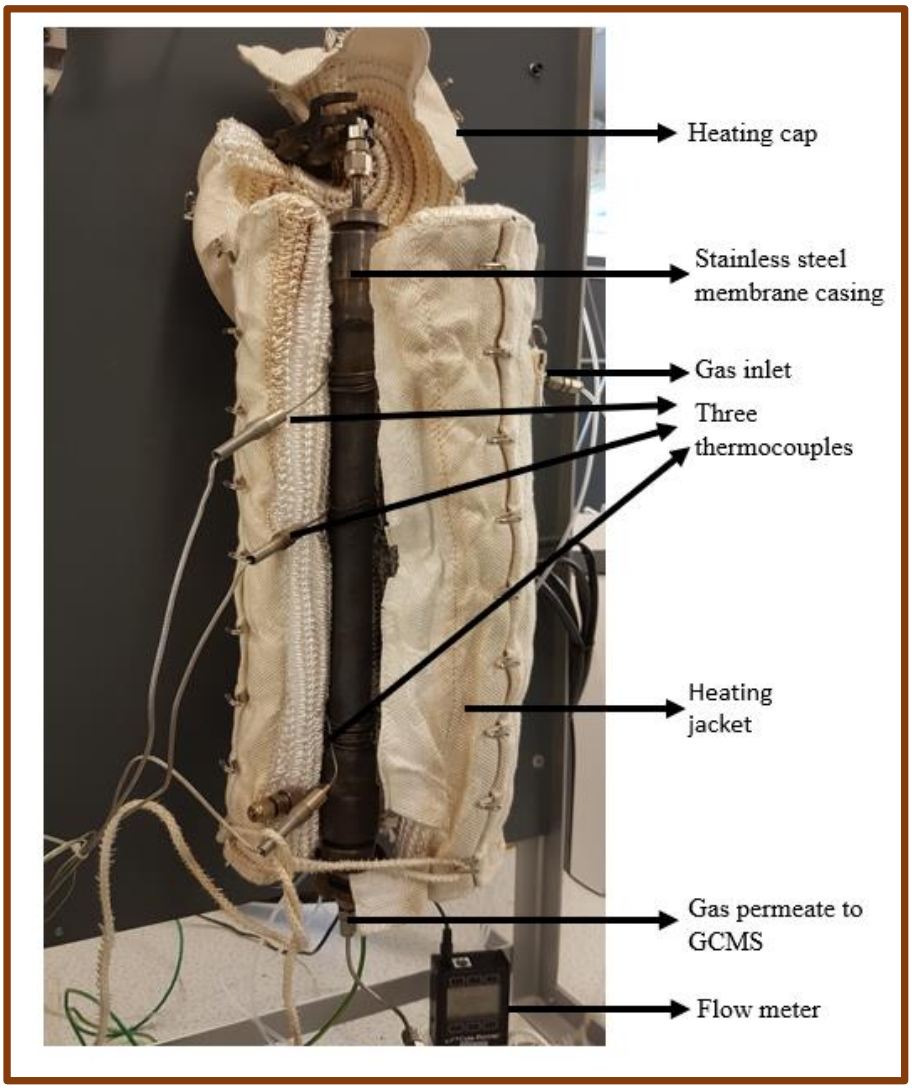

Figure 5-4: Photograph of the membrane reactor enclosed in the heating jacket.

5.6.2 *Gas Flow System*

A diagram of the gas flow module has already been presented in Figure 37 (Chapter 3). The unit can be used for single/mixed gas permeation, in-situ calcinations, reforming reactions and activation of the membrane catalysts. The reactor houses the membrane and allows for the input of the feed gas and also enables the permeate gas flow out of the system. The feed gas can be either pure or mixed, while the permeate gases are sent to the online GC (Agilent Technologies, Santa Clara, California, USA) equipped with a mass spectrometry detector (GC-MS) for analysis using an automated 6-port gas sampling valve (Agilent Technologies, Santa Clara, USA) on a 30 mm Plot H column. The rector consists of a membrane reactor, thermocouples, a heating jacket, power regulator

and temperature controller supplied by Horst, Germany. The pressure inside the membrane tubes was maintained at atmospheric pressure. The flow rate and flow configuration can be regulated through a set of control valves located at the inlet and outlet of the reactor (Figure 5-5). The unit also has a series of back-pressure regulators and control valves.

Prior to catalytic reaction tests, the membrane was heated with helium at the reaction temperature for 2 h to remove any surface impurities. The helium was then replaced with reactant mixtures (CH_4+CO_2+O_2). The outlet of the product stream was connected to the on-line GC-MS for product analysis. Catalytic tests were carried out in the membrane catalytic reactor system once stable temperatures were attained. CH_4, CO_2, and O_2 were then introduced into the reactor as a mixture. The permeate was analysed by on-line GC every 30 minutes over a 6 h period. The steam produced was condensed before the mixture entered the GC-MS. The product selectivity and the conversion were calculated by knowledge of the feed and product composition. The gases exiting the GC were sent to the extraction system in the fume cupboard.

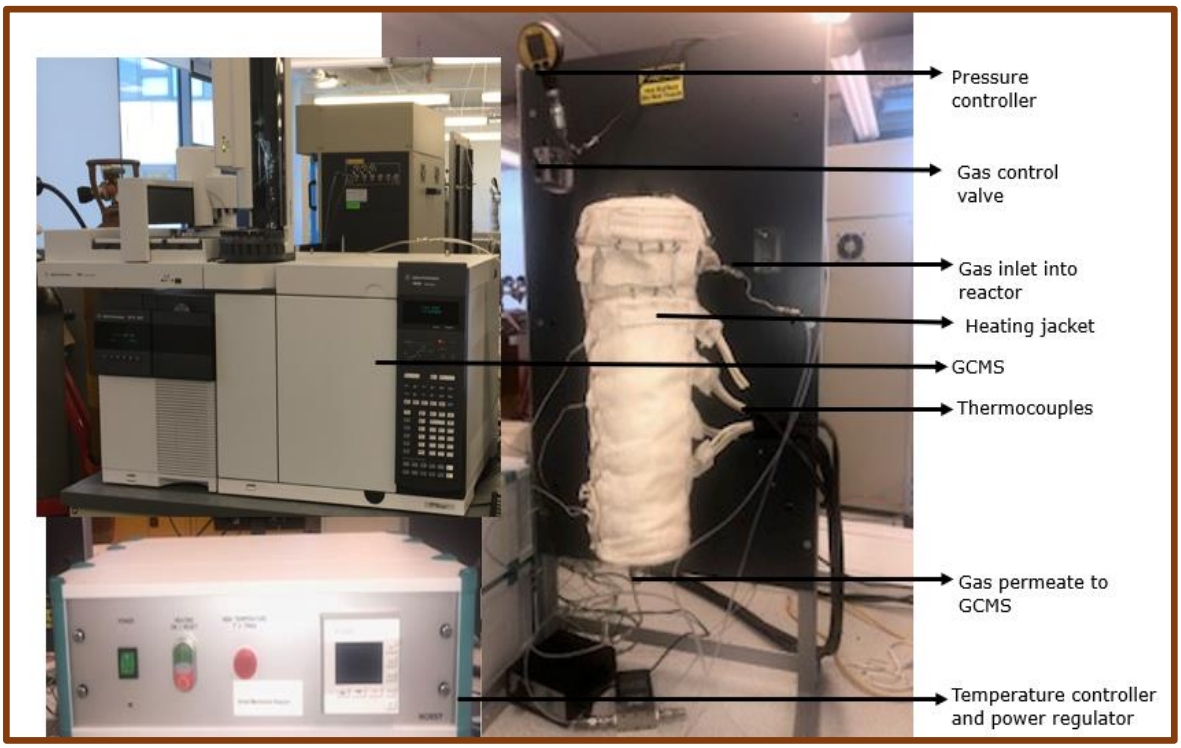

Figure 5-5: Membrane experimental rig.

5.6.3 *Membrane Placement in Reactor System*

The membrane was placed at the centre of the stainless-steel tube in order to take advantage of the uniform furnace heat. This was achieved using the high precision moulded graphite rings. The membrane was placed so that it was possible to measure the temperature at the top and bottom of the reactor. Care was taken to obtain an ideal flow through the reactor system so that the feed gases have maximum contact with all of the dispersed catalyst. The membrane reactor was initially heated to the desired temperature with a ramp rate of 10 °C per minute. Catalytic tests were carried out by allowing the feed gas mixture to enter the reactor, where the gas mixture was maintained at 250 °C in a preheating zone before passing into the main reactor high-temperature or 'hot' zone.

5.6.4 *Membrane Catalyst Activation*

Prior to the catalytic reactions, the rhodium chloride was converted to rhodium by reduction in pure H_2 at 800 °C for 30 mins. The H_2 had a flowrate of 15 ml/min.

5.6.5 *Gas Chromatograph Coupled with Mass Spectrometric (GC-MS) Analysis*

GC-MS (Figure 5-6) is a widely applied separation technique that uses a gaseous mobile phase and a liquid stationary phase that is coated on a column. Species are separated based on their differential distribution between these two phases. The residence time of a species depends on its volatility and its interaction with the stationary phase. GC is an efficient, fast and selective technique of separating gases, non-ionised liquids, solid organic molecules and organometallics.

The basic components of a GC system include,

- The carrier gas with a flow regulator
- Injection port
- A column
- A detector
- A recording device, usually a computer

The operating parameters of the GCMS are given in Table 5.1.

Table 5.1: GCMS operating parameters

	Parameter
Injection source	Manual
Gas inlet temperature	423 K
Split ratio	50:1
Carrier gas flow rate	2 mL min^{-1}

The split ratio which is the ratio of the gas that flows through the injection port from the split line to the column was determined using the vapour calculator on the GCMS. A high slit ratio indicates a small amount of sample on the column. The oven for gas analysis was programmed using the temperature profile in Table 5.2.

Table 5.2: Temprature profile for the GC oven

Temprature (K)	Hold time (min)	Run time (min)
313	5	5
423	10	26

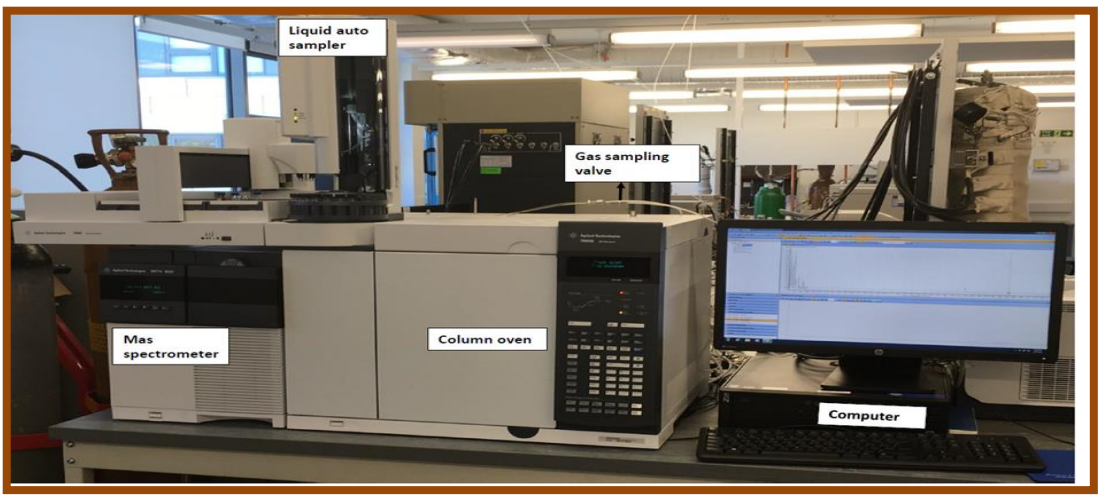

Figure 5-6: Picture of a GC system.

5.6.5.1 Carrier Gas

The function of the carrier gas is to transport species requiring analysis through the column. It must have no direct influence on the separation. Thus, it must be inert, have high purity and be non-flammable. The most common carrier gases are hydrogen, helium and nitrogen. Hydrogen is most widely used; however, it is flammable and may interact with the analytes to form hydrogenated compounds that may produce extra peaks in the chromatogram. The choice of carrier gas is determined by the type of column, detector and the species to be analysed.

A van Deemter plot (Figure 5-7) which is a plot of the Height Equivalent to Theoretical Plate (HETP) against the linear velocity of the gases nitrogen, helium and hydrogen and it shows the effect of the different gasses in an open tubular column. From the figure, nitrogen is shown to have the highest level of efficiency at its optimum flow rate. However, it has a relatively high molecular weight and a corresponding low level of diffusivity, its effectiveness is decreased by longitudinal diffusion. Consequently, it was not chosen as a carrier gas in this work. Moreover, it co-elutes with oxygen and hence oxygen cannot be quantified.

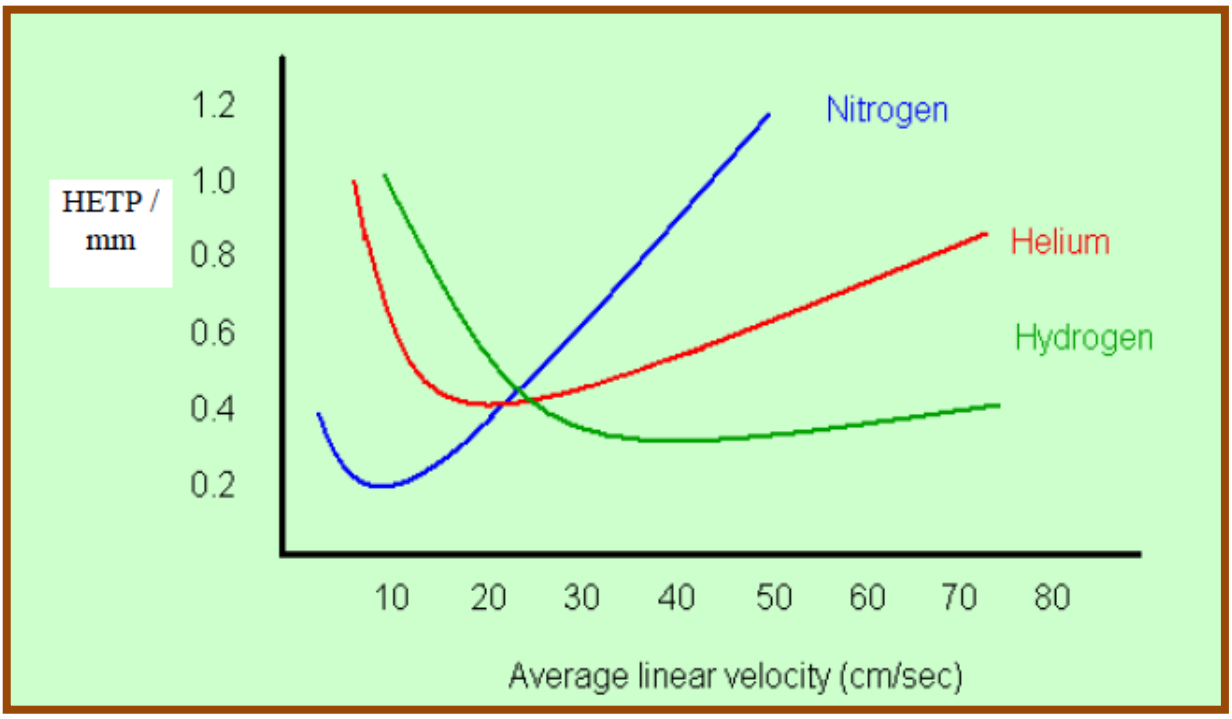

Figure 5-7: van Deemter plot of the effects of N_2, He and H_2 through an open tubular column (242).

The van Deemter plot for H_2 suggests that it is favorable for GC applications. It is the fastest of the three gases and has the lowest viscosity, which is desirable for operation at low inlet pressures. The H_2 curve is the flattest. This suggests that the change in velocity has little effect. This is a measure of the resolving power of the column. One disadvantage of hydrogen is that it is highly flammable. Therefore, helium has been chosen as the carrier gas in this work.

5.6.5.2 GC Column

In an effective GC system, the column plays an important role as it determines the efficiency and selectivity of the separation of the species to be determined. There are characteristics that a column should have in order for it to be suitable and fit for purpose for a particular analysis. For example, if a column is not inert then it can detoriate the samples and hence, alter the results. There are various types of columns used for a GC analysis, these include: support coated open tubular (SCOT) column and porous layer open tubular (PLOT) column. Traditionally, PLOT columns are seldom used for analysis, primarily because the stationary phase layer is not mechanically stable and can lead to particle shedding, but they are ideal for the analysis of gases due to their increased retention and unique selectivity when compared to other columns (243). In this work, a HP PLOT Q was used due to its suitability for the separation of volatile analytes and the properties of this column that made it suitable for application in this work is given in Table 5.3.

Table 5.3: Properties of HP-PLOT Q column

	HP-PLOT Q column
Stationary phase	Bonded, polystyrene divinylbenzene
Temprature limit	Up to 573 K
Hydrocarbon separation	Can elute up to C_{14}. Resolution on C_2 and C_3 isomers, better resolution of hydrocarbon isomers than other columns
Natural gas	Baseline resolution of air/CO_2/CH_4

5.6.5.3 Mass Spectrometry Detector

Several detectors can be coupled to a GC. In this work a mass spectrometer (MS) has been employed. In an MS, detection of species are based on the separation of ionised molecules or their fragments according to their mass-to-charge ratios (m/z). MS work under high vacuum to avoid any collisions between ionised molecules, and to ensure a free mean path until molecules reach the detector.

5.7 Materials and Method

5.7.1 *Materials*

Materials and chemicals used in this work include:

1. Rhodium (III) chloride supplied by Sigma Aldrich (98% w/v)
2. Synthetic off-gas mixture containing 4.5% O_2, 2.5% CH_4, 12.5% CO_2, and balance nitrogen (+/- 2% uncertainty) supplied by BOC, Aberdeen Scotland.
3. 50% CO_2 and 50 % CH_4 (+/- 2% uncertainty) supplied by BOC, Aberdeen Scotland.
4. Analytical grade hydrogen (98% purity) supplied by BOC, Aberdeen Scotland.
5. C106X/1B single stage gas regulator supplied by BOC, Aberdeen Scotland for use with non-corrosive gases.
6. HP 1500 series 851750 single stage gas regulator
7. Synthetic off-gas mixture containing 4.5% O2, 2.5% CH4, 12.5% CO2, 9 ppm NO_2 and balance nitrogen (+/- 2% uncertainty) supplied by BOC, Aberdeen Scotland.
8. Gas connection hose (1/4inch compression fittings).
9. 6000 nm pore size α-alumina support which consists of 77 % alumina and 23% TiO_2 and has a permeable length of 348 mm and an internal and external diameter of 7 and 10 mm respectively, supplied by Ceramiques Techniques et Industrielles (CTI), France
10. Gas Chromatography coupled with Mass Spectrometry from Agilent Technology, UK.

5.7.2 *Method*

Electroless plating deposition of the Rh on 6000 nm pore size tubular ceramic cores has been achieved by dissolving 10 g of 98 % $RhCl_3$ in 500 ml of deionized water (Figure 5-8 a, b, c). This was left to stir for 24 h. 6000 nm α-alumina support was subsequently soaked in water for 2 h and then dipped into the $RhCl_3$ solution and left for 20 h. Catalytic reduction of the $RhCl_3$ and activation of the rhodium metal on the membrane was carried out by passing hydrogen gas through the membrane in the membrane reactor at 573 K for 30 min.

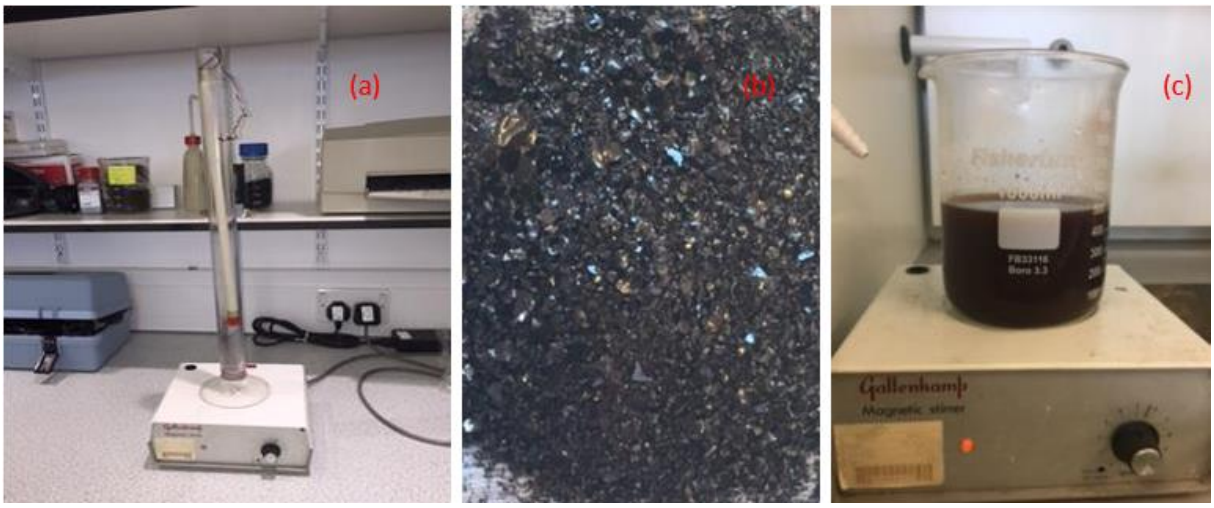

Figure 5-8: Picture of (a) membrane soaked in deionised H_2O, (b) $RhCl_3$ crystals and (c) dissolved $RhCl_3$.

Catalyst loading was determined using equation 59:

$$catalyst\ loading\ (\%) = \frac{wa-wb}{wb} X\ 100 \qquad \textit{Equation 59}$$

Where *wa* is the weight of the membrane before impregnation with Rh and *wb* is the weight of the membrane after Rh deposition.

5.8 Membrane Characterisation

5.8.1 *SEM and EDAX*

SEM applies the use of a beam of high-energy electrons to generate different signals on the catalyst surface. The signals that are obtained from electron-sample

interactions give details such as outer morphology, chemical composition, and crystalline structure and orientation of materials making up the sample. Data was collected over a selected area of a witness sample of the membrane and a two-dimensional image was generated. More details are given in section 2.2.4.2.

5.8.2 *Gas Permeation Test*

A mixed gas permeation test has been carried out and the permeate gases were sent to the online GC (Agilent Technologies, Santa Clara, California, USA) (Figure 5-9) equipped with an MS detector for analysis using an automated 6-port gas sampling valve (Agilent Technologies, Santa Clara, USA) on a 30 mm Plot H column. The experimental rig consists of a membrane reactor that was operated at high temperature using a Horst (Germany) power regulator.

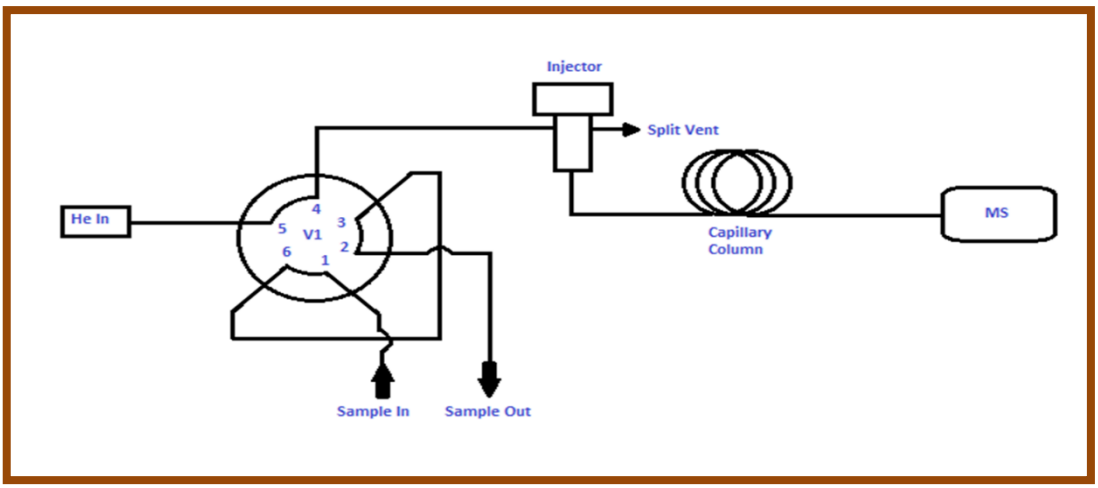

Figure 5-9: 6-port gas sampling valve.

The experimental set-up consisted of a membrane reactor, gas delivery system for pure gases, a permeate and retentate exit, a flow meter and K-type thermocouples fixed on the reactor. Prior to the permeation experiments, the reactor and all connections were tested for leaks. The mixed gas permeation tests involved passing the gas in to the shell-side. This was directed to permeate across the Rh membrane at different fixed feed pressures, but varying flow rates and temperatures. The shell was made from stainless steel, which can withstand high temperatures. The stainless steel shell was covered with heating tape to maintain the heat in the reactor system. The two ends were removable for membrane

replacement purposes. Gas tightness between the shells was maintained by graphite O-rings. Two graphite rings that can withstand high temperature, as well as allow for thermal expansion of the alumina support were used to seal the membrane tube ends. The feed and permeate end of the membrane were connected to the online GC-MS 6-port gas sampling valve.

5.9 Results and Discussion

5.9.1 *SEM and EDAX Analysis*

Morphological studies of the synthesised Rh membrane confirmed that the Rh particles were deposited on the α-alumina support. Figure 5.10 (a) and (b) show the synthesised Rh membrane before and after calcination. A summary of the elemental composition is provided in Table 5.4.

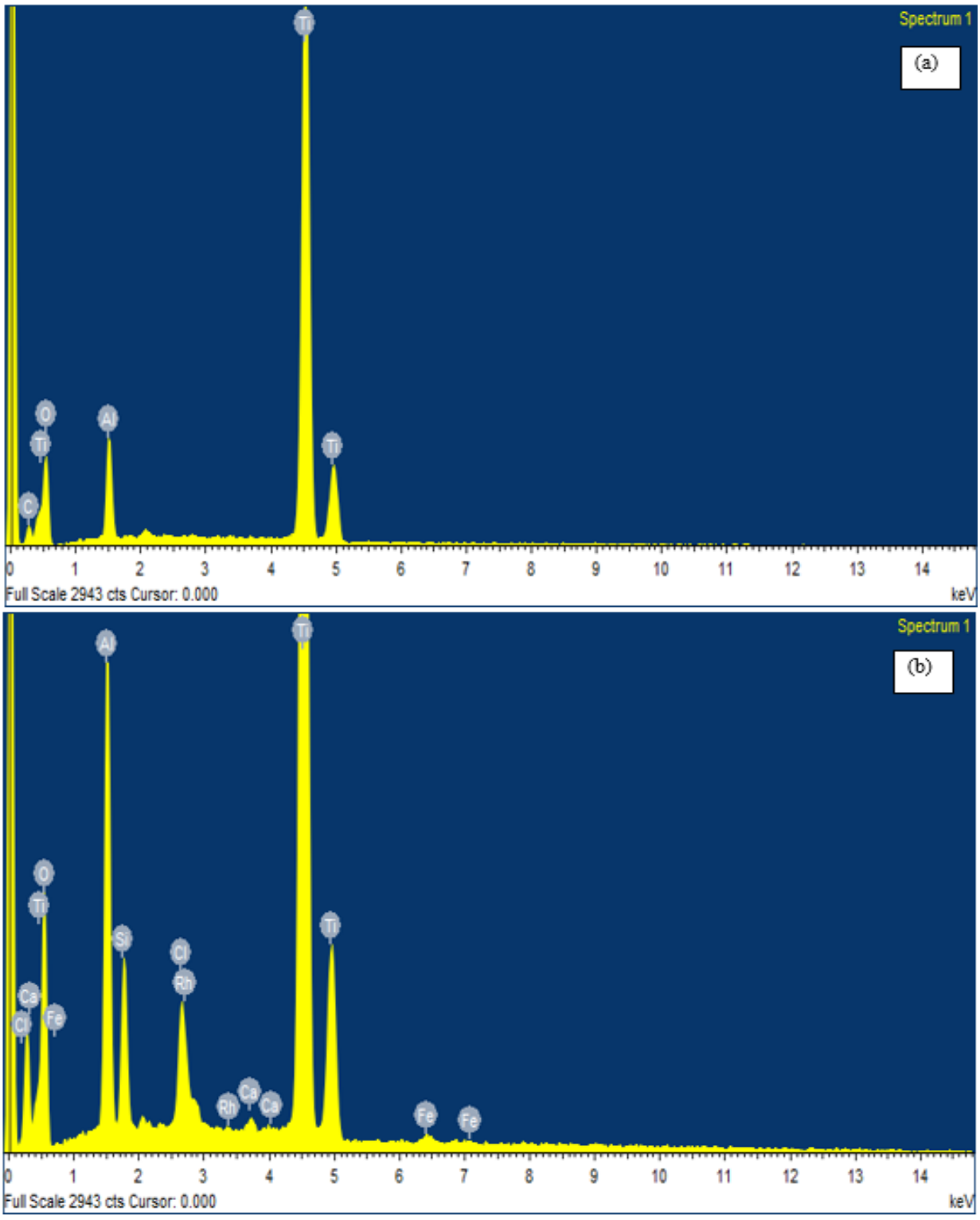

Figure 5-10: EDAX for (a) α-alumina support and (b) Rh/α-alumina membrane.

Table 5.4: Elemental composition of α-alumina and Rh/α-alumina membrane

Elements	% weight composition (α -alumina support)	%weight composition (Rh/α-alumina membrane)
O	7.29	20.5
Al	0.82	3.82
Si		1.43
Cl		0.97
Ca		0.14
Ti	9.68	23.63
Fe		0.23
Rh		0.94
C	0.79	

The EDAX elemental analysis showed the amount of Rh catalyst on the support to be 0.94 %. Moreover, the catalyst loading on the γ-alumina support is 0.52 %.

SEM images of the α-alumina membrane and the rhodium impregnated α-alumina membrane are presented in Figures 5-11 and 5-12.

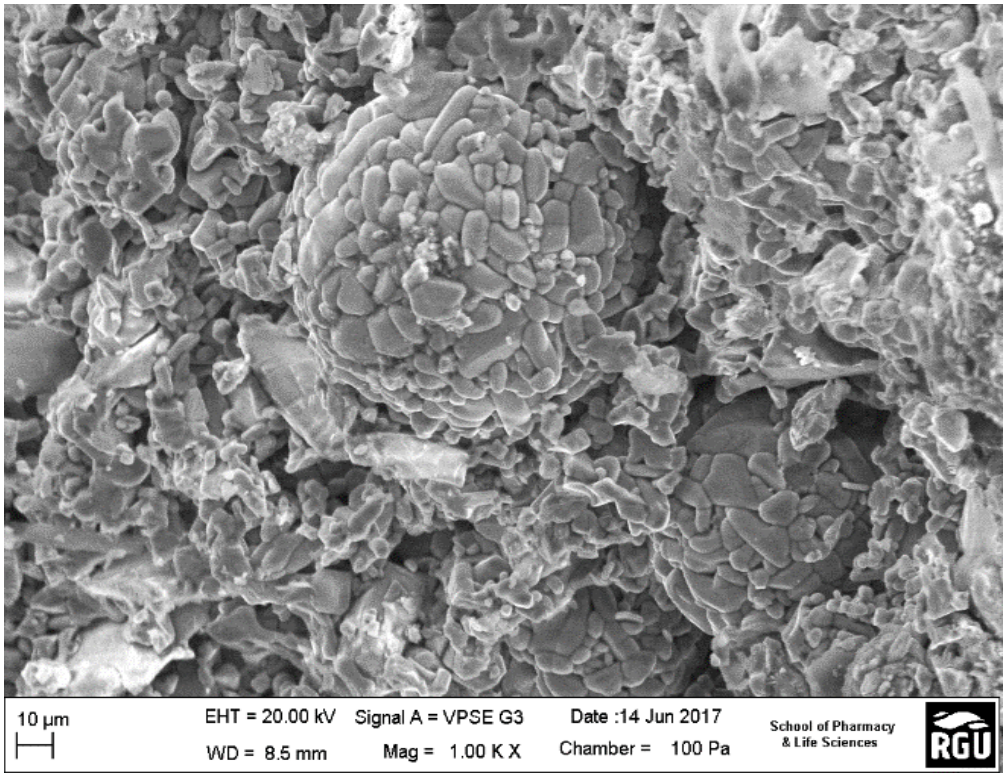

Figure 5-11: α-alumina membrane.

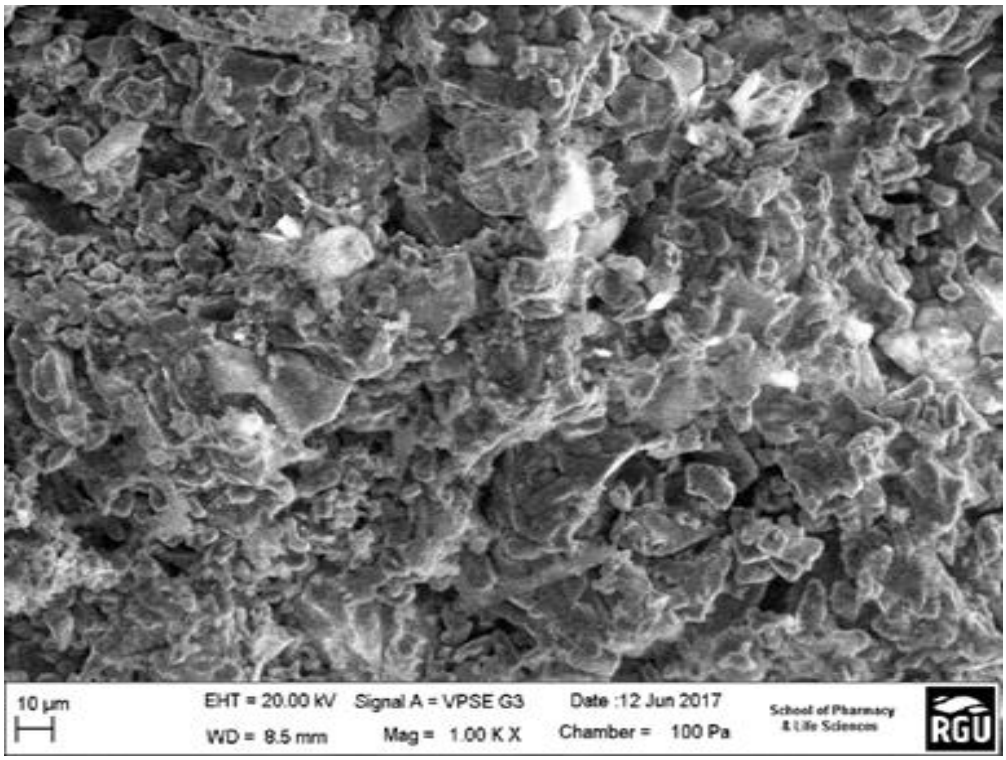

Figure 5-12: Rh/α-alumina membrane.

5.9.2 *Nitrogen Adsorption/Desorption*

Physical adsorption of gases on a materials surface is one of the most important techniques for the characterisation of nanosized porous materials. This method provides details about the surface area, pore volume and pore size distribution. Several different types of physisorption isotherms (Figure 5-13 a and b) have been observed for both the activated and unactivated Rh modified membranes.

The specific surface area of the membranes has been determined from the adsorption of nitrogen on the external and internal surface of the membranes at 77.35 K using a quantachrome adsorption gas analyser.

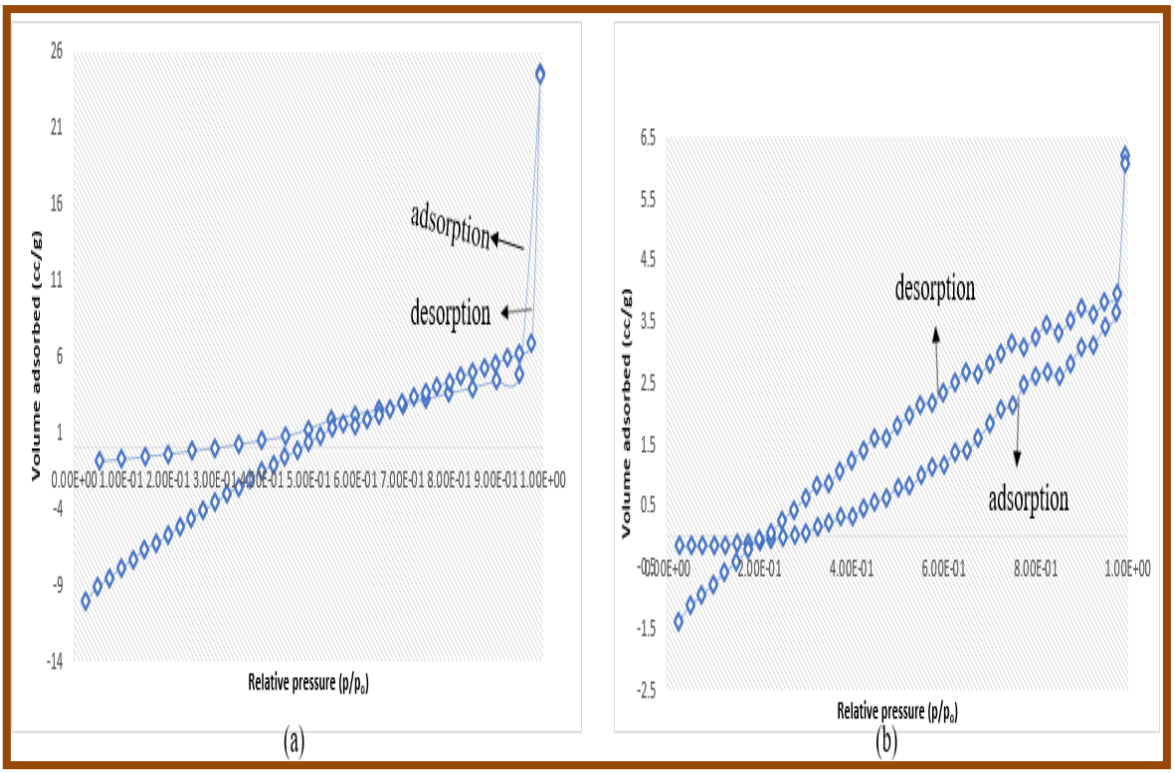

Figure 5-13: N_2 adsorption/desorption isotherm of (a) un-activated Rh membrane and (b) activated Rh membrane.

The difference in the hysteresis isotherms is caused by the difference in adsorbent behaviour of Rh before and after passing H_2 at a temperature of 573 K (Figure 5-13a and b). The observed loop is generally associated with materials that have mesoporic structures. The adsorption behaviour of mesoporous materials can be determined using adsorbent-adsorbate interactions. Hence, the Kelvin equation (equation 60) which is based on cylindrical pores is used for the evaluation of the

pore size distribution of the membrane layer using the Barrett-Joyner-Halenda (BJH) method.

$$r_p = r_k + t \qquad \text{Equation 60}$$

In equation 65, r_p is the pore radius of the membrane layer in nm, r_k is the Kelvin radius and t is the thickness in nm of the membrane layer.

The BJH graph (Figure 5-14) shows the adsorption and desorption branches, which have been used to determine the pore size of the membrane. This was determined to be 2.973 nm with a specific surface area of 17.447 m^2/g.

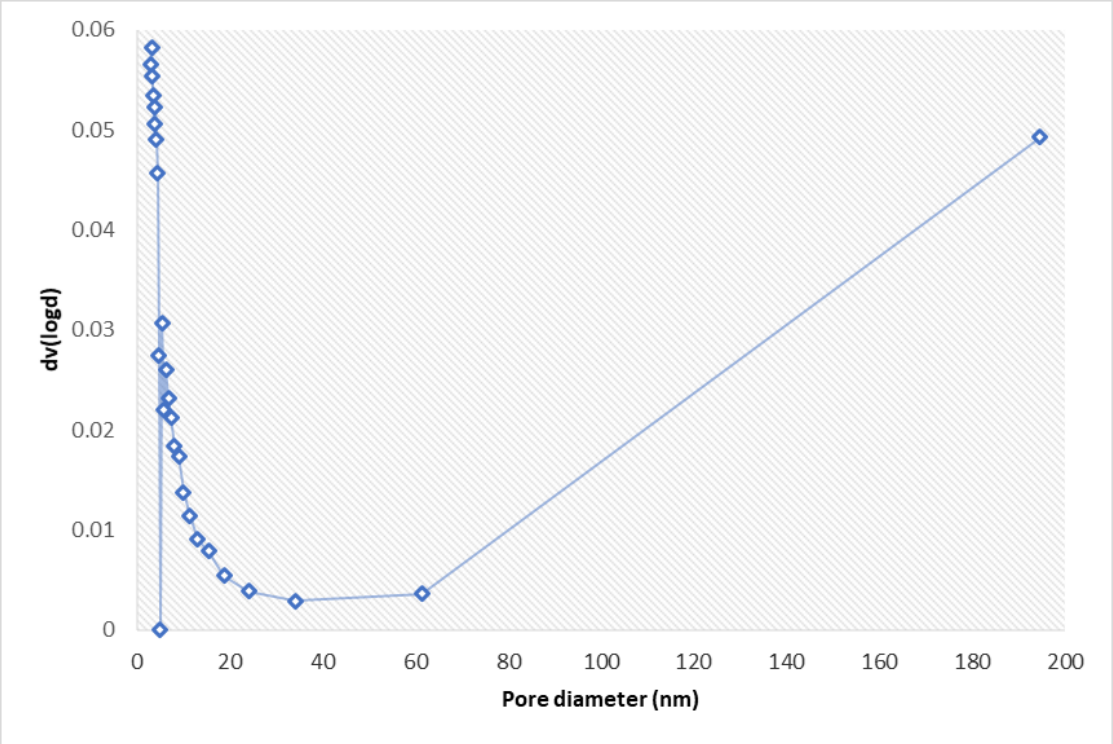

Figure 5-14: BJH pore size distribution of the synthesised Rh membrane.

5.10 Membrane Reactor Performance

5.10.1 *Single Gas Permeation Test*

Single gas permeation of CH_4, CO_2 andH_2 through the α-alumina membrane is presented in Figure 5-15. The permeance of H_2 was shown to increase as the pressure was increased to 1×10^5 Pa. This indicates that the membrane can

selectively remove hydrogen at higher pressures. The order of gas permeance through the membrane was H_2 (2.00 mol/g), CH_4 (16.04 mol/g) and CO_2 (44.00 mol/g). Therefore, the flow mechanism was based on the relative molecular masses of the gases. This is indicative of Knudsen flow mechanism.

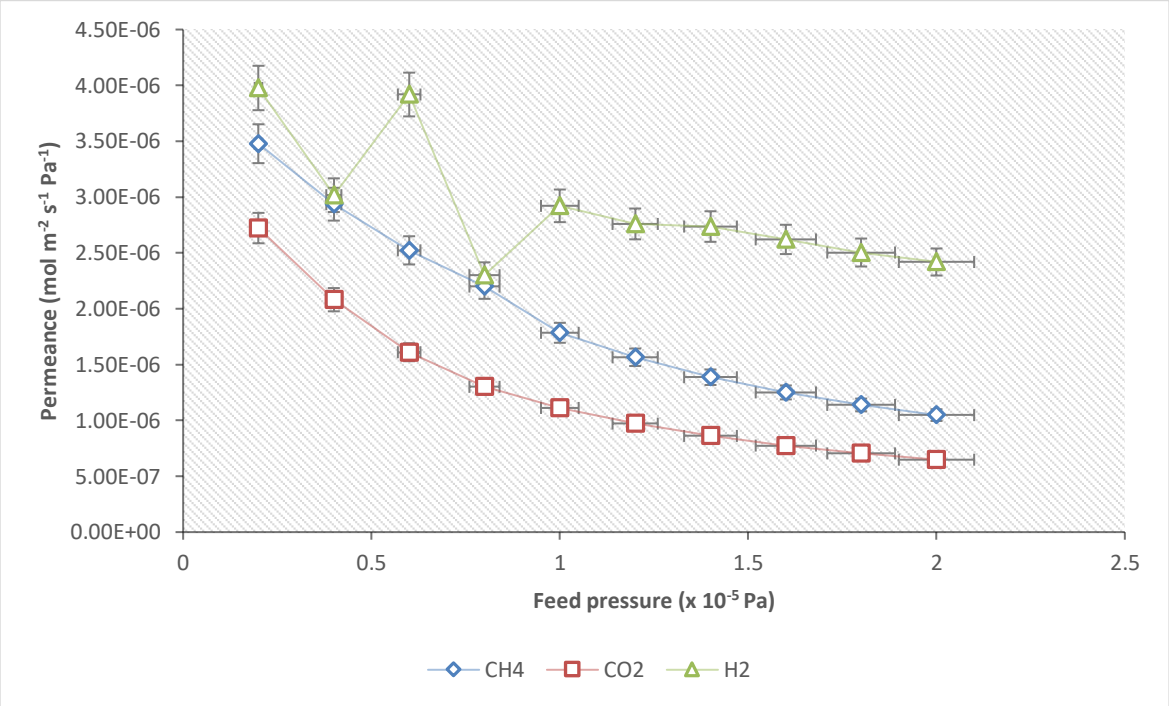

Figure 5-15: Gas permeance through the α-alumina membrane at 293 K.

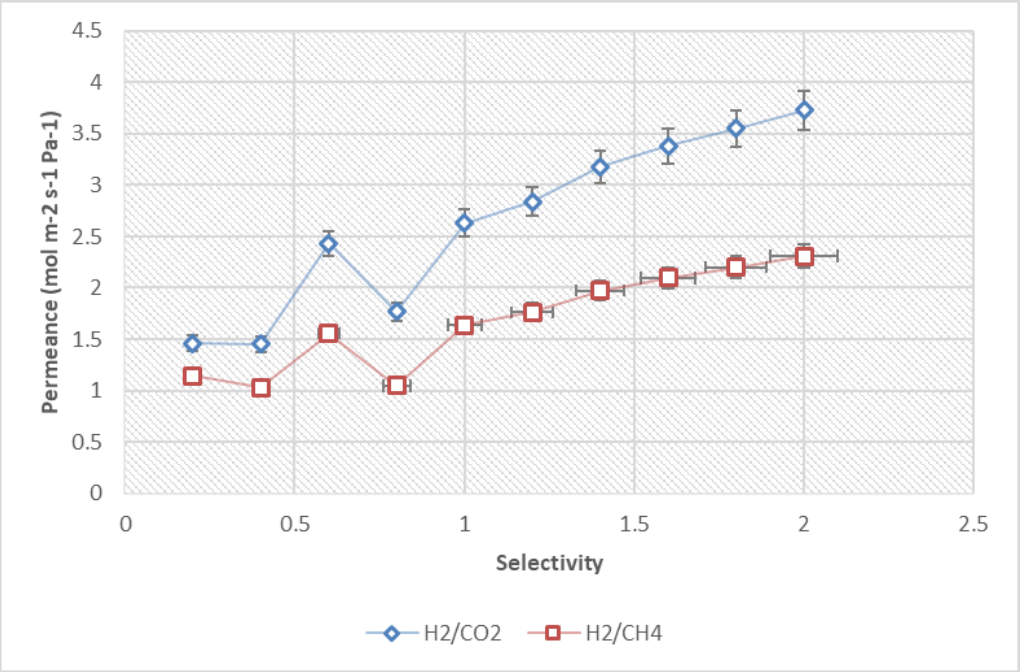

Figure 5-16: Selectivity of the α-alumina membrane at 293 K to hydrogen.

Figure 5-16 shows hydrogen selectivity through the α-alumina membrane. The selectivity was found to increase with increased gas feed pressures. Consequently, continual removal of hydrogen from the gas stream will enhance the CO_2 and CH_4 conversion rates. This is one of the advantages of a membrane reactor over a packed bed reactor (PBR).

Patil *et al.* (225) have previously carried out methane reforming reactions with a noble metal catalyst at 823 K at 2×10^5 Pa in a CMR. This consisted of a palladium based membrane. Moreover, conversion enhancements of 27 – 53% were achieved. Tong and Matsumura (226) also investigated methane reforming reactions with a CMR. They used a commercial nickel catalyst at 773 and 823 K and obtained hydrogen permeances of $1 - 3 \times 10^{-6}$ mol m^{-2} s^{-1} Pa^{-1}. In this work, hydrogen permeances of 2.4 – 3.9 $\times 10^{-6}$ mol m^{-2} s^{-1} Pa^{-1} have been achieved. These are found to be equivalent to those obtained in the literature.

5.10.2 *Effect of Temperature on CO_2 and CH_4 Conversion*

The conversion of CH_4 and CO_2 when passed through a Rh/α-alumina membrane has been calculated using:

$$Conversion\ (\%) = \frac{C_{feed} - C_{permeate}}{C_{feed}} \times 100 \qquad \textit{Equation 61}$$

Where C_{feed} is the initial concentration of the feed gas and $C_{permeate}$ is the final concentration of the gas that permeates out of the membrane. The gas retentate stream is kept closed throughout the reaction time.

5.10.2.1 CH_4 Conversion

Operating temperatures at 1 x 10^5 Pa can affect the equilibrium state by altering the CO_2/CH_4 ratios as follows; conversion of CH_4 increases for temperatures up to 1073 K. Furthermore, CO_2 gas has an oxidative effect on CH_4 as the temperature increases. Nikoo *et al.* (227) made thermodynamic calculations that shows the direct effect of CO_2 on the conversion rates of the CH_4 at temperatures less than 973 K. Hence, the addition of CO_2 to CH_4 as an oxidant produces more activity for CH_4 molecules. Although, exothermic reactions occuring at the side result in decreased methane conversion rate at lower temperatures. Nikoo *et al.* (227) deducted that the equilibrium conversion rate was approximately 82% for an equal CO_2/CH_4 ratio at 873 K. This took into consideration that the decomposition of methane lays the foundation for its conversion. Contrary, Istady (228) calculated a 42% conversion under comparable conditions. Khalesi *et al.* (229) confirmed Nikoo *et al.* calculations experimentally. Furthermore, it was confirmed that the presence of promoted Ni based catalyst led to higher CH_4 conversion at temperatures above 923 K. This was attributed to the low sensitivity of the catalyst to the deposition of carbon at higher temperatures. In this work, CO_2/CH_4 ratio remained constant.

5.10.2.2 CO_2 Conversion

CO_2 conversion is vital, as it has a positive effect on CH_4 conversion. Moreover, CO_2 conversion thermodynamically increases for any CO_2/CH_4 ratio at increased temperatures. Calculations for CO_2 conversion revealed two trends as a function of temperature (227). For any CO_2/CH_4 ratio, CO_2 conversion decreases gradually at 573 K, with differences in the CO_2/CH_4 ratios of 0.5 and 3. These values are 60 % and 15% lower than the original values. These then increase at temperatures in the range 823–873 K, which leads to a conversion of 100%. The conversion of CO_2 reaches a high between 1273 K and 1473 K for any CO_2/CH_4 ratio. Istadi (230)

experimentally proved that CO_2 is absolutely converted at a CO_2/CH_4 ratio of 0.5 at 1273 K. The complete CO_2 consumption in low ratios is due to the fact that it functions as the limiting reactant in the reaction.

In this work, the conversion of CH_4 was 94.5 % at 1073 K. This was higher than the conversion of CO_2 (88.3%). Increasing the temperature lead to an increased CO_2 conversion while the CO_2/CH_4 ratio remained constant. This is because CH_4 plays a more extensive role as a limiting reactant. These results are in agreement with the observations of Wisniewski *et al*. (231), who observed dry methane reforming over a Ce promoted Fe based catalyst, with limited carbon deposition.

5.10.2.3 H_2 Production

For the production H_2 with respect to CO_2/CH_4 ratio, the following conditions are ideally supposed to be considered: CO_2/CH_4 greater than 1 and CO_2/CH_4 less than 1. In this work, the CO_2/CH_4 ratio remained constant at a value greater than 1. Nikoo *et al.* (227) suggested that at a pressure of 1 bar, the production of H_2 gas is dependent on the reaction temperature for CO_2/CH_4 ratios less than 1. Moreover, the production of H_2 was enhanced at the temperature range 573-1473 K. Furthermore, CO_2 is the limiting reactant and the RWGS reaction is not favoured due to the lack of CO_2 (232). However, H_2 produced was not quantified due to the co-elution of hydrogen with the carrier gas. Previous work has shown that the amount of H_2 produced decreases with increasing CO_2/CH_4 ratio (0.5 to 1) at all temperatures. This is because the main reaction is enhanced, and methane decomposition is depressed.

From literature, at CO_2/CH_4 ratios greater than 1, the produced H_2 increased as the temperature increased. A maximum was attained around 973–1023 K. This was observed to reduce at higher temperatures. This decrease was expected as the RWGS reaction increases due to the higher concentration of CO_2, and the consumption of H_2 to produce more CO (230, 232, 233).

5.10.2.4 CO Production

Wang and Millar (234) observed that CO production was favoured at higher temperatures for all CO_2/CH_4 ratios, as all CO production reactions are endothermic and CO production was found to increase with increasing CO_2/CH_4 ratio for a CO_2/CH_4 ratio < 1. At 1173 K, a maximum CO production of 1.3 moles is achieved

for a 0.5 CO_2/CH_4 mix. The highest CO production was obtained with a CO_2/CH_4 ratio of 1. However, with the increase of CO_2/CH_4 ratio to greater than 1 and at increased temperatures, there was a decrease in CO production. This was due to the CH_4 acting as the limiting reactant for the methane dry reforming reaction (233).

From a stoichiometric and thermodynamic point of view, the production of CO was favourable at the temperature range of 1173 K because of the RWGS reactions, where H_2 reacts with CO_2 to produce more CO. This does not agree with the observed decrease in H_2 production for CO_2/CH_4 greater than one and at temperatures greater than 973 K (235). A vital value, derived from the results of the H_2 and the CO production is the product (H_2/CO) ratios that will become the feed stock for gas to liquid (GTL) process (236). Moreover, it becomes very low at temperature above 873 K. This ratio is ideal for industrial implementation, where a value close to unity is desired for the Fischer-Tropsch process (237).

For a rhodium catalyst, stability tests carried out in the presence of nitrous oxide have shown the risk to the catalyst to be low. In the presence of nitrous oxide, CO_2 and CH_4 conversion remained constant for 6 h with the CO_2/CH_4 remaining constant at a ratio of 5.

5.10.2.5 Carbon Production

For carbon formation, the reactions involved can be affected by temperature and ratio of reactants. However, thermodynamic calculations (238) have shown that a number of carbon still remains for a CO_2/CH_4 ratio of ~0.5 at temperatures higher than 1073 K. This is because temperatures become increasingly thermodynamically favourable with methane decomposition. Shamsi (239) showed that the reverse Boudouard reaction which is thermodynamically favourable at the higher temperatures, particularly for CO_2/CH_4 greater than 1, the deposition rate of carbon is reduced. Carbon deposition increase has been predicted for a CO_2/CH_4 ratio of 0.5 at temperatures lower than 723 K (238).

Generally, formation of carbon was expected to decrease as the CO_2/CH_4 ratio increases above one and at a temperature that remains constant. Wang *et al.* (234) deduced that at a particular pressure, the threshold of the temperature required for carbon deposition rises as the CO_2/CH_4 feed ratio is reduced. At the

constant CO_2/CH_4 ratio for the Rh/alumina membrane no reduction in the catalytic activity of the membrane was observed. This is important because the use of excess CO_2 in the feed gas hinders the formation of carbon at reduced temperatures by feeding the reaction with extra oxidation. A study by Claridge (240) revealed two types of carbon deposition for the dry methane reforming process. However, there has been no thermodynamic model that can predict which type of carbon that will be formed during the dry reforming process, as it is ruled by the catalyst/support characteristics and how they interact. One of the goals in methane reforming reactions with the integration of a CMR is to attain high CO_2 and CH_4 conversions while simultaneously producing the desired H_2:CO ratios. A high conversion of CO_2 and CH_4 is environmentally friendly and improves the efficiency in downstream Fischer-Tropsch synthesis for liquid hydrocarbons. From Figure 5-7, it can be observed that the conversion of CO_2 and CH_4 increases with temperature. At 1173 K, CO_2 has a conversion rate of 94% while CH_4 attains a conversion of 95%.

Qualitative analysis using the Agilent mass GC-MS confirmed the gas components in the feed gas and the components at the permeate side. The spectra are presented in Appendix D and E. Appendix B gives the calibration of the GCMS using CH_4, C_3H_8, CO_2, N_2 and CO, it was observed the calibration curve of CO_2 had some contamination thus causing it to have background noise.

A summary of the compounds present in the feed gas and their respective retention times are provided in Table 5.5. Using Table 5.5, the different compounds present in the feed gas can be identified, while those in the permeate are summarised in Table 5.6.

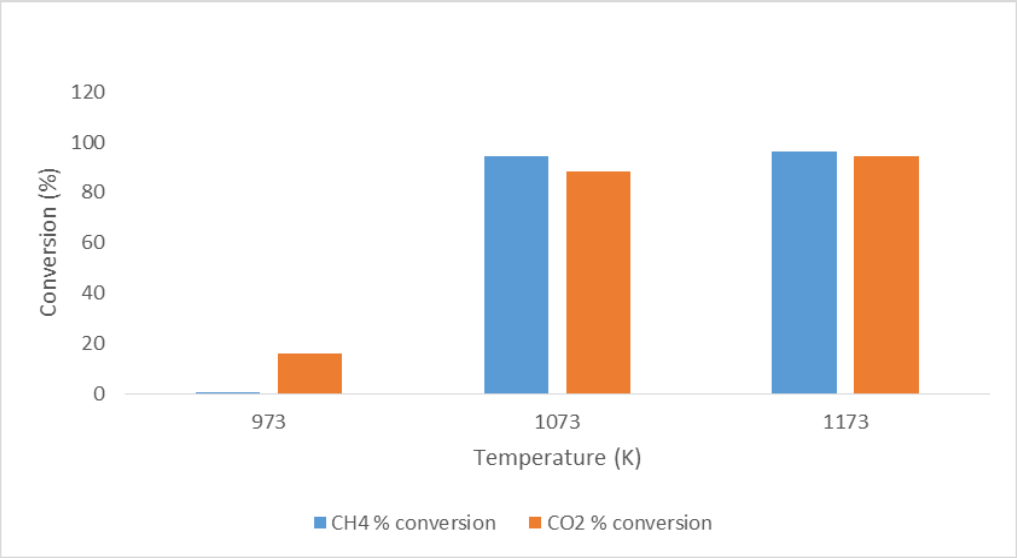

Figure 5-17: Effect of temperature on CO_2 and CH_4 conversion respectively with the Rh/γ-alumina membrane.

Table 5.5: Feed gas compound table.

Compound label	Compound	Retention time (mins)
Cpd 1	Water vapour	5.32
Cpd 2	Nitrogen	1.463
Cpd 3	Methane	1.606
Cpd 4	Carbon dioxide	1.206

Table 5.6: Permeate gas compound table.

Compound label	compound	Retention time
Cpd 1	Water vapour	1.458
Cpd 2	Nitrogen	1.611
Cpd 3	Methane	2.115
Cpd 4	Carbon dioxide	4.12-5.068

5.10.3 *Effect of Feed Flowrate on CO_2 and CH_4 Conversion*

The effect of varying the flow rate of the gas mixture through the membrane has been investigated at 1173 K (Figure 5-18). The intensity of the counts of the methane peak were shown to decrease when methane has been converted to H_2 and CO. The carrier gas used for the experiment was helium, hence in the column hydrogen was expected to co-elute with the carrier gas.

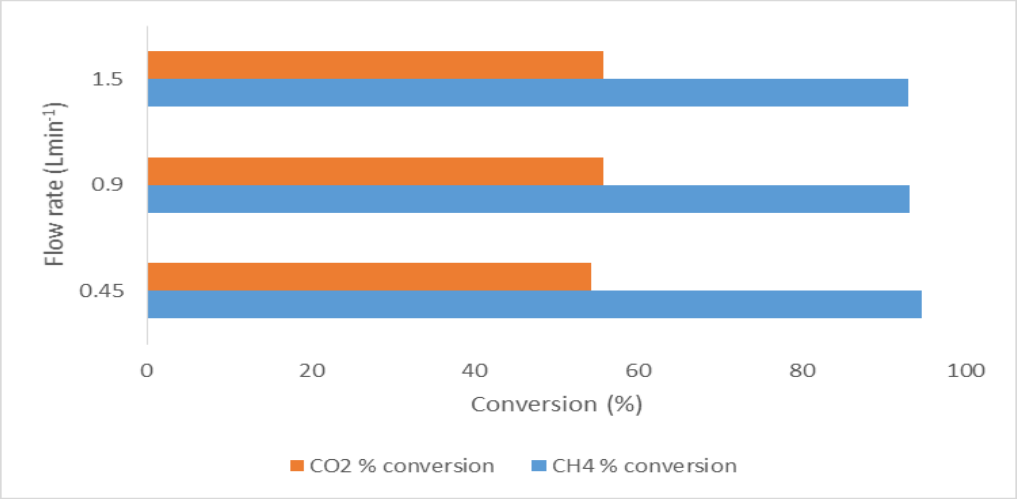

Figure 5-18: Effect of flow rate on CO_2/CH_4 conversion at 1173 K.

Variation of the flow rate at 1173 K did not influence CO_2 and CH_4 conversion. This may imply that the membrane module can be kept at a steady flow rate with the aim of achieving high conversion. In the case of low flow rate of the feed gas, the membrane will still achieve high conversion.

5.10.4 *Stability Test*

The time-dependent activities (stability) of the membranes for NO_2 contaminants on membrane supported Rh catalysts are plotted in Figure 5-19. The conversion of CH_4 remained unchanged during a seven-hour testing period. In addition, CO_2 showed a stable conversion during the period of study and its conversion improved steadily. Initially, CO_2 conversions were slightly lower than those observed for CH_4. However, these increased noticeably after the first 30 minutes, and again after the first 2 hours to become almost unchanged. No significant deactivation of the catalyst has been observed.

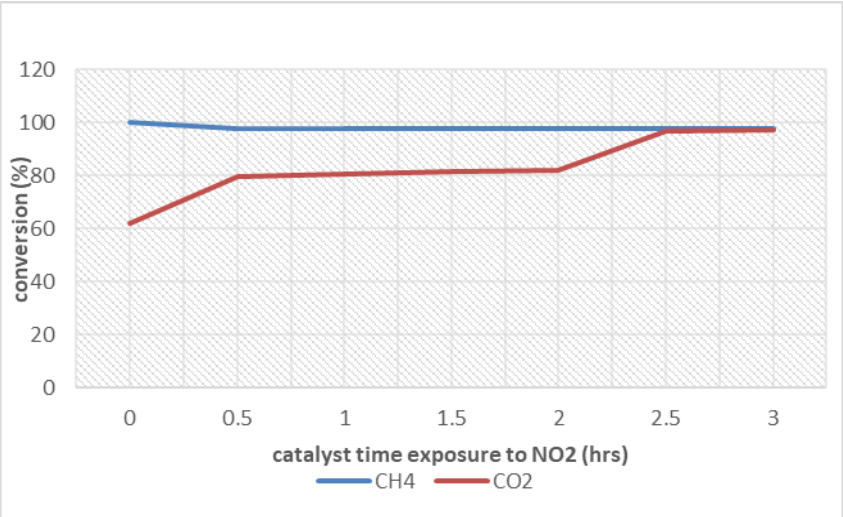

Figure 5-19: Conversion rate stability test when exposed to NO_2.

The use of a catalytic membrane reactor for the dry reforming of methane gas has been proven. An electroless enhanced deposition process followed by drying and reduction using H_2 has been successfully implemented for rhodium catalyst deposition on the γ-alumina membrane. The fresh membrane and the rhodium dispersed membrane have been characterised using SEM coupled with EDAX. The effect of superficial feed gas velocity on CO_2 and CH_4 conversion and catalyst stability under different operating conditions has been tested for the membrane studied. Membrane catalyst and reactor operation have been successfully integrated and tested. Three reaction temperatures 973, 1073 and 1173 K have been studied. Lower CO_2 conversions were observed at 973 K. This indicates that CO_2 reforming of methane was more favourable at high temperatures.

6 Overall Discussion

This chapter summarises the results obtained from the previous chapters and aims to provide a conclusion that can be used to develop a catalytic membrane reactor system for the separation and utilisation of CH_4 and CO_2. It has been observed that the membrane material plays an important role in regard to the functionality of the membrane. Reforming stability tests have shown that coke deposition formation was prevented. The proper selection of membrane material, catalyst and support can lead to optimised off-gas separation and utilisation with enhanced catalytic activity.

This research critically examined the use of silica, Y-type zeolite, Y-type zeolite/polyurethane and rhodium/alumina membranes for the separation and subsequent recovery of hydrocarbon gases under varying conditions of temperature, pressure and flow rate. The following conclusions have been drawn based on investigations regarding suitable membrane materials for off-gas separations. The zeolite membrane has shown potential for the separation of CH_4 from other gases. A high methane flux also confirmed that the zeolite membrane will be suitable for methane separation at 293 K, within a pressure range of 10 to 100 kPa (Figures 6-1 and Figure 6-2). CH_4 permeates faster in the zeolite membrane because zeolite has more affinity for methane. The pressures used are a scale down of the expected operating pressures. Moreover, the flux of methane through the zeolite membrane increases as the pressure increases.

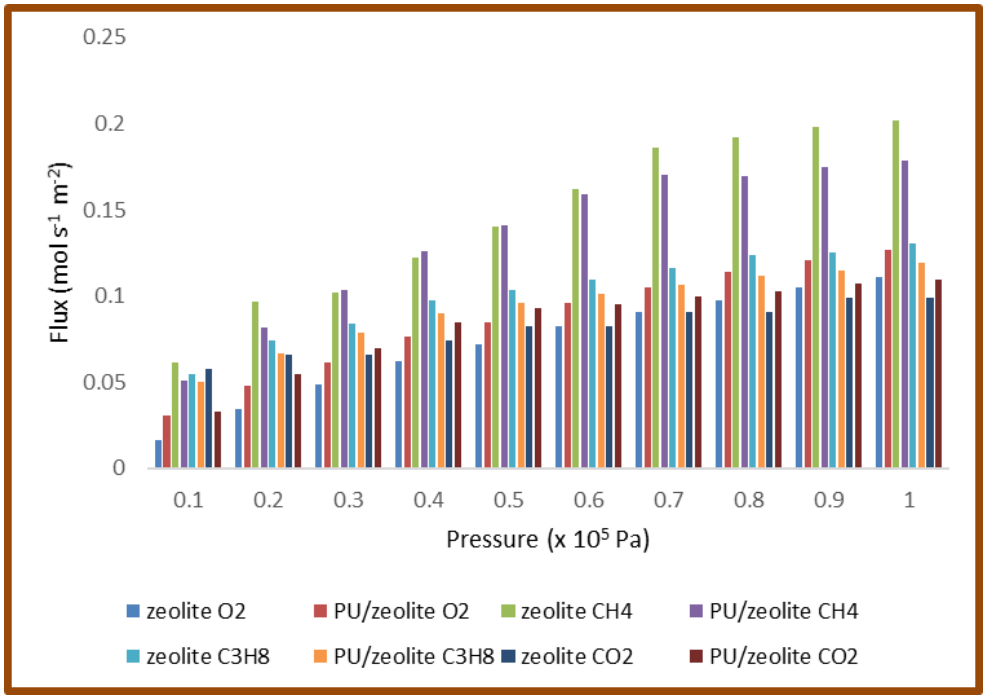

Figure 6-1: Flux of various gases through different membranes at 293 K

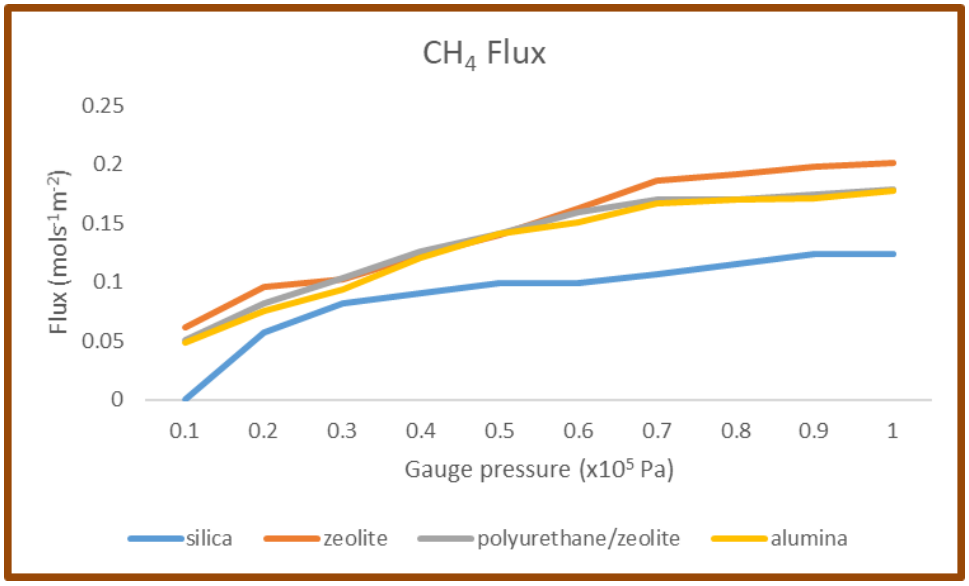

Figure 6-2: CH4 flux through various membranes at 293 K

For CO_2 separation, the silica membrane has shown the most potential. This is due to the high flux of CO_2 through the membrane (Figure 6-3).

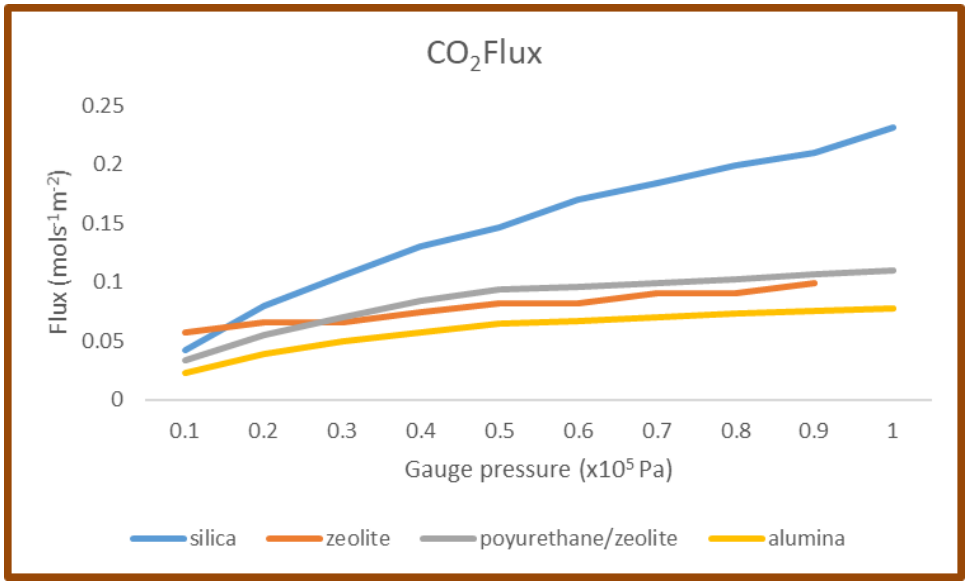

Figure 6-3: CO_2 flux through various membranes at 293 K

Examining the overall target gasses has proved the effectiveness of the silica membrane, in the recovery of CO_2. Silica was found to be unsuitable for the separation of hydrocarbons. However, there was little difference in the flux of C_3H_8, through all the membranes tested (Figure 6-4).

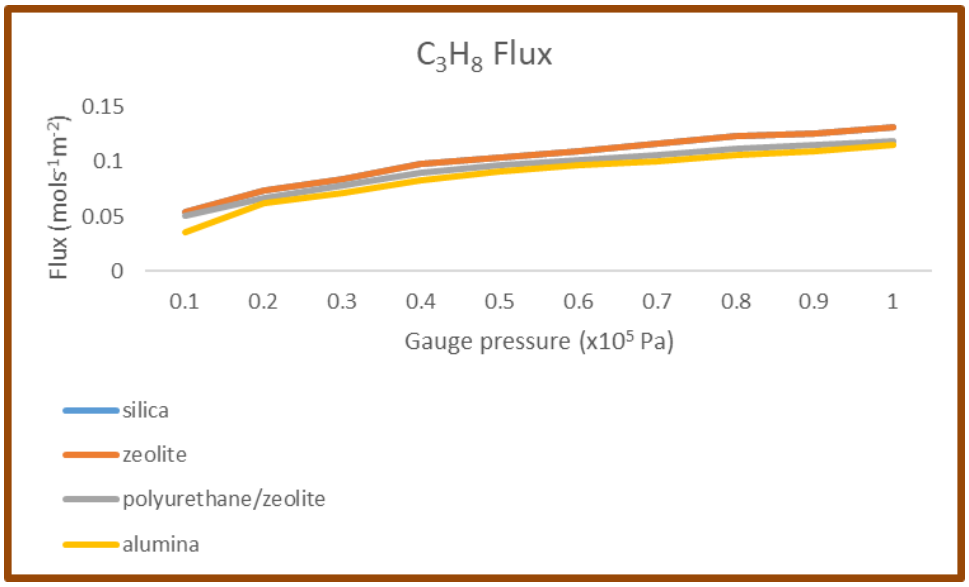

Figure 6-4: Propane flux through various membranes.

The average selectivity of methane, over target gases, has been calculated. It has been observed that low temperatures (298 K and 373 K) produced a better

separation factor for the separation of all the gases. The selectivity of CH_4/C_3H_8 has been shown to reduce with an increase in temperature. However, the selectivity of methane over the inert gases was shown to increase at 373 K and 473 K, but later reduced at 573 K. The high selectivity value of methane over other gases at high temperatures validated the high thermal stability property of the Y-type zeolite membrane. The experimental membrane selectivity values for CH_4/O_2, CH_4/C_3H_8, CH_4/N_2, CH_4/He and CH_4/CO_2 have been compared to the ideal Knudsen selectivity values and found to be higher. Having selectivity higher than Knudsen does not endorse the membrane for a commercial process but it does give a good indication that the membrane material could be suitable for an application Consequently, the use of zeolite membrane for the recovery of methane from oxygen, propane, nitrogen, helium and carbon dioxide could be further investigated.

The morphologies of the membranes have been examined using SEM. This revealed non-uniform pore sizes for all the membranes. Nitrogen adsorption/desorption of the membranes (Table 6.1) showed the zeolite membrane was more suitable for gas separations, even though the silica membrane has a higher surface area.

The elemental composition of the modified zeolite membrane obtained using EDAX indicated a higher weight of elements (*i.e.* C, O, Al, Ti and Si) compared to the unmodified membrane. Silica was found to be present in the modified membrane, indicated the presence of zeolite post modification. The elemental composition of the zeolite powder has been examined. The results indicate that the zeolite powder is made up of tetrahedral units of AlO_4 and SiO_4. The percentage weight of oxygen present is approximately four times that of aluminium and silicon (Table 6.2).

Table 6.1: N_2 adsorption/desorption summary of the membranes studied.

Membrane	BET surface area (m^2/g)	Pore diameter (nm)	Pore volume (cm^3/g)
y-type zeolite membrane	0.106	3.139	0.025
Silica membrane	10.69	4.18	0.027
Polyurethane/zeolite membrane	0.31	3.32	

Table 6.2: EDAX summary of the membranes

Element	Zeolite powder weight (%)	Synthesised y-type zeolite membrane weight (%)	Alumina support weight (%)	Silica membrane weight (%)	Polyurethane/y-type zeolite membrane weight (%)
C	53.72	3.82	6.92	31.97	71.33
Al	34.27	3.11	2.17	5.81	0.31
O	138.04	53.19	40.45	26.74	28.18
Si	37.05	0.50	-	32.21	0.06
Ti	-	60.63	50.46	3.20	-
Na	30.46	-	-	-	-

Based on the observations in the previous chapters, a prototype flow diagram (Figure 6-5) surmmarises the key findings in this work. However, further work needs to be done to improve the selectivities of the synthesised membranes. The disadvantages of using a membrane reactor commercially include: cost price of membrane materials, membrane pollution and the challenge of the membrane having low selectivity.

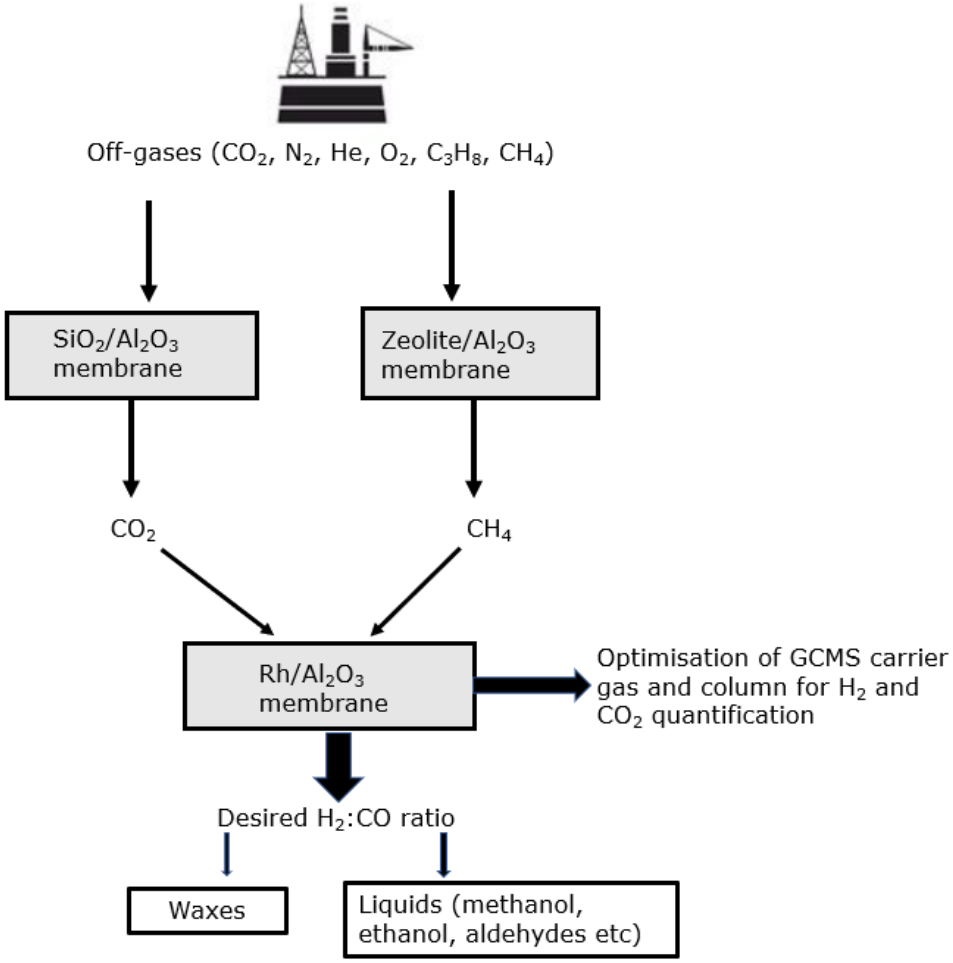

Figure 6-5: Flow diagram for off-gases separation and utilisation

Gas separation using a membrane can be an effective substitute for traditional processes because of its operational ease, economic viability, low maintenance, low energy consumption, small footprint and dependable performances. However, the scale up of membranes for use in industry have two major cost implications: capital investments and operating costs. The capital cost is affected by the membrane area. The higher the membrane area the lower the capital cost for the scale up of that membrane. From Table 6.1, the silica membrane has the highest surface area of 10.69 m^2/g in comparison with the other membranes synthesised. This suggests that the cost for the scale up of the silica membrane will be lower than that of the zeolite membrane, although it is not easy to obtain a reliable cost data for the membranes. The operating cost are determined by the frequency of membrane replacement due to fouling, system maintenance by cleaning, pumping energy and labour. The cost associated with the loss of any valuable gas is also

considered as operating cost. Based on the available literature (244, 245), the following guidelines for the membrane scale up were developed:

1. The average service life of an inorganic membrane is approximately 3 to 5 years as opposed to the 1 to 3 years of an organic polymer membrane, although, the durability of the membrane is dependent on the module design and nature of the feed gas.
2. Maintenance cost is 5 to 10 % of the capital investments.
3. The total system cost is typically 3 to 5 times higher than the module cost.
4. For membrane scale-up in general, the membrane system cost is directly related to the membrane permeation surface area.

A realistic approach to scale up this membrane is to design a concept where the membrane is incorporated into modular configurations, thus allowing different membranes to be run in parallel as shown in Figure 6-5 either in series or as a continuous system. The focus of future scaled up work will be the cost analysis of membrane reactor unit and the cost of the rhodium catalyst.

7 Conclusions and Recommendations for further Work

7.1 Conclusions

Membrane technology has been used as an alternative method for separating gases and for the utilisation of separated gases by incorporating catalysts for the conversion into valuable chemical feedstock. This work has focused on the study of various membrane materials and their suitability for both gas separation and catalytic conversion. A system that combines both the chemical reaction and separation process of a reactant or product is compact. Moreover, it fits with the process intensification (PI) strategy, which focuses on boosting efficiency. Therefore, the following conclusions have been made:

7.1.1 *Gas Separation from Off Gases*

This study has identified that the y-type zeolite membrane is suitable for the separation of methane from off gases in a temperature range of 293 to 573 K, and a pressure range of 0.1 to 1×10^5 Pa. The selectivity of the membrane for CH_4 over C_3H_8, CO_2, N_2, O_2 and He has been determined. The results indicate a higher selectivity for CH_4 when compared to the other membranes. The transport mechanism through the membrane has been shown to closely resemble molecular sieving. At low pressure (2×10^4 Pa to 1.0×10^5 Pa), CH_4 has been found to have the highest permeance through the zeolite membrane. However, He has been shown seen to have the highest permeance at all temperatures at pressures ≥ 1.0×10^5 Pa. This is due to the lower molecular weight of helium. The permeances of O_2, CH_4, N_2, He and CO_2 have been shown to increase with increased temperatures. However, the increase in temperature had little effect on the permeance of C_3H_8. The activation energy values obtained for each gas indicated that it is easier for the inert gases to break the flow barriers and pass through the membrane.

A plot of gas permeance against kinetic diameter has been used to show that the main transport mechanism governing the flow of the gases through the modified y-type zeolite membrane was molecular sieving. He was found to have the smallest

kinetic diameter and greatest permeance, while C_3H_8 had the highest kinetic diameter and lowest permeance. CO_2 and CH_4 were found to deviate from the expected flow pattern. This has been attributed to either an inter-crystalline defect during the seeding procedure of the zeolite membrane or the presence of an alternate flow mechanism.

The effectiveness of the zeolite membrane in recovery of lower hydrocarbons has been tested. This has been investigating by examining the selectivity of CH_4 over C_3H_8, CO_2, N_2, O_2 and He. The average selectivity of methane over the other gases has been calculated and it was observed that lower temperatures of 298 K and 373 K gave rise to better separation factors for the separation of all the gases. The selectivity of CH_4/C_3H_8 was found to reduce with increasing temperatures. However, the selectivity of CH_4/inert gas was found to increase at 373 K and 473 K, followed by a reduction at 573 K. The experimental membrane selectivity values CH_4/O_2, CH_4/C_3H_8, CH_4/N_2, CH_4/He and CH_4/CO_2 have been compared to the ideal Knudsen selectivity values. The experimental selectivity values have been found to be higher. This endorses the use of the y-type zeolite membrane for the recovery of CH_4 from C_3H_8, CO_2, N_2, O_2 and He.

The morphologies of the membrane support and the modified membranes have been investigated using SEM. Unmodified SEM images reveal non-uniform pore sizes. For the zeolite membrane, the outer surface and cross-section of the modified SEM images revealed the zeolite crystals dispersed on the support and were observed to be quite uniform. Moreover, images of the inner surface revealed the formation of an intermediate layer on the support.

The pore volume, surface area, pore diameter, and pore size distribution of the modified zeolite membrane was determined using N_2 desorption/adsorption BJH and BET methods. The modified zeolite membrane was found to be microporous. The surface area of the membrane was found to increase after deposition of zeolite on the support. Moreover, a reduction in the pore diameter of the zeolite membrane was also observed.

7.1.2 *CH_4 Dry Reforming Using CO_2*

CH_4 dry reforming with CO_2 is a highly endothermic reaction that can be used for

CH_4 and CO_2 utilisation to produce highly concentrated CO, useful for other processes. In this research, experimental work has been carried out on the dry reforming of CH_4 with CO_2. A comprehensive review of the catalyst design and preparation, catalytic activity and thermodynamic-kinetic analysis has been carried out. Catalyst deactivation as a result of carbon deposition, off-gas flow rate, reaction temperature and presence of NO_2 contaminant were the main concerns of this process. These are inherently influenced by catalyst design and the chosen reaction conditions.

Four other reforming methods have also been reviewed for comparison. These include, SMR, POA, ATR and Tri reforming. Currently SMR is the most applied industrial technology and is more developed than the other methods. The common feature of all reforming processes, including DRM, is the utilisation of oxidising agents to oxidise CH_4 over a heterogeneous catalyst to produce CO and H_2 syngas in a ratio that depends on both the type of oxidant and on thermodynamic variables. Nevertheless, each of these processes suffers from carbon deactivation and high process costs. Interestingly, methane dry reforming is unique due to its novel utilisation of CO_2 as feedstock material rather than treating it as a waste that can potentially offset increasing future GHG emissions. In the flow-through catalytic membrane reactor setup, the mixed gases flow through the catalytic membrane. This results in complete conversion of $\mathbf{CH_4}$, and $\mathbf{CO_2}$. This takes advantage of intensified catalytic efficiency that occurs from the intimate contact between the reactants and the catalyst. It has been noted that this is the first study to attempt the use of a flow-through catalytic membrane for flue gas methane reforming. The use of a catalytic membrane reactor for the flue gas reforming of CH_4 has been proven. The effect of superficial feed gas velocity on CO_2 and CH_4 conversion and catalyst stability under different operating conditions has been tested for the membranes studied. Three reaction temperatures 973, 1073 and 1173 K have been studied. Lower CO_2 conversions have been observed at 973 K, which implies CO_2 reforming of CH_4 is more favourable at high temperatures. The membrane was found to be stable in an $\mathbf{NO_2}$ environment for up to 2 hours without any deterioration in activity or coke formation. Therefore, it can be concluded that a Rh catalyst on alumina support can have optimal performance for CMR.

7.2 Recommendations for Future Work

The recommendations for future work have been based on some of the challenges experienced during reforming reactions and gas separations. The flue gas used in this work was limited to CO_2, oxides of nitrogen and CH_4 mixtures. There are other important species of off-gases that may impact the conversion for DRM, permeability and selectivity for gas separations using inorganic membranes. Substances including oxygen, water and SO_X could potentially lead to changes in the experimental design. One vital limitation in this work was control of catalyst loading on the membrane. Based on the above factors, the following recommendations for further investigation have been made:

1. The feasibility of the scale up of zeolite membrane for industrial gas recovery should be studied.

2. A reproducibility study to ascertain the repeatability and reproducibility of the synthesis method for the zeolite membrane should be examined.

3. Investigation into improving the synthesis of zeolite membrane in order to synthesise a defect free membrane.

4. Different CO_2/CH_4 ratios of the feed gas should be used to determine the effect of the ratio on the syngas produced.

5. Thermal stability of synthesised zeolite membrane should be investigated at higher temperatures (up to 1173 K), to determine its suitability for methane reforming reactions.

6. The easy clean-ability and catalytic properties of the y-type zeolite membrane should be investigated.

7. A different carrier gas should be used on the GCMS in order to be able to quantify the amount of H_2 and CO produced for the dry reforming reactions. This will help determine the utilisation of the products for future use. For example, in the Fischer-Tropsch process, and for the production of base chemicals such as methanol or dimethyl ether (DME) production.

8. Conduct tests for extended periods of time over and above the 6 h test carried out in this work. Moreover, to monitor CO_2 and CH_4 conversion and syngas yield.

9. The CO_2/CH_4 ratio should be varied to ascertain the effects of ratios that are higher or lower than 1.

References

(1) Teske S, Fattal A, Lins C, Hullin M, Williamson LE. Renewables Global Futures Report: Great debates towards 100% renewable energy. France: 2017.

(2) da Graça Carvalho M. EU energy and climate change strategy. *Energy.* 2012; 40(1): 19-22.

(3) Tamaddoni M, Sotudeh-Gharebagh R, Nario S, Hajihosseinzadeh M, Mostoufi N. Experimental study of the VOC emitted from crude oil tankers. *Process Safety and Environmental Protection.* 2014; 92(6): 929-937.

(4) Martens OM, Oldervik O, Neeraas BO, Strøm T. Control of VOC emissions from crude oil tankers. *Marine Technology.* 2001; 38(3): 208-217.

(5) Gitis V, Rothenberg G. *Ceramic Membranes: New Opportunities and Practical Applications.* New Jersey: John Wiley & Sons; 2016.

(6) Lan R, Irvine JT, Tao S. Ammonia and related chemicals as potential indirect hydrogen storage materials. *International Journal of Hydrogen Energy.* 2012; 37(2): 1482-1494.

(7) Minardi E, Chakraborty S, Curcio S. Membrane reactors for dry reforming of methane. Cambridge: Woodhead; 2015.

(8) Schlögl R. Catalytic Synthesis of Ammonia—A "Never-Ending Story"? *Angewandte Chemie International Edition.* 2003; 42(18): 2004-2008.

(9) Wang ZX, Dong T, Yuan LX, Kan T, Zhu XF, Torimoto Y, et al. Characteristics of bio-oil-syngas and its utilization in Fischer– Tropsch synthesis. *Energy & Fuels.* 2007; 21(4):2 421-2432.

(10) Yin X, Leung DY, Chang J, Wang J, Fu Y, Wu C. Characteristics of the synthesis of methanol using biomass-derived syngas. *Energy & Fuels.* 2005; 19(1): 305-310.

(11) Lee S, Choi I, Chang D. Multi-objective optimization of VOC recovery and reuse in crude oil loading. *Applied Energy.* 2013; 108: 439-447.

(12) Ürge-Vorsatz D, Herrero ST, Dubash NK, Lecocq F. Measuring the co-benefits of climate change mitigation. *Annual Review of Environment and Resources.* 2014; 39: 549-582.

(13) Ghoshal A, Manjare S. Selection of appropriate adsorption technique for recovery of VOCs: an analysis. *Journal of Loss Prevention in the Process Industries.* 2002; 15(6): 413-421.

(14) Derwent RG, Witham CS, Utembe SR, Jenkin ME, Passant NR. Ozone in Central England: the impact of 20 years of precursor emission controls in Europe.

Environmental Science & Policy. 2010; 13(3): 195-204.

(15) Tamaddoni M, Sotudeh-Gharebagh R, Nario S, Hajihosseinzadeh M, Mostoufi N. Experimental study of the VOC emitted from crude oil tankers. *Process Safety and Environmental Protection.* 2013; 92(6): 929-937.

(16) Lalić B. Air pollution prevention from volatile organic compound on shuttle tankers. Croatia: 14th International Reasherch/Expert Conference; 2010 [updated 2010 September 18; cited 2017 February 2]. Available from: http://citeseerx.ist.psu.edu/viewdoc/download?doi=10.1.1.402.8275&rep=rep1&type=pdf.

(17) Wilson J. Shuttle tankers vs. pipelines in the GOM frontier-FPSO developments could create a shuttle tanker service market. *World Oil.* 2008; 149.

(18) Huglen O and Vik R. Reducing VOC Emissions from Large Crude Carriers. Reducing VOC Emissions from Large Crude Carriers. Houston: Offshore Technology Conference; 30th April to 3rd May 2001.

(19) Gupta VK, Verma N. Removal of volatile organic compounds by cryogenic condensation followed by adsorption. *Chemical Engineering Science.* 2002; 57(14):2 679-2696.

(20) Yun J, Choi D, Kim S. Adsorption equilibria of chlorinated organic solvents onto activated carbon. *Industrial & Engineering Chemistry Research.* 1998; 37(4): 1422-1427.

(21) Yun J, Choi D, Kim S. Adsorption of organic solvent vapors on hydrophobic Y-type zeolite. *AIChE Journal.* 1998; 44(6): 1344-1350.

(22) Jiang XC, Ding J, Kumar A. Polyurethane–poly (vinylidene fluoride)(PU–PVDF) thin film composite membranes for gas separation. *Journal of Membrane Science.* 2008; 323(2): 371-378.

(23) Lapkin A, Roschupkina O, Ilinitch O. Transport of C 1–C 3 hydrocarbons in poly (phenylene oxides) membranes. *Journal of Membrane Science.* 1998; 141(2): 223-229.

(24) Tanaka K, Taguchi A, Hao J, Kita H, Okamoto K. Permeation and separation properties of polyimide membranes to olefins and paraffins. *Journal of Membrane Science.* 1996; 121(2): 197-207.

(25) Staudt-Bickel C, Koros WJ. Olefin/paraffin gas separations with 6FDA-based polyimide membranes. *Journal of Membrane Science.* 2000; 170(2): 205-214.

(26) Strathmann H. Membrane separation processes: current relevance and future opportunities. *AIChE Journal.* 2001; 47(5): 1077-1087.

(27) Bernardo P, Drioli E, Golemme G. Membrane gas separation: a review/state of the art. *Industrial & Engineering Chemistry Research.* 2009; 48(10): 4638-4663.

(28) Mokhatab S, Poe WA. *Handbook of natural gas transmission and processing.*

Texas: Gulf professional publishing; 2012.

(29) Watler KG. Membrane Technology and Research Inc, assignee. *Process for separating higher hydrocarbons from natural or produced gas streams.* Google Patent US07139914. 1987-12-31.

(30) Richard W. Baker. *Membrane Technology and Applications.* 3rd edition. Cambridge: John Wiley and Sons Ltd; 2012.

(31) White LS. Evolution of natural gas treatment with membrane systems. *Membrane Gas Separation.* 2010; 313.

(32) Baker RW, Lokhandwala K. Natural gas processing with membranes: an overview. *Industrial & Engineering Chemistry Research.* 2008; 47(7): 2109-2121.

(33) Graham J, Krenek M, Maxon D, Peirson J, Thompson J. Natural Gas Dehydration: Status and Trends. *Gas Research Institute Report GRI-94-099.* 1994.

(34) Baker RW. Future directions of membrane gas separation technology. *Industrial & Engineering Chemistry Research.* 2002; 41(6): 1393-1411.

(35) Tannehill CC, Raven M, Brown K. *Nitrogen Removal Requirements from Natural Gas: Topical Report.* : Gas Research Institute; 1999.

(36) Kidnay AJ, Parrish WR, McCartney DG. *Fundamentals of natural gas processing.* Florida: CRC Press; 2011.

(37) Kohl A, Nielsen R. Gas purification. 5th ed. Texas (Houston) Gulf Professional*;* 1997.

(38) Abedini R, Nezhadmoghadam A. Application of Membrane in Gas Separation Processes: Its Suitability and Mechanisms. *Petroleum & Coal.* 2010; 52(2): 69-80.

(39) Lin Y. Microporous and dense inorganic membranes: current status and prospective. *Separation and Purification Technology.* 2001; 25(1): 39-55.

(40) van de Graaf, Jolinde M, van der Bijl E, Stol A, Kapteijn F, Moulijn JA. Effect of operating conditions and membrane quality on the separation performance of composite silicalite-1 membranes. *Industrial & Engineering Chemistry Research.* 1998; 37(10): 4071-4083.

(41) Stern SA. Polymers for gas separations: the next decade. *Journal of Membrane Science.* 1994; 94(1): 1-65.

(42) Koros WJ. Gas separation membranes: needs for combined materials science and processing approaches. Proceedings of the *Macromolecular symposia*: Wiley Online Library; 2002. p. 13-22.

(43) Kentish SE, Scholes CA, Stevens GW. Carbon dioxide separation through polymeric membrane systems for flue gas applications. *Recent Patents on Chemical Engineering.* 2008; 1(1): 52-66.

(44) Dong X, Jin W, Xu N, Li K. Dense ceramic catalytic membranes and membrane

reactors for energy and environmental applications. *Chemical Communications.* 2011; 47(39): 10886-10902.

(45) Basile A. *Handbook of Membrane Reactors: Fundamental Materials Science, Design and Optimisation.* Cambridge: Woodhead; 2013.

(46) Freeman B, Yampolskii Y, Pinnau I. *Materials science of membranes for gas and vapor separation.* New Jersey: John Wiley & Sons; 2006.

(47) Pandey P, Chauhan R. Membranes for gas separation. *Progress in Polymer Science.* 2001; 26(6): 853-893.

(48) Julian A, Juste E, Chartier T, Del Gallo P and Richet N. Catalytic Membrane Reactor: Multilayer membranes elaboration. Catalytic Membrane Reactor: Multilayer membranes elaboration. *Proceedings of the 10th International Conference of the European Ceramic Society*; 2007. p. 718-722.

(49) Baker RW. *Membrane technology.* New Jersey: John Wiley and Sons; 2000.

(50) Hughes R. *Industrial membrane separation technology.* New York: Springer; 1996.

(51) Mulder M. *Basic Principles of Membrane Technology Second Edition.* Neatherlands: Kluwer Academic Pub; 1996.

(52) Breck D. Ion exchange reactions in zeolites. *Zeolite Molecular Sieves: Structure Chemistry and Use.* 1973; 529-592.

(53) Sidhu PS, Cussler E. Diffusion and capillary flow in track-etched membranes. *Journal of Membrane Science.* 2001; 182(1): 91-101.

(54) Choi J, Do D, Do H. Surface diffusion of adsorbed molecules in porous media: Monolayer, multilayer, and capillary condensation regimes. *Industrial & Engineering Chemistry Research.* 2001; 40(19): 4005-4031.

(55) Burggraaf AJ, Cot L. *Fundamentals of inorganic membrane science and technology.* Amsterdam: Elsevier; 1996.

(56) Chang X, Zhang C, Jin W, Xu N. Match of thermal performances between the membrane and the support for supported dense mixed-conducting membranes. *Journal of Membrane Science.* 2006; 285(1): 232-238.

(57) Kovalevsky A, Kharton V, Maxim F, Shaula A, Frade J. Processing and characterization of La 0.5 Sr 0.5 FeO_3-supported Sr 1− x Fe(Al)O_3–$SrAl_2O_4$ composite membranes. *Journal of Membrane Science.* 2006; 278(1): 162-172.

(58) Feng J, Qiu M, Fan Y, Xu N. The effect of membrane thickness on the co-sintering process of bi-layer ZrO_2/Al_2O_3 membrane. *Journal of Membrane Science.* 2007; 305(1): 20-26.

(59) Kovalevsky A, Yaremchenko A, Kolotygin V, Snijkers F, Kharton V, Buekenhoudt A, et al. Oxygen permeability and stability of asymmetric multilayer Ba 0.5 Sr 0.5 Co

0.8 Fe 0.2 O 3− δ ceramic membranes. *Solid State Ionics.* 2011; 192(1): 677-681.

(60) Julian A, Juste E, Geffroy P, Coudert V, Degot S, Del Gallo P, et al. Elaboration of La 0.8 Sr 0.2 Fe 0.7 Ga 0.3 O_3− δ/La 0.8 M 0.2 FeO_3− δ (M= Ca, Sr and Ba) asymmetric membranes by tape-casting and co-firing. *Journal of Membrane Science.* 2009; 333(1): 132-140.

(61) Watenabe K, Yuasa M, Kida T, Teraoka Y, Yamazoe N, Shimanoe K. High-Performance Oxygen-Permeable Membranes with an Asymmetric Structure Using Ba0. 95La0. 05FeO_3− δ Perovskite-Type Oxide. *Advanced Materials.* 2010; 22(21): 2367-2370.

(62) Yin X, Hong L, Liu Z. Asymmetric tubular oxygen-permeable ceramic membrane reactor for partial oxidation of methane. *The Journal of Physical Chemistry C.* 2007; 111(26):9 194-9202.

(63) Gobina E. Robert Gordon University, assignee. *Apparatus and method for separating gases.* United States Patent 7048778. 2006-23-5.

(64) Qi X, Akin F, Lin Y. Ceramic–glass composite high temperature seals for dense ionic-conducting ceramic membranes. *Journal of Membrane Science.* 2001; 193(2): 185-193.

(65) Hatcher J, Pascual MJ, Poulidi D, Metcalfe IS. Development and testing of an intermediate temperature glass sealant for use in mixed ionic and electronic conducting membrane reactors. *Solid State Ionics.* 2010; 181(15): 767-774.

(66) Pascual M, Guillet A, Durán A. Optimization of glass–ceramic sealant compositions in the system MgO–BaO–SiO_2 for solid oxide fuel cells (SOFC). *Journal of Power Sources.* 2007; 169(1): 40-46.

(67) Chou Y, Stevenson JW, Singh P. Effect of pre-oxidation and environmental aging on the seal strength of a novel high-temperature solid oxide fuel cell (SOFC) sealing glass with metallic interconnect. *Journal of Power Sources.* 2008; 184(1): 238-244.

(68) Chou Y, Thomsen EC, Williams RT, Choi J, Canfield NL, Bonnett JF, et al. Compliant alkali silicate sealing glass for solid oxide fuel cell applications: thermal cycle stability and chemical compatibility. *Journal of Power Sources.* 2011; 196(5): 2709-2716.

(69) Pierson HO. *Handbook of carbon, graphite, diamonds and fullerenes: processing, properties and applications.* New York: William Andrew; 2012.

(70) Balachandran U, Lee TH, Dorris SE. Hydrogen production by water dissociation using mixed conducting dense ceramic membranes. *International Journal of Hydrogen Energy.* 2007; 32(4).

(71) Evdou A, Nalbandian L, Zaspalis V. Perovskite membrane reactor for continuous and isothermal redox hydrogen production from the dissociation of water. *Journal of Membrane Science.* 2008; 325(2): 704-711.

(72) Saracco G, Neomagus HWJP, Versteeg GF, Swaaij WPMv. High-temperature

membrane reactors: potential and problems. *Chemical Engineering Science*. 1999; 54(13).

(73) Yaremchenko A, Kharton V, Valente A, Veniaminov S, Belyaev V, Sobyanin V, et al. Methane oxidation over mixed-conducting $SrFe(Al)O_3-\delta-SrAl_2O_4$ composite. *Physical Chemistry Chemical Physics.* 2007; 9(21): 2744-2752.

(74) Tan X, Li K. Design of mixed conducting ceramic membranes/reactors for the partial oxidation of methane to syngas. *AIChE Journal.* 2009; 55(10): 2675-2685.

(75) Czuprat O, Schiestel T, Voss H, Caro J. Oxidative coupling of methane in a BCFZ perovskite hollow fiber membrane reactor. *Industrial & Engineering Chemistry Research.* 2010; 49(21): 10230-10236.

(76) Olivier L, Haag S, Mirodatos C, van Veen AC. Oxidative coupling of methane using catalyst modified dense perovskite membrane reactors. *Catalysis today.* 2009; 142(1): 34-41.

(77) Czuprat O, Caro J, Kondratenko VA, Kondratenko EV. Dehydrogenation of propane with selective hydrogen combustion: A mechanistic study by transient analysis of products. *Catalysis Communications.* 2010; 11(15): 1211-1214.

(78) Rodriguez ML, Ardissone DE, Heracleous E, Lemonidou AA, López E, Pedernera MN, et al. Oxidative dehydrogenation of ethane to ethylene in a membrane reactor: A theoretical study. *Catalysis Today.* 2010; 157(1): 303-309.

(79) Baldus W, Tillman D. Conditions which need to be fulfilled by membrane systems in order to compete with existing methods for gas separation. *Membranes in Gas Separation and Enrichment.* Neatherlands: Kluwer Acdemic Publishers; 1986.

(80) Stangeland K. *Dry reforming of methane over nickel catalysts modified with noble metals.* Stavanger: University of Stavanger; 2016 [Updated 2016-06; cited 2017-09-01]. Available from: http://hdl.handle.net/11250/2408332.

(81) Dibbern H, Olesen P, Rostrup-Nielsen J, Tottrup P, Udengaard N. Make low H/sub 2//CO syngas using sulfur passivated reforming. *Hydrocarbon Process.;(United States).* 1986; 65(1).

(82) Corthals S, Witvrouwen T, Jacobs P, Sels B. Development of dry reforming catalysts at elevated pressure: D-optimal vs. full factorial design. *Catalysis today.* 2011; 159(1): 12-24.

(83) Rostrup-Nielsen J. 40 years in catalysis. *Catalysis Today.* 2006; 111(1-2): 4-11.

(84) Song X, Guo Z. Technologies for direct production of flexible H_2/CO synthesis gas. *Energy Conversion and Management.* 2006; 47(5): 560-569.

(85) Rostrup-Nielsen JR, Sehested J, Nørskov JK. Hydrogen and synthesis gas by steam-and $C0_2$ reforming. *Advances in catalysis.* 2002; 47: 65-139.

(86) Valderrama G, Goldwasser MR, de Navarro CU, Tatibouët JM, Barrault J, Batiot-Dupeyrat C, et al. Dry reforming of methane over Ni perovskite type oxides. *Catalysis*

Today. 2005; 107: 785-791.

(87) Hu Y, Ruckenstein E. An optimum NiO content in the CO_2 reforming of CH_4 with NiO/MgO solid solution catalysts. *Catalysis letters.* 1996; 36(3): 145-149.

(88) Pompeo F, Nichio NN, Souza MM, Cesar DV, Ferretti OA, Schmal M. Study of Ni and Pt catalysts supported on α-Al_2O_3 and ZrO_2 applied in methane reforming with CO_2. *Applied Catalysis A: General.* 2007; 316(2): 175-183.

(89) Gigola CE, Moreno MS, Costilla I, Sánchez MD. Characterization of Pd–CeO x interaction on α-Al_2O_3 support. *Applied Surface Science.* 2007; 254(1): 325-329.

(90) Bartholomew CH. Mechanisms of catalyst deactivation. *Applied Catalysis A: General.* 2001; 212(1): 17-60.

(91) Samuel P. GTL technology-challenges and opportunities in catalysis. *Bulletin of Catalysis Society of India.* 2003; 2(5): 82-99.

(92) Ghoneim SA, El-Salamony RA, El-Temtamy SA. Review on innovative catalytic reforming of natural gas to syngas. *World Journal of Engineering and Technology.* 2015; 4(01): 116.

(93) Rafiq MH, Hustad J. Synthesis gas from methane by using a plasma-assisted gliding arc catalytic partial oxidation reactor. *Industrial & Engineering Chemistry Research.* 2011; 50(9): 5428-5439.

(94) Neiva L, Gama L. A study on the characteristics of the reforming of methane: a review. *Brazilian Journal of Petroleum and Gas.* 2010; 4(3): 119-127.

(95) Gadalla AM, Bower B. The role of catalyst support on the activity of nickel for reforming methane with CO_2. *Chemical Engineering Science.* 1988; 43(11): 3049-3062.

(96) Wolf D, Buyevskaya O, Baerns M. An evolutionary approach in the combinatorial selection and optimization of catalytic materials. *Applied Catalysis A: General.* 2000; 200(1): 63-77.

(97) Shishido T, Yamamoto Y, Morioka H, Takaki K, Takehira K. Active Cu/ZnO and Cu/ZnO/Al_2O_3 catalysts prepared by homogeneous precipitation method in steam reforming of methanol. *Applied Catalysis A: General.* 2004; 263(2): 249-253.

(98) Widegren JA, Finke RG. A review of the problem of distinguishing true homogeneous catalysis from soluble or other metal-particle heterogeneous catalysis under reducing conditions. *Journal of Molecular Catalysis A: Chemical.* 2003; 198(1): 317-341.

(99) Eriksson S, Nylén U, Rojas S, Boutonnet M. Preparation of catalysts from microemulsions and their applications in heterogeneous catalysis. *Applied Catalysis A: General.* 2004; 265(2): 207-219.

(100) Sahli N, Petit C, Roger A, Kiennemann A, Libs S, Bettahar MM. Ni catalysts from $NiAl_2O_4$ spinel for CO_2 reforming of methane. *Catalysis Today.* 2006; 113(3): 187-

193.

(101) Ashcroft A, Cheetham A, Green M, Vernon P. Partial oxidation of methane to synthesis gas using carbon dioxide. *Nature.* 1991; 352(6332): 225-226.

(102) Chen D, Lødeng R, Anundskås A, Olsvik O, Holmen A. Deactivation during carbon dioxide reforming of methane over Ni catalyst: microkinetic analysis. *Chemical Engineering Science.* 2001; 56(4): 1371-1379.

(103) de Sousa FF, de Sousa HS, Oliveira AC, Junior MC, Ayala AP, Barros EB, et al. Nanostructured Ni-containing spinel oxides for the dry reforming of methane: effect of the presence of cobalt and nickel on the deactivation behaviour of catalysts. *International Journal of Hydrogen Energy.* 2012; 37(4): 3201-3212.

(104) Zhang Z, Verykios XE. Carbon dioxide reforming of methane to synthesis gas over Ni/La_2O_3 catalysts. *Applied Catalysis A: General.* 1996; 138(1): 109-133.

(105) Al-Fatesh AS, Fakeeha AH, Abasaeed AE. Effects of promoters on methane dry reforming over Ni catalyst on a mixed (a-Al_2O_3 TiO_2) support. *International Journal of Physical Sciences.* 2011; 6(36): 8083-8092.

(106) Amin MH, Putla S, Hamid SBA, Bhargava SK. Understanding the role of lanthanide promoters on the structure–activity of nanosized Ni/γ-Al_2O_3 catalysts in carbon dioxide reforming of methane. *Applied Catalysis A: General.* 2015; 492: 160-168.

(107) Yu M, Zhu Y, Lu Y, Tong G, Zhu K, Zhou X. The promoting role of Ag in Ni-CeO_2 catalyzed CH_4-CO_2 dry reforming reaction. *Applied Catalysis B: Environmental.* 2015; 165: 43-56.

(108) Rossetti I, Pernicone N, Forni L. Promoters effect in Ru/C ammonia synthesis catalyst. *Applied Catalysis A: General.* 2001; 208(1): 271-278.

(109) Qiu Y, Chen J, Zhang J. Effect of CeO_2 and CaO promoters on ignition performance for partial oxidation of methane over Ni/MgO-Al_2O_3 catalyst. *Journal of natural gas chemistry.* 2007; 16(2): 148-154.

(110) Qiu Y, Chen J, Zhang J. Effects of CeO_2 and CaO composite promoters on the properties of eggshell Ni/MgO-Al_2O_3 catalysts for partial oxidation of methane to syngas. *Reaction Kinetics and Catalysis Letters.* 2008; 94(2): 351-357.

(111) Qin H, Guo C, Wu Y, Zhang J. Effect of La_2O_3 promoter on NiO/Al_2O_3 catalyst in CO methanation. *Korean Journal of Chemical Engineering.* 2014; 31(7): 1168-1173.

(112) Nagaoka K, Seshan K, Aika K, Lercher JA. Carbon deposition during carbon dioxide reforming of methane—comparison between Pt/Al_2O_3 and Pt/ZrO_2. *Journal of Catalysis.* 2001; 197(1): 34-42.

(113) Zhang Z, Tsipouriari V, Efstathiou A, Verykios X. Reforming of methane with carbon dioxide to synthesis gas over supported rhodium catalysts: I. Effects of support and metal crystallite size on reaction activity and deactivation characteristics. *Journal of Catalysis.* 1996; 158(1): 51-63.

(114) Ruckenstein E, Hu YH. Role of Support in CO_2 Reforming of CH_4 to Syngas over Ni Catalysts. *Journal of Catalysis.* 1996; 162(2): 230-238.

(115) Nakamura J, Aikawa K, Sato K, Uchijima T. Role of support in reforming of CH_4 with CO_2 over Rh catalysts. *Catalysis letters.* 1994; 25(3-4): 265-270.

(116) Guo J, Lou H, Zhao H, Chai D, Zheng X. Dry reforming of methane over nickel catalysts supported on magnesium aluminate spinels. *Applied Catalysis A: General.* 2004; 273(1): 75-82.

(117) Goula M, Lemonidou A, Efstathiou A. Characterization of Carbonaceous Species Formed during Reforming of CH_4 with CO_2 over Ni/CaO–Al_2O_3 Catalysts Studied by Various Transient Techniques. *Journal of Catalysis.* 1996; 161(2): 626-640.

(118) Li Y, Wang Y, Zhang X, Mi Z. Thermodynamic analysis of autothermal steam and CO 2 reforming of methane. *International Journal of Hydrogen Energy.* 2008; 33(10): 2507-2514.

(119) Benguerba Y, Dehimi L, Virginie M, Dumas C, Ernst B. Numerical investigation of the optimal operative conditions for the dry reforming reaction in a fixed-bed reactor: role of the carbon deposition and gasification reactions. *Reaction Kinetics, Mechanisms and Catalysis.* 2015; 115(2): 483-497.

(120) Pakhare D, Spivey J. A review of dry (CO_2) reforming of methane over noble metal catalysts. *Chemical Society Reviews.* 2014; 43(22): 7813-7837.

(121) Tomishige K, Chen Y, Fujimoto K. Studies on Carbon Deposition in CO_2 Reforming of CH_4 over Nickel–Magnesia Solid Solution Catalysts. *Journal of Catalysis.* 1999; 181(1): 91-103.

(122) Djinović P, Črnivec IGO, Batista J, Levec J, Pintar A. Catalytic syngas production from greenhouse gasses: Performance comparison of Ru-Al_2O_3 and Rh-CeO_2 catalysts. *Chemical Engineering and Processing: Process Intensification.* 2011; 50(10): 1054-1062.

(123) Djaidja A, Messaoudi H, Kaddeche D, Barama A. Study of Ni–M/MgO and Ni–M–Mg/Al (M= Fe or Cu) catalysts in the CH_4–CO_2 and CH_4–H_2O reforming. *International Journal of Hydrogen Energy.* 2015; 40(14): 4989-4995.

(124) Fidalgo B, Zubizarreta L, Bermúdez JM, Arenillas A, Menéndez J. Synthesis of carbon-supported nickel catalysts for the dry reforming of CH_4. *Fuel Processing Technology.* 2010; 91(7): 765-769.

(125) Ma J, Sun N, Zhang X, Zhao N, Xiao F, Wei W, et al. A short review of catalysis for CO_2 conversion. *Catalysis Today.* 2009; 148(3): 221-231.

(126) Takanabe K, Nagaoka K, Nariai K, Aika K. Titania-supported cobalt and nickel bimetallic catalysts for carbon dioxide reforming of methane. *Journal of Catalysis.* 2005; 232(2): 268-275.

(127) Djinović P, Batista J, Pintar A. Efficient catalytic abatement of greenhouse gases: methane reforming with CO_2 using a novel and thermally stable Rh–CeO_2

catalyst. *International Journal of Hydrogen Energy.* 2012; 37(3): 2699-2707.

(128) Yoshida K, Okumura K, Miyao T, Naito S, Ito S, Kunimori K, et al. Oxidative steam reforming of methane over Ni/α-Al_2O_3 modified with trace Pd. *Applied Catalysis A: General.* 2008; 351(2): 217-225.

(129) Erdohelyi A, Cserényi J, Solymosi F. Activation of CH_4 and its reaction with CO_2 over supported Rh catalysts. *Journal of Catalysis.* 1993; 141(1): 287-299.

(130) Jones G, Jakobsen JG, Shim SS, Kleis J, Andersson MP, Rossmeisl J, et al. First principles calculations and experimental insight into methane steam reforming over transition metal catalysts. *Journal of Catalysis.* 2008; 259(1): 147-160.

(131) Ferreira-Aparicio P, Guerrero-Ruiz A, Rodrıguez-Ramos I. Comparative study at low and medium reaction temperatures of syngas production by methane reforming with carbon dioxide over silica and alumina supported catalysts. *Applied Catalysis A: General.* 1998; 170(1): 177-187.

(132) Bitter J, Seshan K, Lercher J. The State of Zirconia supported platinum catalysts for CO_2/CH_4 reforming. *Journal of Catalysis.* 1997; 171(1): 279-286.

(133) Bradford M, Vannice M. CO_2 reforming of CH_4. *Catalysis Reviews.* 1999; 41(1): 1-42.

(134) Ferreira-Aparicio P, Marquez-Alvarez C, Rodrıguez-Ramos I, Schuurman Y, Guerrero-Ruiz A, Mirodatos C. A transient kinetic study of the carbon dioxide reforming of methane over supported Ru catalysts. *Journal of Catalysis.* 1999; 184(1): 202-212.

(135) Hou Z, Chen P, Fang H, Zheng X, Yashima T. Production of synthesis gas via methane reforming with CO_2 on noble metals and small amount of noble (Rh) promoted Ni catalysts. *International Journal of Hydrogen Energy.* 2006; 31(5): 555-561.

(136) Ghelamallah M, Granger P. Supported-induced effect on the catalytic properties of Rh and Pt-Rh particles deposited on La 2 O 3 and mixed α-Al_2O_3-La_2O_3 in the dry reforming of methane. *Applied Catalysis A: General.* 2014; 485: 172-180.

(137) Arandiyan H, Peng Y, Liu C, Chang H, Li J. Effects of noble metals doped on mesoporous LaAlNi mixed oxide catalyst and identification of carbon deposit for reforming CH_4 with CO_2. *Journal of Chemical Technology and Biotechnology.* 2014; 89(3): 372-381.

(138) Nematollahi B, Rezaei M, Khajenoori M. Combined dry reforming and partial oxidation of methane to synthesis gas on noble metal catalysts. *International Journal of Hydrogen Energy.* 2011; 36(4): 2969-2978.

(139) Matsui N, Anzai K, Akamatsu N, Nakagawa K, Ikenaga N, Suzuki T. Reaction mechanisms of carbon dioxide reforming of methane with Ru-loaded lanthanum oxide catalyst. *Applied Catalysis A: General.* 1999; 179(1): 247-256.

(140) de Vos RM, Verweij H. High-selectivity, high-flux silica membranes for gas

separation. *Science (New York, N.Y.).* 1998; 279(5357): 1710-1711.

(141) Hsieh H. Inorganic membrane reactors. *Catalysis Reviews.* 1991; 33(1-2): 1-70.

(142) Eng D, Stoukides M. Catalytic and electrocatalytic methane oxidation with solid gxide membranes. *Catalysis Reviews.* 1991; 33(3-4): 375-412.

(143) Reyes SC, Iglesia E, Kelkar C. Kinetic-transport models of bimodal reaction sequences—I. Homogeneous and heterogeneous pathways in oxidative coupling of methane. *Chemical Engineering Science.* 1993; 48(14): 2643-2661.

(144) Mohan K, Govind R. Analysis of equilibrium shift in isothermal reactors with a permselective wall. *AIChE Journal.* 1988; 34(9): 1493-1503.

(145) Van Dyk L, Miachon S, Lorenzen L, Torres M, Fiaty K, Dalmon J. Comparison of microporous MFI and dense Pd membrane performances in an extractor-type CMR. *Catalysis today.* 2003; 82(1): 167-177.

(146) ten Hove M, Nijmeijer A, Winnubst L. Facile synthesis of zirconia doped hybrid organic inorganic silica membranes. *Separation and purification technology.* 2015; 147: 372-378.

(147) Yoshioka T, Nakanishi E, Tsuru T, Asaeda M. Experimental studies of gas permeation through microporous silica membranes. *AIChE Journal.* 2001; 47(9): 2052-2063.

(148) Boffa V, Blank DH, ten Elshof JE. Hydrothermal stability of microporous silica and niobia–silica membranes. *Journal of Membrane Science.* 2008; 319(1-2): 256-263.

(149) Gobina EN, Oklany JS, Hughes R. Elimination of ammonia from coal gasification streams by using a catalytic membrane reactor. *Industrial & Engineering Chemistry Research.* 1995; 34(11): 3777-3783.

(150) Li A, Zhao H, Gu J, Xiong G. Preparation of γ-Al_2O_3 composite membrane and examination of membrane defects. *Science in China Series B: Chemistry.* 1997; 40(1): 31-36.

(151) Goldstein JI, Newbury DE, Echlin P, Joy DC, Lyman CE, Lifshin E, et al. Generation of X-rays in the SEM specimen. *Scanning Electron Microscopy and X-Ray Microanalysis.* : Springer; 2003. p. 271-296.

(152) Jia C, Schwickardi M, Weidenthaler C, Schmidt W, Korhonen S, Weckhuysen BM, et al. Co_3O_4–SiO_2 nanocomposite: a very active catalyst for CO oxidation with unusual catalytic behavior. *Journal of the American Chemical Society.* 2011; 133(29): 11279-11288.

(153) Weidenthaler C. Pitfalls in the characterization of nanoporous and nanosized materials. *Nanoscale.* 2011; 3(3): 792-810.

(154) Beganskienė A, Sirutkaitis V, Kurtinaitienė M, Juškėnas R, Kareiva A. FTIR, TEM

and NMR investigations of Stöber silica nanoparticles. *Material Science (Medžiagotyra).* 2004; 10: 287-290.

(155) Kusakabe K, Kuroda T, Murata A, Morooka S. Formation of a Y-type zeolite membrane on a porous α-alumina tube for gas separation. *Industrial & Engineering Chemistry Research.* 1997; 36(3): 649-655.

(156) Li H, Schygulla U, Hoffmann J, Niehoff P, Haas-Santo K, Dittmeyer R. Experimental and modeling study of gas transport through composite ceramic membranes. *Chemical Engineering Science.* 2013; .

(157) Messaoud SB, Takagaki A, Sugawara T, Kikuchi R, Oyama ST. Alkylamine–silica hybrid membranes for carbon dioxide/methane separation. *Journal of Membrane Science.* 2015; 477: 161-171.

(158) Basile A. *Handbook of Membrane Reactors: Fundamental Materials Science, Design and Optimisation.* Amsterdam: Elsevier; 2013.

(159) Baerlocher C, McCusker LB, Olson DH. *Atlas of zeolite framework types.* Amsterdam: Elsevier; 2007.

(160) McLeary E, Jansen J, Kapteijn F. Zeolite based films, membranes and membrane reactors: Progress and prospects. *Microporous and Mesoporous Materials.* 2006; 90(1): 198-220.

(161) Caro J, Noack M, Kölsch P. Zeolite membranes: from the laboratory scale to technical applications. *Adsorption.* 2005; 11(3): 215-227.

(162) Geus E, Jansen J, Van Bekkum H. Calcination of large MFI-type single crystals: Part 1. Evidence for the occurrence of consecutive growth forms and possible diffusion barriers arising thereof. *Zeolites.* 1994; 14(2): 82-88.

(163) Jia M, Chen B, Noble RD, Falconer JL. Ceramic-zeolite composite membranes and their application for separation of vapor/gas mixtures. *Journal of Membrane Science.* 1994; 90(1-2): 1-10.

(164) Yan Y, Davis ME, Gavalas GR. Preparation of zeolite ZSM-5 membranes by in-situ crystallization on porous. alpha.-Al_2O_3. *Industrial & Engineering Chemistry Research.* 1995; 34(5): 1652-1661.

(165) Vroon Z, Keizer K, Gilde M, Verweij H, Burggraaf A. Transport properties of alkanes through ceramic thin zeolite MFI membranes. *Journal of Membrane Science.* 1996; 113(2): 293-300.

(166) Tavolaro A, Drioli E. Zeolite membranes. *Advanced Materials.* 1999; 11(12): 975-996.

(167) Pan M, Lin Y. Template-free secondary growth synthesis of MFI type zeolite membranes. *Microporous and Mesoporous Materials.* 2001; 43(3): 319-327.

(168) Lai Z, Bonilla G, Diaz I, Nery JG, Sujaoti K, Amat MA, et al. Microstructural optimization of a zeolite membrane for organic vapor separation. *Science (New York,*

N.Y.). 2003; 300(5618): 456-460.

(169) Hedlund J, Sterte J, Anthonis M, Bons A, Carstensen B, Corcoran N, et al. High-flux MFI membranes. *Microporous and Mesoporous Materials.* 2002; 52(3): 179-189.

(170) Miachon S, Ciavarella P, Van Dyk L, Kumakiri I, Fiaty K, Schuurman Y, et al. Nanocomposite MFI-alumina membranes via pore-plugging synthesis: specific transport and separation properties. *Journal of Membrane Science.* 2007; 298(1): 71-79.

(171) Illgen U, Schäfer R, Noack M, Kölsch P, Kühnle A, Caro J. Membrane supported catalytic dehydrogenation of iso-butane using an MFI zeolite membrane reactor. *Catalysis Communications.* 2001; 2(11): 339-345.

(172) Qi B, Lu X, Zhou D, Xia Q, Tang Z, Fang S, et al. Catalytic epoxidation of alkenes with 30% H_2O_2 over Mn_2 exchanged zeolites. *Journal of Molecular Catalysis A: Chemical.* 2010; 322(1): 73-79.

(173) Gu X, Tang Z, Dong J. On-stream modification of MFI zeolite membranes for enhancing hydrogen separation at high temperature. *Microporous and Mesoporous Materials.* 2008; 111(1): 441-448.

(174) Rohde MP, Unruh D, Schaub G. Membrane application in Fischer–Tropsch synthesis reactors—Overview of concepts. *Catalysis today.* 2005; 106(1): 143-148.

(175) Melian-Cabrera I, Espinosa S, Groen J, Kapteijn F, Moulijn J. Utilizing full-exchange capacity of zeolites by alkaline leaching: preparation of Fe-ZSM5 and application in N_2O decomposition. *Journal of Catalysis.* 2006; 238(2): 250-259.

(176) Zhu X, Liu S, Song Y, Xu L. Catalytic cracking of C4 alkenes to propene and ethene: influences of zeolites pore structures and Si/Al_2 ratios. *Applied Catalysis A: General.* 2005; 288(1): 134-142.

(177) van de Graaf, Jolinde M, Zwiep M, Kapteijn F, Moulijn JA. Application of a zeolite membrane reactor in the metathesis of propene. *Chemical engineering science.* 1999; 54(10): 1441-1445.

(178) Hasegawa Y, Kusakabe K, Morooka S. Selective oxidation of carbon monoxide in hydrogen-rich mixtures by permeation through a platinum-loaded Y-type zeolite membrane. *Journal of Membrane Science.* 2001; 190(1): 1-8.

(179) Bernardo P, Algieri C, Barbieri G, Drioli E. Hydrogen purification from carbon monoxide by means of selective oxidation using zeolite catalytic membranes. *Separation and Purification Technology.* 2008; 62(3): 629-635.

(180) Burggraaf A. Single gas permeation of thin zeolite (MFI) membranes: theory and analysis of experimental observations. *Journal of Membrane Science.* 1999; 155(1): 45-65.

(181) Den Exter M, Jansen J, van de Graaf J, Kapteijn F, Moulijn J, Van Bekkum H. Zeolite-based membranes preparation, performance and prospects. *Studies in Surface Science and Catalysis.* 1996; 102: 413-454.

(182) Barrer RM. Porous crystal membranes. *Journal of Chemical Society: Faraday Trans.* 1990; 86(7): 1123-1130.

(183) Krishna R, Van Baten J. Describing binary mixture diffusion in carbon nanotubes with the Maxwell-Stefan equations. An investigation using molecular dynamics simulations. *Industrial & Engineering Chemistry Research.* 2006; 45(6): 2084-2093.

(184) Xiao J, Wei J. Diffusion mechanism of hydrocarbons in zeolites—I. Theory. *Chemical Engineering Science.* 1992; 47(5): 1123-1141.

(185) White JC, Dutta PK, Shqau K, Verweij H. Synthesis of ultrathin zeolite Y membranes and their application for separation of carbon dioxide and nitrogen gases. *Langmuir.* 2010; 26(12): 10287-10293.

(186) Robeson LM. The upper bound revisited. *Journal of Membrane Science.* 2008; 320(1): 390-400.

(187) Süer MG, Baç N, Yilmaz L. Gas permeation characteristics of polymer-zeolite mixed matrix membranes. *Journal of Membrane Science.* 1994; 91(1-2): 77-86.

(188) Afarani HT, Sadeghi M, Moheb A. The Gas Separation Performance of Polyurethane–Zeolite Mixed Matrix Membranes. *Advances in Polymer Technology.* 2016; 37(2): 309-640.

(189) Tantekin-Ersolmaz ŞB, Şenorkyan L, Kalaonra N, Tatlıer M, Erdem-Şenatalar A. n-Pentane/i-pentane separation by using zeolite–PDMS mixed matrix membranes. *Journal of Membrane Science.* 2001; 189(1):59-67.

(190) Sadeghi M, Afarani HT, Tarashi Z. Preparation and investigation of the gas separation properties of polyurethane-TiO_2 nanocomposite membranes. *Korean Journal of Chemical Engineering.* 2015; 32(1): 97-103.

(191) Kim S, Marand E. High permeability nano-composite membranes based on mesoporous MCM-41 nanoparticles in a polysulfone matrix. *Microporous and Mesoporous Materials.* 2008; 114(1): 129-136.

(192) Alhoshan M, Alam J, Dass LA, Al-Homaidi N. Fabrication of polysulfone/ZnO membrane: influence of ZnO nanoparticles on membrane characteristics. *Advances in Polymer Technology.* 2013; 32(4).

(193) Li Y, Chung T, Cao C, Kulprathipanja S. The effects of polymer chain rigidification, zeolite pore size and pore blockage on polyethersulfone (PES)-zeolite A mixed matrix membranes. *Journal of Membrane Science.* 2005; 260(1): 45-55.

(194) Sadeghi M, Semsarzadeh MA, Barikani M, Chenar MP. Gas separation properties of polyether-based polyurethane–silica nanocomposite membranes. *Journal of Membrane Science.* 2011; 376(1): 188-195.

(195) Sadeghi M, Talakesh MM, Ghalei B, Shafiei M. Preparation, characterization and gas permeation properties of a polycaprolactone based polyurethane-silica nanocomposite membrane. *Journal of Membrane Science.* 2013; 427: 21-29.

(196) Mohagheghian M, Sadeghi M, Chenar MP, Naghsh M. Gas separation properties of polyvinylchloride (PVC)-silica nanocomposite membrane. *Korean Journal of Chemical Engineering.* 2014; 31(11): 2041-2050.

(197) Lin Y, Wang J, Zhang Z, Bai H, Li Y, Zhu D, et al. An electron acceptor challenging fullerenes for efficient polymer solar cells. *Advanced Materials.* 2015; 27(7): 1170-1174.

(198) Rajesh S, Murthy Z. In Situ Synthesis and Characterization of 2, 2′-Methylenebis (6-tert-butyl-4-ethylphenol)-Incorporated Polymeric Membranes. *Advances in Polymer Technology.* 2014; 33(1). 70-304

(199) Tirouni I, Sadeghi M, Pakizeh M. Separation of C_3H_8 and C_2H_6 from CH_4 in polyurethane–zeolite 4Å and ZSM-5 mixed matrix membranes. *Separation and Purification Technology.* 2015; 141(3): 94-402.

(200) Ismail AF, Khulbe KC, Matsuura T. *Gas Separation Membranes.* New York: Springer; 2015.

(201) Cong H, Radosz M, Towler BF, Shen Y. Polymer–inorganic nanocomposite membranes for gas separation. *Separation and Purification Technology.* 2007; 55(3): 281-291.

(202) Li C, Shao H, Zhong S. Preparation technology of organic-inorganic hyhrid membrane. *Progress in Chemistry.* 2004; 16(1): 83-89.

(203) Genné I, Kuypers S, Leysen R. Effect of the addition of ZrO_2 to polysulfone based UF membranes*. Journal of Membrane Science.* 1996; 113(2): 343-350.

(204) Wara NM, Francis LF, Velamakanni BV. *Addition of alumina to cellulose acetate membranes.* 1995ID: 271357.

(205) Stephen R, Ranganathaiah C, Varghese S, Joseph K, Thomas S. Gas transport through nano and micro composites of natural rubber (NR) and their blends with carboxylated styrene butadiene rubber (XSBR) latex membranes. *Polymer Science*. 2006; 47(3): 858-870.

(206) Mascia L, Zhang Z, Shaw SJ. *Carbon fibre composites based on polyimide/silica ceramers: aspects of structure-properties relationship.* 1996ID: 271638.

(207) Liu H. Synthesis of TiO_2 nanopowder enwrapped by organic membrane with microwave induced plasma method. *Huaxue Tongbao.* 1997; 10: 44-46.

(208) Wang S, Liao X, Hu J, Cao D, Li Y, Wang J, et al. Kinetic aspect of CO_2 reforming of CH_4 on Ni (111): a density functional theory calculation. *Surface Science.* 2007; 601(5): 1271-1284.

(209) Rostrupnielsen J, Hansen JB. CO_2-reforming of methane over transition metals. *Journal of Catalysis.* 1993; 144(1): 38-49.

(210) Gronchi P, Centola P, Del Rosso R. Dry reforming of CH_4 with Ni and Rh metal catalysts supported on SiO_2 and La_2O_3. *Applied Catalysis A: General.* 1997; 152(1):

83-92.

(211) Richardson J, Paripatyadar S. Carbon dioxide reforming of methane with supported rhodium. *Applied Catalysis.* 1990; 61(1): 293-309.

(212) Fisher F, Tropsch H. Conversion of methane into hydrogen and carbon monoxide. *Brennst.-Chem.* 1928; 9.

(213) Iyer MV, Norcio LP, Kugler EL, Dadyburjor DB. Kinetic modeling for methane reforming with carbon dioxide over a mixed-metal carbide catalyst. *Industrial & Engineering Chemistry Research.* 2003; 42(12): 2712-2721.

(214) Wei J, Iglesia E. Structural requirements and reaction pathways in methane activation and chemical conversion catalyzed by rhodium. *Journal of Catalysis.* 2004; 225(1): 116-127.

(215) Mark MF, Maier WF, Mark F. Reaction kinetics of the CO_2 reforming of methane. *Chemical Engineering & Technology.* 1997; 20(6): 361-370.

(216) Bitter J, Seshan K, Lercher J. On the contribution of X-ray absorption spectroscopy to explore structure and activity relations of Pt/ZrO_2 catalysts for CO_2/CH_4 reforming. *Topics in Catalysis.* 2000; 10(3-4): 295-305.

(217) Chen C, Cheng W, Lin S. Study of iron-promoted Cu/SiO_2 catalyst on high temperature reverse water gas shift reaction. *Applied Catalysis A: General.* 2004; 257(1): 97-106.

(218) Junke X, Wei Z, Jihui W, Zhaojing L, Jianxin M. Characterization and analysis of carbon deposited during the dry reforming of methane over $Ni/La_2O_3/Al_2O_3$ catalysts. *Chinese Journal of Catalysis.* 2009; 30(11): 1076-1084.

(219) Ferreira-Aparicio P, Rodrıguez-Ramos I, Anderson J, Guerrero-Ruiz A. Mechanistic aspects of the dry reforming of methane over ruthenium catalysts. *Applied Catalysis A: General.* 2000; 202(2): 183-196.

(220) Zhang Z, Verykios X. Carbon dioxide reforming of methane to synthesis gas over supported Ni catalysts. *Catalysis Today.* 1994; 21(2-3): 589-595.

(221) Wei J, Iglesia E. Isotopic and kinetic assessment of the mechanism of reactions of CH_4 with CO_2 or H_2O to form synthesis gas and carbon on nickel catalysts. *Journal of Catalysis.* 2004; 224(2): 370-383.

(222) Ferreira-Aparicio P, Fernandez-Garcia M, Guerrero-Ruiz A, Rodrıguez-Ramos I. Evaluation of the role of the metal–support interfacial centers in the dry reforming of methane on alumina-supported rhodium catalysts. *Journal of Catalysis.* 2000; 190(2): 296-308.

(223) Li C, Yan W, Xin Q. Interaction of methane with surface of alumina studied by FT-IR spectroscopy. *Catalysis letters.* 1994; 24(3): 249-256.

(224) Solymosi F, Cserényi J. Decomposition of CH_4 over supported Ir catalysts. *Catalysis today.* 1994; 21(2-3): 561-569.

(225) Patil CS, van Sint Annaland M, Kuipers J. Fluidised bed membrane reactor for ultrapure hydrogen production via methane steam reforming: Experimental demonstration and model validation. *Chemical Engineering Science.* 2007; 62(11): 2989-3007.

(226) Tong J, Matsumura Y. Pure hydrogen production by methane steam reforming with hydrogen-permeable membrane reactor. *Catalysis today.* 2006; 111(3): 147-152.

(227) Nikoo MB, Mahinpey N. Simulation of biomass gasification in fluidized bed reactor using ASPEN PLUS. *Biomass and Bioenergy.* 2008; 32(12): 1245-1254.

(228) Istadi I, Amin NAS. Modelling and optimization of catalytic–dielectric barrier discharge plasma reactor for methane and carbon dioxide conversion using hybrid artificial neural network—genetic algorithm technique. *Chemical Engineering Science.* 2007; 62(23): 6568-6581.

(229) Khalesi A, Arandiyan HR, Parvari M. Effects of lanthanum substitution by strontium and calcium in La-Ni-Al perovskite oxides in dry reforming of methane. *Chinese Journal of Catalysis.* 2008; 29(10): 960-968.

(230) Istadi I, Amin NAS, Aishah N. Co-generation of C_2 hydrocarbons and synthesis gases from methane and carbon dioxide: a thermodynamic analysis. *Journal of Natural Gas Chemistry.* 2005; 14: 140-150.

(231) Wisniewski M, Boréave A, Gélin P. Catalytic CO_2 reforming of methane over Ir/Ce 0.9 Gd 0.1 O 2− x. *Catalysis Communications.* 2005; 6(9): 596-600.

(232) Li Y, Jin B, Xiao R. Carbon dioxide reforming of methane with a free energy minimization approach. *Korean Journal of Chemical Engineering.* 2007; 24(4): 688-692.

(233) Takano A, Tagawa T, Goto S. Carbon dioxide reforming of methane on supported nickel catalysts. *Journal of Chemical Engineering of Japan.* 1994; 27(6): 727-731.

(234) Wang S, Lu G, Millar GJ. Carbon dioxide reforming of methane to produce synthesis gas over metal-supported catalysts: state of the art. *Energy & Fuels.* 1996; 10(4): 896-904.

(235) Naeem MA, Al-Fatesh AS, Fakeeha AH, Abasaeed AE. Hydrogen production from methane dry reforming over nickel-based nanocatalysts using surfactant-assisted or polyol method. *International Journal of Hydrogen Energy.* 2014; 39(30): 17009-17023.

(236) Al-Sobhi S, Elkamel A. Simulation and optimization of natural gas processing and production network consisting of LNG, GTL, and methanol facilities. *Journal of Natural Gas Science and Engineering.* 2015; 23: 500-508.

(237) Seshan K, Bitter J, Lercher J. Design of stable catalysts for methane—carbon dioxide reforming. *Studies in Surface Science and Catalysis.* 1998; 113: 187-191.

(238) Nikoo MK, Amin N. Thermodynamic analysis of carbon dioxide reforming of methane in view of solid carbon formation. *Fuel Processing Technology.* 2011; 92(3): 678-691.

(239) Shamsi A, Johnson CD. Effect of pressure on the carbon deposition route in CO_2 reforming of 13CH4. *Catalysis today.* 2003; 84(1): 17-25.

(240) Claridge JB, Green ML, Tsang SC, York AP, Ashcroft AT, Battle PD. A study of carbon deposition on catalysts during the partial oxidation of methane to synthesis gas. *Catalysis Letters.* 1993; 22(4): 299-305.

(241) Dalane K, Dai Z, Mogseth G, Hillestad M, Deng L. Potential applications of membrane separation for subsea natural gas processing: A review. *Journal of Natural Gas Science and Engineering.* 2017; 39:101-117.

(242) Van Deemter JJ, Zuiderweg F, Klinkenberg Av. Longitudinal diffusion and resistance to mass transfer as causes of nonideality in chromatography. *Chemical Engineering Science.* 1956; 5(6): 271-289.

(243) Zhou Y, Wang C, Firor R. *Analysis of permanent gases and methane with the Agilent 6820 gas chromatograph.* Shanghai: Agilent Technologies*;* 2003 [Updated 2003; cited 2017-20-12]. Available from: https://www.agilent.com.

(244) Johnson H, Schulman BL. *Assessment of the potential for refinery applications of inorganic membrane technology: An identification and screening analysis.Final report.* California: US Department of Energy; 1993 [Updated May 1993; cited 20018-02-27] Available from: https://www.osti.gov.

(245) Spillman RW and Cooley T. Membrane gas treating, in: Proceedings of the sixty-eighth Gas Processors Association Annual Convention; 1989 March 13th -14th: San Antonio, Texas.

Appendix A

Calculations

1. Area of the Membrane

$$Area = 2\pi l_o \frac{r_2 - r_1}{ln(r_2/r_1)}$$

Where l_o is the effective length, r_2 the outer radius and r_1 is the inner radius of the membrane.

$l_o = 0.342\ m$

$r_2 = 0.005\ m$

$r_1 = 0.0035\ m$

$$Area = (2 * 3.14 * 0.342)\left({(0.005 - 0.0035)}\Big/{ln\left(\frac{0.005}{0.0035}\right)}\right)$$

Area of membrane = 0.009032 m^2

2. Molar gas flow rate through the membrane

From Avogadro's theory (Amedeo Avogadro 1811); one mole of an ideal gas occupies 22.4 L at standard temperature and pressure (STP) or Standard Ambient Temperature and Pressure (SATP).

Gas flowrate was measured in L min^{-1} and converted to molar flowrate in mol s^{-1}.

$$molar\ flowrate\ (mol\ s^{-1}) = \left(flowrate\ (L\ min^{-1}/_{60}\right)\ /22.4$$

Appendix B

GCMS Calibration

Methane

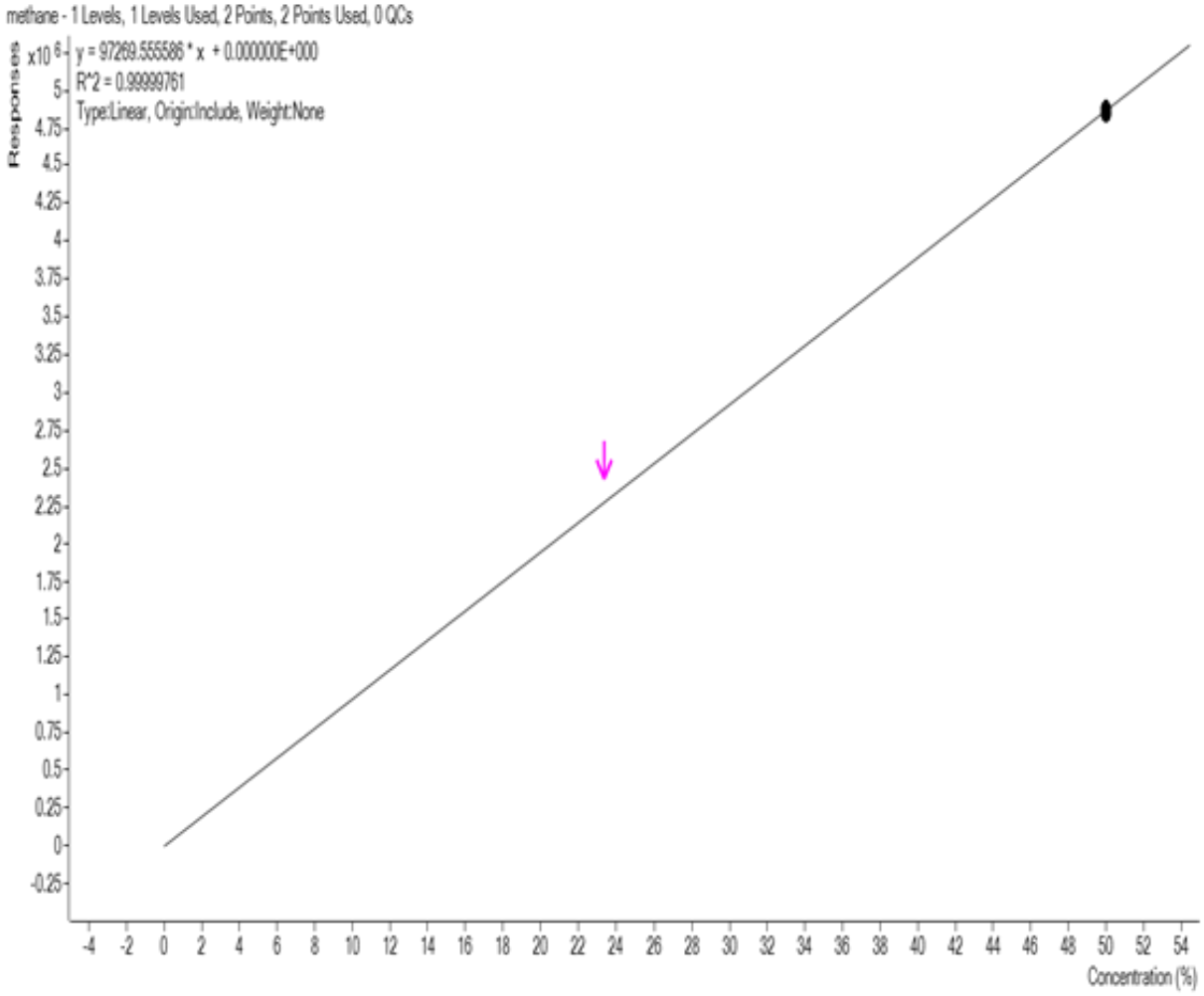

Figure-A 1: Calibration curve of methane gas

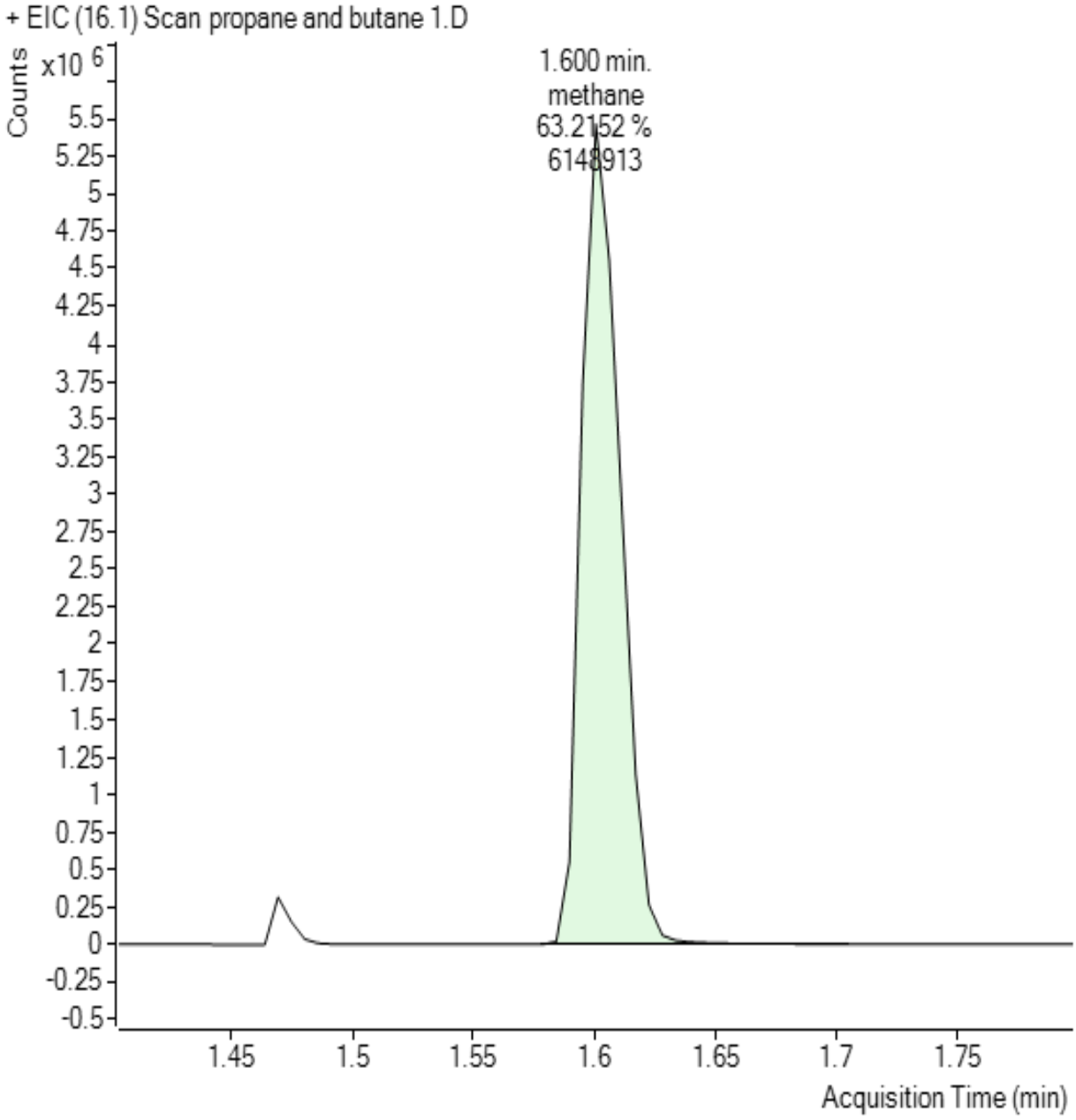

Figure-A 2: Methane calibration showing acquisition time

Propane

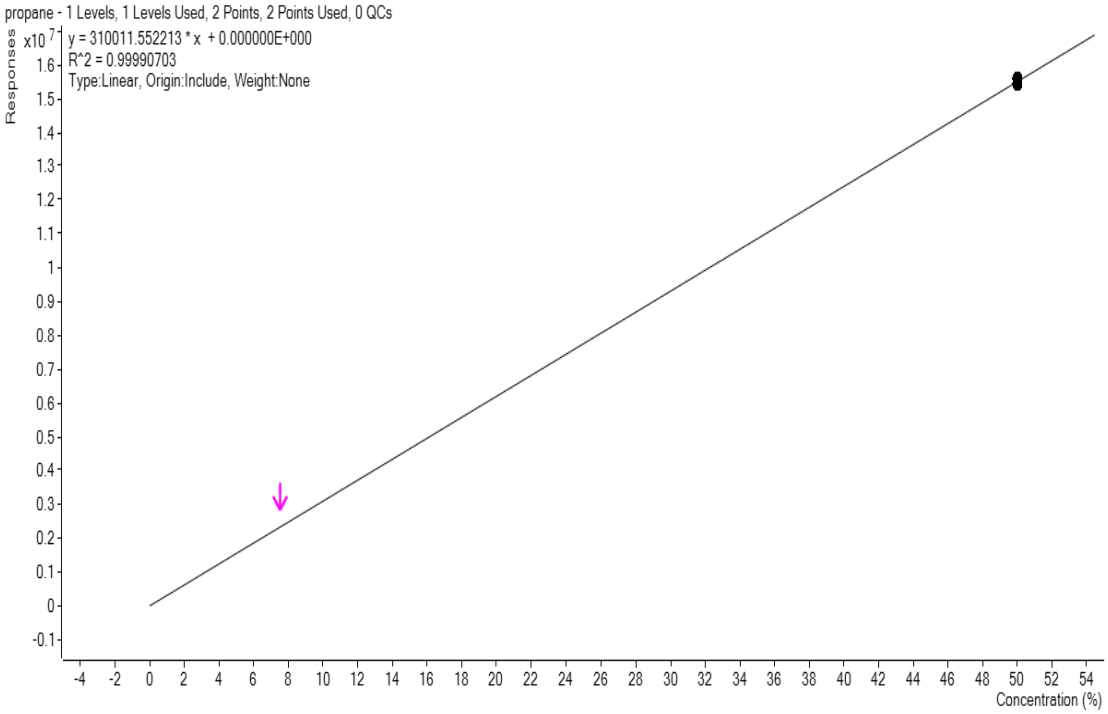

Figure-A 3: Propane calibration curve

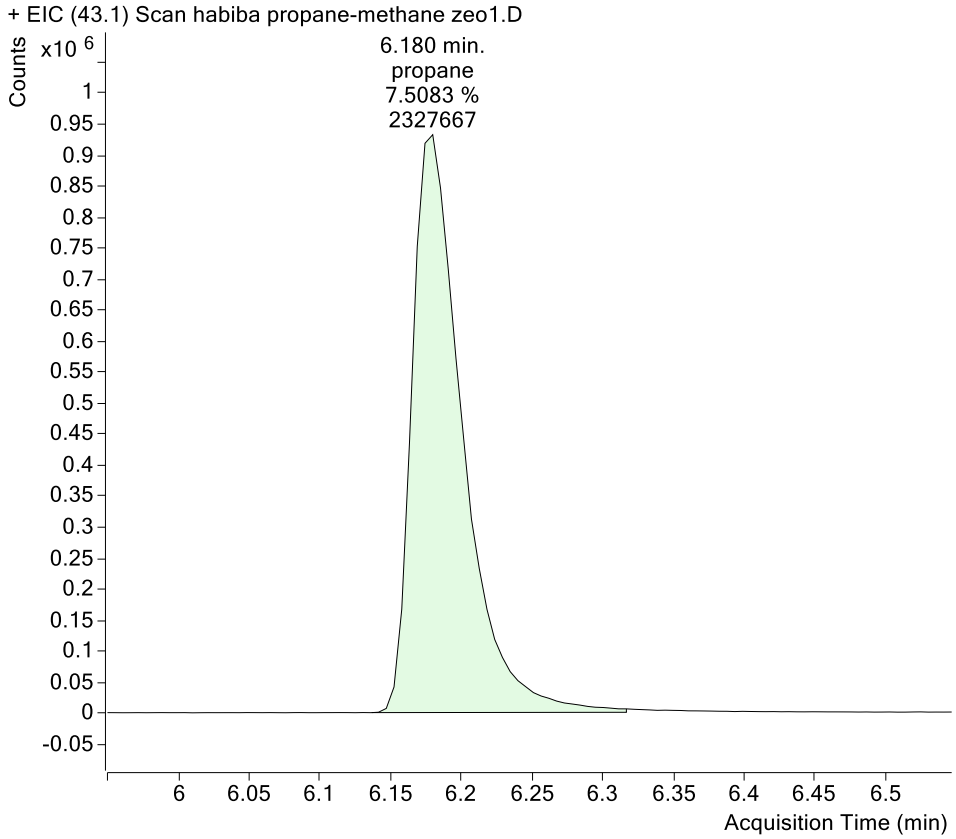

Figure-A 4: Propane calibration showing acquisition time

Nitrogen

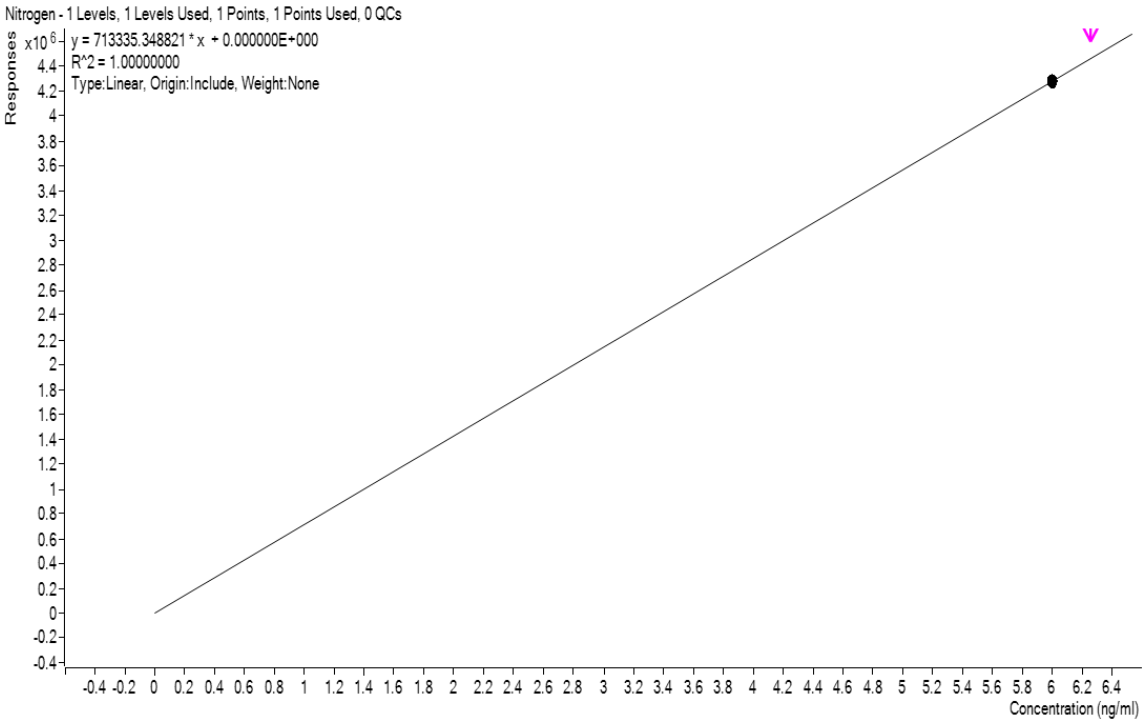

Figure-A 5: Nitrogen calibration curve

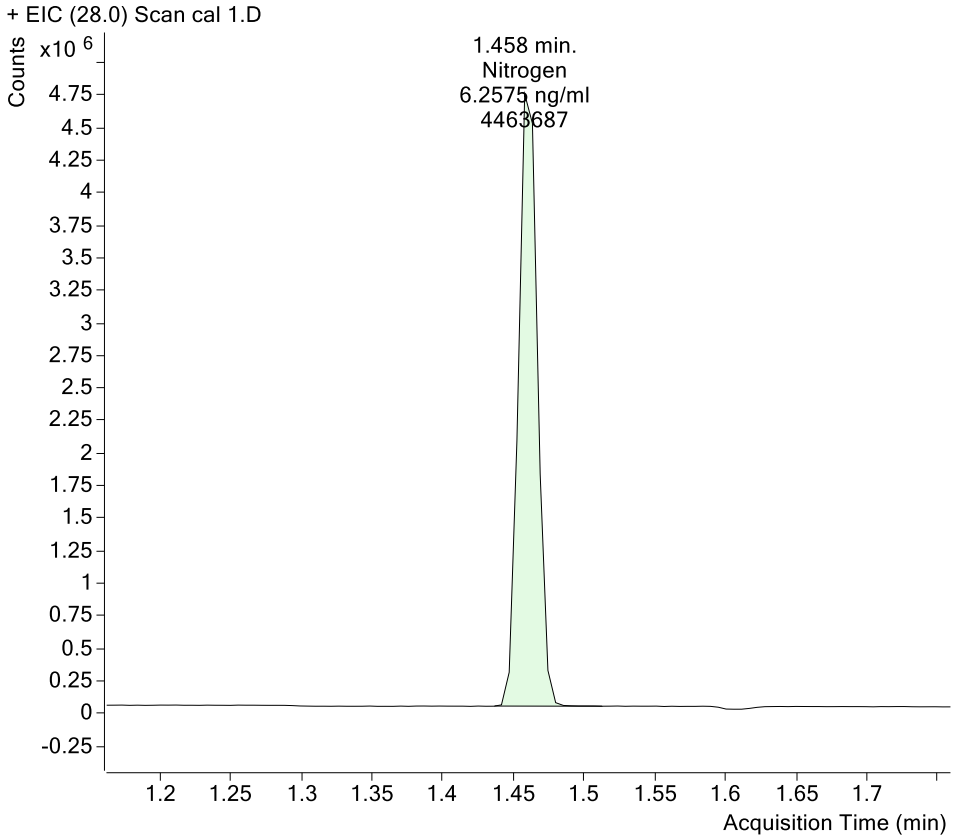

Figure-A 6: Nitrogen calibration showing acquisition time

Carbon dioxide

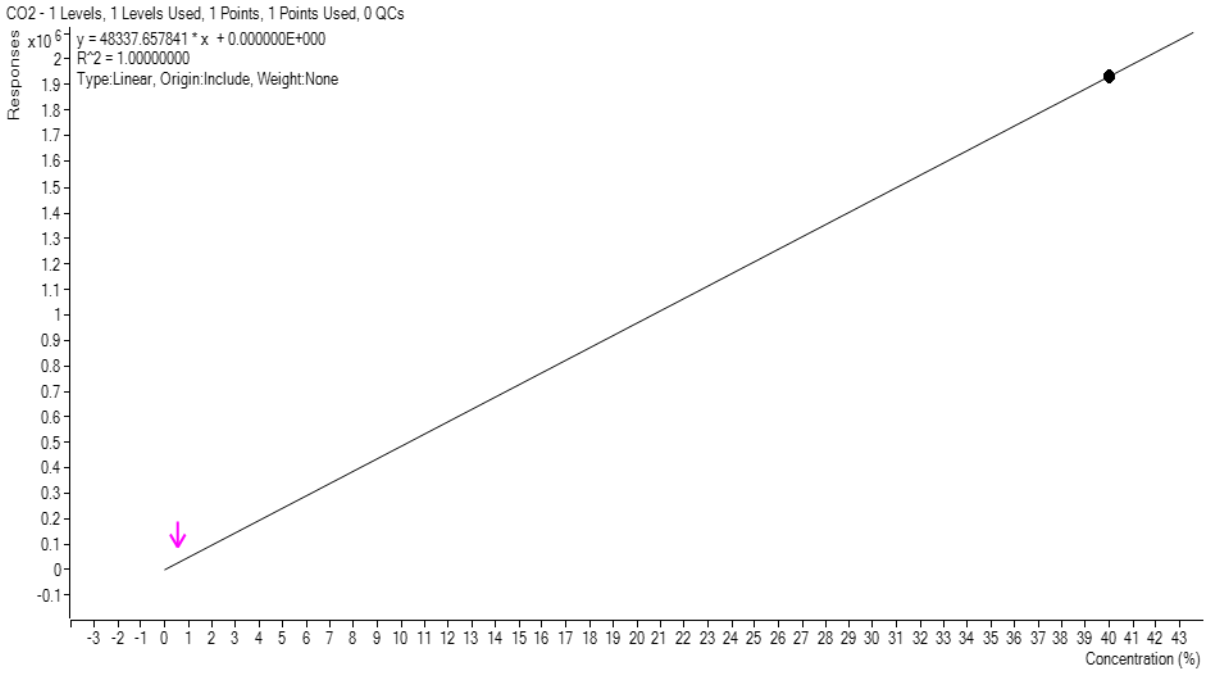

Figure-A 7: Carbon dioxide calibration curve

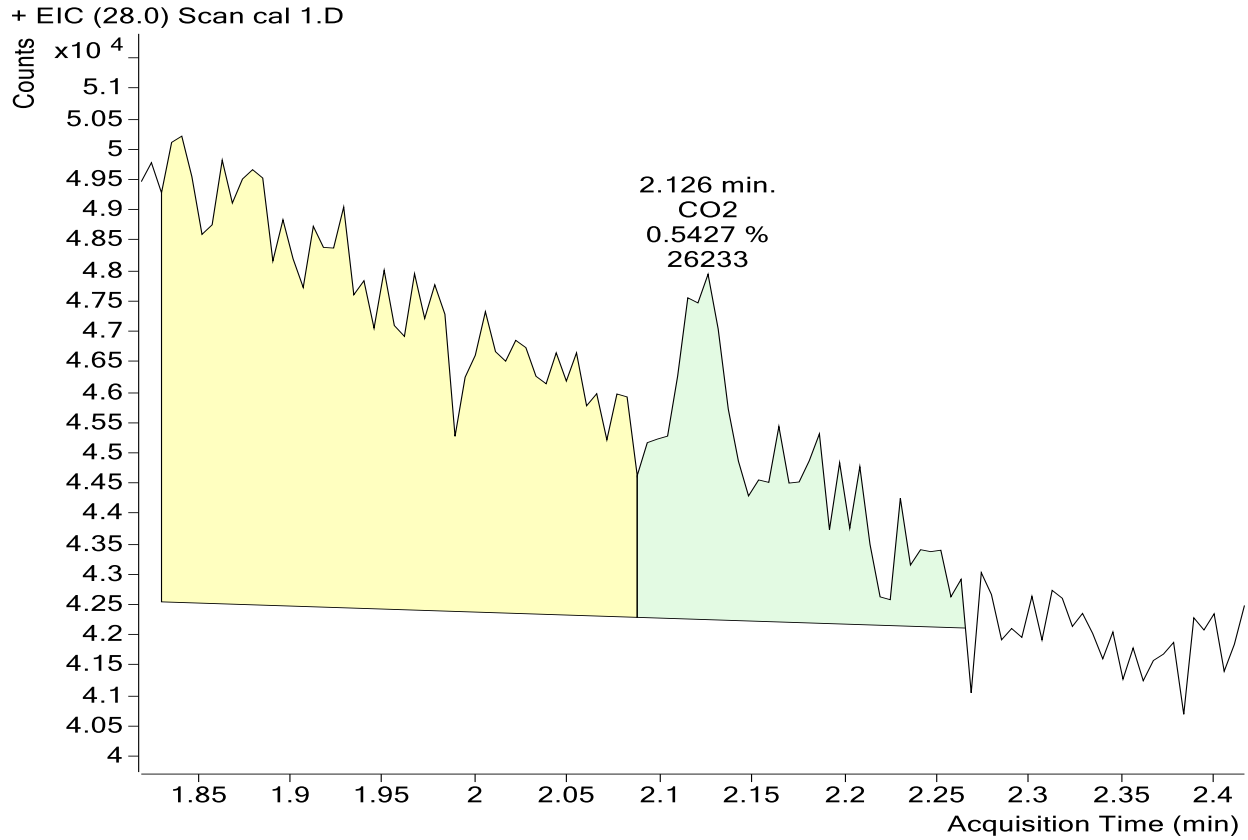

Figure-A 8: Carbon dioxide calibration showing acquisition time

Carbon Monoxide

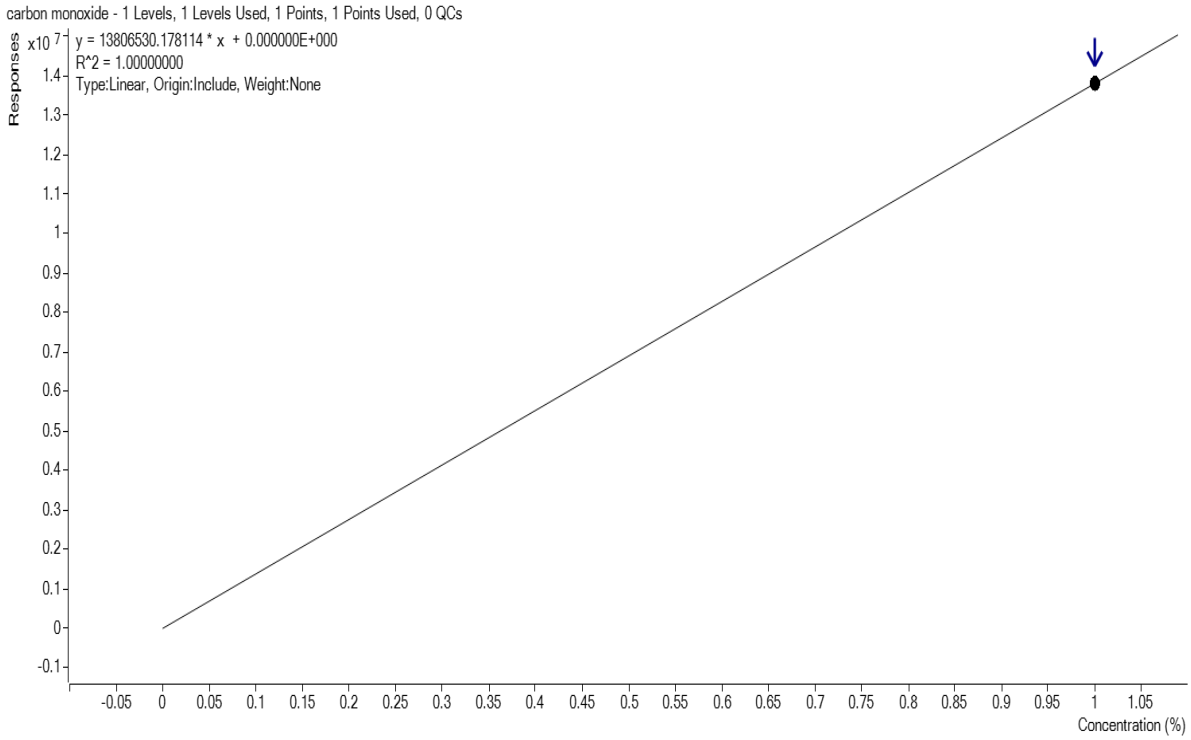

Figure-A 9: Carbon monoxide calibration curve

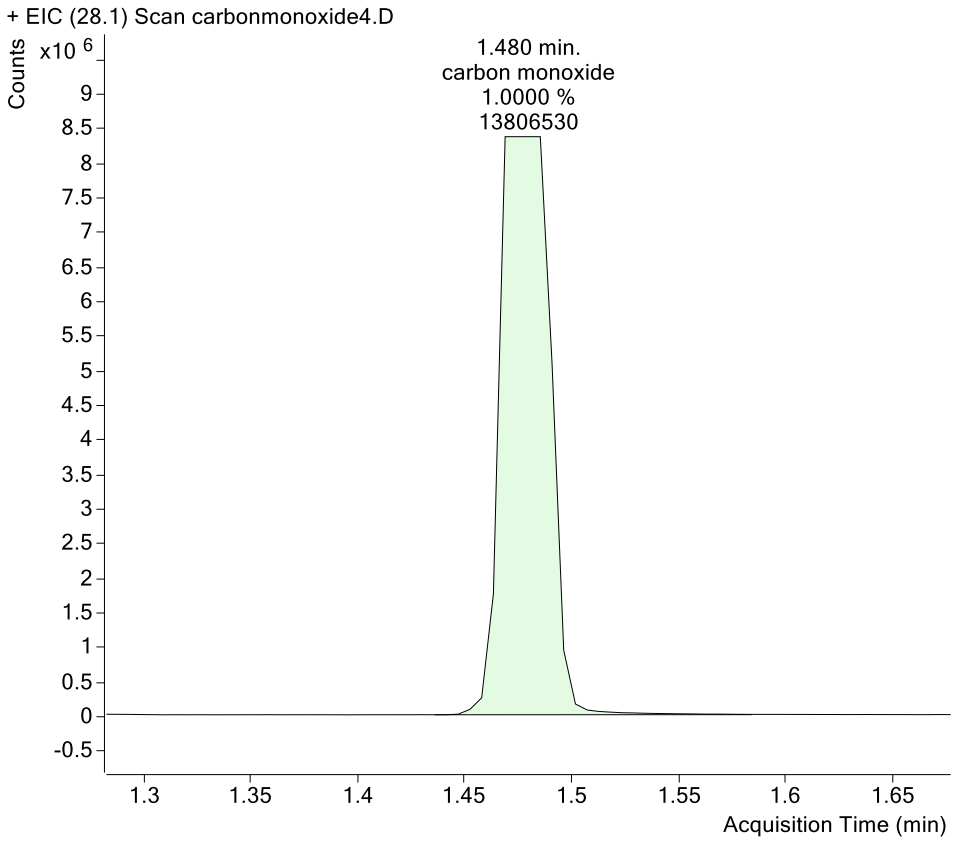

Figure-A 10: Carbon monooxide calibration showing acquisition time

Appendix C

Qualitative compound report for mixed gases through the zeolite membrane

Data File	Zeolite mix3.D	**Sample Name**	Zeolite mix3
Sample Type		**Position**	1

Instrument Name	5977A MSD	**User Name**	
Acq Method	Sequence Gas Analysis 11-05-2017.M	**Acquired Time**	5/19/2017 11:33:38 AM
IRM Calibration Status	Not Applicable	**DA Method**	RGU Routine.m
Comment	propane,CO2, O2, CH4 N2 mixture with fr 0.6Lmin		
Expected Barcode		**Sample Amount**	
Dual Inj Vol	1	**TuneName**	etune.u
TunePath	D:\MassHunter\GCMS\1\5977\	**TuneDateStamp**	2017-05-10T14:11:30+01:00
MSFirmwareVersion	6.00.34	**OperatorName**	
RunCompletedFlag	True	**Acquisition SW Version**	MassHunter GC/MS Acquisition B.07.05.2479 23-Aug-2016 Copyright © 1989-2016 Agilent Technologies, Inc.

Compound Table

Compound Label	RT	Mass	Name	DB Formula	Hits (DB)
Cpd 1: Nitrogen	1.458		Nitrogen	N2	5
Cpd 2: Methane	1.611		Methane	CH4	3
Cpd 3: Carbon dioxide	2.121		Carbon dioxide	CO2	7
Cpd 4: Water	5.249		Water	H2O	1
Cpd 5: Water	5.287		Water	H2O	1
Cpd 6: 5.380	5.38				0
Cpd 7: 5.440	5.44				0
Cpd 8: Water	5.49		Water	H2O	1
Cpd 9: Water	5.637		Water	H2O	1
Cpd 10: Propane	6.174		Propane	C3H8	10
Cpd 11: Butane	8.453		Butane	C4H10	10

Compound Label	Name	RT	Algorithm
Cpd 1: Nitrogen	**Nitrogen**	1.458	Find by Integration

Compound Chromatograms

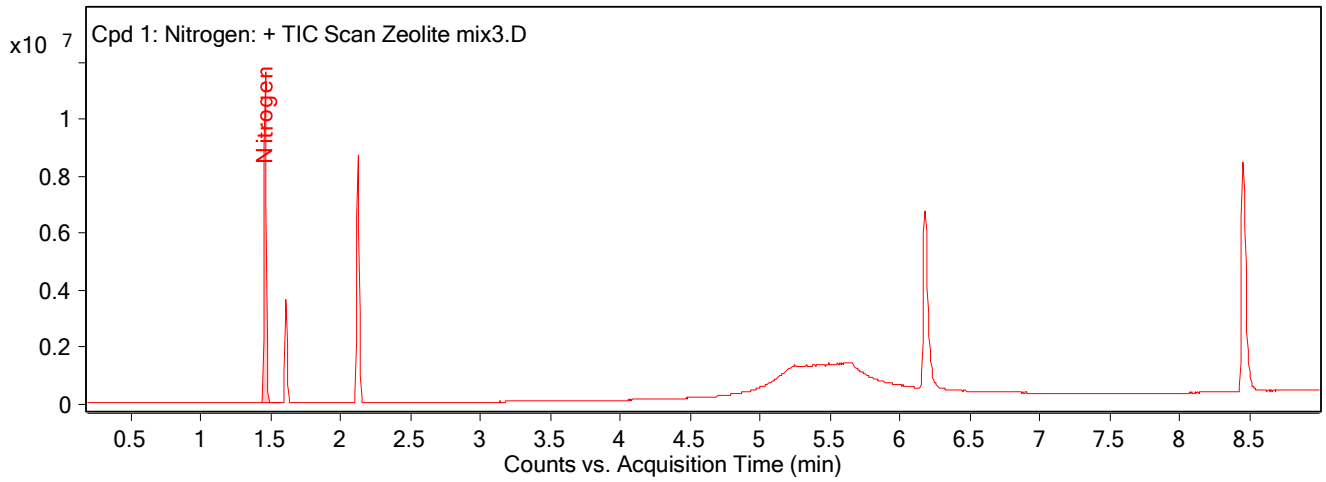

MS Spectrum

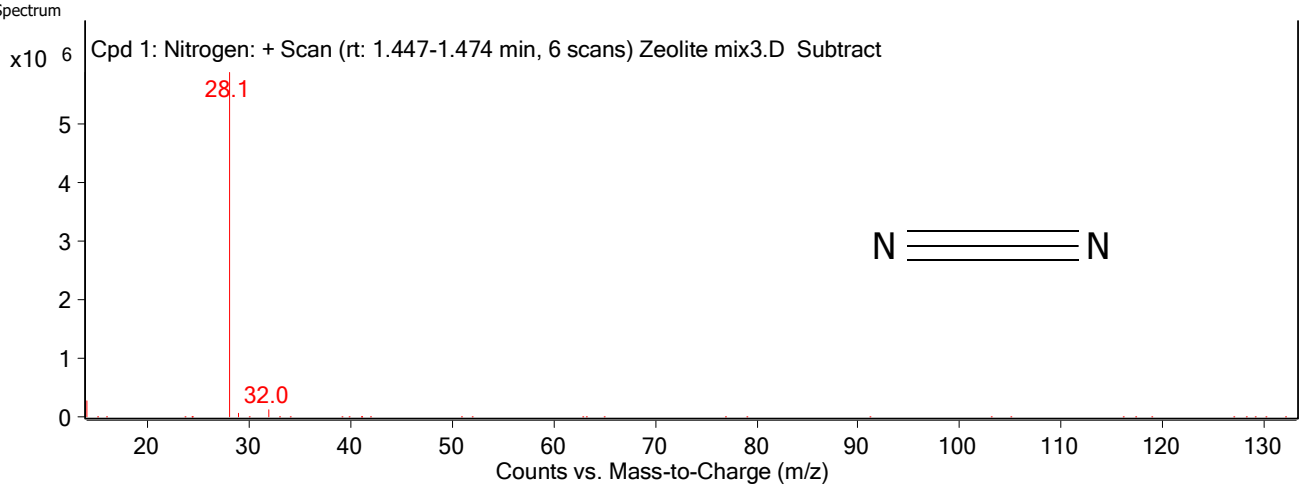

MS Zoomed Spectrum

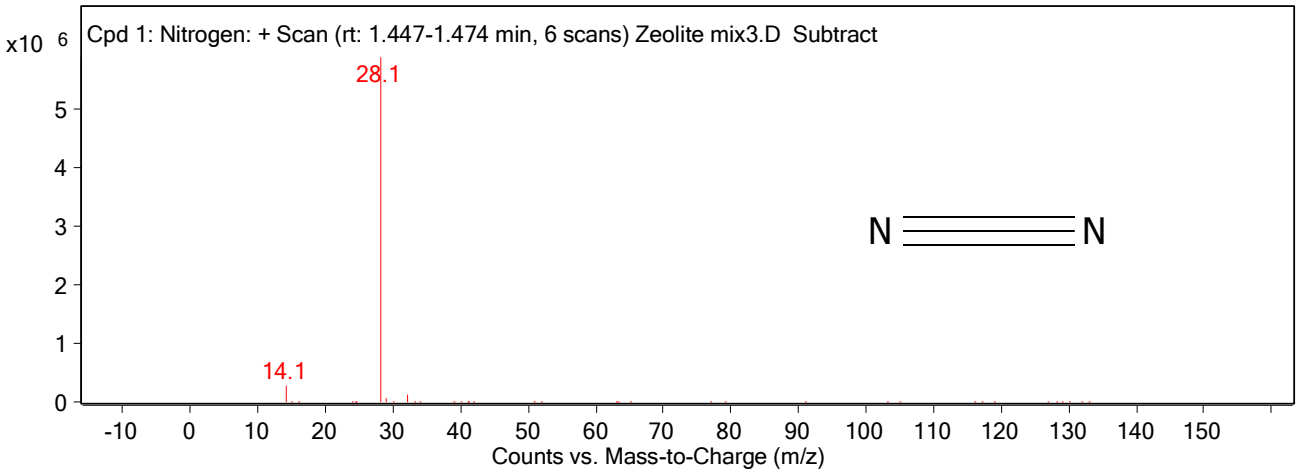

MS Spectrum Peak List

m/z	Abund
14.1	265906.31

28.1	5882379.5
29.1	75337.7
32	114733.53

Compound Structure

Compound Label	Name	RT	Algorithm
Cpd 2: Methane	**Methane**	1.611	Find by Integration

Compound Chromatograms

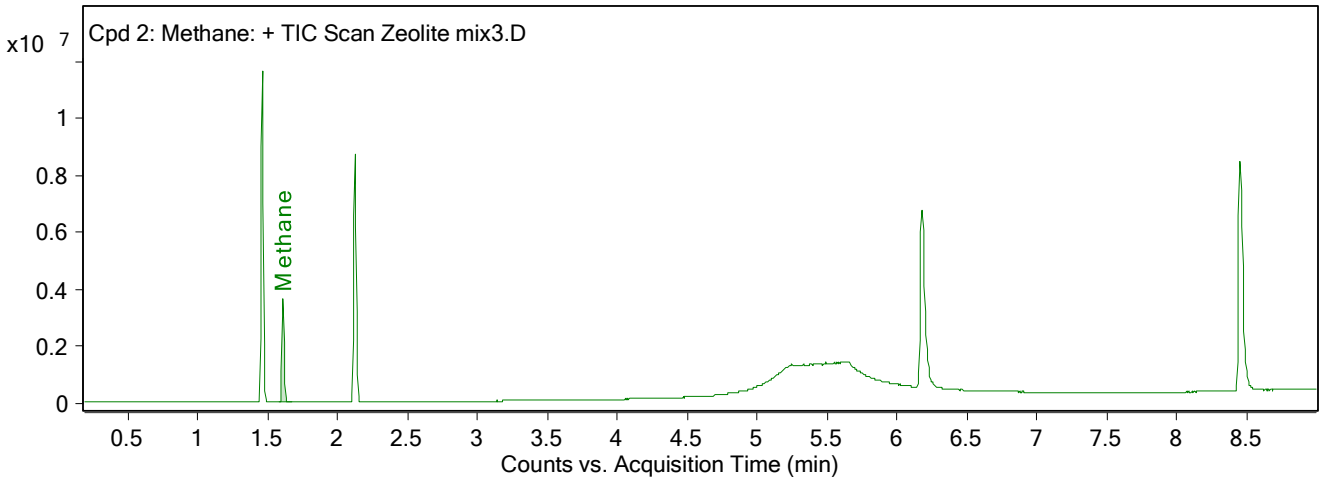

MS Spectrum

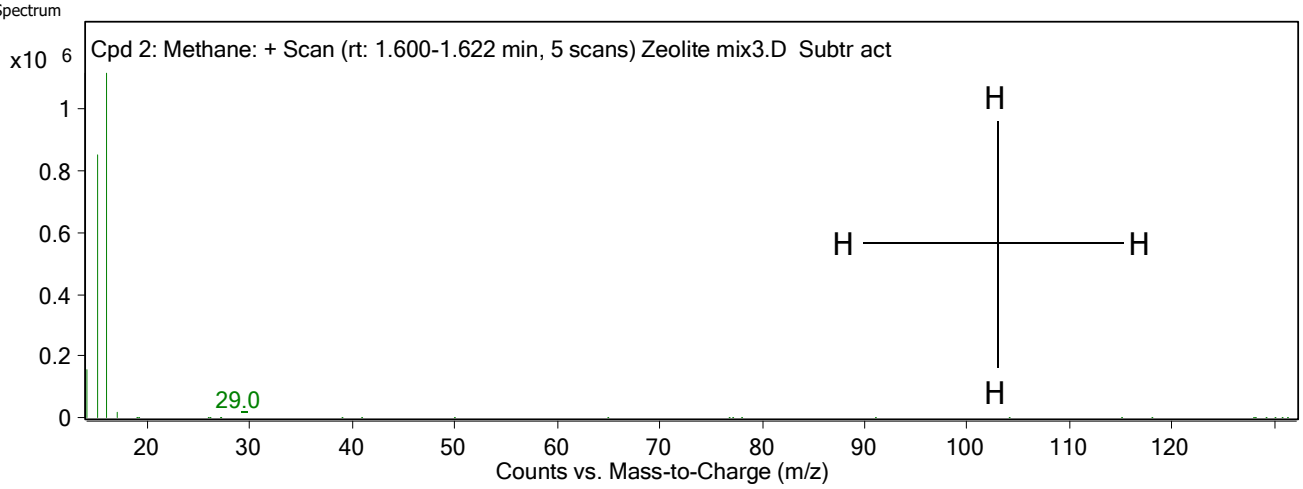

MS Zoomed Spectrum

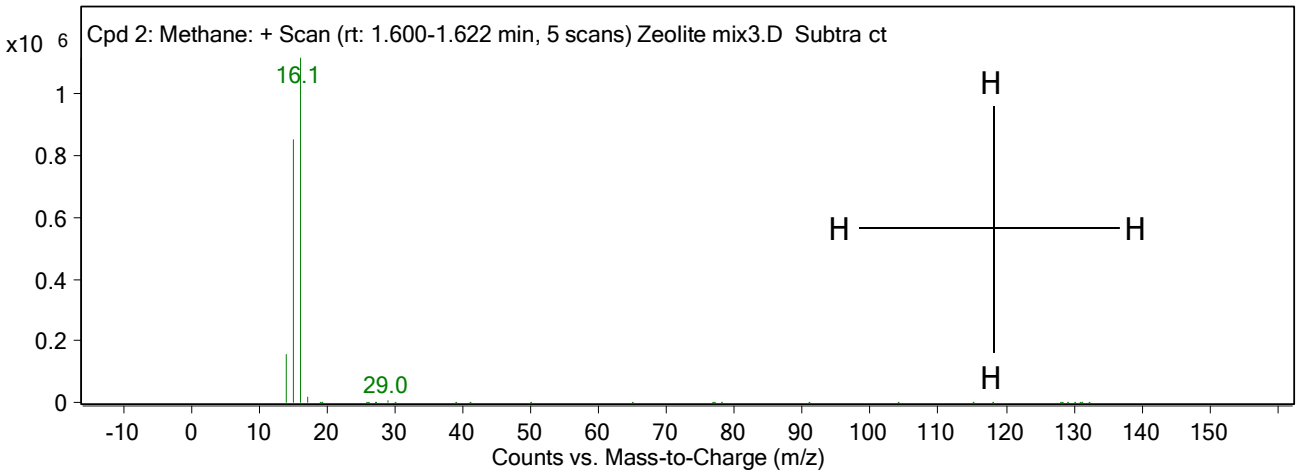

MS Spectrum Peak List

m/z	Abund
14.1	156547.06
15.1	851105.81
16.1	1117473.13
17.1	18557.78
29	8535.59

Compound Structure
Compound Chromatograms

Compound Label	Name	RT	Algorithm
Cpd 3: Carbon dioxide	**Carbon dioxide**	2.121	Find by Integration

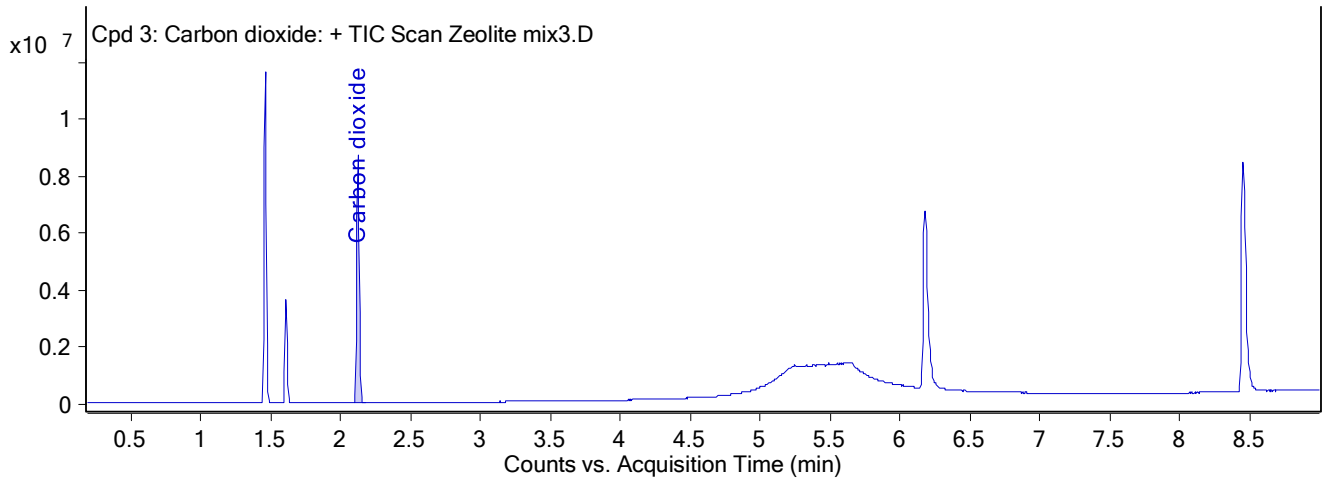

MS Spectrum

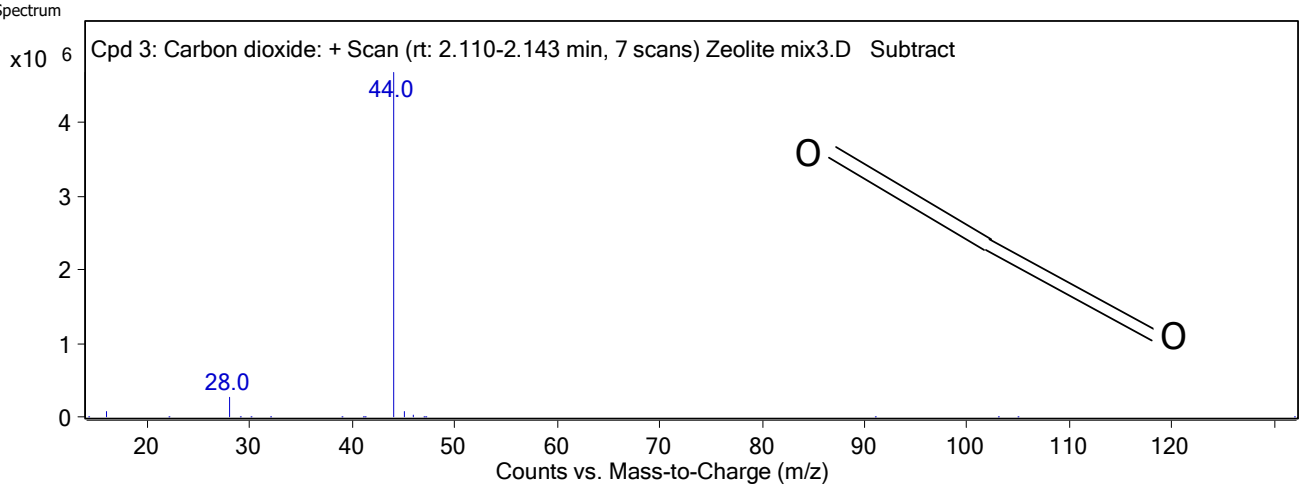

MS Zoomed Spectrum

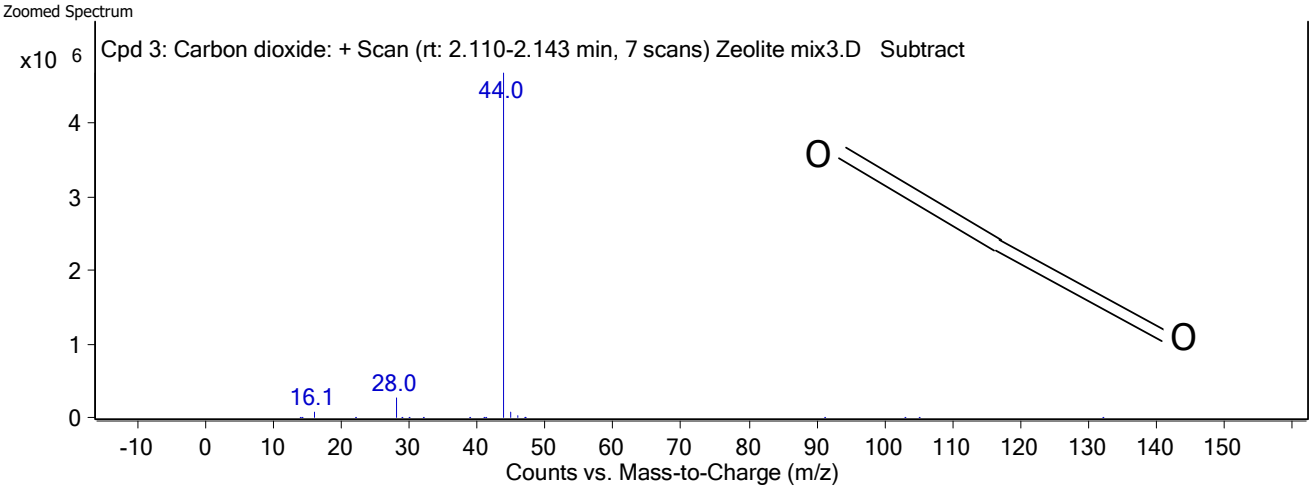

MS Spectrum Peak List

m/z	Abund
16.1	68543.09

28	275641.91
44	4679142.5
45	67062.96
46	23841.11

Compound Structure

Compound Label	Name	RT	Algorithm
Cpd 4: Water	**Water**	5.249	Find by Integration

Compound Chromatograms

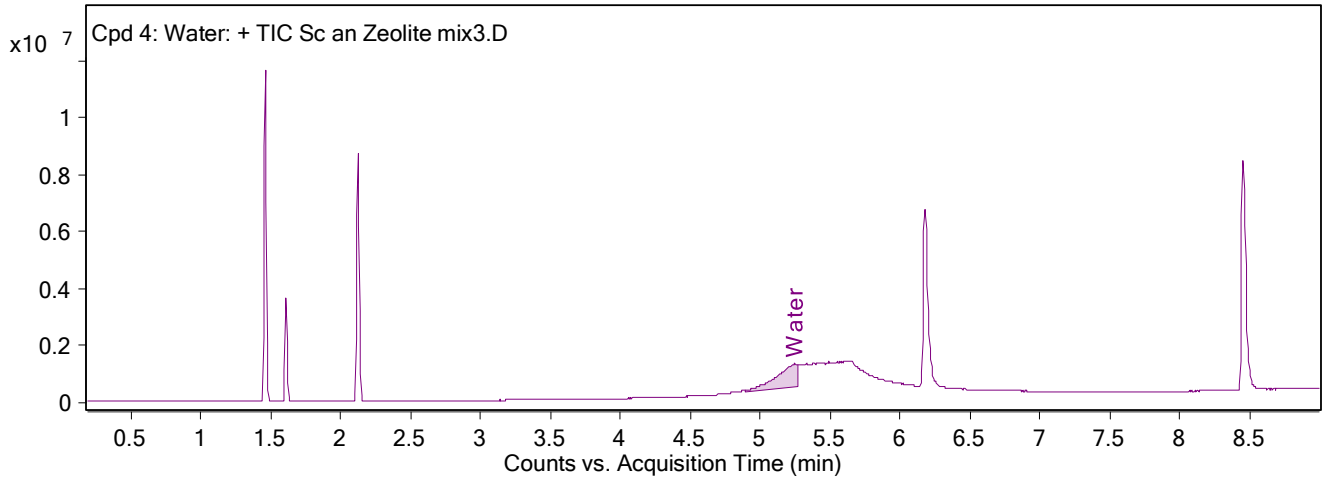

MS Spectrum

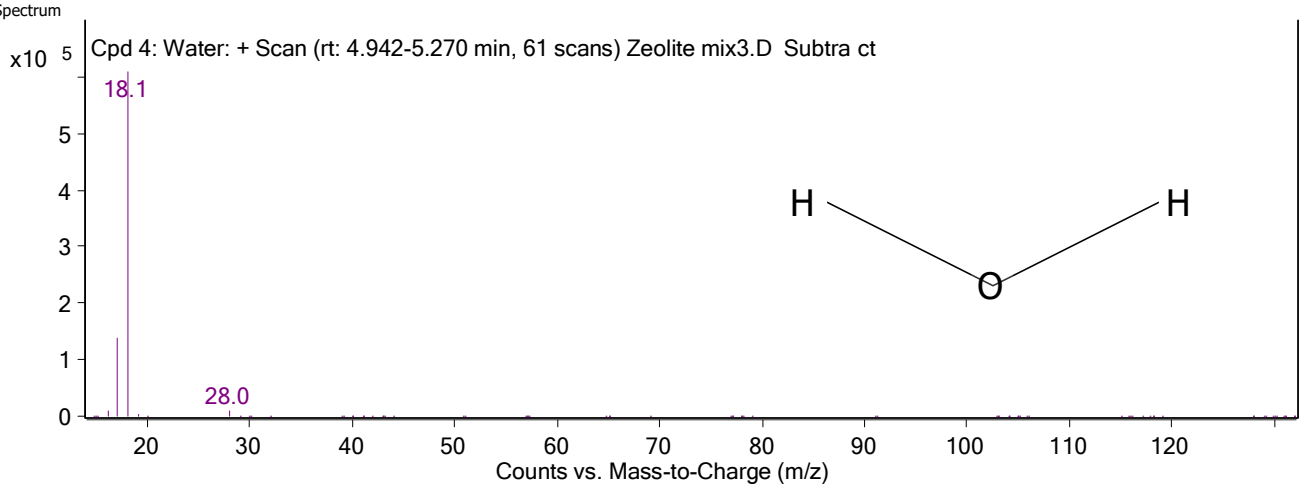

MS Zoomed Spectrum

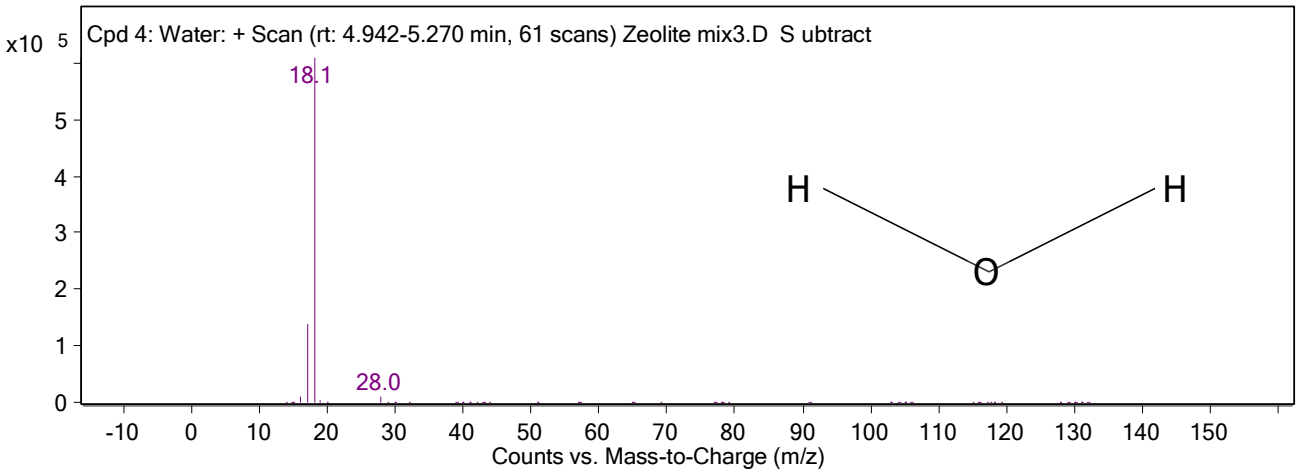

MS Spectrum Peak List

m/z	Abund
16.1	10129.63
17.1	138870.08
18.1	609328.75
19.1	3294.93
28	8179.73

Compound Structure

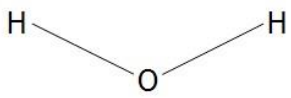

Compound Label	Name	RT	Algorithm
Cpd 5: Water	**Water**	5.287	Find by Integration

Compound Chromatograms

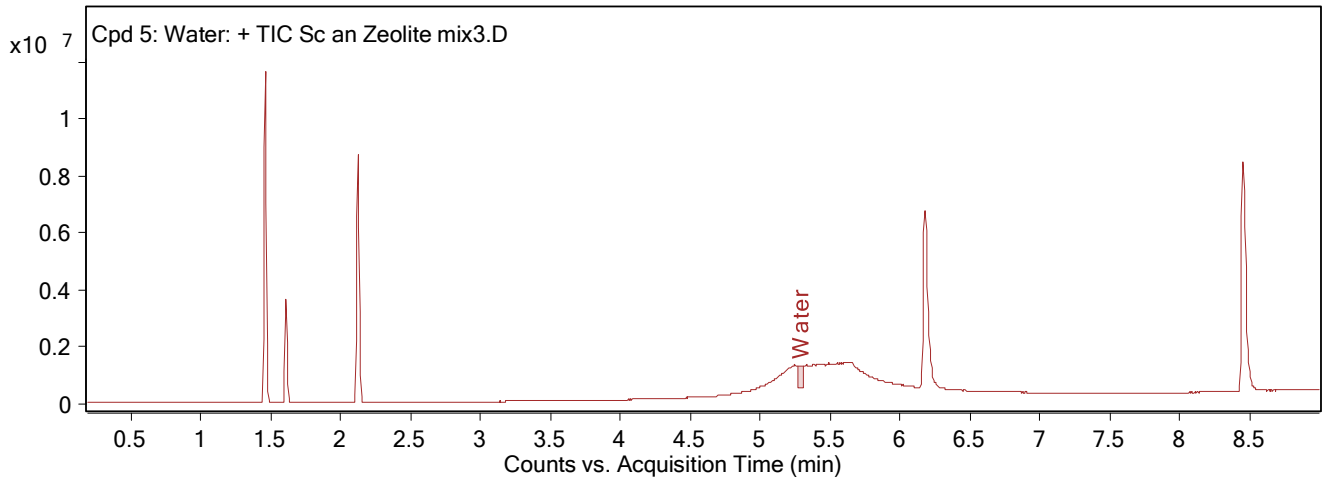

m/z	Abund
14.1	115.54

16.1	132.01
17.1	1579.34
18.1	14536.63
19.1	226.8
20.1	124.1
32	106.06
57	167.88
78	139.83
132.2	119.52

MS Spectrum

MS Zoomed Spectrum

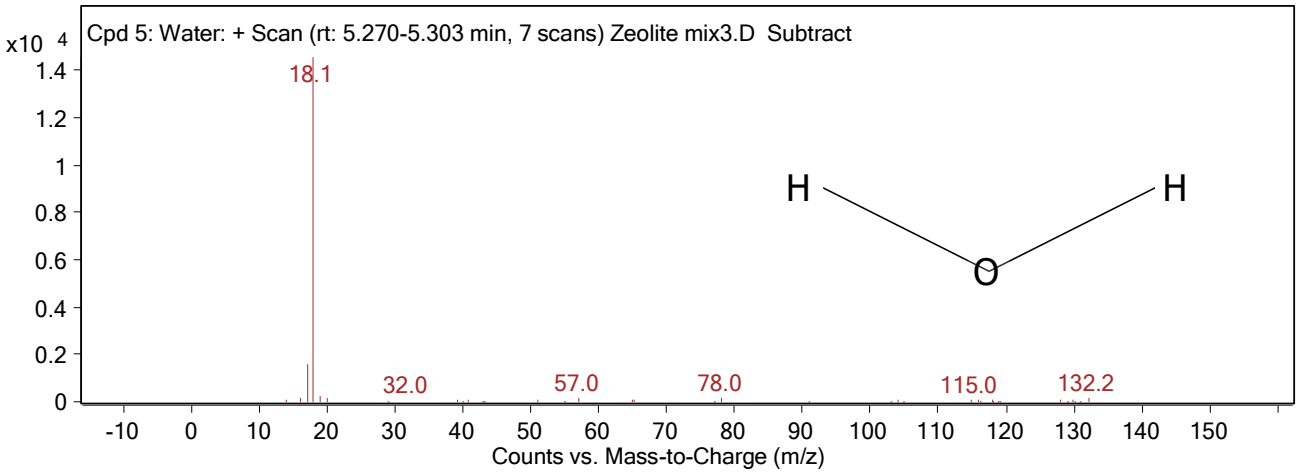

MS Spectrum Peak List

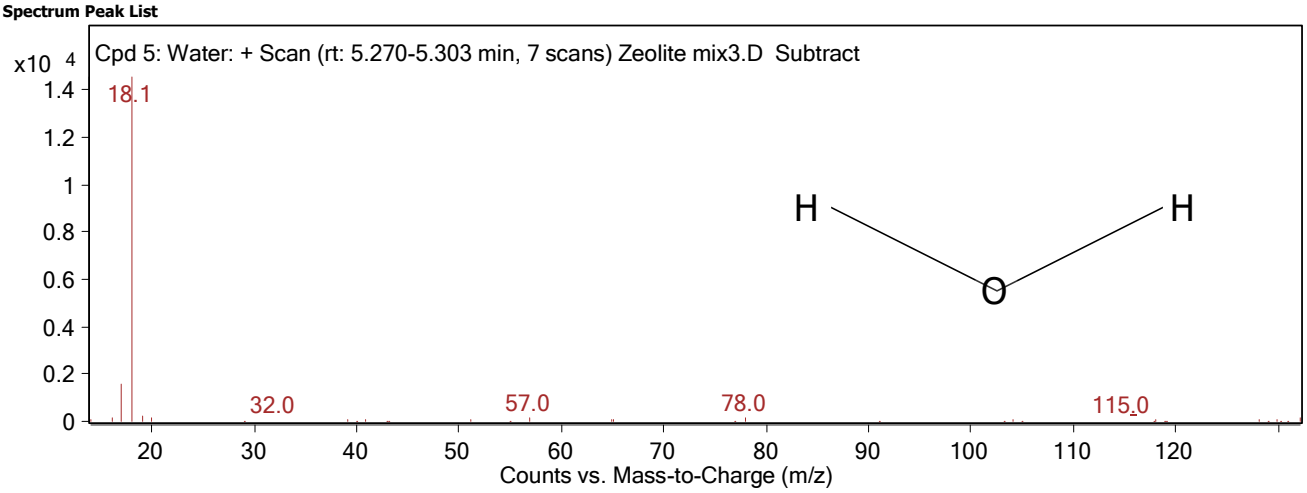

Compound Structure

Compound Chromatograms

Compound Label	RT	Algorithm
Cpd 6: 5.380	5.38	Find by Integration

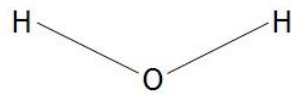

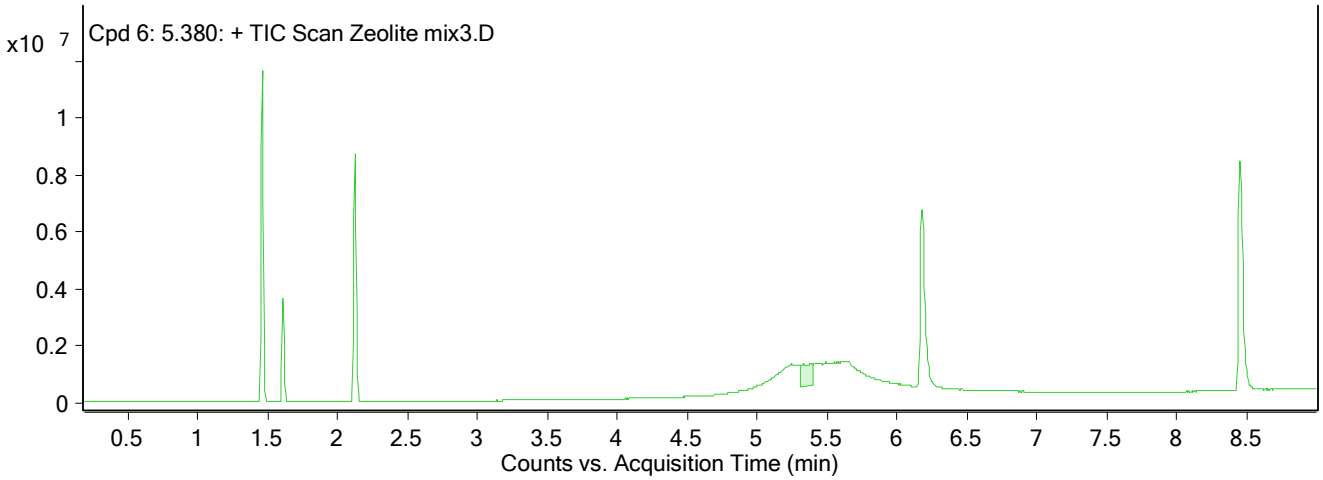

MS Spectrum

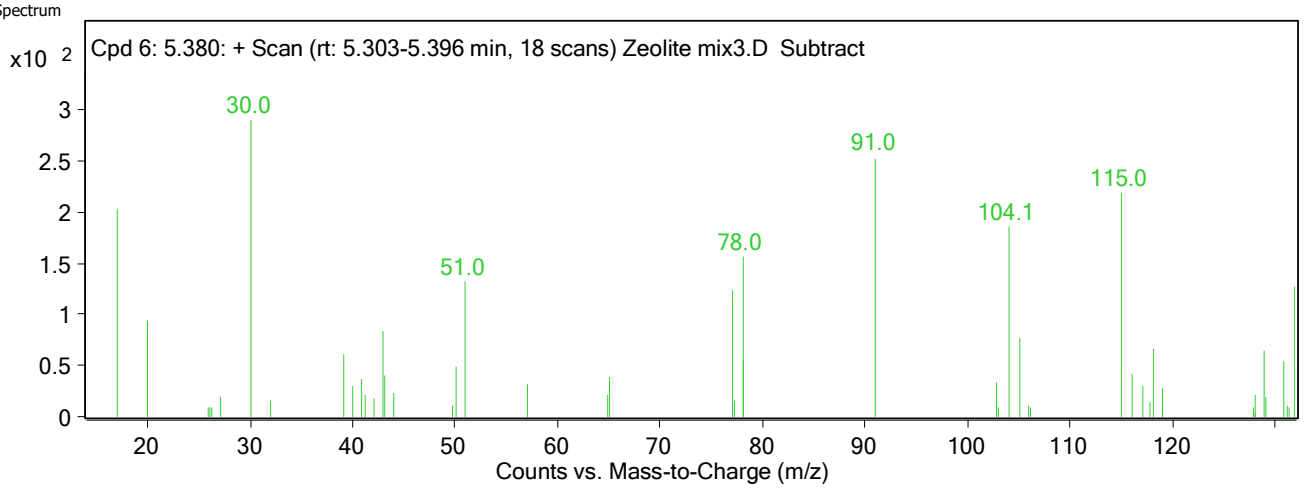

MS Zoomed Spectrum

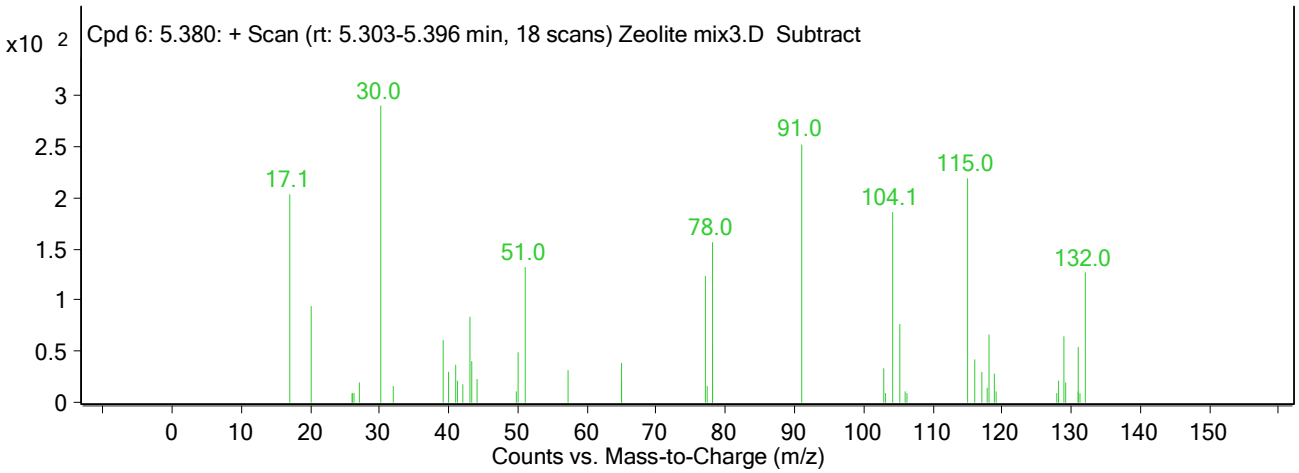

MS Spectrum Peak List

m/z	Abund
17.1	203.72
30	291.24
51	132.61
77	123
78	156.54
91	253.09
104.1	185.34
115	218.71
132	126.99

Compound Label	RT	Algorithm
Cpd 7: 5.440	5.44	Find by Integration

Compound Chromatograms

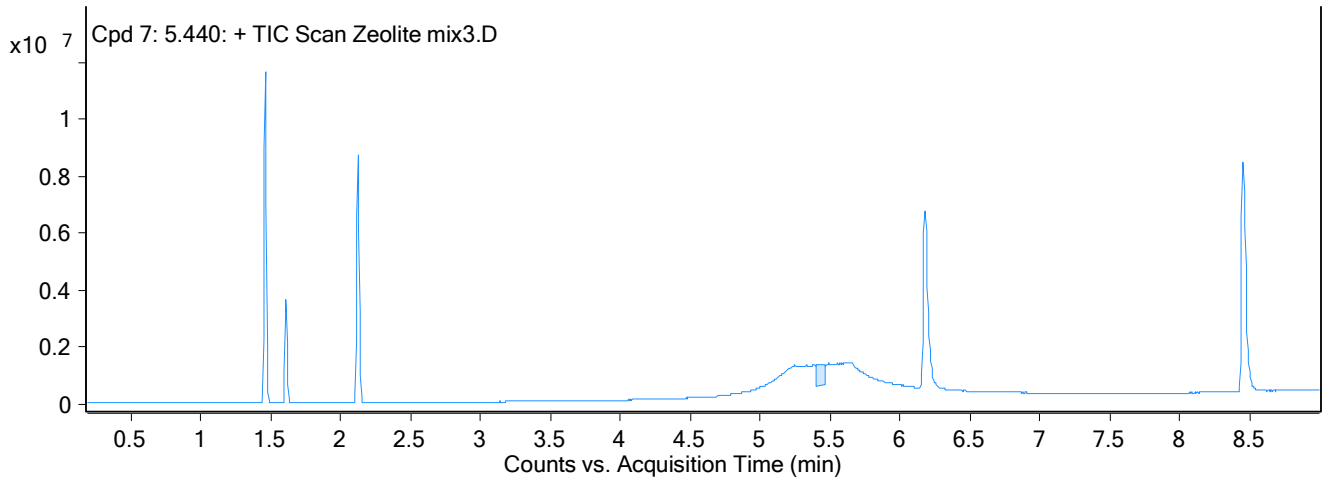

MS Spectrum

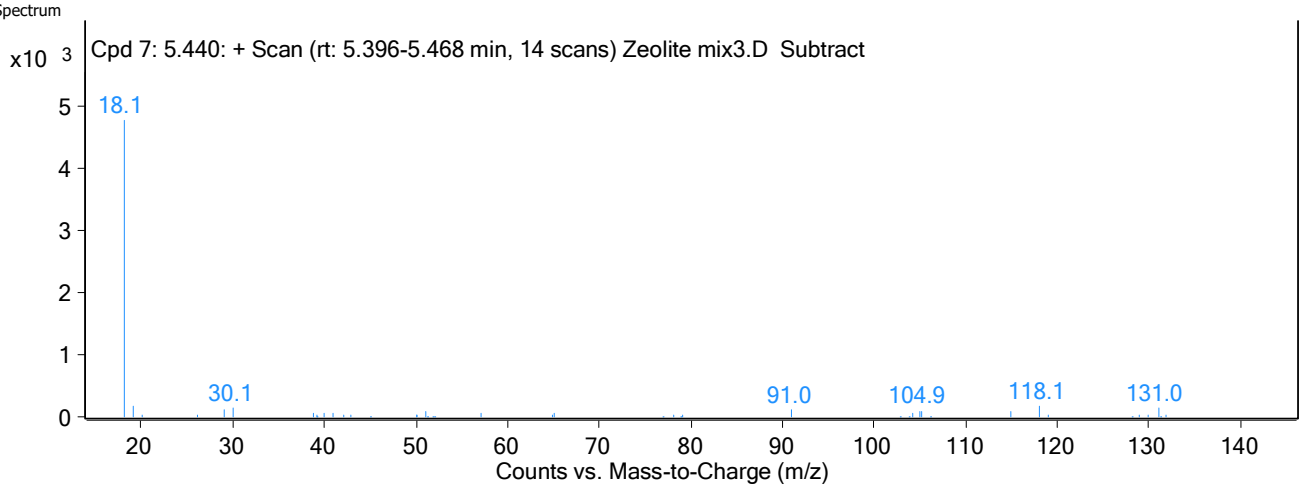

MS Zoomed Spectrum

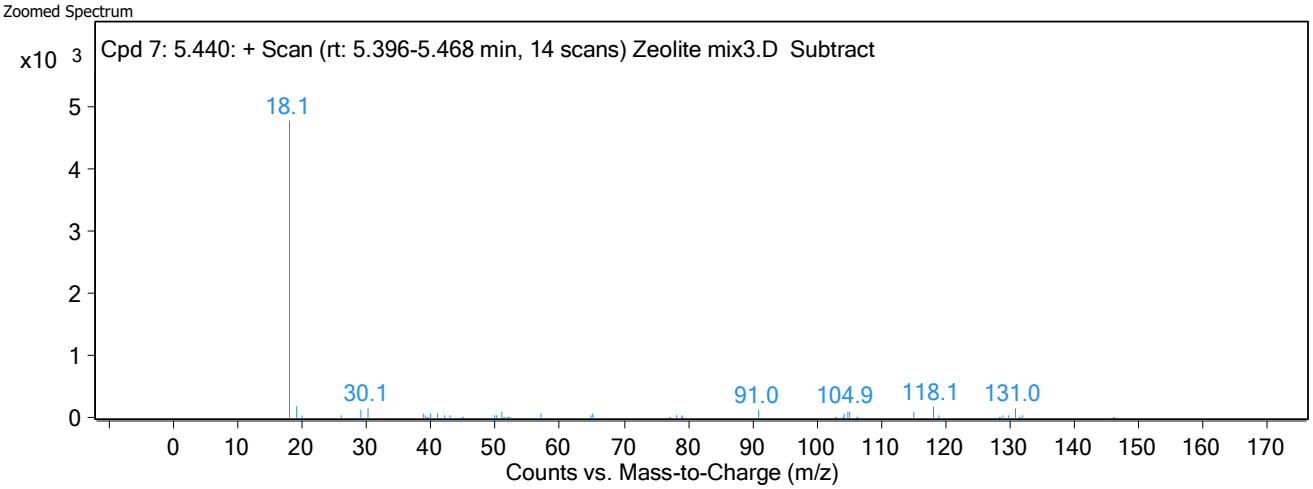

MS Spectrum Peak List

m/z	Abund
18.1	4781.88

19.1	185.79
29	129.65
30.1	156.11
91	120.86
104.9	101.69
118.1	185.72
131	141.45

Compound Label	Name	RT	Algorithm
Cpd 8: Water	**Water**	5.49	Find by Integration

Compound Chromatograms

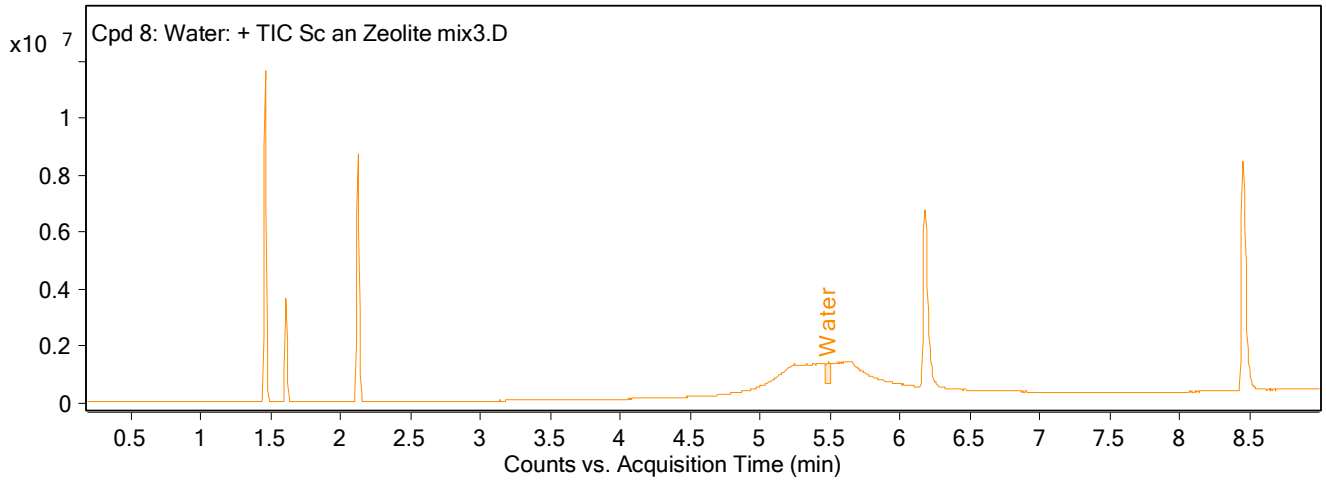

MS Spectrum

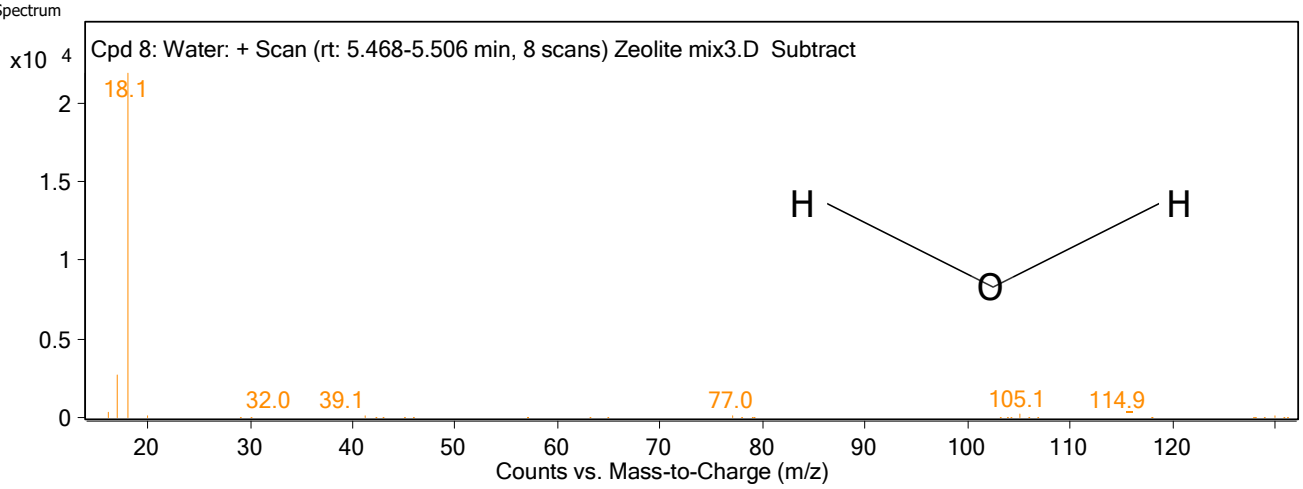

MS Zoomed Spectrum

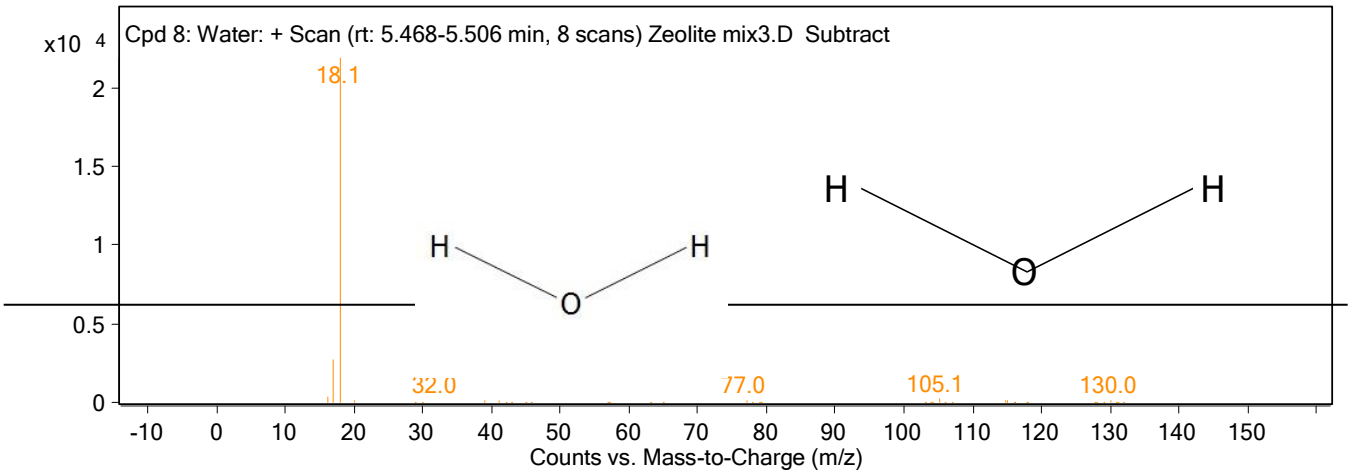

MS Spectrum Peak List

m/z	Abund
16.1	323.07
17.1	2669.44
18.1	21899.75
32	124.62
39.1	120.57
77	140.74
105.1	199.94
114.9	116.3
115.1	111.31
130	154.21

Compound Structure

Compound Chromatograms

Compound Label	Name	RT	Algorithm
Cpd 9: Water	**Water**	5.637	Find by Integration

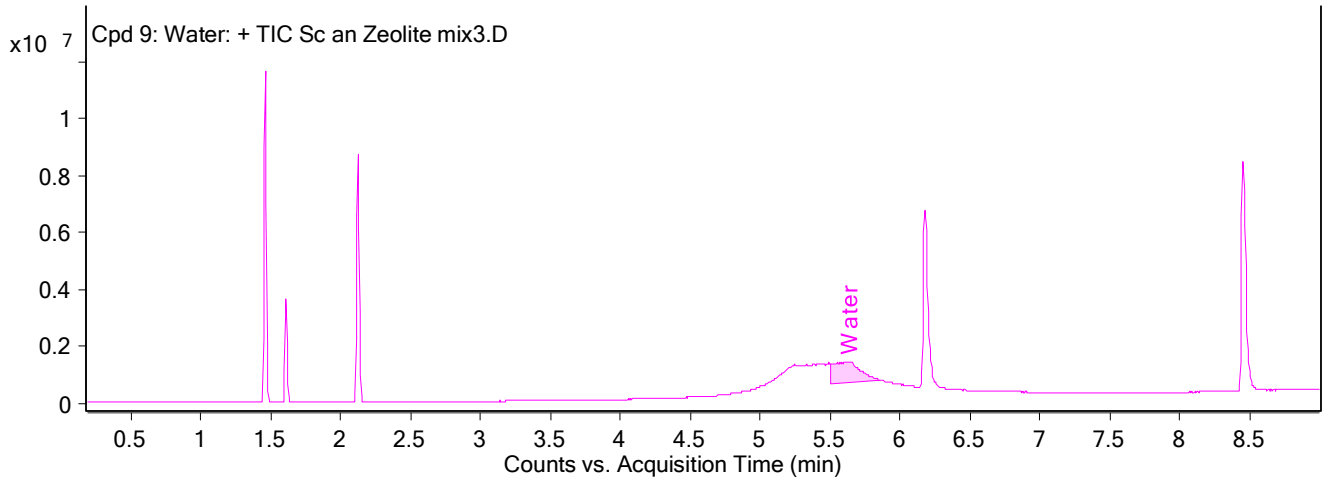

MS Spectrum

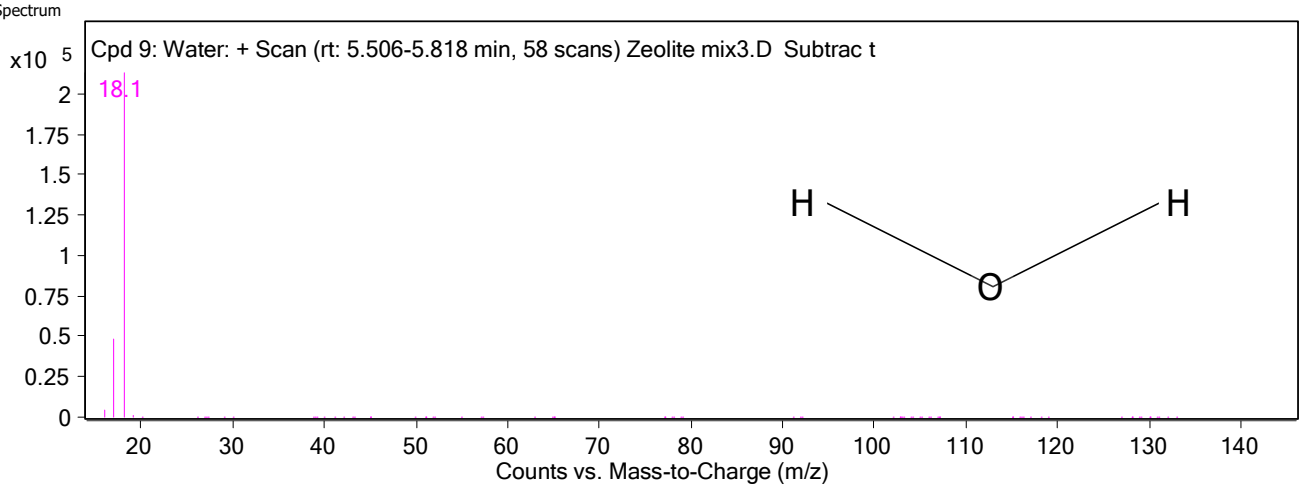

MS Zoomed Spectrum

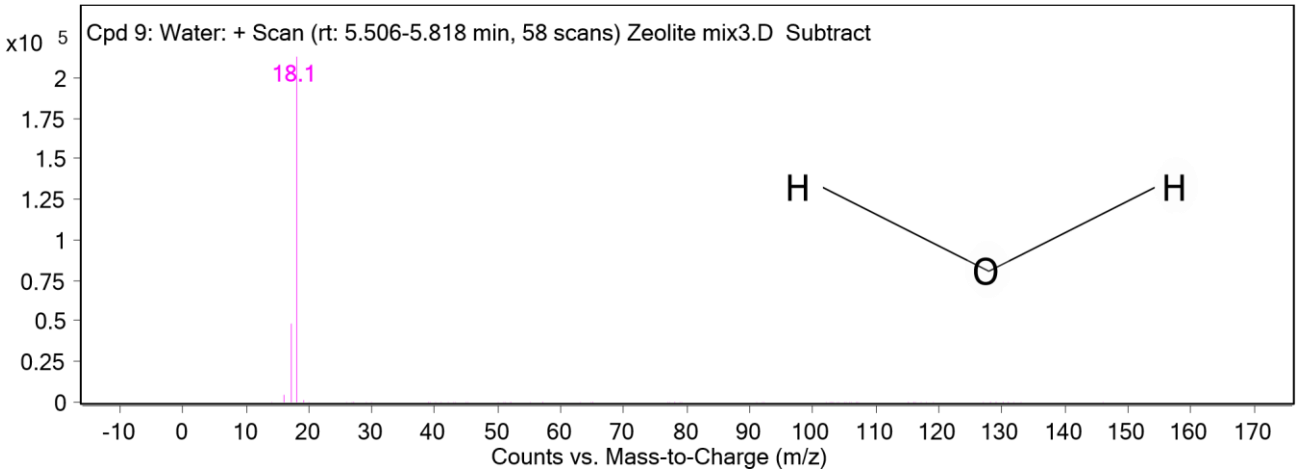

MS Spectrum Peak List

m/z	Abund
16.1	4034.28
17.1	48481.7
18.1	213067.25
19.1	1503.51

Compound Structure

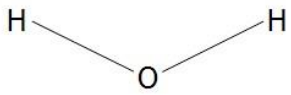

Compound Label	Name	RT	Algorithm
Cpd 10: Propane	**Propane**	6.174	Find by Integration

Compound Chromatograms

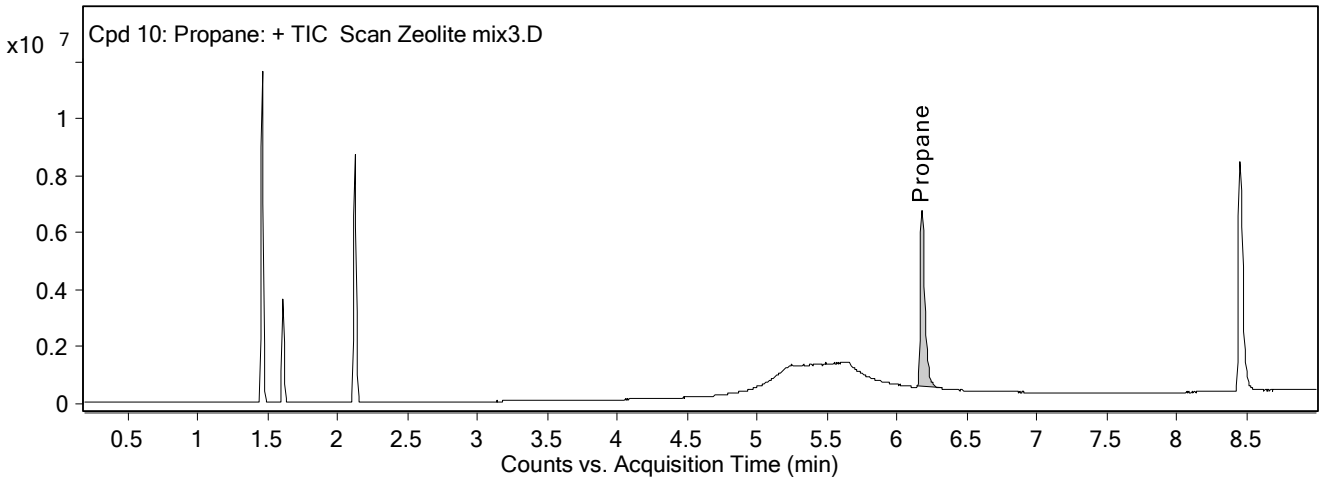

MS Spectrum

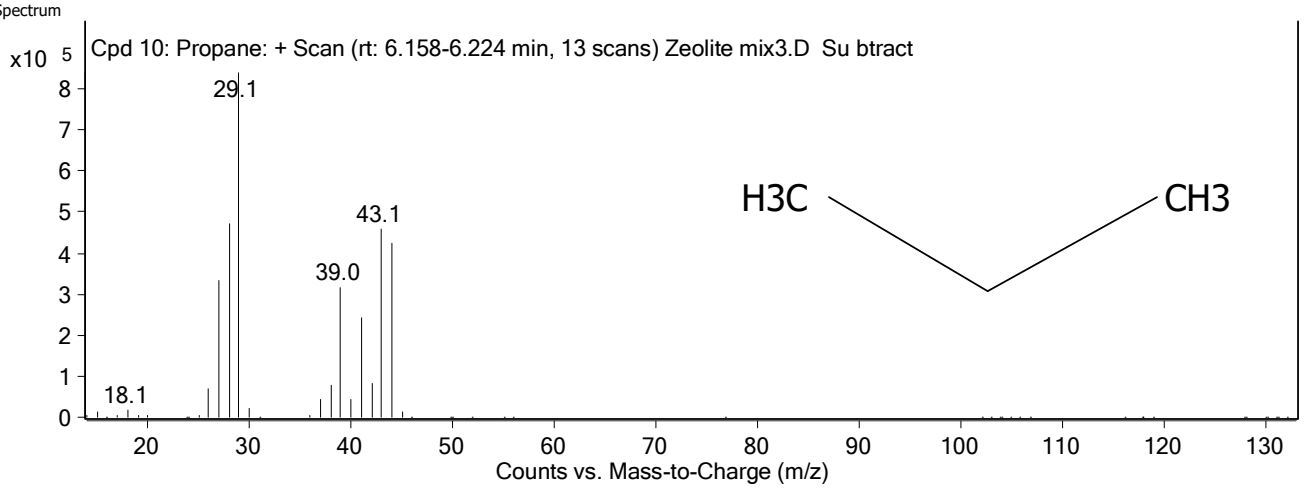

MS Zoomed Spectrum

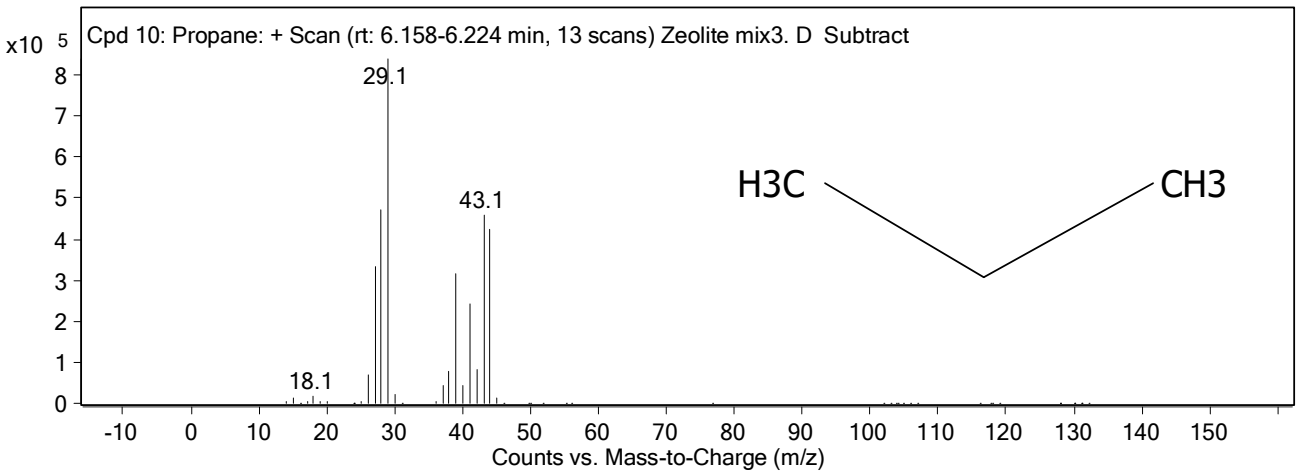

MS Spectrum Peak List

m/z	Abund
26.1	69291.09
27.1	334173.94
28.1	472039.56
29.1	839220.88
38	78321.27
39	315011.25
41	242247.42
42.1	82644.62
43.1	458569.53

44.1	426307.75

Compound Structure

Compound Label	Name	RT	Algorithm
Cpd 11: Butane	**Butane**	8.453	Find by Integration

Compound Chromatograms

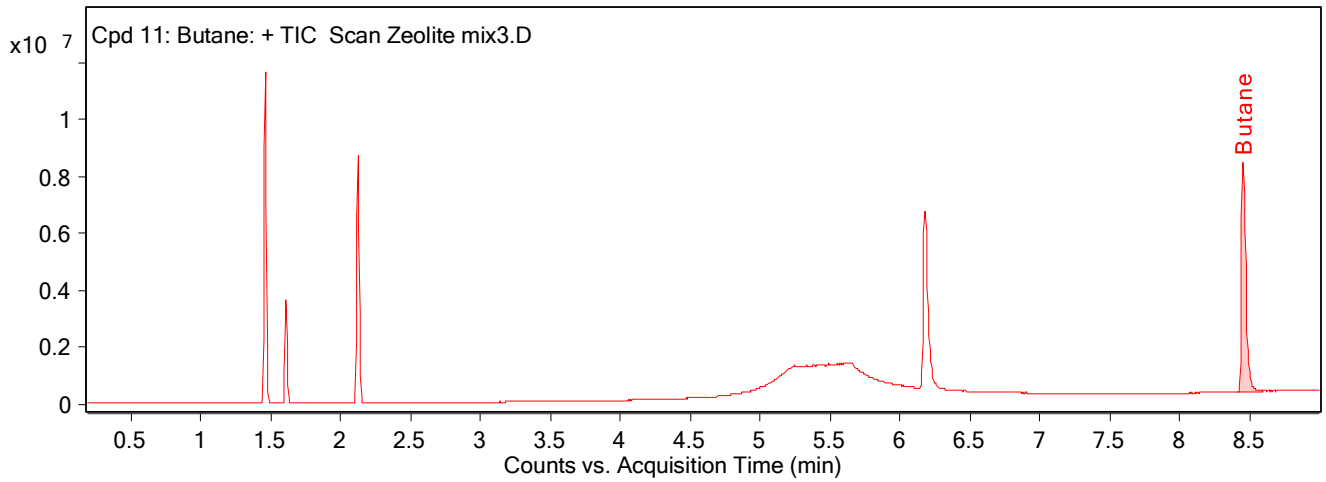

MS Spectrum

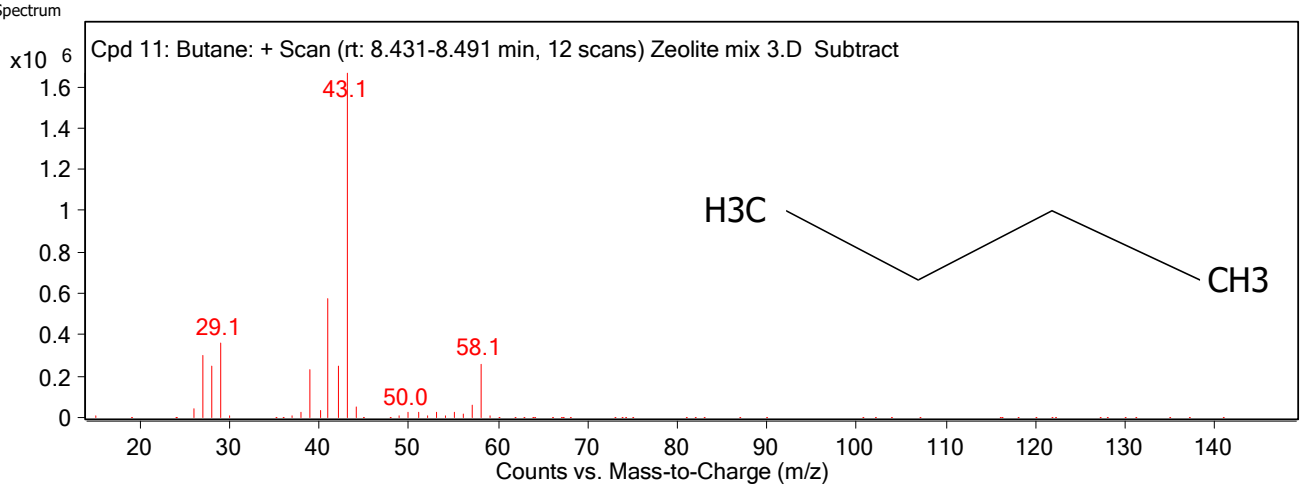

MS Zoomed Spectrum

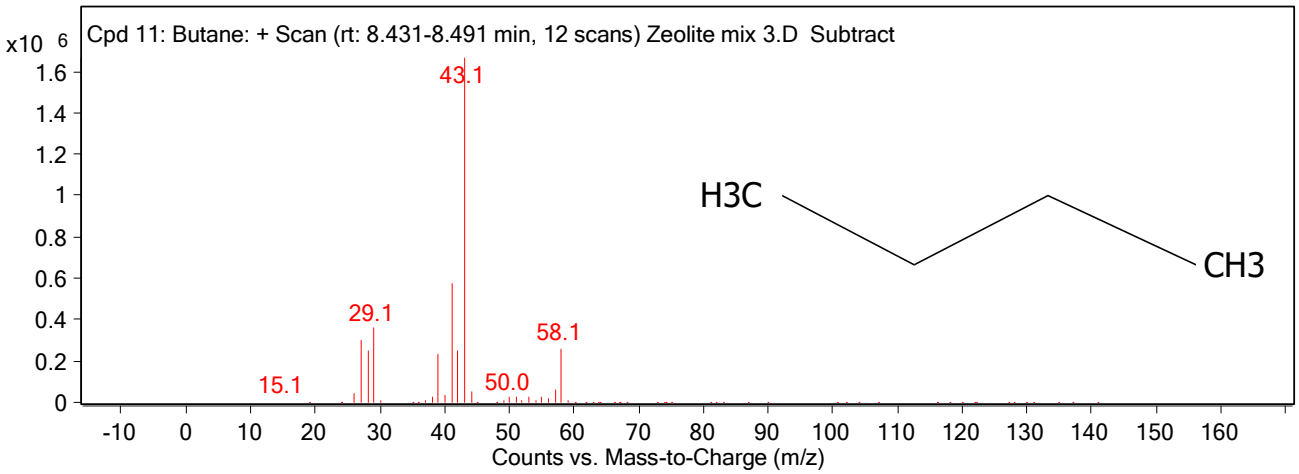

MS Spectrum Peak List

m/z	Abund
27.1	296774.78
28.1	250353.27
29.1	361228.34
39	230452.64
41.1	578612.19
42.1	245086.92
43.1	1664489.25
44.1	55733.14
57.1	57689.26
58.1	262149.41

Compound Structure

--- End Of Report ---

Appendix D

Qualitative compound report of CO_2 reforming of CH_4 using Rh/alumina membrane (feed gas)

Data File	CCEME Rh SM2.D	**Sample Name**	CCEME Rh SM2
Sample Type		**Position**	1
Instrument Name	5977A MSD	**User Name**	
Acq Method	Sequence Gas Analysis 11-05-2017.M	**Acquired Time**	5/16/2017 12:50:37 PM
IRM Calibration Status	Not Applicable	**DA Method**	RGU Routine.m
Comment	0.45mLmin 800C		
Expected Barcode		**Sample Amount**	
Dual Inj Vol	1	**TuneName**	etune.u
TunePath	D:\MassHunter\GCMS\1\5977\	**TuneDateStamp**	2017-05-10T14:11:30+01:00
MSFirmwareVersion	6.00.34	**OperatorName**	
RunCompletedFlag	True	**Acquisition SW Version**	MassHunter GC/MS Acquisition B.07.05.2479 23-Aug-2016 Copyright © 1989-2016 Agilent Technologies, Inc.

Compound Table

Compound Label	RT	Mass	Name	DB Formula	Hits (DB)
Cpd 1: 1.200	1.2				0
Cpd 2: Nitrogen	1.458		Nitrogen	N2	5
Cpd 3: Methane	1.611		Methane	CH4	3
Cpd 4: Carbon dioxide	2.121		Carbon dioxide	CO2	7
Cpd 5: 3.386	3.386				0
Cpd 6: Water	5.265		Water	H2O	1
Cpd 7: Water	5.292		Water	H2O	1
Cpd 8: 5.391	5.391				0
Cpd 9: Water	5.429		Water	H2O	1
Cpd 10: 5.462	5.462				0
Cpd 11: 5.544	5.544				0
Cpd 12: Water	5.577		Water	H2O	1
Cpd 13: Water	5.627		Water	H2O	1
Cpd 14: 8.968	8.968				0

Compound Label	RT	Algorithm
Cpd 1: 1.200	1.2	Find by Integration

Compound Chromatograms

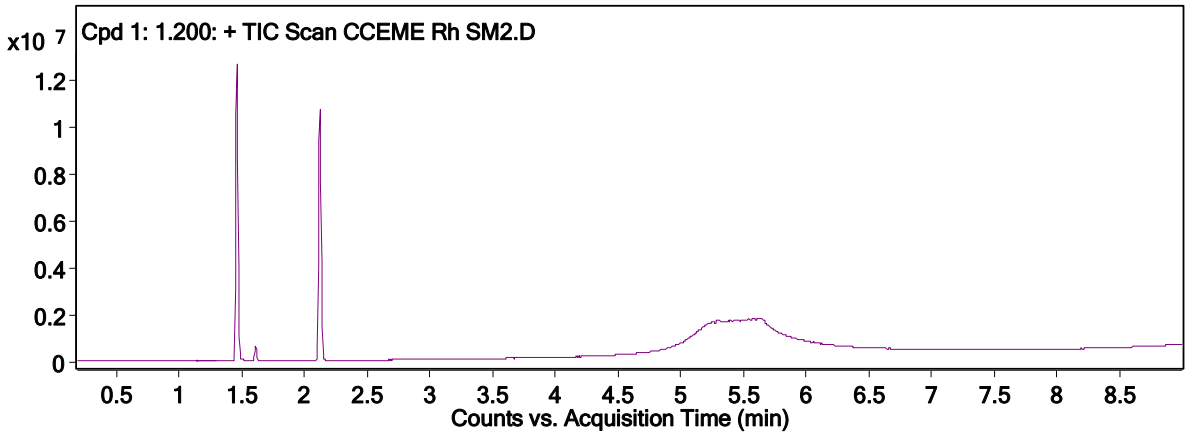

MS Spectrum

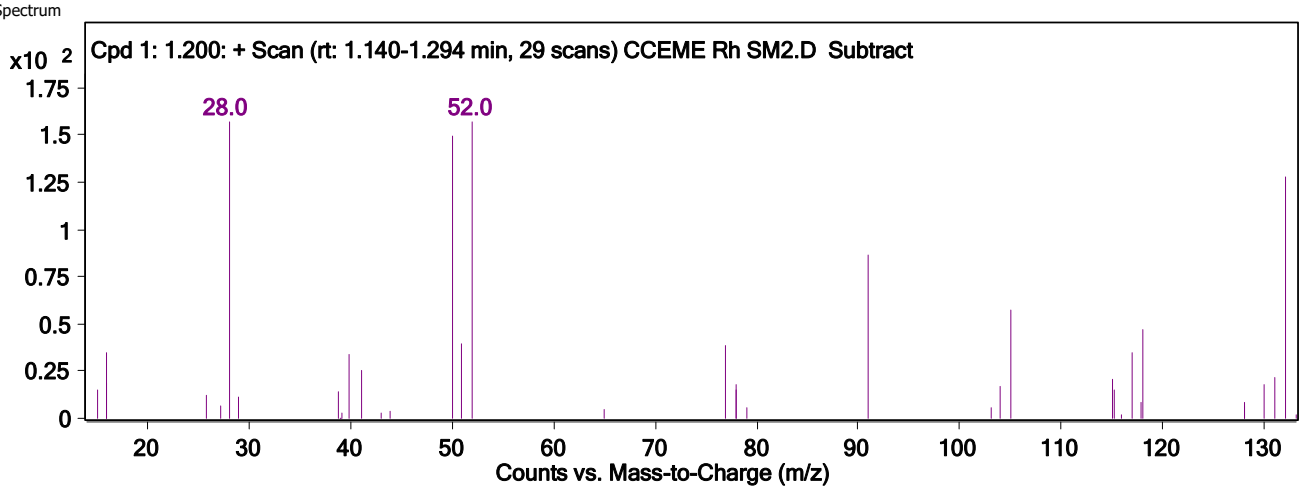

MS Zoomed Spectrum

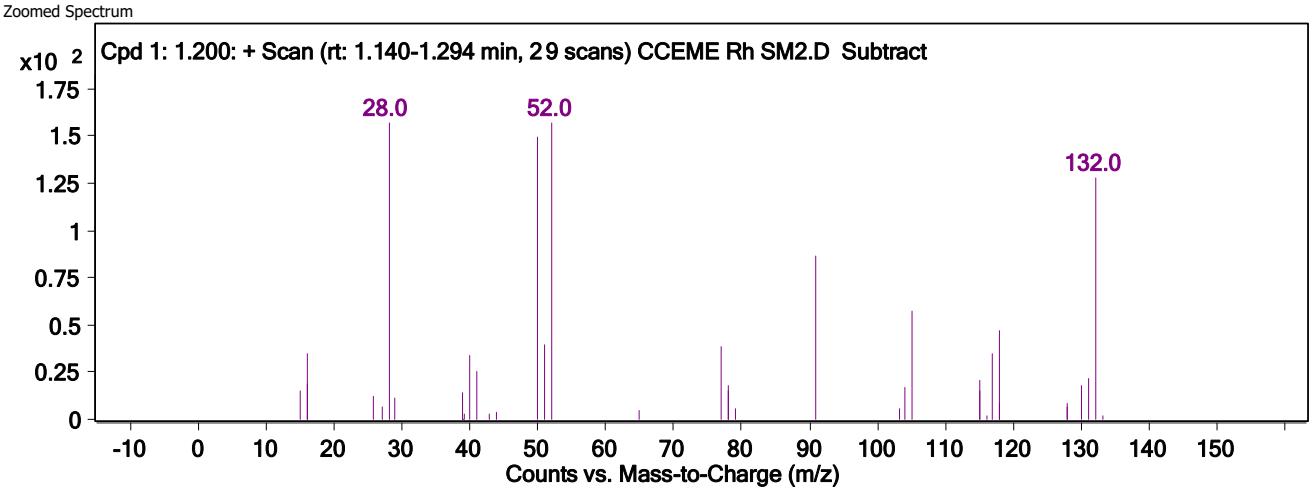

MS Spectrum Peak List

m/z	Abund
28	157.11
50	149.21

52	156.98
132	127.95

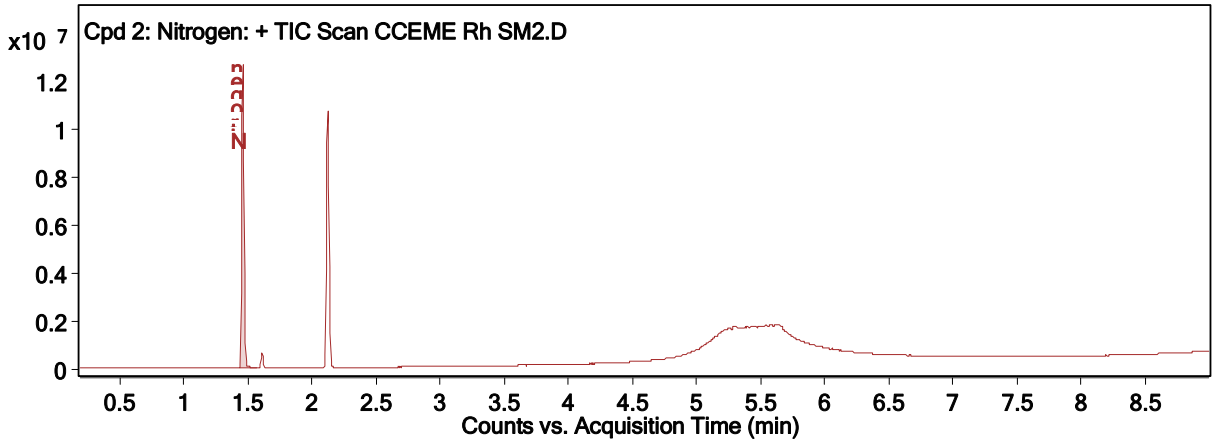

MS Spectrum

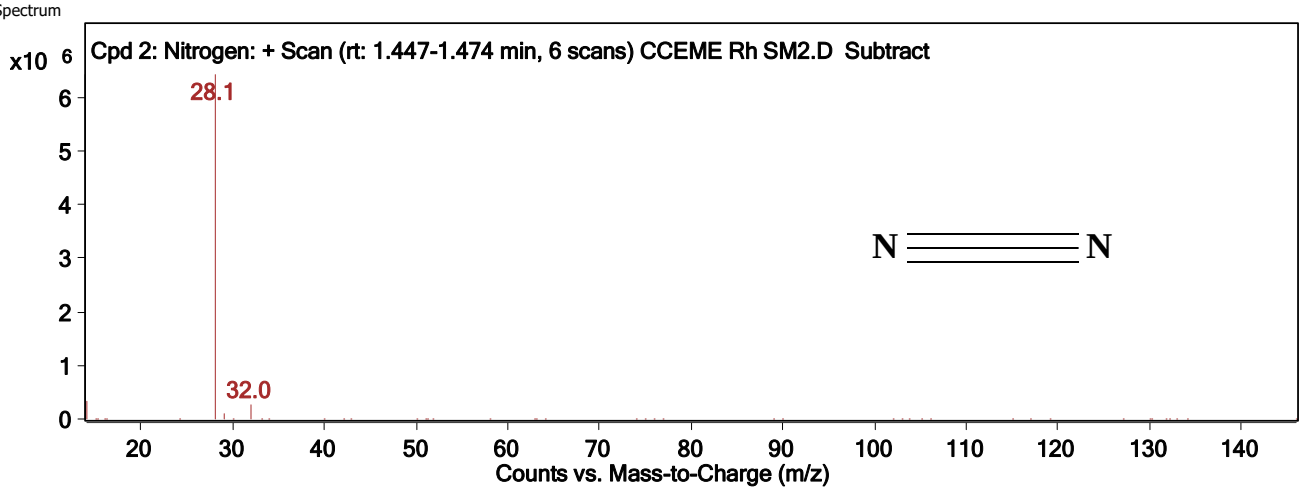

MS Zoomed

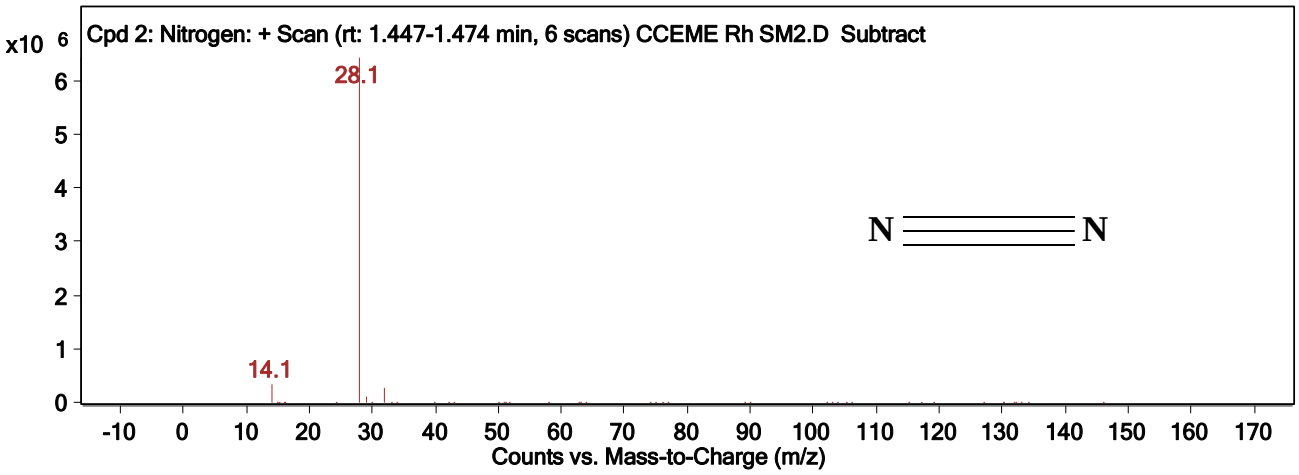

MS Spectrum Peak List

m/z	Abund
14.1	324845.28
28.1	6426583.5
29.1	98017.7
32	269590.09

Compound Label	Name	RT	Algorithm
Cpd 3: Methane	**Methane**	1.611	Find by Integration

Compound Structure

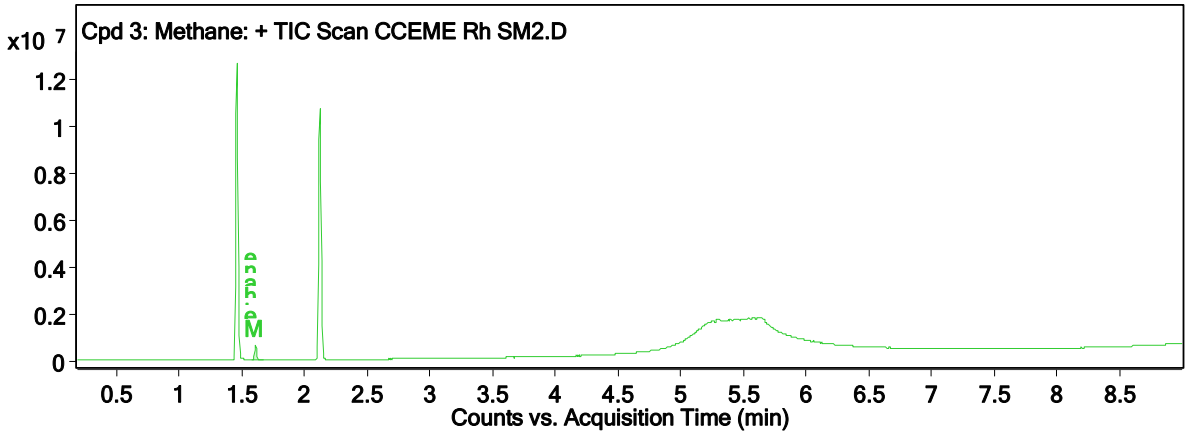

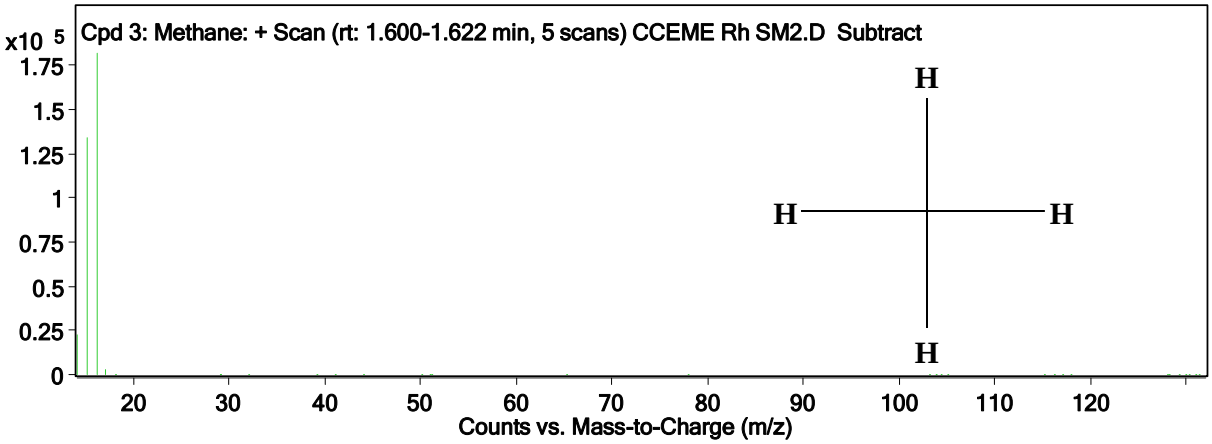

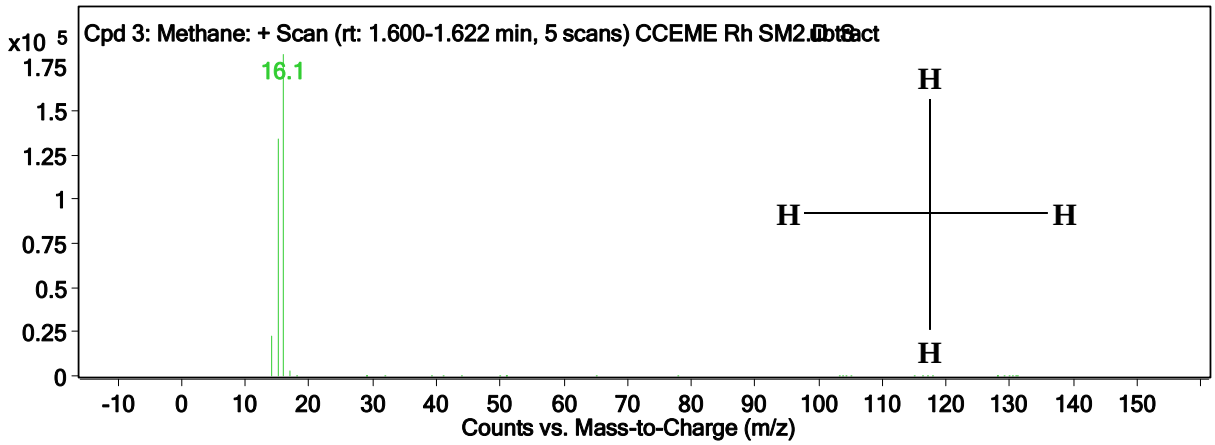

m/z	Abund
14.1	22753
15.1	134048.09
16.1	182023.52
17.1	2539.19

Compound

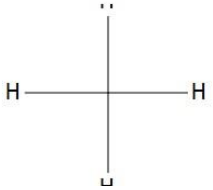

Compound Label	Name	RT	Algorithm
Cpd 4: Carbon dioxide	**Carbon dioxide**	2.121	Find by Integration

Compound Chromatograms

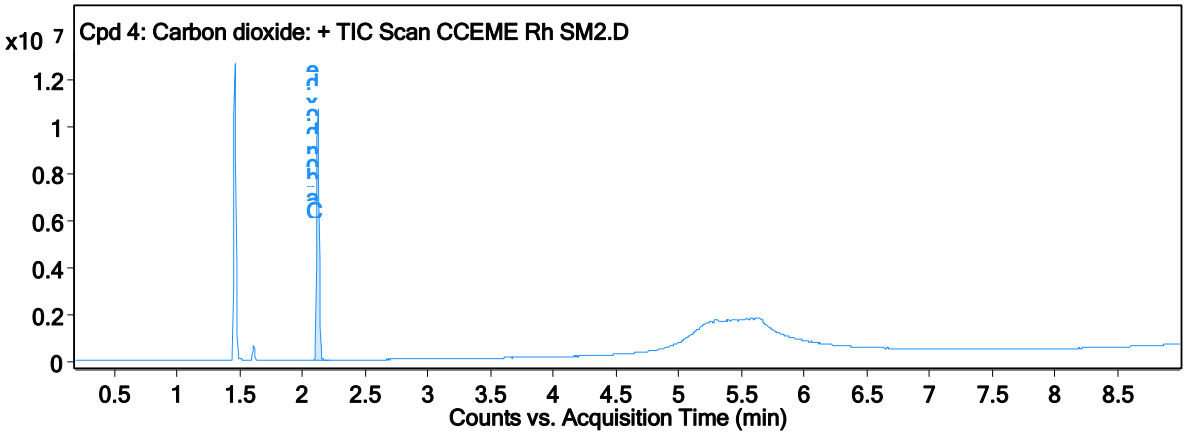

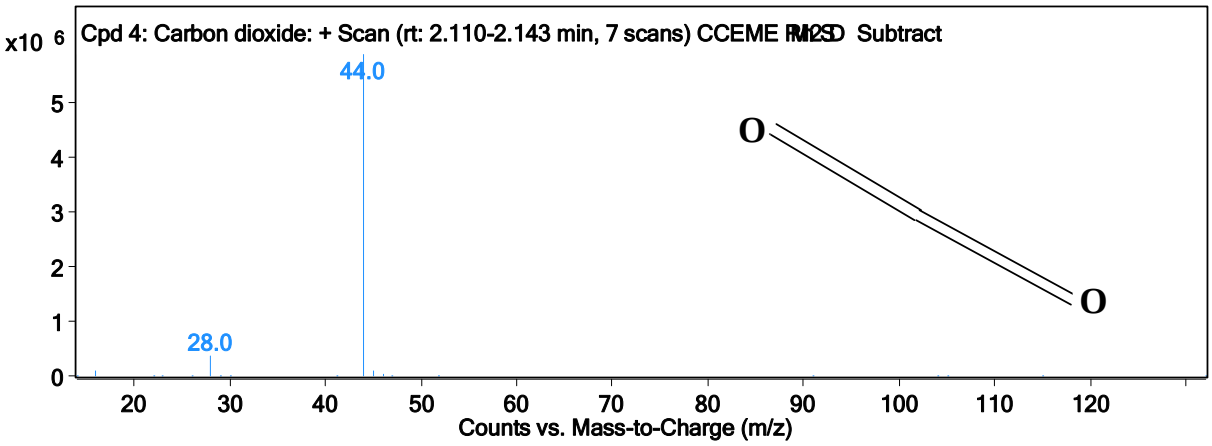
x10 6
Cpd 4: Carbon dioxide: + Scan (rt: 2.110-2.143 min, 7 scans) CCEME RM2SD Subtract
44.0
28.0
O
O
5
4
3
2
1
0
20
30
40
50
60
70
80
90
100
110
120
Counts vs. Mass-to-Charge (m/z)

Appendix E

Qualitative compound report of CO_2 reforming of CH_4 using Rh/alumina membrane (permeate gas)

Data File	CCEME Rh SM2.D	**Sample Name**	CCEME Rh SM2
Sample Type		**Position**	1
Instrument Name	5977A MSD	**User Name**	
Acq Method	Sequence Gas Analysis 11-05-2017.M	**Acquired Time**	5/16/2017 12:50:37 PM
IRM Calibration Status	Not Applicable	**DA Method**	RGU Routine.m
Comment	0.45mLmin 800C		
Expected Barcode		**Sample Amount**	
Dual Inj Vol	1	**TuneName**	etune.u
TunePath	D:\MassHunter\GCMS\1\5977\	**TuneDateStamp**	2017-05-10T14:11:30+01:00
MSFirmware Version	6.00.34	**OperatorName**	
RunCompleted Flag	True	**Acquisition SW Version**	MassHunter GC/MS Acquisition B.07.05.2479 23-Aug-2016 Copyright © 1989-2016 Agilent Technologies, Inc.

Compound Table

Compound Label	RT	Mass	Name	DB Formula	Hits (DB)
Cpd 1: 1.200	1.2				0
Cpd 2: Nitrogen	1.458		Nitrogen	N2	5
Cpd 3: Methane	1.611		Methane	CH4	3
Cpd 4: Carbon dioxide	2.121		Carbon dioxide	CO2	7
Cpd 5: 3.386	3.386				0
Cpd 6: Water	5.265		Water	H2O	1
Cpd 7: Water	5.292		Water	H2O	1
Cpd 8: 5.391	5.391				0
Cpd 9: Water	5.429		Water	H2O	1
Cpd 10: 5.462	5.462				0
Cpd 11: 5.544	5.544				0
Cpd 12: Water	5.577		Water	H2O	1
Cpd 13: Water	5.627		Water	H2O	1
Cpd 14: 8.968	8.968				0

Compound Label	RT	Algorithm
Cpd 1: 1.200	1.2	Find by Integration

Compound Chromatograms

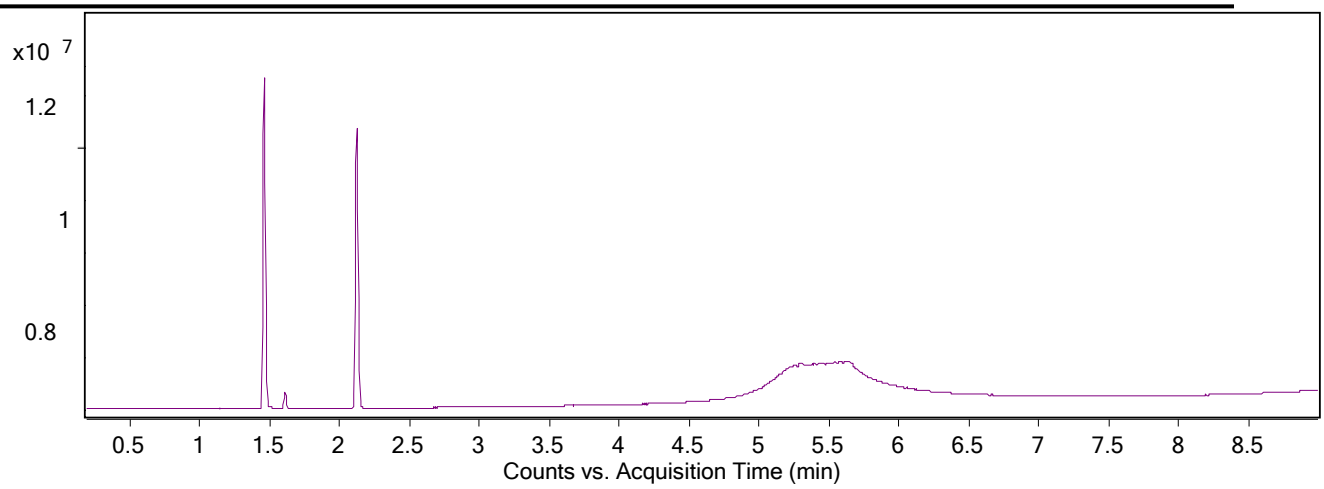

MS Spectrum

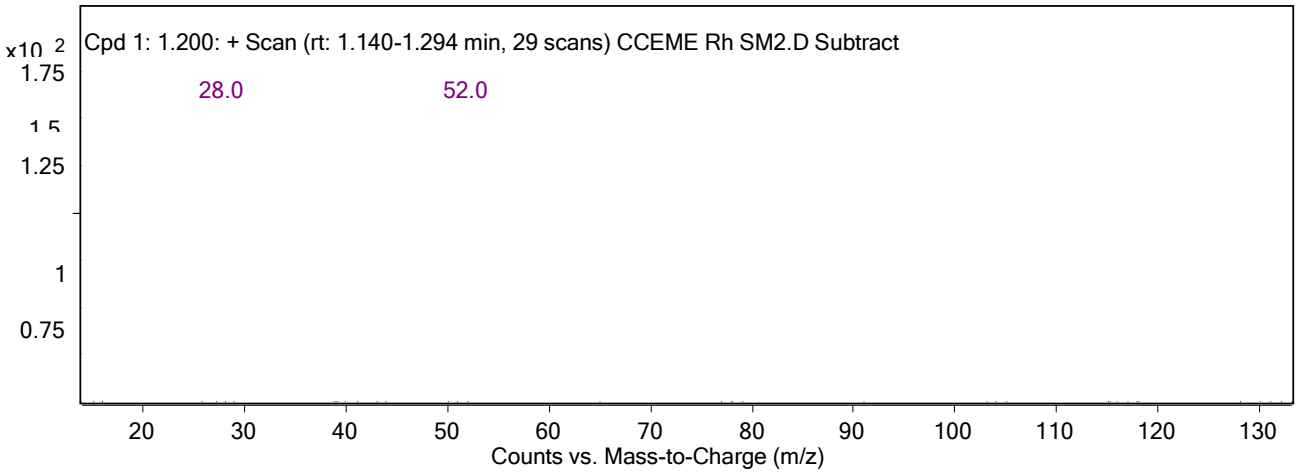

MS Zoomed Spectrum

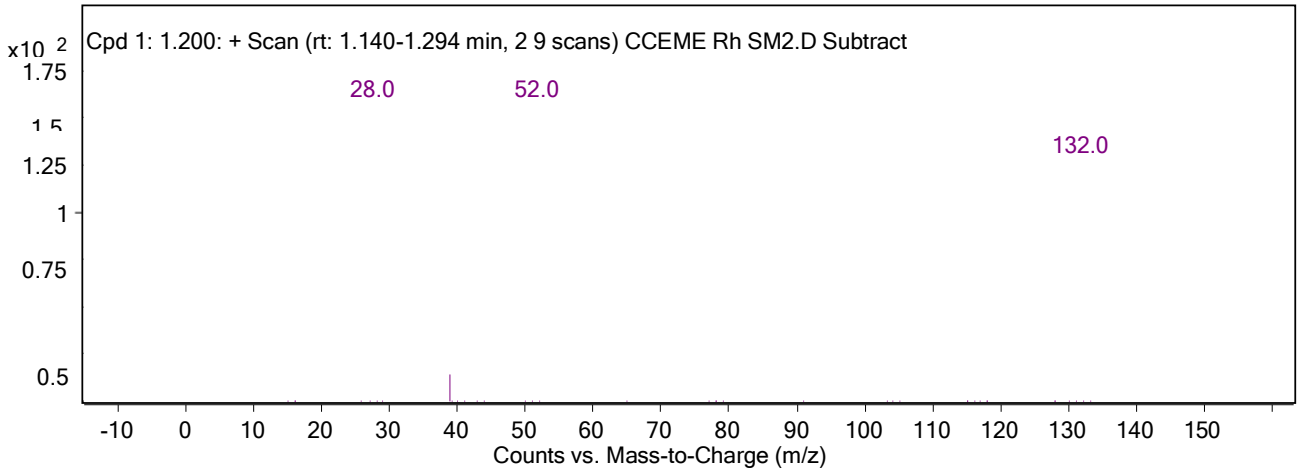

MS Spectrum Peak List

m/z	**Abund**
28	157.11
50	149.21
52	156.98

132	127.95

Compound Label	Name	RT	Algorithm
Cpd 2: Nitrogen	**Nitrogen**	1.458	Find by Integration

Compound Chromatograms

x10 7

MS Spectrum

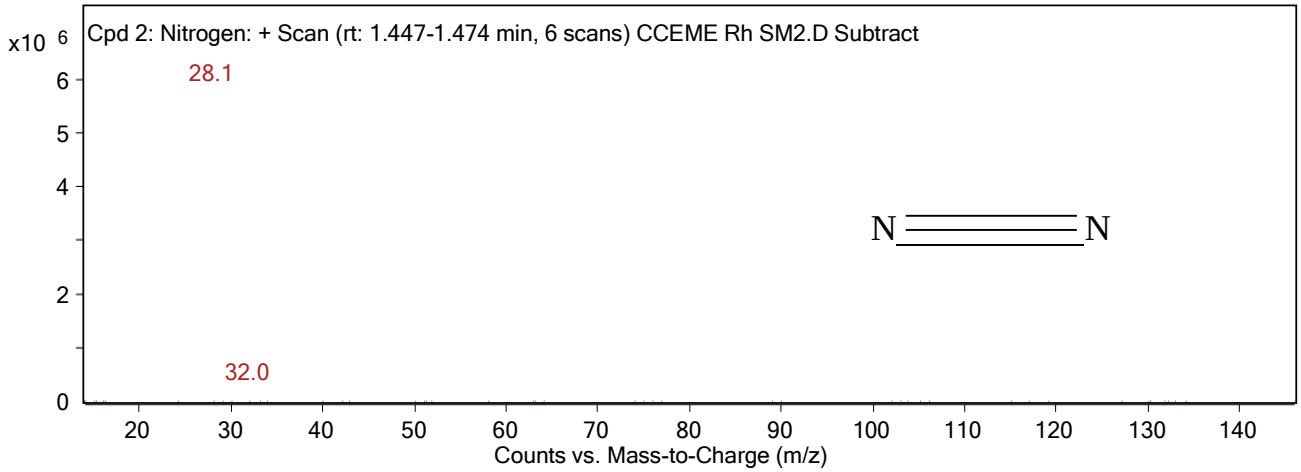

MS Zoomed Spectrum

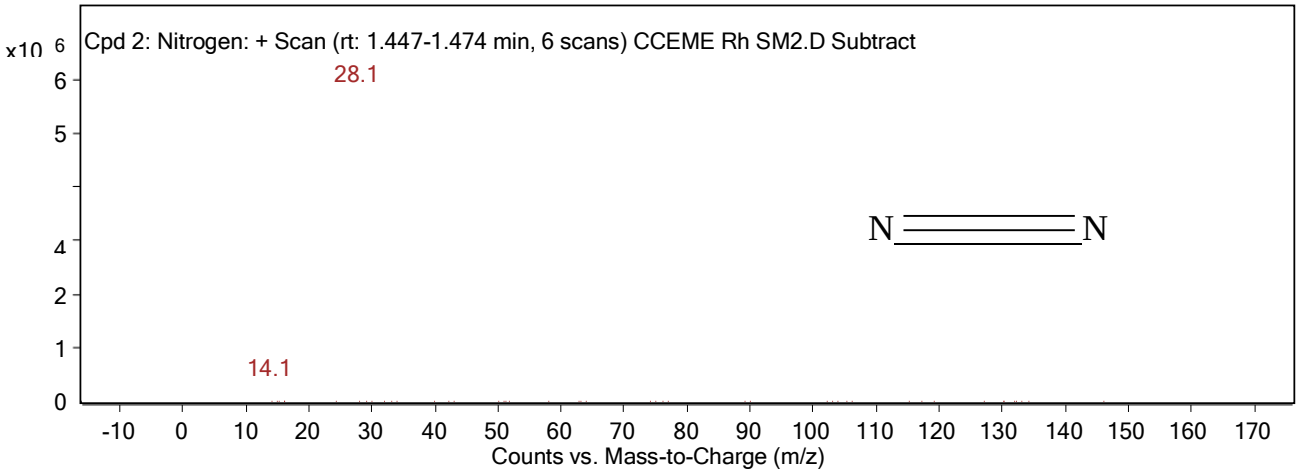

MS Spectrum Peak List

m/z	**Abund**
14.1	324845.28
28.1	6426583.5
29.1	98017.7
32	269590.09

Compound Label	**Name**	**RT**	**Algorithm**	
Cpd 3: Methane	**Methane**	1.611	Find by Integration	

Compound Structure Compound Chromatograms

x10 7

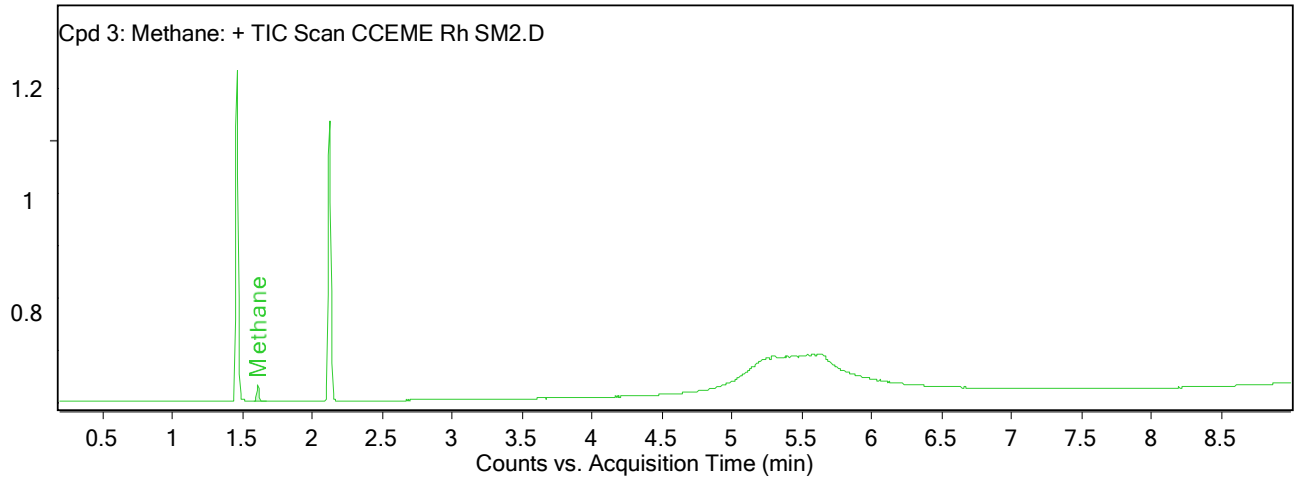

MS Spectrum

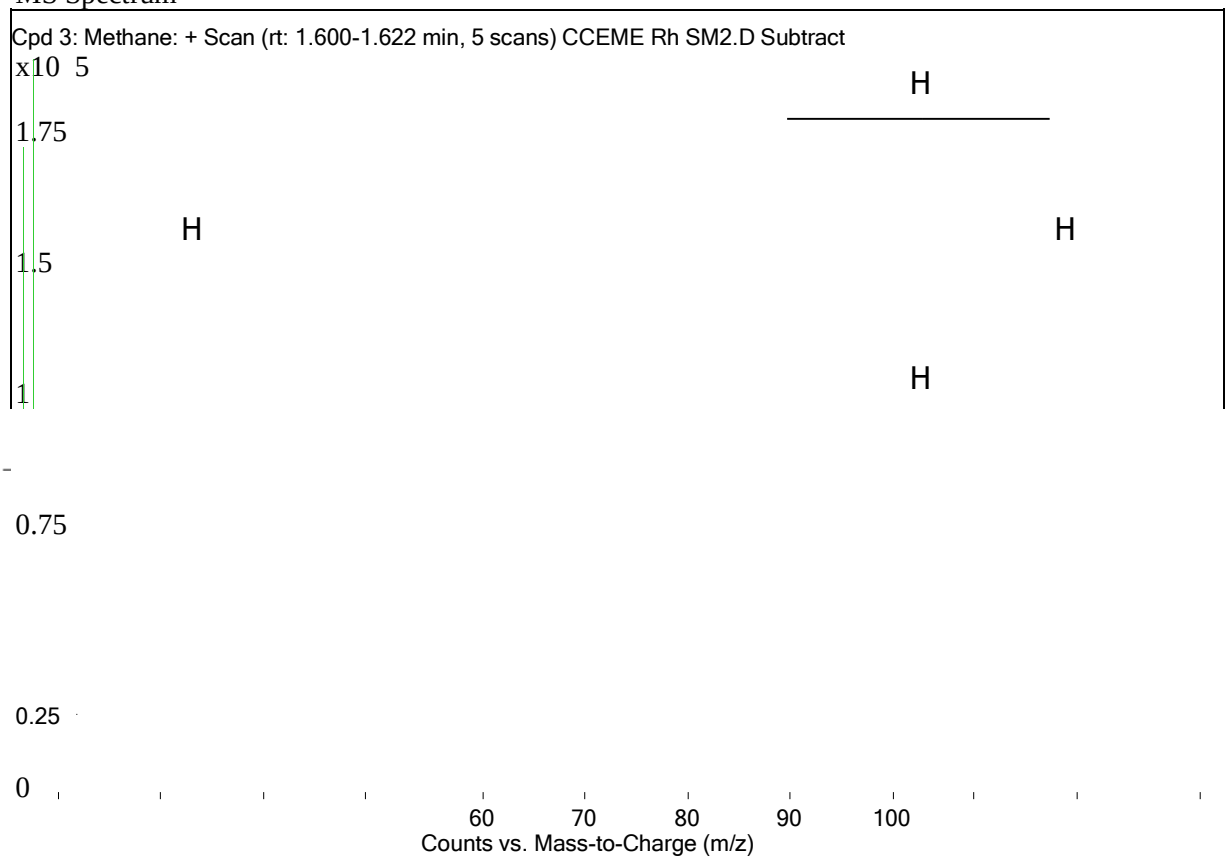

MS Zoomed Spectrum

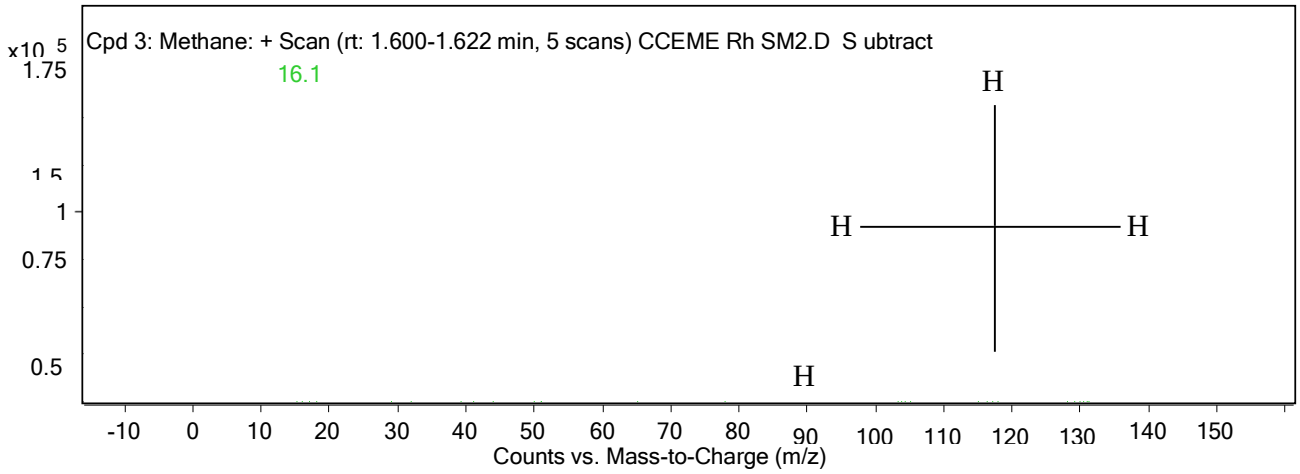

MS Spectrum Peak List

m/z	**Abund**
14.1	22753
15.1	134048.09
16.1	182023.52
17.1	2539.19

Compound Structure

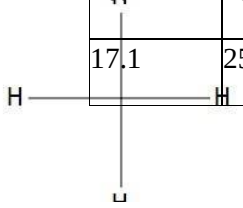

Compound Label	Name	RT	Algorithm
Cpd 4: Carbon dioxide	**Carbon dioxide**	2.121	Find by Integration

Compound Chromatograms

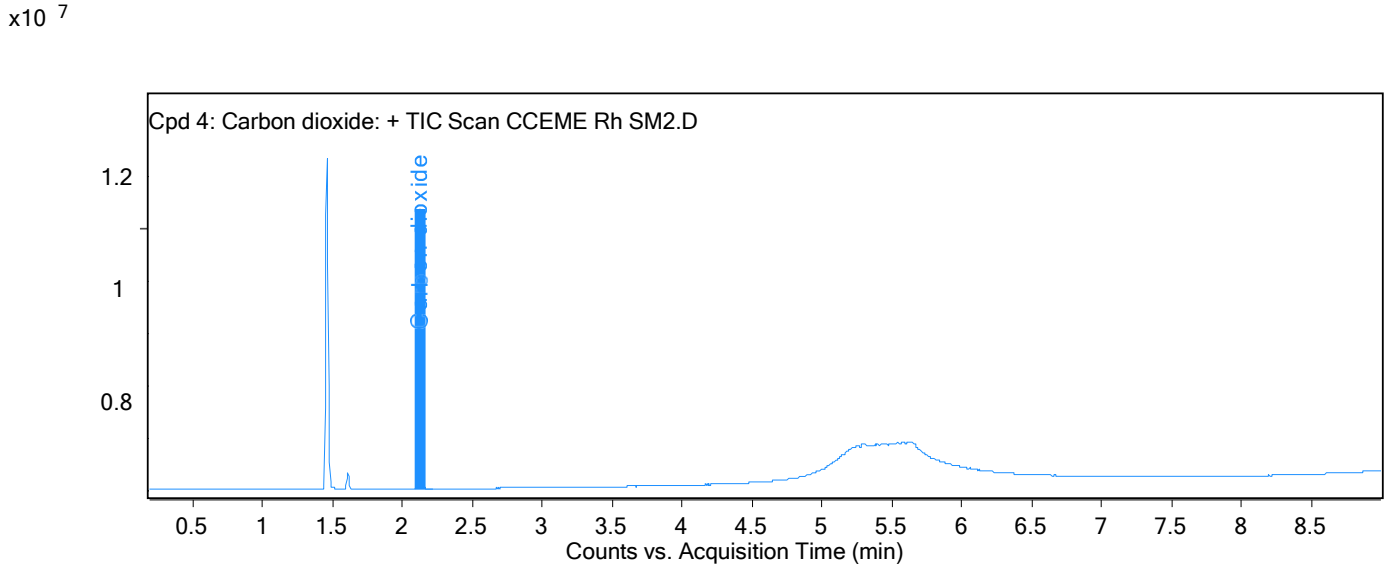

MS Spectrum

x10

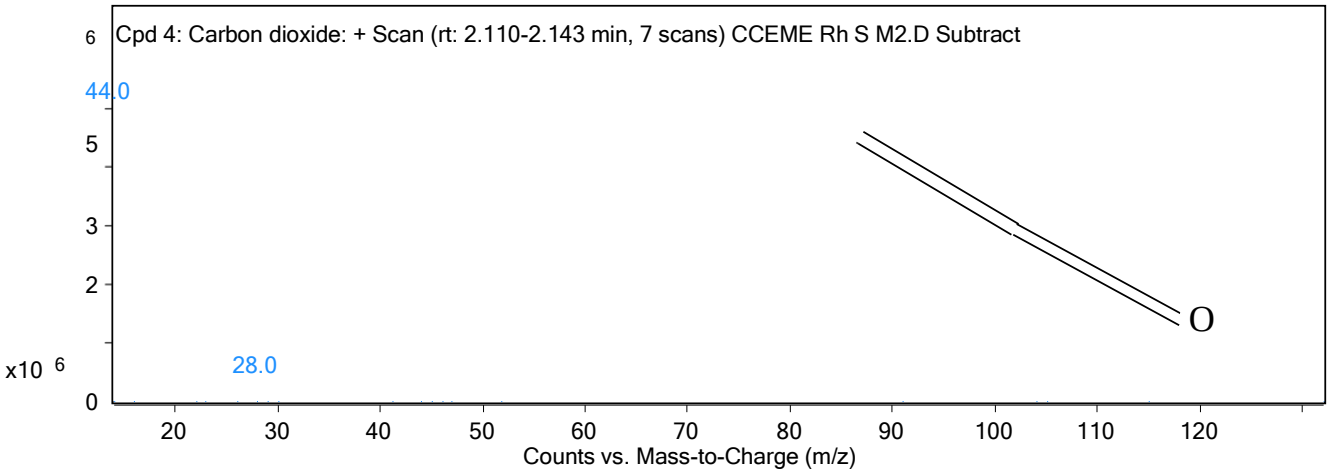

MS Zoomed Spectrum

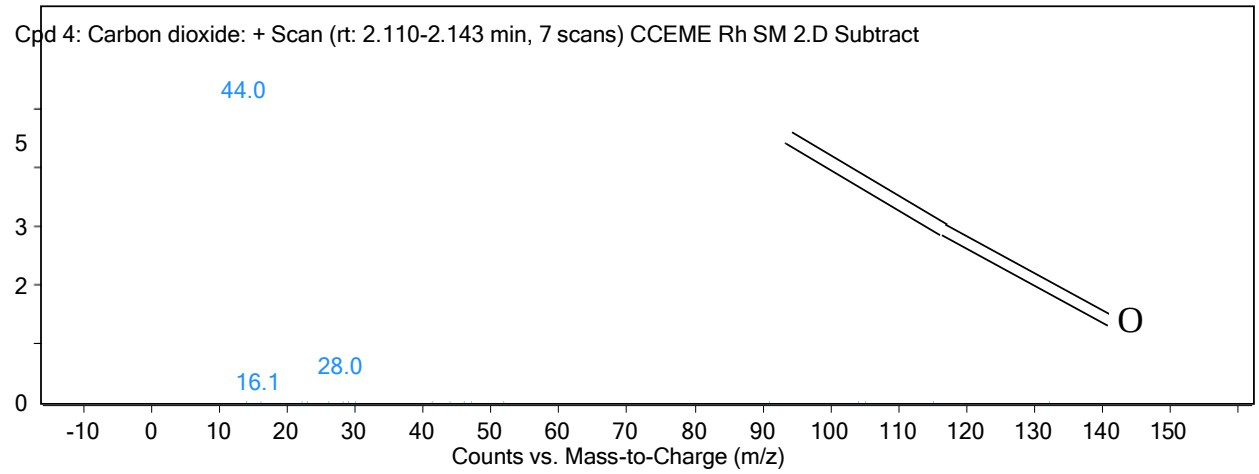

MS Spectrum Peak List

m/z	**Abund**
16.1	100051.04
28	379442.84
44	5887222
45	97332.57

Compound Structure

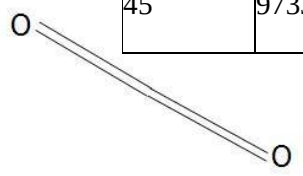

46	34495.53

Compound Label	RT	Algorithm
Cpd 5: 3.386	3.386	Find by Integration

Compound Chromatograms

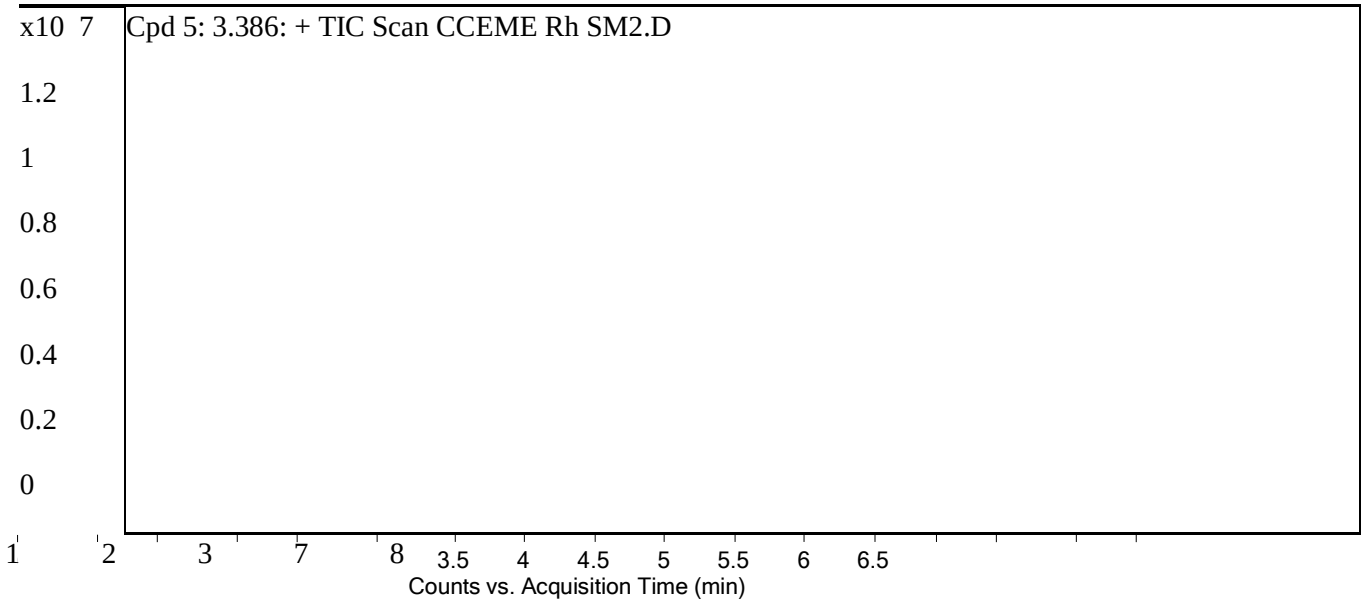

MS Spectrum

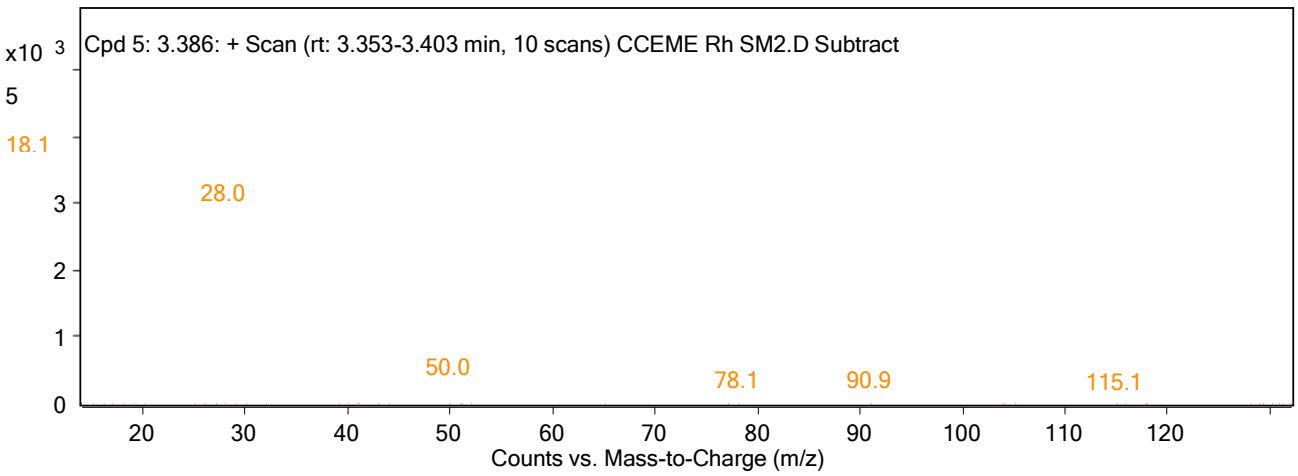

MS Zoomed Spectrum

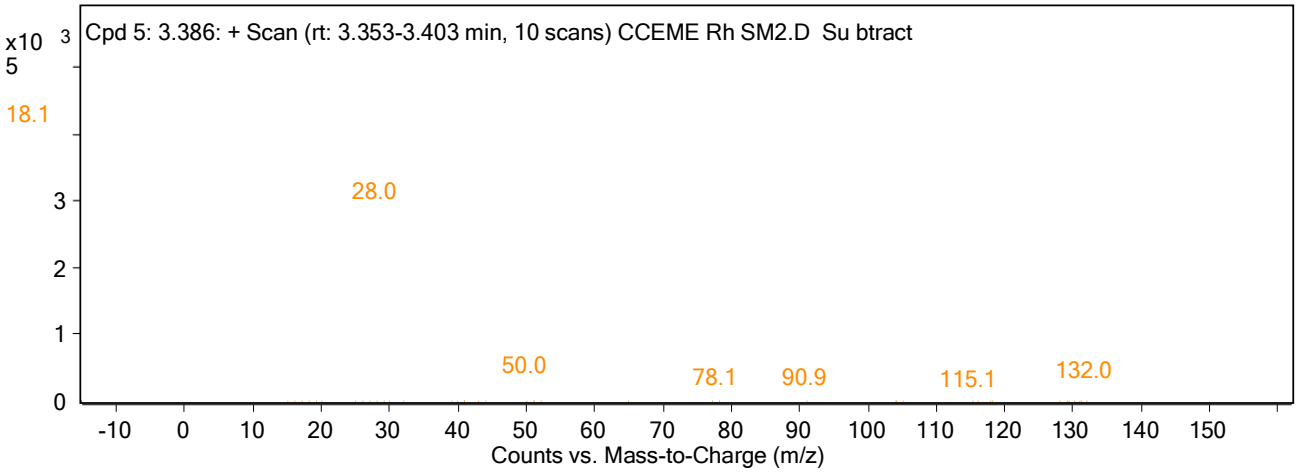

MS Spectrum Peak List

m/z	**Abund**
17.1	1117.65
18.1	4453.58
26	677.8
27.1	963.77

28	2919.91
29	615.94
30	750.77
50	320.6
90.9	133.2
132	249

Compound Label	Name	RT	Algorithm
Cpd 6: Water	**Water**	5.265	Find by Integration

Compound Chromatograms

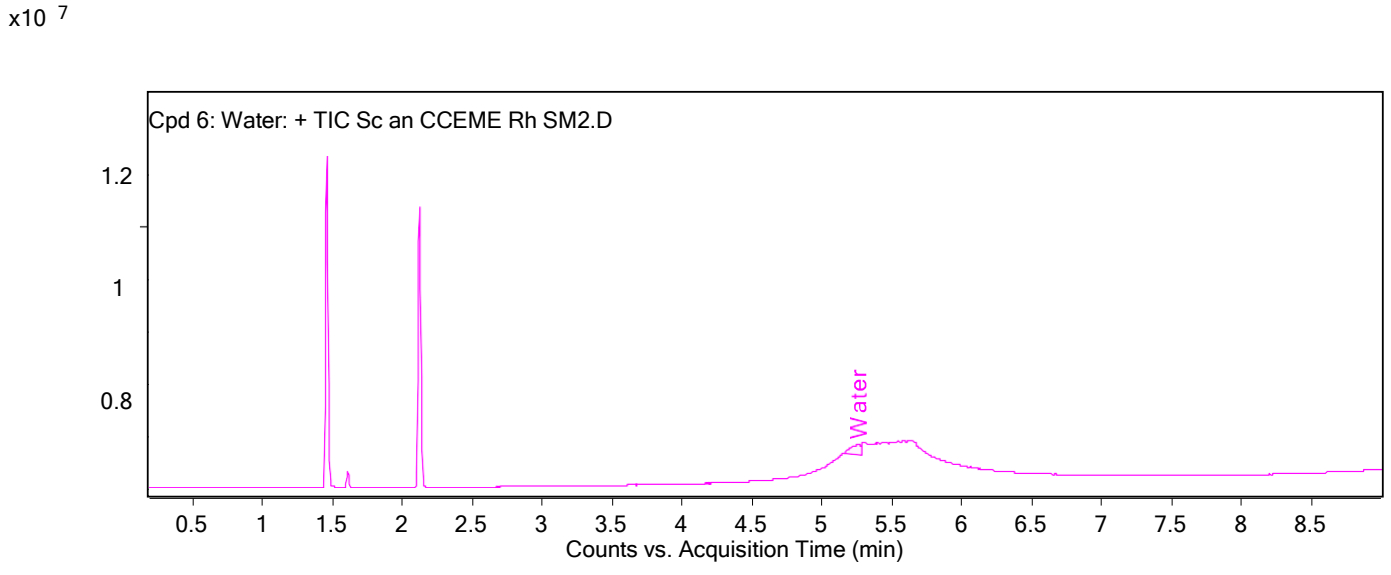

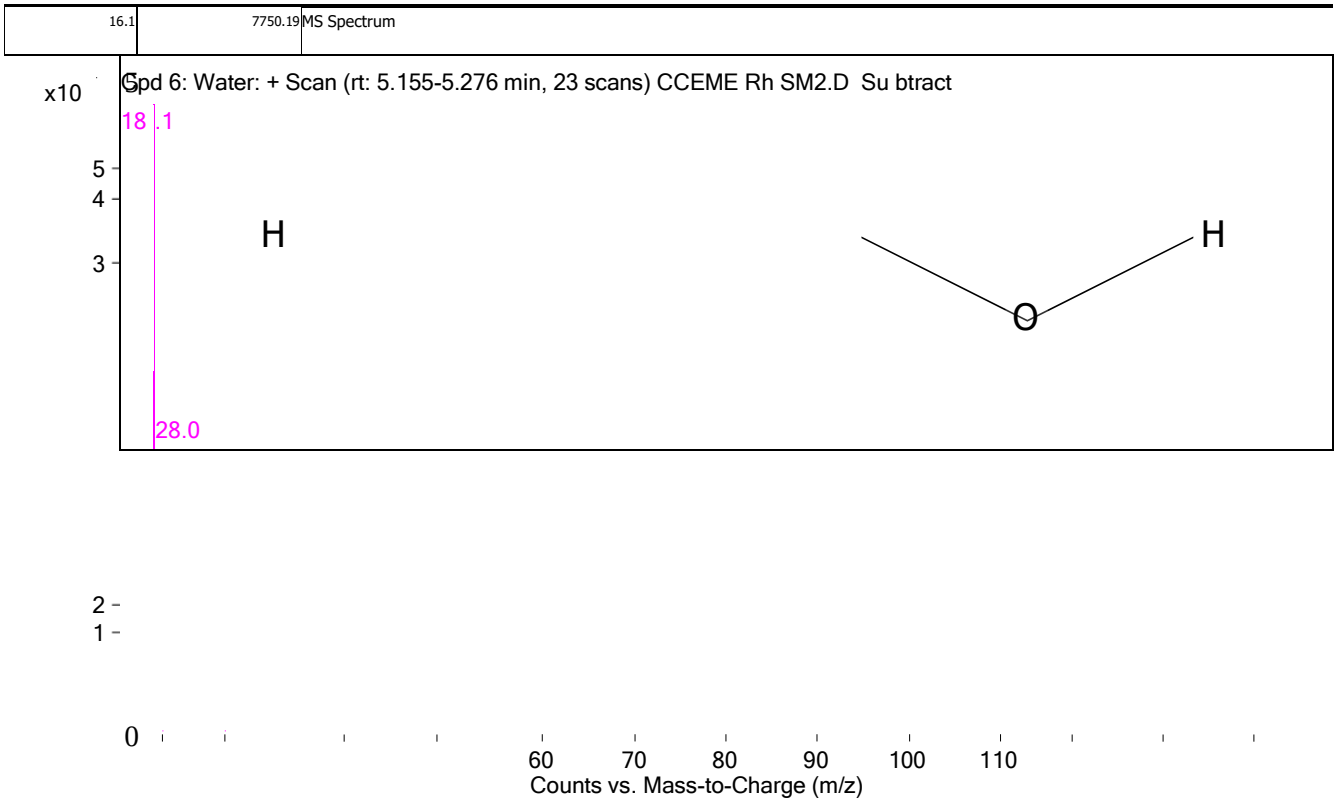

MS Zoomed Spectrum

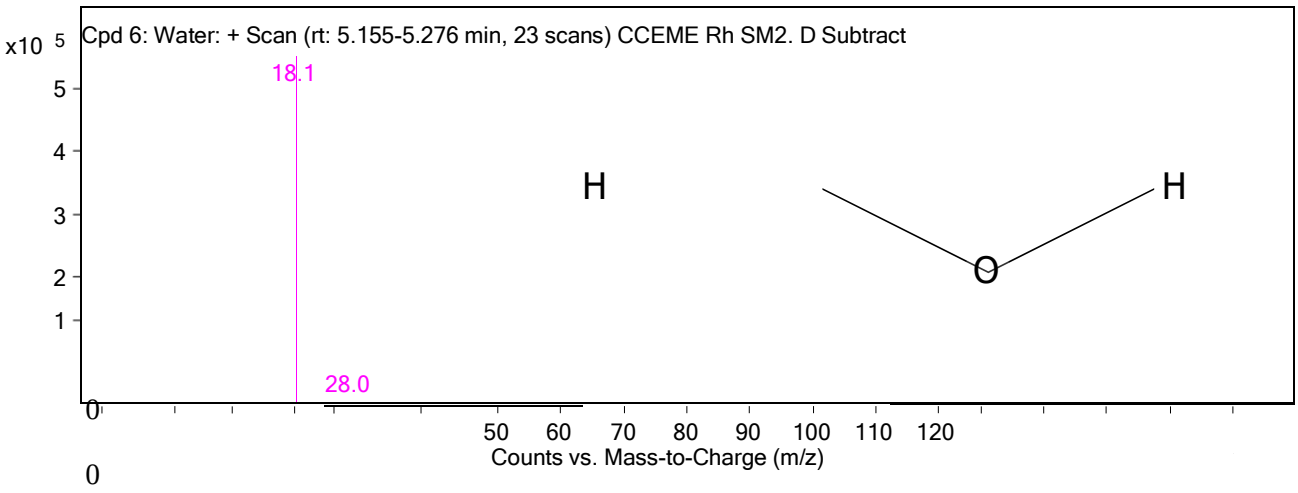

MS Spectrum Peak List

17.1	118637.06
18.1	547895.25
19.1	3099.02
28	3414.56

Compound Structure Compound Chromatograms

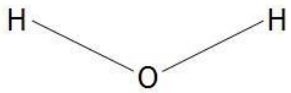

Compound Label	**Name**	**RT**	**Algorithm**
Cpd 7: Water	**Water**	5.292	Find by Integration

Cpd 7: Water: + TIC Sc an CCEME Rh SM2.D

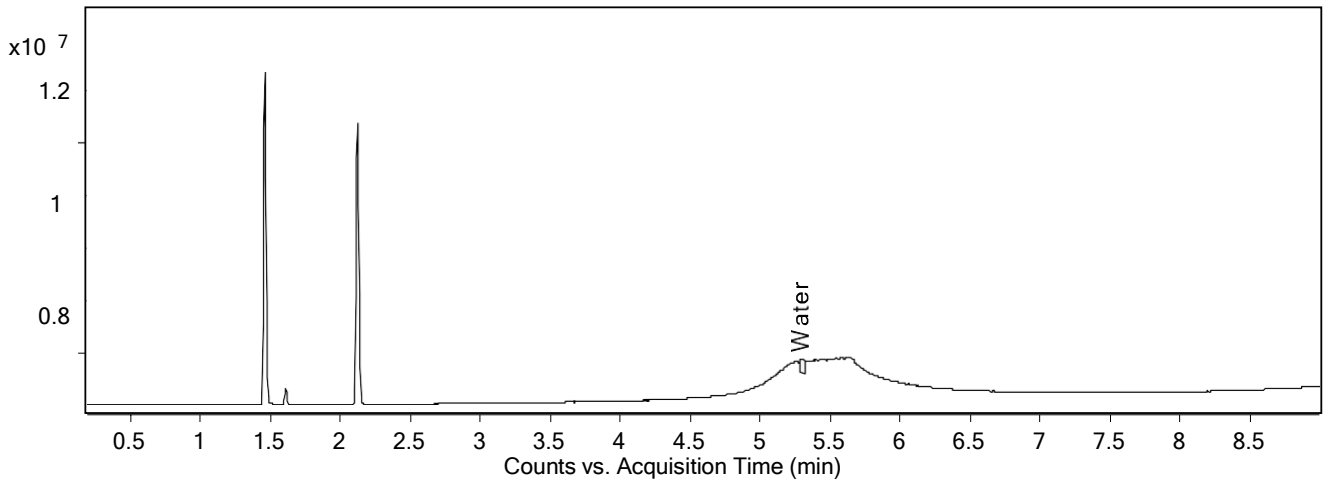

MS Spectrum

x10

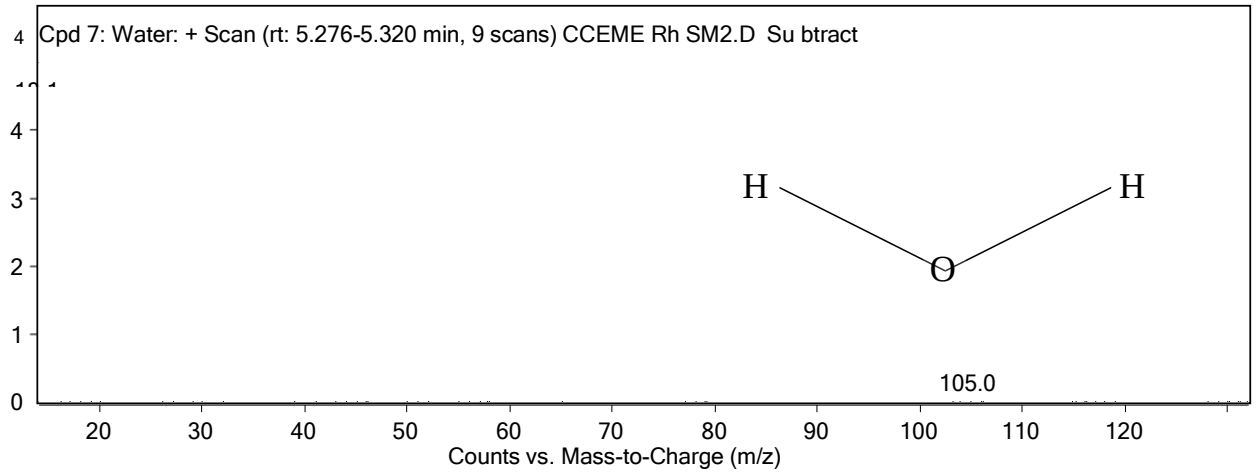

MS Zoomed Spectrum

x10 4

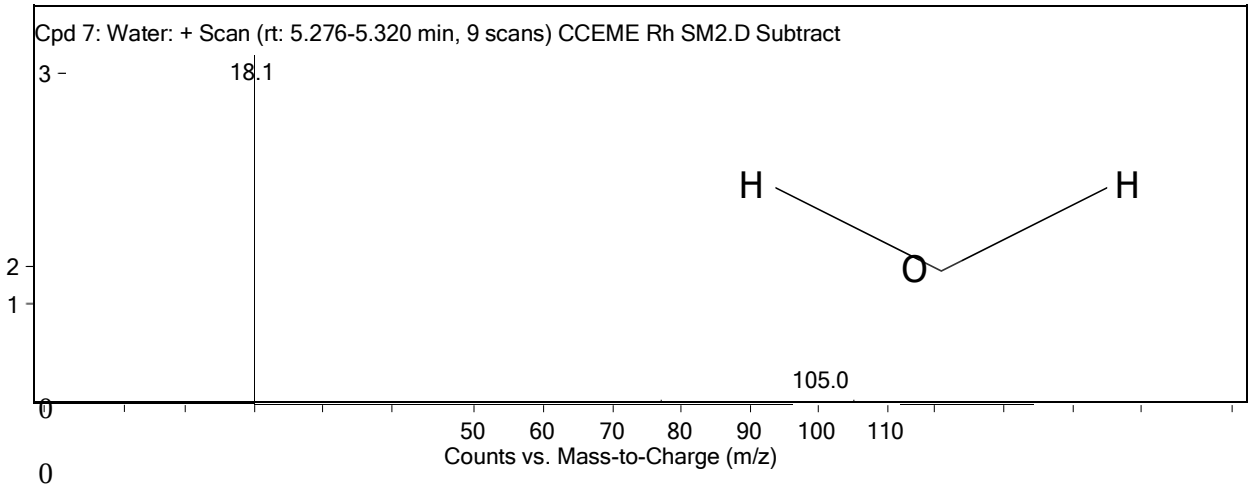

MS Spectrum Peak List

m/z	**Abund**
16.1	856.09

Compound Structure

17.1	10351.47
18.1	50848
19.1	428.09
105	405.75

Compound Label	RT	Algorithm
Cpd 8: 5.391	5.391	Find by Integration

Compound Chromatograms

x10 7

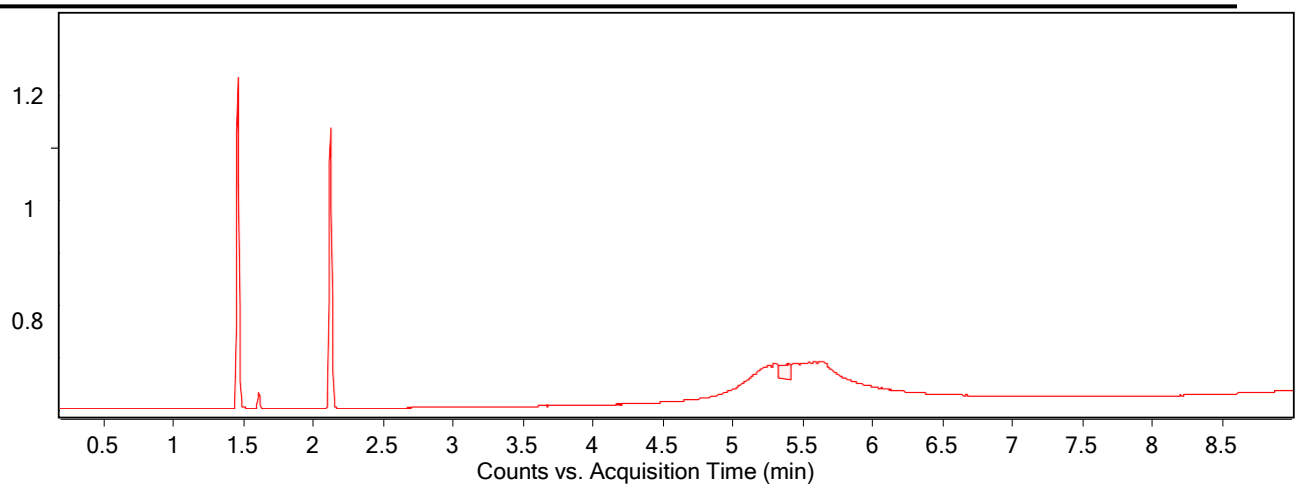

MS Spectrum

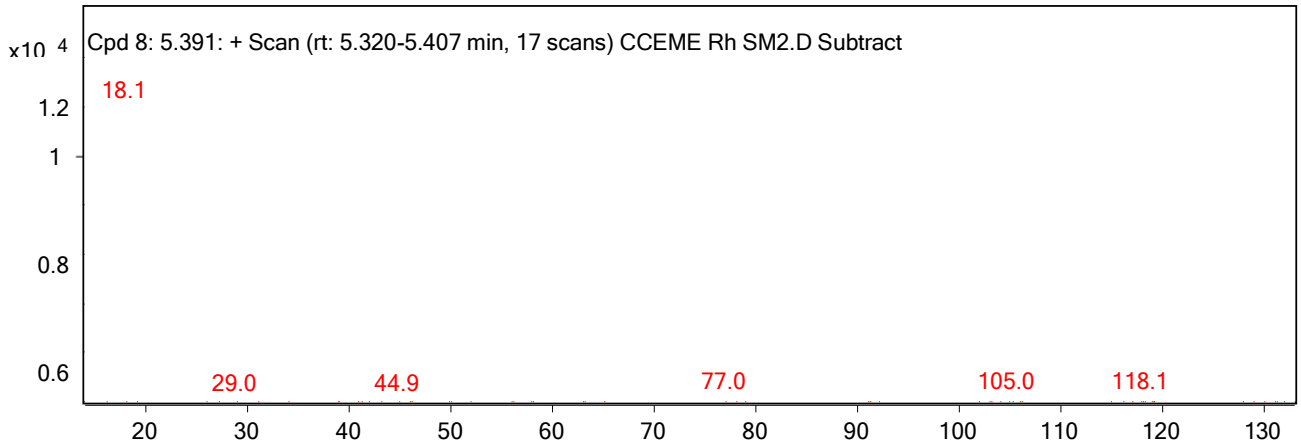

MS Zoomed Spectrum

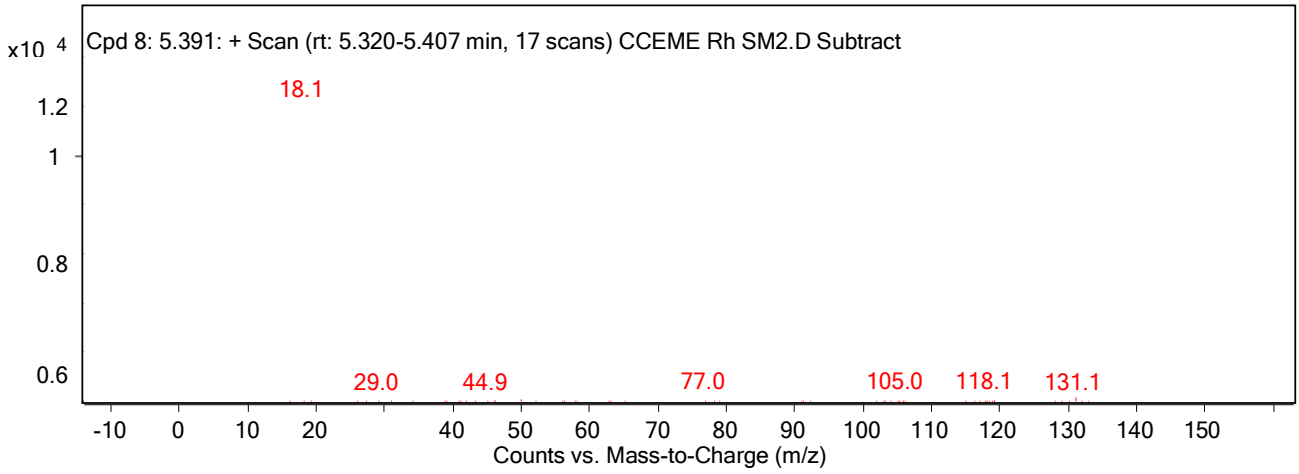

MS Spectrum Peak List

m/z	**Abund**
16.1	540.99
18.1	12077.75
19.1	230.61

29	123.29
77	218.84
103.9	128.78
105	186.87
115	145.82
118.1	202.5
131.1	127.72

Compound Label	Name	RT	Algorithm
Cpd 9: Water	**Water**	5.429	Find by Integration

Compound Chromatograms

x10 ^{7}

MS Spectrum

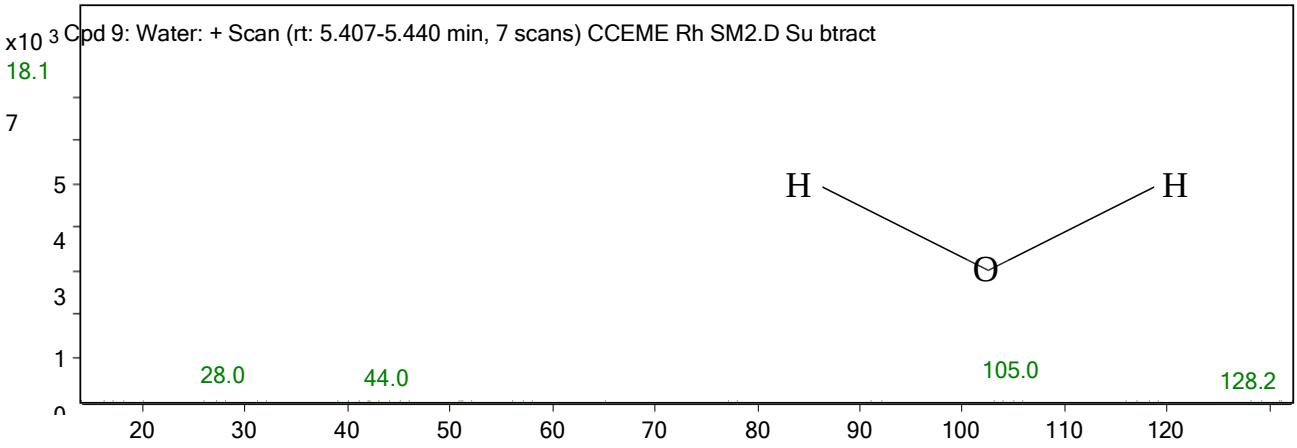
Cpd 9: Water: + Scan (rt: 5.407-5.440 min, 7 scans) CCEME Rh SM2.D Su btract
x10 3
18.1
7
5
4
3
1
0
28.0
44.0
105.0
128.2
H
H
O
20
30
40
50
60
70
80
90
100
110
120

S Zoomed Spectrum **Compound Structure**

x10 3 Cpd 9: Water: + Sca

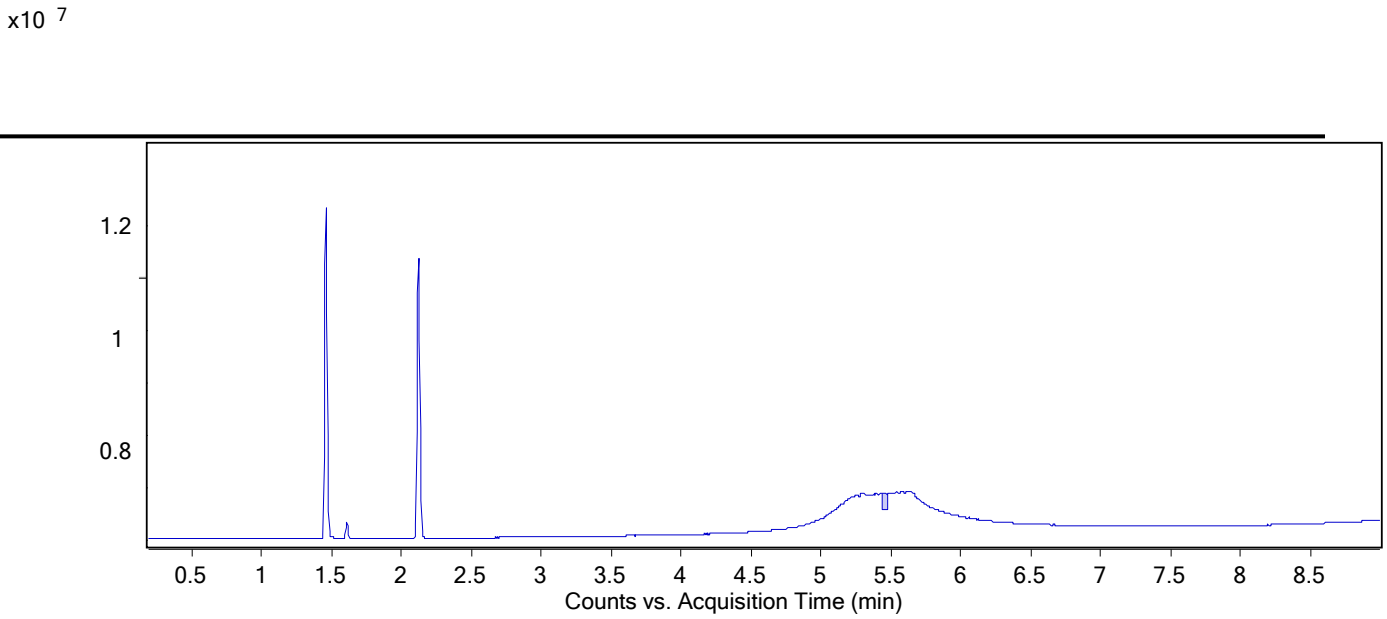

MS Spectrum

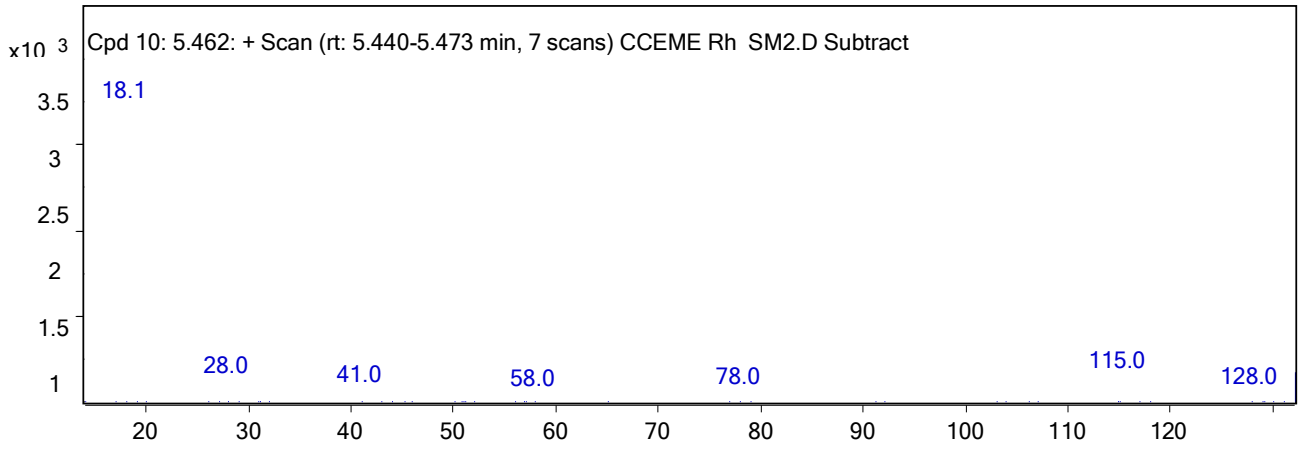

MS Zoomed Spectrum

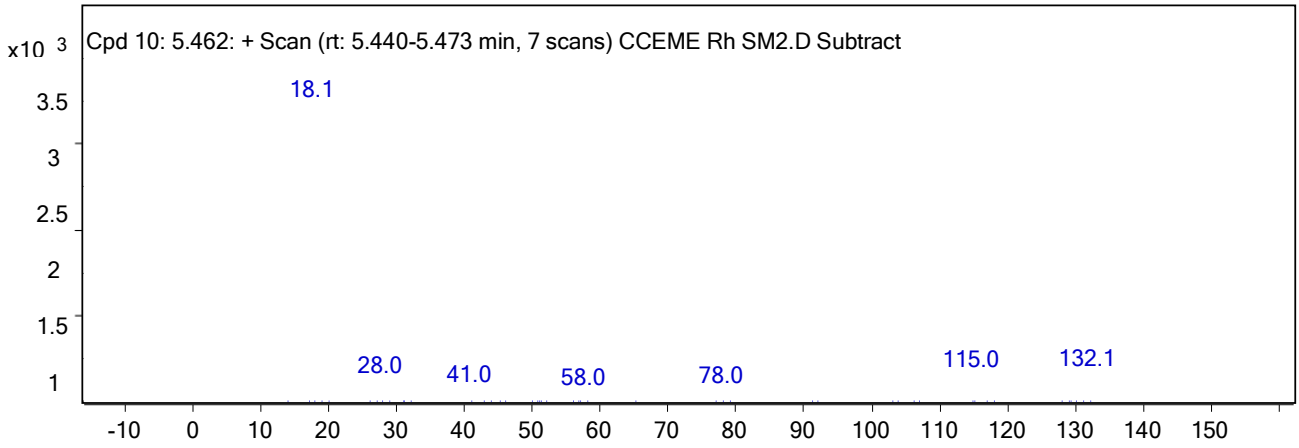

MS Spectrum Peak List

m/z	**Abund**
14.1	611.3
17.1	1989.81
18.1	3465.88

28	248.33
41	144.19
114.9	145.92
115	319.44
118	137.33
128	132.14
132.1	333.46

Compound Label	**RT**	**Algorithm**
Cpd 11: 5.544	5.544	Find by Integration

Compound Chromatograms

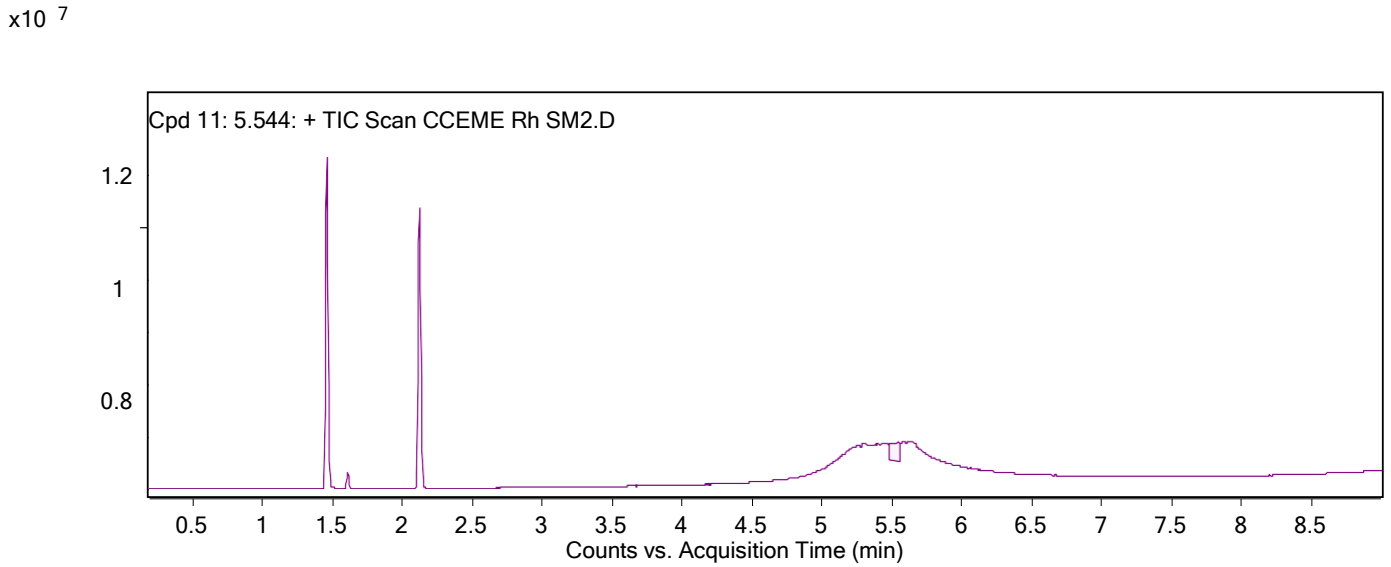

MS Spectrum

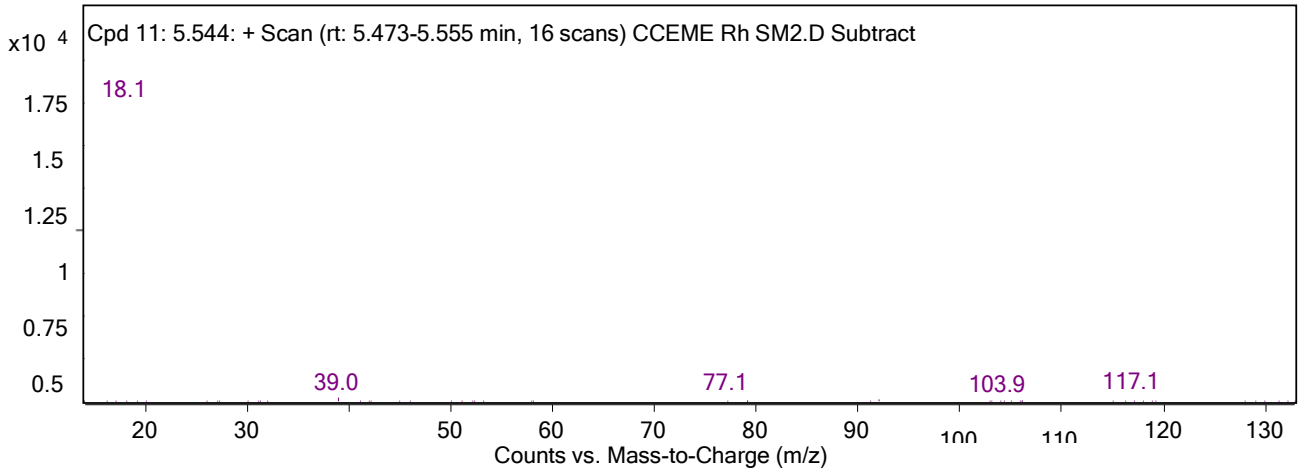

MS Zoomed Spectrum

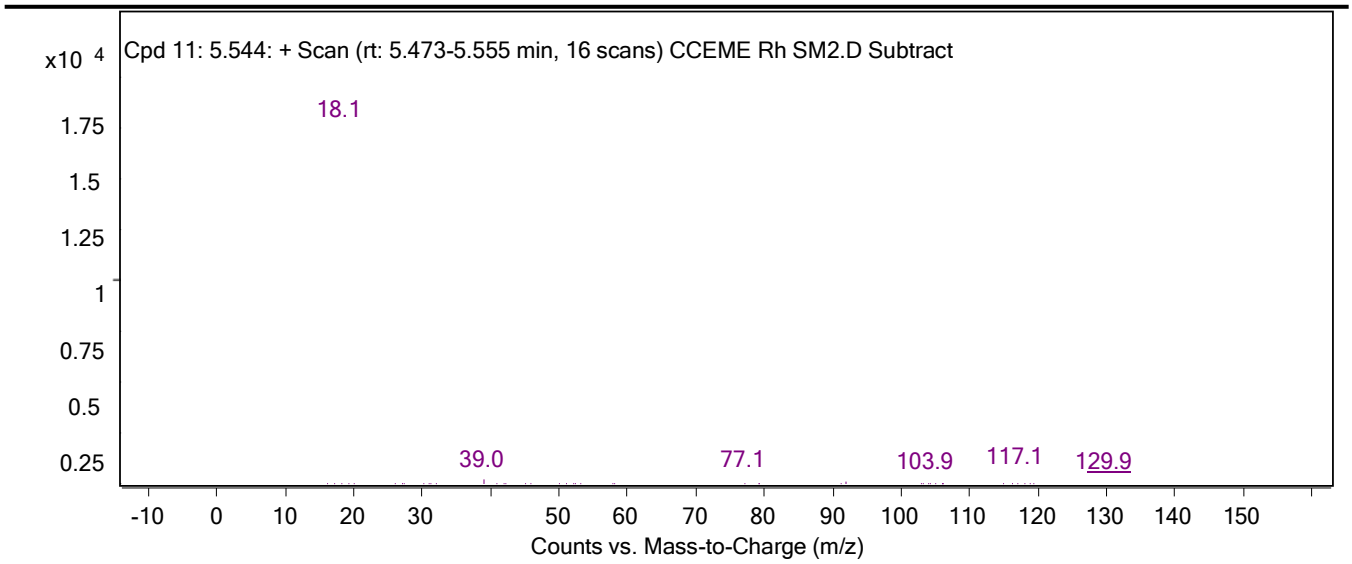

MS Spectrum Peak List

m/z	**Abund**
16.1	217.74
17.1	1944.44
18.1	17413.5
39	254.94
41	165.51
77.1	202.66
117.1	304.94
118	145.14
129	135.53
129.9	142.34

Compound Label	Name	RT	Algorithm
Cpd 12: Water	**Water**	5.577	Find by Integration

Compound Chromatograms

x10 7

MS Spectrum

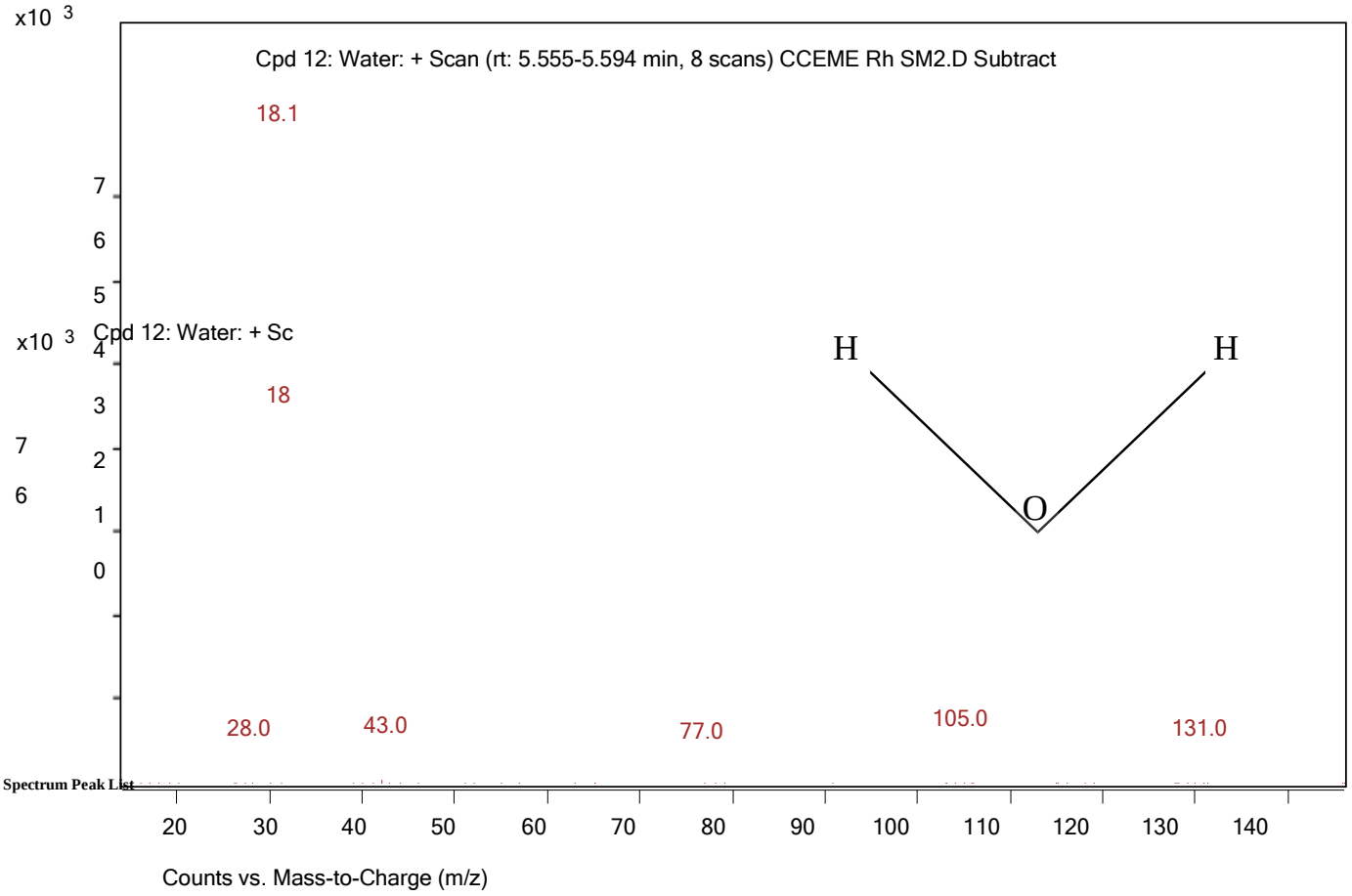

MS Spectrum Peak List

MS Zoomed Spectrum

m/z	**Abund**
17.1	5813.09
18.1	7905.38
27.2	131.29
28	175.58
40.1	128.38
43	198.98
46	107.14
77	119.84
105	300.38
131	144.93

Compound Structure Compound Chromatograms

Compound Label	**Name**	**RT**	**Algorithm**
Cpd 13: Water	**Water**	5.627	Find by Integration

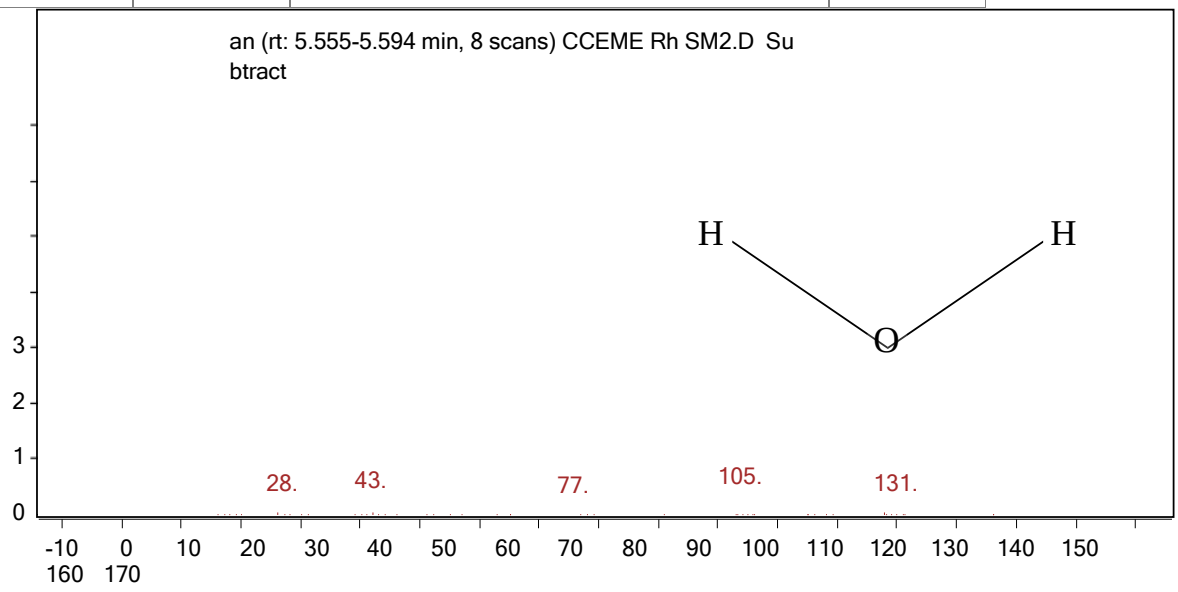

x10 7

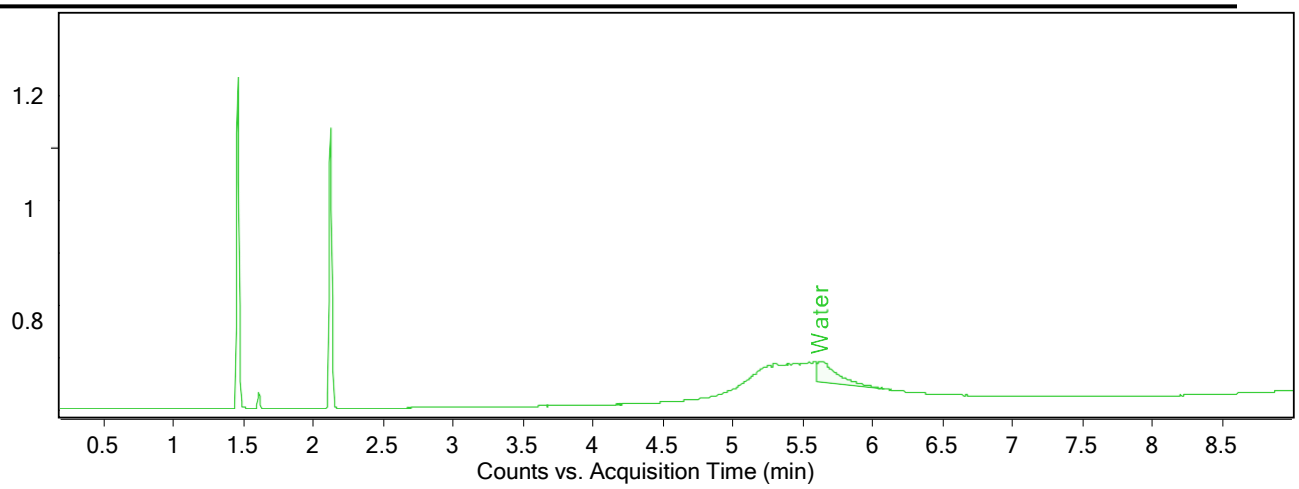

MS Spectrum

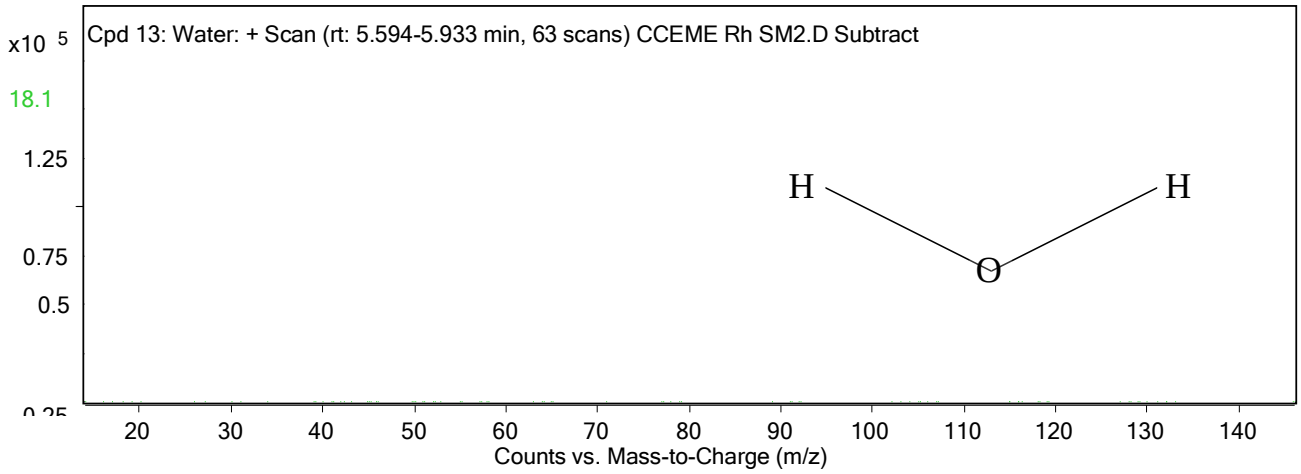

MS Zoomed Spectrum

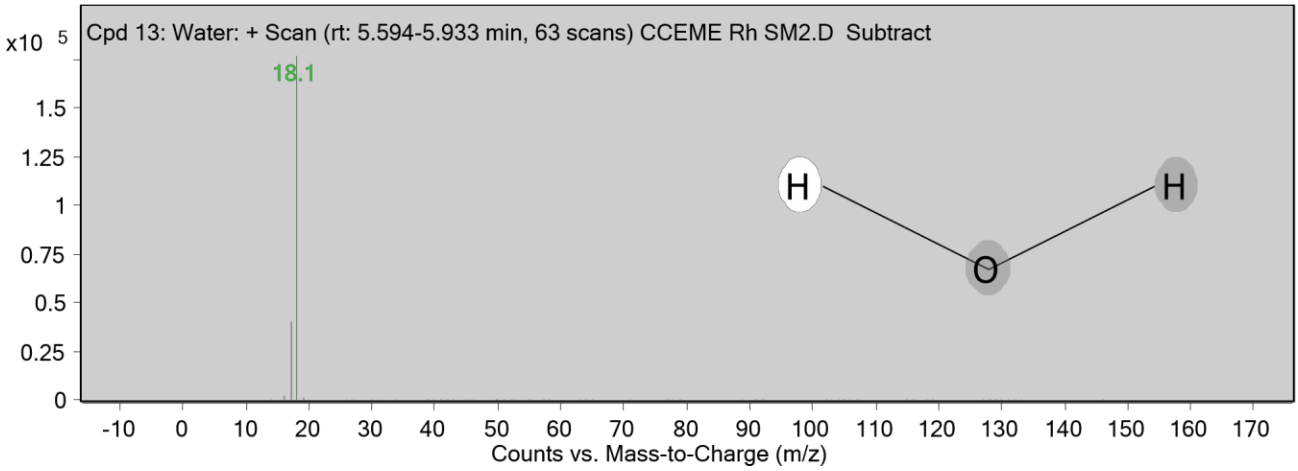

MS Spectrum Peak List

m/z	**Abund**
16.1	2327.33
17.1	40533
18.1	176674.13

Compound Structure

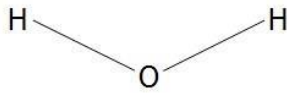

Compound Label	RT	Algorithm
Cpd 14: 8.968	8.968	Find by Integration

Compound Chromatograms

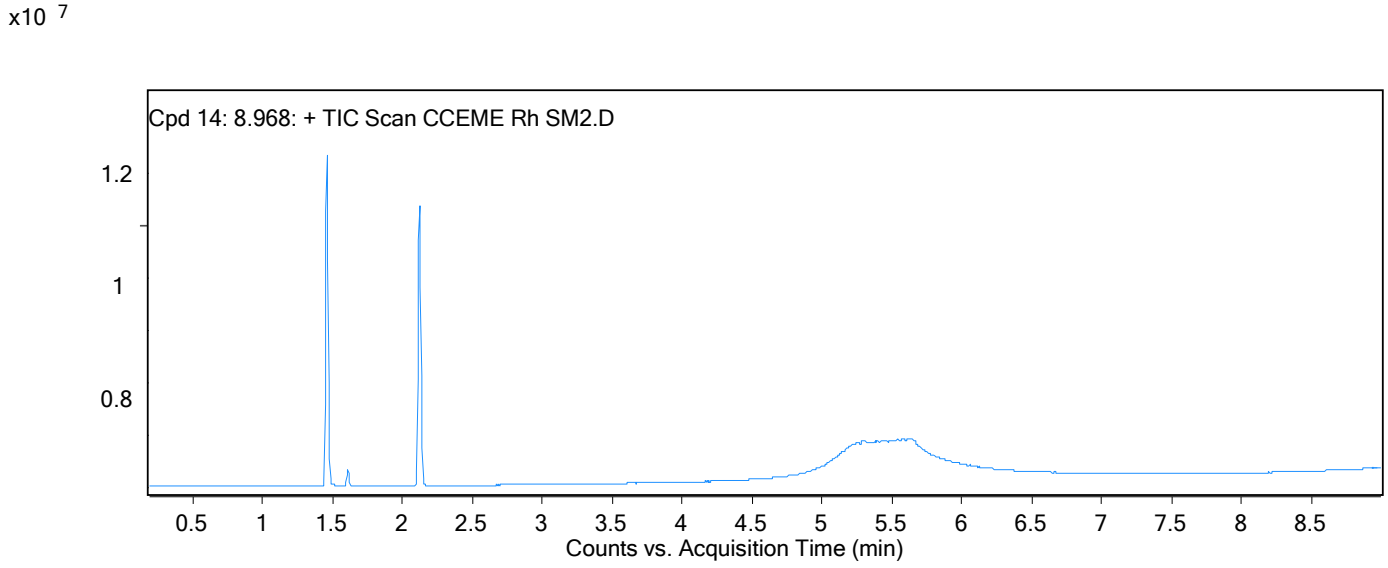

MS Spectrum

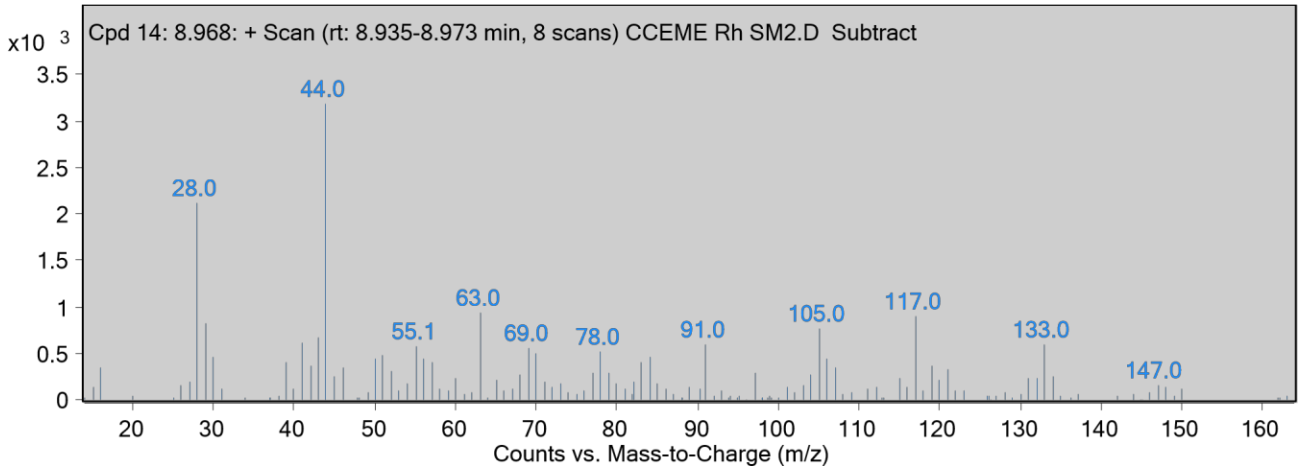

MS Zoomed Spectrum

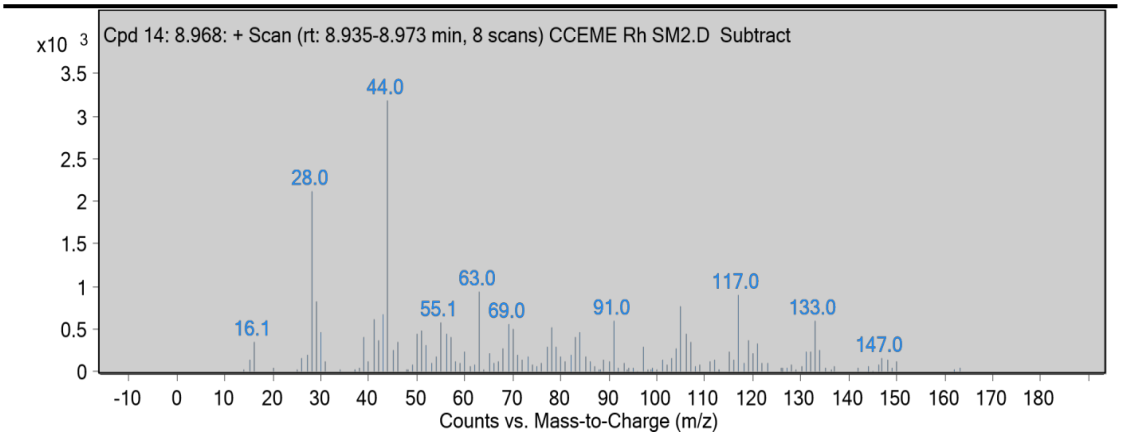

MS Spectrum Peak List

m/z	**Abund**
28	2107.37
29	820.89
41	615.32
43	674.49
44	3186.92
63	934.22
91	594.51
105	769.87
117	905.7
133	590.62

--- End Of Report ---